



THE UNIVERSITY OF
WAIKATO
Te Whare Wānanga o Waikato

Research Commons

<http://researchcommons.waikato.ac.nz/>

Research Commons at the University of Waikato

Copyright Statement:

The digital copy of this thesis is protected by the Copyright Act 1994 (New Zealand).

The thesis may be consulted by you, provided you comply with the provisions of the Act and the following conditions of use:

- Any use you make of these documents or images must be for research or private study purposes only, and you may not make them available to any other person.
- Authors control the copyright of their thesis. You will recognise the author's right to be identified as the author of the thesis, and due acknowledgement will be made to the author where appropriate.
- You will obtain the author's permission before publishing any material from the thesis.

**Laser-induced breakdown spectroscopy applied to pasture,
titanium, and bioplastics**

A thesis
submitted in fulfilment
of the requirements for the degree
of
Doctor of Philosophy in Engineering
at
The University of Waikato
by
HARRISSON BALABAT JULL



THE UNIVERSITY OF
WAIKATO
Te Whare Wānanga o Waikato

2018

Abstract

Precision agriculture is a farming practice that makes production more efficient. Farmers are able to treat infield variability optimising efficiency, growth, and yield by tailoring the time, rate, and type of fertilizer that is applied. This reduces costs, waste, and environmental side effects such as runoff and leaching caused by over-fertilization. Precision agriculture technology measures the nutritional status of crops to inform what, and where, nutrients are needed. The sensors need to be precise, discriminative, and work in real time to ensure that optimal windows for nutrition are not missed. These sensor systems provide aerial imaging, and crop, or soil, colour index maps.

A technology that has proven effective on some agricultural specimens is laser-induced breakdown spectroscopy (LIBS). LIBS is an optical emission technique that utilizes a high-powered pulsed laser to create a plasma on the sample surface. As the plasma cools, photons are emitted at distinct wavelengths corresponding to the elemental composition in the plasma, which should represent the sample. This thesis investigates using LIBS as a sensor for precision agriculture. Multiple chemometric methods have been used on the pasture spectra to build calibration models. There are large deviations between spectra belonging to a single sample. This is due to surface inhomogeneity, particle size, lens-to-sample distance, temperature fluctuations between plasmas, and other causes. Temperature corrections were investigated using Boltzmann plots, Saha-Boltzmann plots, and intensity ratios.

With limited success in mitigating the variations in pasture spectra, LIBS was used to investigate non-aqueous systems. The ability to selectively sinter the surface of injection moulded titanium was examined. Titanium metal injection moulding allows the creation of complex metal parts that are lightweight, biocompatible, and costs less than machining. Multiple LIBS pulses produced sintering in the ablation crater of injection moulded titanium by sufficiently heating the titanium particles so that fusion occurred. The spectra from LIBS can be used to monitor the extent to which the surface is sintered by measuring the reduction in carbon emissions. An autofocus system, based on the triangulation method, was used to minimise variations caused by lens-to-sample distance (LTSD).

With the success of sintering titanium, LIBS was used to investigate non-aqueous organic systems. Employing LIBS to discriminate bioplastics from regular plastics was explored in recycle waste streams. If bioplastics are present in the recovery process of regular plastics the resulting product contains impurities. This study was undertaken to determine the feasibility of incorporating bioplastics in the curbside pickup of recyclables in New Zealand. The common recyclables are plastics, glass, tin cans, and aluminium cans. The setup was designed to emulate a one-shot LIBS detection system in a recycling plant. Models were created using k nearest neighbours and soft independent modelling class analogy from the spectra. 100 % discrimination between bioplastics and regular plastics was achieved. An autofocus system, combining dual lasers, was used to overcome the occlusions produced by sample geometry.

Acknowledgments

I am not a man of many words, so I hope these few words can express my immense thanks to those who helped me along this journey.

“If I have seen further it is by standing on the shoulders of giants!”

- Isaac Newton

First and foremost, I would like to thank God, who without, this work would not have come to fruition. I would also like to thank my family for helping me throughout the years and for supporting me even when they had no idea what my research was about. Especially my parents Colin and Camila. You were always there giving me encouragement and telling me how proud you were. Also, thanks to my siblings Angelina, Chiquitita, Gerrard and their spouses for allowing me to take my mind off my studies and be the best uncle in the world.

Thanks to the late Dr Sadhana Talele, who unfortunately could not see this work complete, for seeing something in me and approaching me to pursue a doctorate. I appreciate your effort in changing my mind and not giving up on me. Thank you for the opportunities to demonstrate, tutor, and teach. I was your first PhD student that you were chief supervisor over and I hope I did you proud. Thanks to my supervisor and friend Associate Professor Rainer Künemeyer for your help, guidance, support, knowledge, comradery, and for always lightening the mood with your great sense of humour. I would not have completed this work without your encouragement and direction. Thank you for always having an open door and giving me opportunities to learn. Thanks to Dr Peter Schaare for your direction, for allowing me to use your facilities, and for your sense of humour. Our research discussions were always enlightening and joyful. To my final supervisor Dr Marcus Wilson, thank you for stepping in and helping out after the passing of Dr Talele.

There are many staff at the University of Waikato that I would like to thank also. To Mary Dalbeth for all the help you have given me with all my forms and for the friendly greetings every time I had to bother you with something. To Gwenda Pennington for encouraging me to apply for scholarships and for her instrumental part in helping me receive a Fulbright Science & Innovation Graduate Student

Award. The time and effort you put in to help me were not unnoticed and I appreciate it all. To all the staff in the Interlibrary Loan office for dealing with my numerous interloan requests (literally hundreds).

I would like to especially thank the University of Waikato for the University of Waikato Doctoral Scholarship which allowed me to undertake this endeavour. This scholarship provided for my needs and helped me pay off my student loan. To the Todd Foundation, thank you for the Todd Foundation Award for Excellence (Universities) with which I attended the Euro-Mediterranean Symposium on LIBS. I was able to meet with some of the forerunners in the LIBS field and listen to some amazing presentations. The conference also provided me passage to Italy where I explored Rome, one of my lifelong dreams. To Fulbright New Zealand for the Fulbright Science & Innovation Graduate Student Award with which I travelled to the United States to perform research. To the Dodd-Walls Centre for Photonic and Quantum Technologies for the Dodd-Walls Centre PhD Extension Scholarship which gave me the funding to finish this thesis. And finally, grateful acknowledgement to the New Zealand Ministry of Business, Innovation and Employment for financial assistance from under contract C11X1209 without which this work would not have taken place.

For the Fulbright Science & Innovation Graduate Student Award I spent a year in Florida doing research at Nova Southeastern University under the supervision of Professor José Ramos. I would like to thank Professor Ramos for extending the invitation with open arms and for all the work he put in to help me adjust to life in America. Thank you for your comradery, friendship, supervision, teaching me system identification, inviting me into your home, and for everything that you have done for me. My time in Florida is a cherished memory. Te extraño y tu familia. To all my friends in Florida thank you for helping me adjust, sharing your culture, and including me in everything. There were hard times being in a new country feeling homesick and you all made me feel like Florida was a new home.

A huge thank you to my friends. Dane, Gus, Chris, Elye, Cam, and Josh for all the laughs we had at university and for taking my mind off the stress and worry that comes with a doctorate. To Lehi and Brooke for making me a part of the family and always looking out for me. To Courty and Riri for keeping me grounded through

this long voyage and helping me have fun. To Celeste and Leah for making my off time from university more enjoyable with the competitive card nights. To Mereana for friendship and the deep conversations about anything and everything. Seeing you every day helped with the demanding work that I undertook. To all of you for always being there and helping me out when I needed it. For always laughing with me. Someone once said, “when you find a friend, you find a treasure” and you are the treasures that kept me strong until the end.

To everyone else that has helped me along the way, thank you!

Table of Contents

Abstract	i
Acknowledgements	iii
Chapter 1 Introduction.....	1
Chapter 2 Literature Review	8
Chapter 3 Nutrient quantification in fresh and dried mixtures of ryegrass and clover leaves using laser-induced breakdown spectroscopy.....	20
Chapter 4 Laser-Induced Breakdown Spectroscopy Analysis of Sodium in Pelletised Pasture Samples.....	38
Chapter 5 Considerations needed for sensing mineral nutrient levels in pasture using a benchtop laser-induced breakdown spectroscopy system ...	46
Chapter 6 Identification of Contamination Levels and the Microstructure of Metal Injection Moulded Titanium.....	87
Chapter 7 Selective Surface Sintering Using a Laser-Induced Breakdown Spectroscopy System	97
Chapter 8 Classification of recyclables using laser-induced breakdown spectroscopy for waste management	109
Chapter 9 Process monitoring using LIBS	130
Chapter 10 Conclusion	140
References	144
Appendix A Summary of LIBS analysis of plant material including various parameters for experimental setup and emission lines investigated.	158
Appendix B Agricultural robot platform.....	203
Appendix C Conferences presentations	224
Appendix D Co-authorship forms	227

Chapter 1

Introduction

Introduction

Financial and environmental benefits are created by the precision agriculture (PA) strategy of applying the right fertilizer, at the right time and in the right place. This enables land users to maximise yield and profit, minimize expenses and reduce environmental side-effects caused by over-fertilisation such as leaching and excessive run-off into waterways. This is achieved by spatially measuring the macro (N, P, K, Ca, S, and Mg) and micro (B, Cl, Mn, Fe, Zn, Cu, Mo, and Ni) nutrients in the field of interest. This information can then be used to develop a fertilisation strategy that would apply different types of fertilizer at different rates and in specific sites. The current technologies used for PA that are capable of real-time, in-field nutritional assessment of plants evaluate only a few of the essential nutrients. Greenseeker[®] is one of these technologies that focus on N [1]. Focussing on N alone diminishes improvements to crops and reduces the effectiveness of fertilizer application.

The ideal technology for PA would be cost-effective, portable, make measurements in-situ and present information in real time [2]. Laser-induced breakdown spectroscopy (LIBS), also known as laser-induced plasma spectroscopy, caters to all the above and requires minimal preparation to samples, no chemical usage, non-contact analysis of samples while removing a surface area of only a few hundred microns in diameter (almost non-destructive). LIBS can be used on samples irrespective of their state (solid, liquid or gas). For these reasons, LIBS is a perfect candidate for PA. The hypothesis is that LIBS technology can provide detailed, real-time information on the nutritional status of pasture and can be used to tailor fertiliser application rates. This will provide savings to New Zealand farmers, and to the country as a whole.

LIBS is a spectroscopic technique that utilizes a short, high powered, pulsed laser focused on the surface of a sample (solid/liquid) or inside a sample (liquid/gas). The incident focused beam (usually $>1 \text{ GW cm}^{-2}$) rapidly melts and/or vaporizes a small amount of the sample surface, through inverse Bremsstrahlung, creating a plasma. As the plasma cools, electrons transition from high energy levels to lower ones. These transitions cause photons to be emitted at specific wavelengths

corresponding to the change in energy. Each atom and ion have particular energy levels, therefore particular wavelengths that will be present in the spectrum of the plasma's radiated emission. To achieve the best signal-to-background ratio (S/B) experimental parameters such as spot size [3, 4], wavelength [5, 6], pulse duration [4], pulse energy [3-5, 7], power density [8], gate delay [3, 9], integration time [10], incident angle [11-13], lens-to-sample distance (LTSD) [11, 13-15], and power density [7] need to be optimized. To optimize these parameters, emission lines need to be chosen for the atoms and ions of interest because they do not react to the same set of values for each parameter [9, 16]. There is no standard set of values since each matrix behaves differently [13, 17-22]. Examples of these matrix effects are found in studies by Moros et al. [3] where graphs were produced displaying how the spot size, laser pulse energy, and delay time effect the emission lines in different types of explosive samples, Gomes et al. [17] in which particle sizes of different plant species effect the intensities of emission lines, and Gornushkin et al. [18] where no consistent calibration behaviour was found between spectra from organic and inorganic powders both containing magnesium. Other ways to improve S/B is by controlling the pressure and surrounding atmosphere of the sample [23].

To evaluate the spectra obtained from the plasma, chemometric techniques are used on the emission lines. This provides qualitative and quantitative information on the chemical makeup of the sample. The calibrations made from the chemometric analysis are only specific to that particular sample because each matrix responds differently to the same set of experimental parameters [13, 17-22]. Common chemometric techniques include principal component analyses (PCA) to identify samples from their spectra and partial least squares regression (PLS) which is used to build a calibration curve for quantitative analysis of samples. A method known as calibration-free LIBS can also be used to perform quantitative analysis on materials [24-27]. This technique assumes that the plasma is in local thermodynamic equilibrium (LTE) and utilises the Saha equation and Boltzmann plot on spectral lines to determine the concentration of the analysed element. These can help mitigate matrix effects. Another way to combat matrix effects is to build calibration curves using an internal standard [27-42]. The internal standard is usually of an element that comprises the majority of the sample. The sample can also be doped with an element of a known concentration which is used for the

internal standard. Other novel methods have also been used to increase model predictive capabilities [43].

A field deployable instrument needs to be able to work at varying distances. Standoff LIBS (ST-LIBS) is the art of performing LIBS at large distances [44]. Also known as open-path LIBS, it is not to be confused with remote LIBS where a fibre optic cable is used for covering large distances. The distances involved cover a few meters [45] to a few hundred meters [46]. This is achieved by changing the optics in the delivery system by increasing lens sizes and focal lengths, or by using telescopes. The important aspect is being able to vary the position of the optical arrangement so that the beam can be focused at varying distances. It is important not to increase the LTSD beyond the focal distance of the optics as an air plasma can be created above the sample surface and the spectra recorded would not be comparable to the sample [13]. The effect of decreasing the LTSD below the focal distance of the optics varies depending on the emission line. Different emission lines have peak intensities at different values of LTSD. This is caused by changes in spot size, mass ablated, and irradiance on the sample among other factors. There are also changes in plasma temperatures [13, 14]. Autofocus systems greatly increase the accuracy and speed of varying the LTSD. This concept also applies to focusing the LIBS beam within small deviations on the surface material of the investigated sample.

The purpose of this thesis is to determine if LIBS is a suitable sensor technology for precision agriculture. This system would evaluate the nutritional status of pasture at variable distances in a minimal amount of time. The calibration curves created for the macro and micro nutrients in pasture should be accurate. This will allow in-field, real-time analysis of pasture so that the correct fertilisers can be applied on time and in the right place. This would increase yield and profits, at the same time eliminating over-fertilisation and the effects associated with it. This will also reduce costs connected with fertiliser application such as frequency of application and type of fertilizer used.

These specific objectives were addressed in seven chapters, made up of five peer-reviewed journal publications, a peer-reviewed conference publication, and a concluding discussion.

Chapter 2 discusses the studies that have been done on grass with mention of other important literature on agriculture. The literature on ST-LIBS and LIBS systems with autofocus are explored. An in-depth up-to-date list of LIBS for agriculture is found in Appendix A.

Chapter 3 is a peer-reviewed publication that has been accepted [47]. It investigates using LIBS on fresh and dried pelletized pasture to predict nutrient levels. PLS was used to build models for each macro and micro nutrient. Spectra taken using an argon atmosphere are compared with spectra taken in air. A discussion on the prediction limitation for each nutrient is included.

Chapter 4 is a book chapter to be submitted to a Springer published book titled “Smart Sensors for Precision Agriculture” [48]. It discusses using various chemometric methods to increase the predictive ability of LIBS on pasture. The methods explored were Savitzky Golay filtering, multiple linear regression, principal component regression, PLS, Gaussian process regression, and artificial neural networks. Categorical information, such as the dates and plots the samples were gathered from, were investigated to determine whether prediction accuracy would increase.

Chapter 5 is a peer-reviewed, international conference publication [49]. It examines the emission line equation to determine the main contributors of within-sample spectral variation. These are namely the temperature dependence of the partition function and the Boltzmann factor. The temperature of the plasma for each spectrum was determined by Boltzmann plots and Saha-Boltzmann plots. It was then used to remove the partition function and Boltzmann factor from the equation. PLS was used on the result to build models for sodium. This chapter also discusses using internal references to improve the predictive ability of the calibration curves for sodium. Different combinations of internal references were used on the Na I 818.326 nm line.

Chapter 6 is a peer-reviewed publication which is published [50]. With the moisture being the main source of variation in fresh pasture, Chapter 6 investigates using LIBS on inorganic non-aqueous systems to confirm the performance of the technology. This chapter identifies the inaccuracies when measuring contamination levels in metal injection moulded titanium. Scanning electron microscopy imaging, electron dispersion spectroscopy point and area mapping, Trace analysis and X-ray diffraction elemental mapping are used to analyse samples. The relevant portion of this chapter, with regards to this thesis, is the work performed using LIBS. LIBS is used as a trial method to determine the binder levels in green, grey, brown, and sintered forms of the part. The ratio of Ti II 282.81 nm with C I 247.86 nm is used to give a relative measure of residual carbon. Energy-dispersive X-ray spectroscopy (EDS) results are compared with the LIBS results. An autofocus system based on the triangulation method is used to minimise LTSD variations. The system is described in this chapter.

Chapter 7 is a peer-reviewed publication that is published [51]. It continues analysis of inorganic non-aqueous systems. This chapter explores the idea of using LIBS to selectively sinter the surface of injection moulded titanium. Repetitive LIBS laser pulses are fired on the same location increasing the heat on the sample surface fusing the titanium particles together. With the small amount of ablated surface in the plasma, the surface composition can be determined. Taking the ratio of Ti II 282.81 nm and the C I 247.86 nm lines gives a relative indication of the extent to which the surface under the laser has been sintered. EDS is used on the ablation craters to determine the amount of residual carbon and the results are compared to traditionally sintered titanium. The process of selective surface sintering is employed using an autofocus system.

With the success of proving the performance of LIBS on inorganic non-aqueous systems, Chapter 8 investigates using LIBS on organic non-aqueous systems. Chapter 8 is a peer-reviewed publication under review [52]. This chapter discusses using LIBS to sort through common recycle waste streams in New Zealand. These are namely glass bottles, plastics bottles (polyethylene terephthalate and high-density polyethylene), tin cans, and aluminium cans. Two bioplastics (polylactic acid (PLA) and Novatein[®] Thermoplastic Protein (NTP)) are investigated to

determine whether they can be added to the current recycling stream. This chapter focuses on the classification of recyclables using k -nearest neighbour (k -NN) and soft independent modelling by class analogy (SIMCA) on the principal components from PCA. PCA was performed on spectra of glass bottles, plastic bottles, a tin can, an aluminium can, PLA, and NTP. A dual laser autofocus system based on the triangulation method is implemented to ensure the correct LTSD and to overcome obstructions which limit single laser triangulation.

Chapter 9 synthesizes chapters 3 through 8. This chapter adds further discussion on the limitations on using LIBS for precision agriculture and considerations for further work. The reasoning for the improved performance of LIBS on non-aqueous systems compared to aqueous systems is given.

Finally, a conclusion is given which highlights the main findings of each chapter and offers discussion on further work and considerations.

Chapter 2

Literature Review

Literature review

2.1 LIBS analysis of grass

LIBS has been evaluated in laboratories on various plant materials, for various purposes. Appendix A contains a comprehensive up-to-date list of the plant material used in the literature with a detailed description of experimental parameters. This is not a complete list of literature dealing with agricultural material, but it is sufficient for the needs of this thesis and is an extension of the list published in Chapter 3. There are only seven articles that have been found with references to LIBS on the assessment of grass samples. A summary of the relevant parts of these studies is presented here.

Only two studies have been performed on fresh grass. Chauhan et al. [53] studied the distribution of Si in Bermuda Grass (*Cynodon dactylon*). A 532 nm, 4 ns, 10 Hz Nd:YAG (neodymium-doped yttrium aluminium garnet) laser with a 10 mJ pulse was used to map the samples using a single shot. The spectrum recorded showed the presence of Si, Mg, Ca, C, Al, Zn, N and Sr in the leaves. The intensity of the Si I 288.15 nm line was used to find the Si concentration in various locations on the leaves. It was higher in leaf blades than leaf sheaths and stems. The strongest concentration of silica was found in the midrib area of the leaf. Reference is made to Boltzmann's law that spectral lines are directly proportional to the concentration of the elements in the sample but no quantitative LIBS analysis was performed.

Boyain-Goitia et al. [54] assessed the use of LIBS for analysing bioaerosols, namely pollen from lilies and marguerites. A 1064 nm, 5 Hz Nd:YAG laser with a 20-30 mJ pulse was focused to produce a 150 μm spot size. The single shot spectra obtained from the pollen was collected using a spectrometer with a 1 μs delay and integrated over 4 μs . The relevant portion of this study is where the pollen spectra were compared with spectra from fresh grass fragments. Both sets of data were normalised with the CN (Cyano radical) band peaks to reduce matrix effects. The differences found were that the grass fragments did not emit Cr and Fe lines, there were Si lines in the grass spectra, and the phenylalanine concentration in grass seems to be considerably lower than pollen. The Si was attributed to soil dust on the grass blade. The Ca and Al concentrations in the grass fragments were of similar

orders of magnitude to that of the pollen samples. Due to the limited samples, since the study was performed in autumn, it is difficult to distinguish between grass and pollen. No quantitative analysis was performed on the grass spectra. Only the normalized intensities of the emission lines of interest were compared.

The remaining studies do not examine fresh grass samples. Braga et al. [36] investigated the efficiency of multivariate (PLS) and univariate linear regression calibrations to determine micro nutrients (B, Cu, Fe, Mn and Zn) in pelletized plant samples. The plant material used was from an aquatic plant, aquatic moss, bush branches and leaves, cabbage, soya flour, rice flour, wheat flour, spinach leaves, brachiaria, banana leaves, coffee leaves, maize leaves, mango leaves, pepper leaves, and soya leaves. Olive leaves, apple leaves, guava leaves, grass (*Axonopus obtusifolius*) and jackfruit leaves were used in the validation set for model calibrations. A 532 nm, 12 ns, 10 Hz Nd:YAG laser with a 71 mJ pulse was focused to produce a spot size of 600 μm with a fluence and irradiance of 25 J cm^{-2} and 2.0 GW cm^{-2} respectively. Ar was pumped into the ablation chamber to increase emission line intensities. The spectra were collected using an echelle spectrometer with a delay and integration time of 9 μs and 1.1 μs . 10 locations were chosen on each sample and 30 consecutive laser pulses were taken in each location. These spectra were averaged to produce a single spectrum. This procedure was replicated five times for each sample. The replicates for each sample displayed shot-to-shot variation and matrix effects. To try to mitigate this, the emission lines for univariate linear regression (B I 249.773, Cu I 327.395, Fe II 238.200, Mn II 257.610, and Zn II 206.200 nm lines) and the spectra for PLS were normalised with the C I 193.090 nm emission line. The spectra were split up into regions and PLS was performed on them.

Mixed results were obtained using normalisation and sub-intervals of the spectra. The C I 193.090 nm normalisation only improved correlations for Fe and B but not for Cu, Mn, and Zn. There was no significant difference between using the entire spectra and regions of the spectra. The only micro nutrient that benefited from this was Fe. Of particular interest is that the data suggested that the multivariate model for B in grass followed the expected values whereas the univariate model did not. One of the conclusions is that a specific calibration method should be done for each

plant species using plant material that closely resembles the chemical and physical makeup of the sample to be studied. This will reduce matrix effects and make the calibration matrix dependent.

Martin et al. [55] assessed the use of LIBS for identifying endophyte-infected Tall Fescue Grass (*Festuca arundinacea*). The grass was ground and passed through a 20-mesh screen then pressed into pellets. A 532 nm Nd:YAG laser with a 23 mJ pulse was focused to ablate the pelletized samples with an irradiance of $>10 \text{ GW cm}^{-2}$. The spectra were collected using a spectrometer with a delay and integration time of 0.5 μs and 10 μs . The specific elements investigated were Fe, Mn, Mg, Pb, Ca, Zn, and Cd. The study found that LIBS was more sensitive to Cd detection than ICP-MS. It was also found that when endophyte was present the concentrations of Mg, Ca, Fe and Mn were different. Due to the lack of samples, no definite method was found to differentiate whether endophyte affected the concentrations of metals in the grass. However, LIBS was successful in qualitatively detecting Fe, Mn, Mg, Pb, Ca, Zn, and Cd.

Rai et al. [35] investigated the effectiveness of Bermuda Grass (*Cynodon dactylon*) as a treatment for diabetics. Diabetes was induced in a group of male albino Wistar rats and the rats were feed the grass. There were different groups of rats to compare the treatment with other treatments. The grass samples were shade-dried, extracted with distilled water, and filtered. A 1 Hz Nd:YAG laser with a 175 mJ pulse was used on the samples. Each spectrum was an average of 100 shots. The LIBS analysis was used to detect the glycaemic elements present in Bermuda grass. The concentration ratios of Mg, Na, K, H, and N against C III 229.6 nm and O against N were calculated and compared to the results obtained from plantains (*Musa paradisiaca*). Mg/C was stronger in grass, whereas K/C and Na/C were weaker in grass. These ratios were possibly responsible for the antidiabetic effect in the rats studied. There is no mention of the actual concentration of these elements in the article other than that the spectral line is proportional to the concentration of the element.

LIBS was compared to inductively coupled plasma-optical emission spectroscopy (ICP-OES) for measuring macro and micro nutrients (Na, K, Mg, Ca, Mn, Fe, Cu,

Zn, B, P, and S) in pasture by Devey et al. [56]. The pasture samples, comprised mainly of ryegrass (*Lolium perenne*) and white clover (*Trifolium repens*), were dried and ground to less than a millimetre and pressed into pellets. A 1064 nm Nd:YAG laser with a 200 mJ pulse was used on the samples. One cleaning shot was used followed by a measuring shot. 80 shots were taken, each in a different location, then averaged. The spectra were collected after a 1 μ s delay. Savitzky Golay (SG) smoothing, vector normalization, and wavelet smoothing were performed on the spectra before analysis. The correlation of each wavelength was calculated and the peak with the highest correlation and the region surrounding it were used in PLS regression. The peaks of the elements analysed were 819.4 nm (Na), 696.4 nm (K), 882.4 nm (Mg), 212.3 nm (Ca), 257.6 nm (Mn), 248.5 nm (Fe), 213.8 nm (Zn), 249.7 nm (B), and 214.9 nm (P). There were no strong correlations for Cu and S. Wavelengths at the expected emission lines, 324.7 nm (Cu) and 921.3 nm (S), were used. Using PLS on these regions, rather than the whole spectra, increased the accuracy of the models. The best results were found for Na, K, Ca, and P. These results were similar to that of ICP-OES. LIBS had poorer correlation for Zn and Cu than ICP-OES.

Kunz et al. [57] explored using the plasma temperature to distinguish between different plant species. The tested samples were dried leaves from dallisgrass (*Paspalum dilatatum*), wheat (*Triticum aestivum*), soybean (*Glycine max*), and bell pepper (*Capsicum annuum*). An 800 nm, 35 fs, 1 kHz Ti:Sapphire laser with a 0.3 mJ pulse was focused to produce a spot size of $\sim 100 \mu\text{m}$ with a fluence and irradiance of 3.8 J cm^{-2} and $\sim 3.8 \text{ kW cm}^{-2}$ respectively. The spectra were collected using a spectrometer with an integration time of 0.5 s. 500 laser pulses were taken for each of the 10 spectra on both replicates of each species. Each spectrum was gathered from a different surface on the leaf. Boltzmann plots were created using the Ca I 422.874, Ca I 518.542, and Ca I 559.849 nm lines. The temperature of each plasma was calculated from the gradient of the line of best fit through the points from these three lines. The R^2 value for the Boltzmann plot of dallisgrass was 0.7 and the average temperature was 5638 K. The average temperatures of the different species were diverse enough that they could be used to identify each sample. A main source of variation is the inhomogeneity of the samples. The authors state that their method produces semi-quantitative results.

From these articles, only Braga et al. [36] and Devey et al. [56] performed quantitative analysis of grass. Explanations of the origin of the variances for each nutrient have not been discussed in depth and quantitative models specifically for fresh grass have not been created.

2.2 Focusing of LIBS at various distances

Changes in the distance to the sample introduce a number of complications in beam focusing, emission collection, and shot-to-shot variation [58, 59]. One of the major issues is that as the distance to the sample increases the intensity of the emission line decreases and broadens thus decreasing the S/B [60, 61]. Wiens et al. [62] suggest that emission line ratios can be used, instead of individual line intensities, to disregard the effects of changes in distance. This fact is demonstrated by Stepputat and Noll [63]. By investigating the methods used for focusing ST-LIBS a similar approach can be taken for focusing the LIBS beam on a sample close to the system with deviations on the sample surface. The majority of experiments for ST-LIBS have used telescopes to both focus the beam and collect the radiated emissions. This reduces the spot size, increases the irradiance, as well as increases the solid angle of the received light waves thus increasing the intensity of the signal. Almost all of the ST-LIBS investigations have been at specific distances which suggest that the optical setup has been adjusted to be only used at that specific distance. Very few papers have expressed what mechanical systems were used to achieve variable focal distances or how the distance to sample was obtained let alone any automated process involved.

Gaona et al. [64] surveyed the main façade of the Cathedral of Malaga with LIBS to identify the chemical composition of the architecture at an average distance of 35 m. A Cassegrain telescope was used to deliver the LIBS beam and receive the radiated emissions from the plasma. A 632 nm laser was utilized to accurately align the LIBS system. A motorized mirror shift mechanism was used to adjust the focus of the telescope. There was no mention made of how the distance was found or how the distance was used to focus the telescope. The group (Lucena et al.) used the same setup in other experiments [65].

Gotfried et al. [66] developed a double-pulse ST-LIBS system to detect hazardous material at 20 m. The laser pulses were expanded with two lenses and focused on the target with a three-inch lens. A Schmidt-Cassegrain telescope was used to collect the radiated emissions from the plasma. A 632 nm diode laser, coincident with the LIBS beam, was used for alignment. A wireless range finder measured the distance to the sample with a digital camera remotely viewing the target. There was no further expansion on how the distance from the range finder correlated to an autofocus mechanism for the laser and telescope. This setup was known as the first-generation system. The same setup was used in their following experiments [67-69]. In the fourth-generation system [70] controls for the autofocus of the laser and collection optics were automated, but there is no mention of how this was achieved. An important observation of the study is that at 20 m the double-pulse significantly enhanced the emission lines in the spectra compared to single pulsed LIBS. For the Al lines, there was an increase by a factor of 20.

Palanco et al. [60] created a field-deployable LIBS instrument for making measurements in the range of hundreds of meters. The system was made using a Herschelian telescope to deliver the LIBS beam and receive the radiated plasma emissions. A motorized flat aluminium mirror was used to adjust the distance to the diverging lens thus changing the focal point. This design was optimized to 120 m. To increase the useful range of the instrument, mention is given to motorisation of the remaining optical components. This additional setup was not used in their study. The combination of using a single telescope for beam focusing and emission collection simplifies focusing since the same focus is used for both. No mention is made to how the distance to the sample was found or if there was an autofocus regime employed. An important highlight of the study was that the LIBS signal strongly decayed with range because of plasma formation and emission collection. The beam divergence and size of the optical elements are also important. In later work by the same group [12], the beam focusing was done by a pair of lenses with a motorized linear stage to separate the lenses. There is no mention of distance acquisition or automation.

Stepputat and Noll [63, 71] used LIBS to analyze heavy metals in electric and electronic waste and implemented an automatic on-line LIBS analyser. A Nokra

laser triangulation sensor in conjunction with a dynamic focusing unit (VarioSCAN, SCANLAB) was used to measure the distance to the surface of a sample and focus the LIBS. It was used in a feedback loop to adjust a variable optics system in the autofocus unit. The sensor and optical system are both standalone products that have been combined to achieve autofocus. The design had a measuring frequency and accuracy of 50 Hz and $\pm 70 \mu\text{m}$ with a working range of 50 mm. To measure the overall system accuracy multiple shots were taken at various places within the 50 mm range. The intensities of these shots were averaged and then different distances compared. This produced a 5 % variation between the observed intensities. There is no statement on how fast focusing was or the algorithm used to achieve autofocus. This system was used by the same group in later studies [72].

Werheit et al. [73] developed a fast identification of metals for recycling using LIBS. An autofocus unit was integrated into a recycling LIBS system that had a conveyer belt which moved at 2-4 m per second. The unit used a 3D CCD camera in conjunction with a line-projection laser to locate and track the scrap metal. Through triangulation, the distance to the sample was found and sent to the galvo-scanner mirrors which focus the LIBS beam onto the sample. The unit could move the focal position of the LIBS laser through a range of 100 mm. This was achieved using a fast diverging lens followed by a fixed focusing lens. One problem was that when the sample moved after it was scanned, and before plasma formation, the focal position would be incorrect. With the current setup, if there was an object between the camera and the reflected autofocus laser line, the LIBS beam would not be focused in the correct place. Noll et al. [74], from the same group, used a triangulation sensor in their inspection system, called LIFT, to identify different high-alloy steel grades. The sensor used a 670 nm laser diode, collinear to the LIBS beam, to measure the distance between a reference plane and the surface of the sample. Noll [71] also described the TeleLis system for ST-LIBS that uses an integrated rangefinder coaxial to the LIBS laser to find the distance to the sample. Once the distance was found the system automatically adjusts the optics in the Galilean telescope to focus the beam.

Balzer et al. [75] used LIBS to acquire a depth profile of sheet steel. A triangulation sensor was employed to keep the focus of the laser on the surface of the steel in the

presence of vibrations. The working distance was 1.5 mm. The beam from the triangulation sensor is transmitted through two dichroic mirrors then through the focusing lens onto the sample surface. The reflection is observed using a CCD camera inside the sensor and the distance calculated. Software was then used to control a diverging lens in the telescope used to focus the LIBS beam. The focus is adjusted to coincide with the surface. There is no mention of the accuracy or speed of the autofocus unit.

Wiens et al. [62] incorporated LIBS in their Mars rover design for determining the elemental composition of rock and soil targets. The system was aimed using bore-sighted cameras. A simple two-lens system was used to focus the LIBS laser on working distances of 2-6 m. An off-axis rangefinder was used to acquire the distance to the sample then the concave lens was moved, via a linear programmable translation stage, to focus the LIBS beam on the target. There was no discussion on whether the programmed displacement of the translation stage, which corresponded to the distance to sample, was based on calculation or experiment. Also, there is no mention of how accurate the system was or the time taken to focus.

The same group developed the autofocus system for ChemCam[®] [76, 77]. The first mention of the autofocus unit for ChemCam[®] [76] employs a modulated (to increase S/N) 785 nm continuous-wave (CW) laser reflected off the target to find the distance to the sample with a working range of 1-9 m. This is done by moving the secondary mirror on a Schmidt telescope with a stepper micro-motor and sensing the intensity of the reflected light with a photodiode. Moving the translation stage through its entire range would produce a hill shape on an intensity versus mirror position plot. A digital processor then calculates the best focus position by using the data obtained between 15-80 % of the maximum received signal and computing where the two symmetric lines would intersect. A problem that arose was that the distance to target obtained from the autofocus was not in the same position as the optimal position for plasma collection. This is due to an offset that can be programmed out using a lookup table for calibrations. The electronic noise was also found to contribute to errors. This autofocus system is used in a later experiment by the same group [78]. Again, there is no mention of the speed of the

routine or whether the routine takes into consideration movement of the sample while evaluating the position of best focus.

The final design of the ChemCam[®] autofocus system is described in detail by Maurice et al. [77]. The Schmidt-Cassegrain telescope had a working range of 1.5-9 m. This was achieved by a 2-phase stepper micro-motor driving a screw-nut [79] setup through a range of 15 mm connected to the secondary mirror. The screw-nut design was employed because of the strict mass and volume requirements for the spacecraft. The time taken to focus, within 0.5 % of the distance to sample, is two minutes but can be up to three minutes at lower temperatures. To accomplish this, the NavCam unit estimates the distance to a target within 5 % using stereo vision. The position of the secondary mirror is then changed to correspond to the estimated target distance by using the relationship between motor steps and distance to the target. This relationship has already been determined. The autofocus routine is the same as [76], with the CW laser being modulated at 10 kHz. Using a modulated CW laser reduces the effect of ambient light on the photodiode. Even though slight beam wander is considered, the technique used is intended for a stationary target which limits its uses for alternate applications. There is a large amount of time taken to focus because of the number of intensity readings taken at each displacement of the secondary mirror. There is no mention as to whether the method of taking a large number of readings is for the extreme accuracy needed for the rover or if it is a standard number for the technique. The speed of the stepper motor also impacts on the time taken to focus. This may be adjusted if one is not concerned with the robustness needed for space exploration.

Barnett et al. [80] used ST-LIBS to investigate the performance of their spatial heterodyne LIBS spectrometer. A Schmidt-Cassegrain telescope was used to focus the laser onto the samples 20 m away. Focusing on the sample was done by using an amplified electret microphone and oscilloscope to monitor the shockwave produced by the LIBS spark. The acoustic signals of the sparks were taken within a range of distances to find the optimal focal point. The intensity of the shockwave was found to be proportional to the irradiance on the sample. There is no mention of the speed of focusing or how the telescope was focused.

Grönlund et al. [81] investigated using LIBS for remote imaging and ablative cleaning for cultural heritage. A Newtonian telescope was used to deliver the LIBS beam and receive the emitted radiation from the plasma 60 m away. A mirror, controlled with stepper motors, was used to fold the LIBS beam so that the targets could be scanned. A lidar system was used to find the distance to the targets. It was equipped with two cameras to identify the location of the laser spot. There is no mention of the speed or accuracy of the focusing mechanism.

The papers above are the only literature that has been found with mention of focusing for ST-LIBS. There are two LIBS papers, which do not use ST-LIBS, that have been found which use focusing mechanisms. Novotný et al. [82] which compares image processing autofocus techniques used for distances of 16 mm and 100 mm. The method employs a CCD camera to detect the sharpness, through image processing, of the image taken at a particular focus. The time taken to focus was between 1.37-5.75 s depending on which method is chosen. The intended use was for two-dimensional surface analysis. This method may be adopted in a three-dimensional environment. This would be an intense algorithm which would only assess the target spot and disregard the rest of the image. Also, the algorithm would need to differentiate between the different planes of focus. The new method would have a huge increase in the time taken to focus.

Ashrafkhani et al. [83] used an autofocus system to improve the repeatability of LIBS. Their method uses point auto-focus. A CW diode laser is reflected off a mirror, so that it is parallel with the LIBS beam, then transmitted through the focusing lens of the LIBS system onto the sample surface. The reflected beam is transmitted, off-axis, back through the optics and finally through a lens which focuses it onto a CCD camera. The image captured by the CCD camera is filtered so that only the beam spot is visible. A reference image of the focal point is compared to the current filtered image to find which way the sample should be shifted so that the correct position is achieved. The autofocus system increased the relative standard deviation of emission lines from 24-46 % to 2-16 % on aluminium samples. There is no mention of the speed of the system or how the CW laser beam obstructions are dealt with.

From the reviewed literature, there are multiple ways of focusing a laser. The use of a rangefinder parallel with the LIBS laser is not suitable for targets smaller than the distance between the parallel beams. The rangefinder can be made to be collinear so that it can point at targets along the axis of the LIBS laser. Having a detection system off-axis can introduce problems such as obstructions that are only in one optical path. The same problem for the rangefinder applies to all off-axis collection. This is not a concern in most of the literature because their targets are larger than a blade of grass. The gradient-based methods of focusing have a large number of problems primarily with the processing algorithm. The ChemCam[®] instrument uses a simple technique, but there is still major room for improvement. The concerns with lidar are the cost of the system and if the accuracy of the system could deal with small blades of grass. The acoustic method needs to be close to the sample and would need to be in an environment free from high-frequency noises. This may work for precision agriculture, but there may be situations in which it would fail. A robust method is needed infield. The point autofocus method is a simple proven method, but the issue is obstructions to either the transmitted or reflected beams. This is highly likely when investigating pasture.

Chapter 3

Nutrient quantification in fresh and dried mixtures of ryegrass and clover leaves using laser-induced breakdown spectroscopy

a peer-reviewed publication
in revision following reviewers' comments in
Precision Agriculture

by

H. Jull, R. Künnemeyer, and P. Schaare

Nutrient quantification in fresh and dried mixtures of ryegrass and clover leaves using laser-induced breakdown spectroscopy

H. Jull¹  · R. Künnemeyer¹ · P. Schaare²

© Springer Science+Business Media, LLC, part of Springer Nature 2018

Abstract Laser-induced breakdown spectroscopy (LIBS) is an analytical technique that can be used to facilitate variable rate fertilizer application, potentially increasing yield, reducing costs and reducing environmental side effects of nutrient loss. LIBS can give real-time information about macro and micro nutrients with little to no sample preparation. The study reported in this paper investigated whether LIBS can predict nutrient levels of fresh and dried pelletized pasture and what the limitations are. Spectra were acquired in air and under argon. Partial least square regression was used to build models for each macro and micro nutrient. The best results were for potassium, sodium and manganese with root mean square errors of cross-validation of 0.20, 0.029 and 0.0008 wt%, respectively, coefficient of determination of 0.92, 0.93 and 0.90, limits of detection of 0.99, 0.11 and 0.0027 wt%, and precisions of 0.30, 0.042 and 0.0012 wt%. LIBS can be used to assess nutrient levels of fresh pasture. Reducing the shot-to-shot variation will lead to improved calibrations.

Keywords Laser-induced breakdown spectroscopy · Pasture · Partial-least squares regression · Plant Nutrition

Introduction

Insufficient fertilizer deprives soil and crops of much needed nutrients, while too much fertilizer increases cost and pollution in streams and rivers. Knowing what nutrients are needed and where to apply them may overcome these problems. Precision agriculture is creating financial and environmental benefits through site-specific and precisely timed crop management. This is achieved through technologies guiding variable rate applications of

✉ H. Jull
harrison.jull@gmail.com

¹ School of Engineering, The Dodd Walls Centre for Photonic and Quantum Technologies, The University of Waikato, Hamilton 3240, New Zealand

² Plant and Food Research, Hamilton 3240, New Zealand

fertilizer (van Maarschalkerweerd and Husted 2015). Essential elements required for plant growth are classified according to the quantities required as either macro or micro nutrients (Barker and Pilbeam 2006). Generally macro nutrients [nitrogen (N), phosphorus (P), potassium (K), calcium (Ca), sulfur (S) and magnesium (Mg)] are larger than 0.1 wt% and micro nutrients [boron (B), chlorine (Cl), manganese (Mn), iron (Fe), zinc (Zn), copper (Cu), molybdenum (Mo) and nickel (Ni)] are less than 0.01 wt%. Na is not an essential nutrient but can be beneficial in stimulating growth (Gorham 2006). Precision agriculture is based on measurements which must be rapid and cost-effective so sufficient data can be acquired for spatial and temporal precision. The measurements must be selective to avoid interference and unstable calibration and they need to be sensitive if measuring low concentrations. Laser induced breakdown spectroscopy (LIBS) is a method that could potentially satisfy these requirements.

LIBS has become a very popular analytical method in the last decade, due to unique features such as applicability to any type of sample, practically no sample preparation, remote sensing capability and speed of analysis. Analysis of leaf nutrient content is a complex laboratory-based process involving wet chemistry and powerful chemicals for digesting plant fiber; it typically costs tens of dollars per sample and requires considerable time. Consequently, when evaluating nutrient requirements, leaf material is sampled at coarse spatial resolution, reducing potential benefits of variable rate application. LIBS can eliminate these constraints.

LIBS is a type of optical emission spectroscopy where a high powered pulsed laser, usually a Q-switched laser, is focused onto the surface of a material. The high power density breaks down the surface material and creates a plasma once the breakdown threshold is exceeded (Cremers and Radziemski 2013a). The breakdown threshold depends on the surface material of the sample. When the plasma is created, the remaining part of the laser pulse is absorbed causing the plasma temperature to increase (Cremers and Radziemski 2013b). As the plasma cools, electrons transition from high to low energy levels. Each element has specific energy levels where transitions can take place resulting in emission of photons of distinct wavelength. The intensities of these emissions are related to the concentrations of the elements observable in the recorded spectrum (Thakur 2007).

A major problem when creating calibration models for LIBS is the lack of repeatability (Hahn and Omenetto 2012). The variations between spectra from the same sample, and between samples, are caused by many factors including inhomogeneity, matrix effects and perturbations in experimental parameters. Sample moisture is another factor that changes the intensities between identical samples. The moisture in a sample has been found to reduce the intensity of emission lines and the limits of detection (Lazic et al. 2007; Rauschenbach et al. 2008). Reduction of moisture in a sample reduces the power density required to produce breakdown in the sample. This increases the amount of ablated sample, temperature in the plasma and the intensity of the emission. The temperature dependence of plasmas, caused by the exponential Boltzmann factor and the partition function within the emission line intensity equation, is one of the leading factors contributing to variability between spectra from the same sample. There are various techniques to reduce the adverse effects these factors have on a calibration curve including averaging multiple spectra from the same sample, using internal standards and using chemometric techniques. Argon atmospheres have also been used to increase the temperature in the plasma which increases the intensity of the spectral lines and also increases the number of emission lines observed. This creates more lines to analyze with higher signal to noise ratio which increases the predictive capability of LIBS. Temperature correction and internal standardization, to improve the prediction of the calibration curves on pelletized pasture, was investigated in a

previous paper (Jull et al. 2015). Considerations of emission line selection for normalizations specifically for pasture were discussed. Some of these considerations include emission lines having similar ionization energies, excitation energies and intensities (Barnett et al. 1968).

Few studies have been done using LIBS on pasture and, to the authors' knowledge, none on fresh pasture. LIBS, on pelletized samples, was used by Martin et al. (2010) to determine whether endophyte infection in Tall Fescue Grass (*Festuca arundinacea*) could be identified. Differentiation between healthy and infected samples was unsuccessful due to the lack of samples. Calcium, magnesium, iron, manganese, zinc, lead and cadmium were detected in the grass samples. The efficiency of multivariate and univariate calibrations on micro nutrients in pelletized plant materials was studied by Braga et al. (2010). Grass (*Axonopus obtusifolius*) was used to validate their calibration models. To reduce shot-to-shot variations and matrix effects, all emission lines were normalized by the C I 193.09 nm emission line. The expected values could be predicted by the multivariate model but not by the univariate model. The authors concluded that the chemical and physical makeup of the material used for calibration should be similar to the plant species to be studied if a reduction in matrix effects was to be observed.

Bermuda grass (*Cynodon dactylon*) and Plantain stems (*Musa paradisiaca*) were examined by Rai et al. (2009) to find which elements are responsible for their glycemic attributes. Powdered extracts were dissolved in distilled water and multiple LIBS spectra were recorded. Emission lines for both samples were normalized with the C III 229.7 nm line and compared. The Mg, K and Na concentrations were responsible for the antidiabetic effects of Bermuda grass. The distribution of silicon in Bermuda grass was studied by Chauhan et al. (2011). Phytolith analysis was used to determine the concentration of silicon in the grass samples. The spectra showed that the highest concentration of Si is found in the leaf blade, followed by the leaf sheath and stem.

Spectra from grass fragments and pollen were compared by Boyain-Goitia et al. (2003) in their work on bio-aerosols. A reduction in matrix effects was achieved by normalizing the spectra by the CN violet bands. Chromium and iron lines were observed only in the spectra from pollen. Calcium and aluminum were similar in both samples. Silicon emissions were found in spectra from grass which was likely caused by soil dust on the samples. A lack of samples was responsible for the struggle differentiating between pollen and grass fragments. Devey et al. (2015) compared LIBS results for pelletized pasture samples with inductively coupled plasma-optical emission spectroscopy (ICP-OES). Savitzky–Golay smoothing followed by vector normalization and wavelet smoothing was performed before partial least-squares regression (PLS) models were created on selected spectral regions. Sodium, potassium, calcium and phosphorus had accuracies similar to the ICP-OES results. Manganese, iron and boron had reasonable results but zinc, copper and sulphur did not.

The work presented in this paper investigates, for the first time, the viability of using LIBS in-field to measure micro and macro nutrients in fresh untreated pasture. Measurements were made on fresh and dried, pelletized pasture both in air and under an argon atmosphere. Precision, limits of detection and root-mean square error of cross-validation were used to compare prediction models.

Materials and methods

A commercial LIBS system (LIBS-6, Applied Photonics, Skipton, UK) system with a Nd:YAG laser (Big Sky Ultra, Quantel, France) operating at 1064 nm with a pulse width of 7 ns, and pulse energy of 100 mJ was focused perpendicular to the sample surface to generate the plasma. The setup had a fixed distance to the sample. The LIBS-6 has a built-in beam expander which was focused to roughly 80 mm from the beam expander. The surfaces of the samples were placed 79 mm from the beam expander which corresponded to the lens-to-sample distance that produced the highest emission line intensities. The spot size on the sample was 450 μm , measured from the crater, which produced an irradiance of 9.0 GW cm^{-2} . Each spectrum was acquired with the six (Avantes, Apeldoorn, The Netherlands) spectrometers in the LIBS-6 unit covering the range 182.26–908.07 nm. All spectrometers were set to start recording after a delay time of 1.27 μs with respect to the laser pulse and an integration time of 1 ms. A 3-axis translation stage was employed so that each sample surface was at the same height. The translation stage moved the sample so that each LIBS pulse was aimed at a new location.

Fresh pasture (a mix of ryegrass and clover leaves), from 20 different plots of typical grazing paddocks in the Waikato region of New Zealand, was harvested over a 13 month period creating a total of 280 samples. The herbage was pressed flat in a holder. An accumulation of 100 shots under an air atmosphere, and 100 shots under an argon purge were taken for each batch. Each shot was taken from a new location on the sample. The pasture samples were sent to a commercial analytical laboratory where they were dried at 62 $^{\circ}\text{C}$ overnight and ground to pass through a 1 mm screen. Nitrogen was estimated by NIR calibration based on N by Dumas combustion. All other elements were determined by nitric acid/hydrogen peroxide digestion followed by inductively coupled plasma optical emission spectrometry. Table 1 shows the variation in the dataset and the limits of detection for the quantitative analysis performed by the laboratory. A portion of the powder was returned and pellets were pressed for each batch of harvested pasture. An accumulation of 100 shots under an air atmosphere, and 100 shots under an argon purge were taken for each pellet. Each shot was taken from a new location on the sample.

Partial least squares regression (PLS) is a statistical technique that has been employed to overcome the drawbacks of variability between spectra. PLS is a technique that is used

Table 1 Concentration range (wt%) of the data set and detection limits of the commercial analytical laboratory

Element	Mean	SD	Detection limit of reference
N	2.8	0.49	0.1
P	0.36	0.054	0.02
K	2.7	0.68	0.1
S	0.33	0.042	0.02
Ca	0.68	0.18	0.02
Mg	0.19	0.03	0.02
Na	0.26	0.12	0.002
Fe	0.01	0.0082	0.0005
Mn	0.0061	0.0025	0.0003
Zn	0.0044	0.0057	0.0002
Cu	0.00075	0.00018	0.0001
B	0.00062	0.0003	0.0001

when there are many variables, compared to observations, and when there is high collinearity, in the data, between variables. This is well suited to LIBS spectra that have thousands of variables, many of which are collinear. By projecting the elemental concentrations (responses) and the spectra (predictors) to a new space, PLS finds a fundamental linear relationship between the predictors and responses. An underlying relationship can be found that is not necessarily visually apparent. This relationship is conveyed through the Latent Variables (LV). PLS has found great success building calibration curves that perform better than simple linear regression of a single emission line (Fink et al. 2002; Nunes et al. 2010). There are various methods of determining which variables are important in a PLS model (Mehmood et al. 2011). Variable Importance on Projections (VIP) scores on the predictors is an indication of the significance of the projections to find the latent variables. VIPs are calculated as (Wold et al. 1993):

$$\text{VIP}_j = \sqrt{p \sum_{m=1}^M w_{mj}^2 \text{SS}(b_m t_m) / \left(\sum_{m=1}^M \text{SS}(b_m t_m) \right)} \quad (1)$$

where p is the number of variables in a predictor, M is the number of LVs, $\text{SS}(b_m t_m)$ is the percentage of y explained in the m th latent variable and w_{mj} is the weight for the j th variable for the m th latent variable. A cut-off criterion for variable selection of VIP scores greater than one is usually used, since the average value of all VIP scores equals one. Performing VIP after PLS has produced excellent results in detecting relevant predictors and has outperformed other variable selection methods (Chong and Jun 2005).

The accuracy of a PLS model is measured by the difference between the predicted values and actual values. The Root Mean Squared Error of Cross-Validation (RMSECV) parameter is one measure of these differences. The RMSECV is calculated as:

$$\text{RMSECV} = \sqrt{\frac{\sum_{i=1}^n (\hat{y}_i - y_i)^2}{n}} \quad (2)$$

where \hat{y} contains the predictions from the cross-validation for the i th samples which was not used in building the model for that fold, y contains the actual responses and n is the number of samples.

There are various figures of merit used to assess the performance of an analysis method. These include precision and limits of detection. Precision is used as a metric for measurement repeatability. This is usually represented in the standard deviation of a group of measurements on the same sample. Precision is calculated as (ASTM E1655-05 2012):

$$s = \sqrt{\frac{\sum_{i=1}^n \sum_{j=1}^m (\hat{y}_i - \hat{y}_{ij})^2}{n(m-1)}} \quad (3)$$

where \hat{y} is the mean of the predictions for the replicates in a sample, \hat{y} are the predictions for a sample, n is the number of samples and m is the number of replicates. In this study, n and m are five and ten respectively and each replicate is the average of ten measurements.

The limit of detection (LOD) is the smallest concentration that can be detected with reasonable certainty (Boqué and Rius 1996). For PLS this value can be calculated as (Allegrini and Olivieri 2014; Ortiz et al. 2003):

$$\text{LOD} = 3.3s_{pu}^{-1} \left[\left(1 + \frac{\bar{y}_{cal}^2}{\sum_{i=1}^I y_i^2} + 1/I \right) \text{var}_{pu} \right]^{1/2} \quad (4)$$

where s_{pu} is the slope of the calibration line, var_{pu} is the variance of the regression residuals, \bar{y}_{cal} is the mean calibration concentration, I is the number of samples, and y_i is the centered concentration.

All spectra were corrected for background and dark current. Three samples were removed because of false laboratory results. The 100 spectra for each sample were averaged but not normalized. The resulting spectra were then analyzed using PLS with 10-fold cross-validation in Matlab (R2012a, MathWorks, Natick, USA). Matlab uses the SIMPLS algorithm which centers both the predictors and responses. Calibration models were generated for N, P, K, S, Ca, Mg, Na, Fe, Mn, Zn, Cu and B.

Results and discussion

A typical LIBS spectrum for fresh and pelletized pasture is shown in Fig. 1. The strongest emission lines for each element are listed in Table 2. The spectra display increased intensities for samples under argon and an intensity reduction for the oxygen triplet around 777 nm. This is expected as argon has a low ionization energy which contributes more electrons into the plasma, and the presence of argon reduces the surrounding oxygen concentration.

Fig. 1 Typical spectra for fresh pasture in air (a), fresh pasture under argon (b), pelletized pasture in air (c), and pelletized pasture under argon (d)

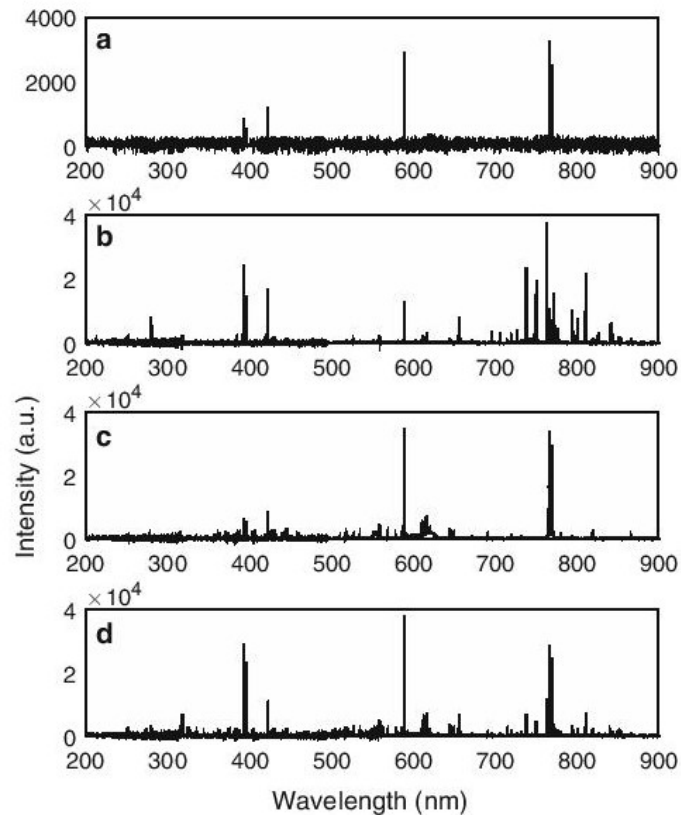


Table 2 Strong emission lines of nutrients in pasture

Species	Strong emission lines (nm)
N I	742.36, 744.23, 746.83, 862.92, 868.03, 868.34
P I	167.97, 177.50
K I	691.11, 693.88, 766.49, 769.90
S I	142.50, 147.40, 180.73
Ca I	422.67, 442.54, 443.50, 445.48
Ca II	315.89, 317.93, 393.37, 396.85
Mg I	285.21, 382.94, 383.23, 383.82, 516.73, 517.27, 518.36
Na I	589.00, 589.59, 818.33, 819.48
Fe I	358.12, 371.99, 373.71, 374.56, 374.59, 374.83
Fe II	238.20, 239.56, 240.49, 241.05, 241.33
Mn I	403.08, 403.31, 403.45
Zn I	213.86, 334.50, 481.05
Cu I	324.75, 327.40, 521.82
B I	249.68, 249.77

Multiple PLS models were built for each element by repeatedly performing 10-fold cross-validation on the spectra then increasing the number of LVs. The RMSECVs were observed and the number of optimal LVs were chosen corresponding to lowest RMSECVs. Table 3, Figs. 2 and 3 display the PLS prediction results from the 10-fold cross-validations for the elemental concentrations in the samples. Precision was calculated from the pooled values in each fold of the cross-validation. The calculated RMSECV for the dried pellets were similar to the results obtained by Devey et al. (2015).

The use of argon on fresh pasture produced models with greater coefficient of determination (R^2) for all elements except P (R^2 results for fresh samples under argon are not shown). It produced inferior precision for all elements and reduced the RMSECV in all elements except P, Ca and Cu. It also improved LOD for Ca with slight increases for S, Mg, Na, Fe, Mn and Zn. Using argon on pelletized pasture reduced the RMSECV for all elements and enhanced the R^2 for all elements except S, Ca, Mn and B (R^2 results for pellet samples in air are not shown). The LOD improved for N, P, Mg, Na, Fe, Zn and Cu. Precision for N, K, Ca, Mg, Fe, Zn and Cu were also improved. When comparing fresh and dried pasture, there was a reduction in RMSECV for all elements in dried pasture and an increase in R^2 for all elements. Fresh pasture had better precision for N, P, S, Fe, Zn and Cu, but worse LOD for all elements. The best correlations were found for K and Na in pellets sampled under argon and Mg in pellets sampled in air. The values of R^2 were 0.92, 0.93 and 0.90 respectively. K and Mg were the only elements to have R^2 over 0.7 for fresh pasture in air.

Dried pellets had better RMSECV and R^2 results because there is less between-sample variation caused by the different moisture levels between each fresh sample. During March 2014, the middle of the 13 month period, there was a drought in New Zealand. K, Mg and Fe concentrations were affected by this. Mg and Fe levels were significantly higher and K levels were significantly lower. This provided a wider range of concentrations to build models on and accounts for the two groupings seen in some of the calibration curves for some elements.

Table 3 Accuracy of PLS models created for the macro and micro nutrients in pasture

	Element	In air				Under argon			
		LV	Precision	RMSECV	LOD	LV	Precision	RMSECV	LOD
Fresh	N	6	0.31	0.4	1.7	7	0.79	0.36	2.5
Pasture	P	10	0.026	0.043	0.16	6	0.088	0.044	0.3
	K	24	0.45	0.35	1.2	12	0.63	0.33	1.6
	S	7	0.029	0.037	0.15	31	0.07	0.035	0.13
	Ca	3	0.16	0.14	0.82	10	0.25	0.14	0.56
	Mg	18	0.025	0.021	0.078	16	0.037	0.02	0.075
	Na	6	0.056	0.084	0.29	35	0.11	0.08	0.27
	Fe	21	0.0039	0.0051	0.017	35	0.0068	0.0041	0.014
	Mn	21	0.0012	0.0013	0.0044	23	0.0021	0.001	0.0036
	Zn	26	0.00084	0.0009	0.0029	14	0.001	0.0008	0.0026
	Cu	23	0.00011	0.00011	0.00039	15	0.00021	0.00011	0.00039
	B	6	0.000097	0.00025	0.00087	10	0.00032	0.00024	0.00086
Pellets	N	14	0.44	0.31	1.3	43	0.39	0.26	0.97
	P	27	0.044	0.032	0.12	48	0.05	0.032	0.11
	K	19	0.42	0.22	0.93	12	0.3	0.2	0.99
	S	44	0.041	0.029	0.11	46	0.046	0.032	0.12
	Ca	41	0.15	0.066	0.22	18	0.13	0.08	0.31
	Mg	27	0.022	0.013	0.05	48	0.021	0.013	0.047
	Na	15	0.04	0.03	0.12	18	0.042	0.029	0.11
	Fe	42	0.0044	0.0033	0.011	50	0.004	0.0029	0.0096
	Mn	38	0.0012	0.00075	0.0025	37	0.0012	0.0008	0.0027
	Zn	38	0.00089	0.00069	0.0026	39	0.00081	0.00058	0.002
	Cu	31	0.00015	0.000095	0.00034	46	0.0001	0.000089	0.00031
B	34	0.000097	0.00025	0.00042	45	0.00032	0.00024	0.00049	

Concentrations are in wt%

Nitrogen

The nitrogen emission lines are very weak in the collected spectra. One reason is that the upper level energies of the strong nitrogen emission lines are about 12.0 eV. The plasmas created in this study do not have sufficient energy to allow sufficient population of these states. Another reason is the contribution of nitrogen from the atmosphere. The atmospheric nitrogen would add to, or even overwhelm, the nitrogen concentration in the samples when measured in air. Under an argon atmosphere, the effect of atmospheric nitrogen is reduced, improving results. Figure 4 displays the intensity of the strongest nitrogen line (N I 746.83 nm) for fresh pasture in air which had a VIP score of 18. The emission line intensities were larger even though the nitrogen concentrations were lower. These larger intensities are from samples collected March 2014 when there was a drought in New Zealand. The high intensities are likely caused by a reduction of moisture in the sample. Nitrogen line intensities appeared more consistent outside the drought period. The highest VIP scores for fresh pasture in air were 1777, 1016, 642 and 491 for K I

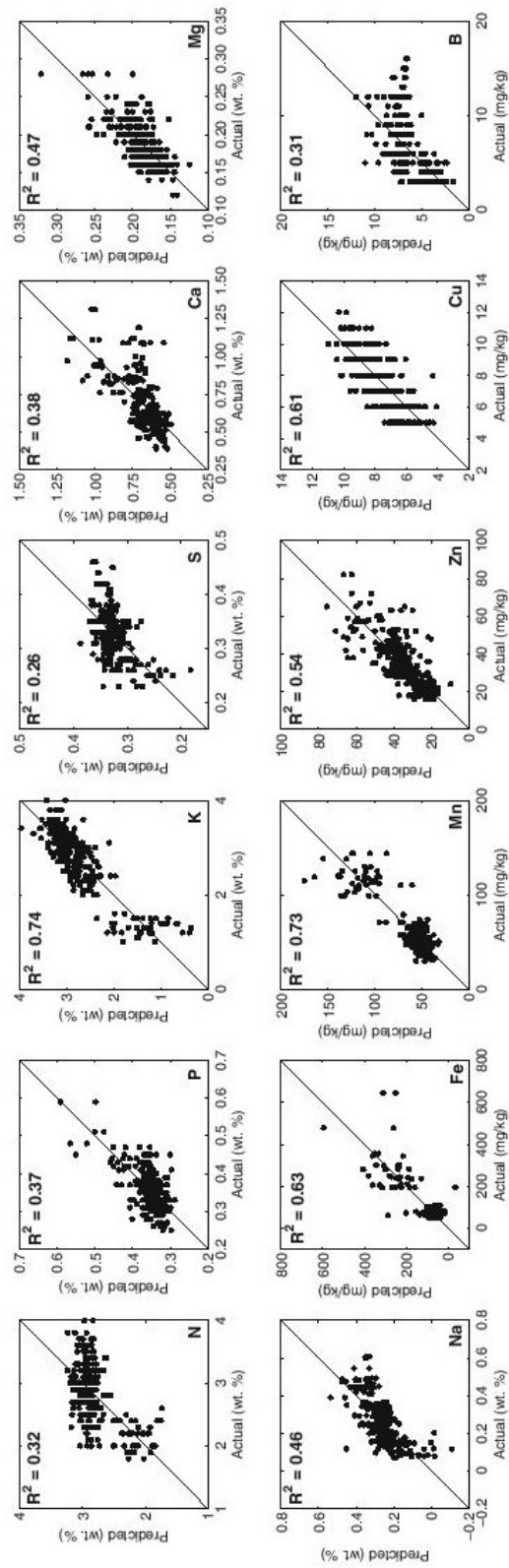


Fig. 2 Predictions created from PLS 10-fold cross-validation on fresh pasture in air

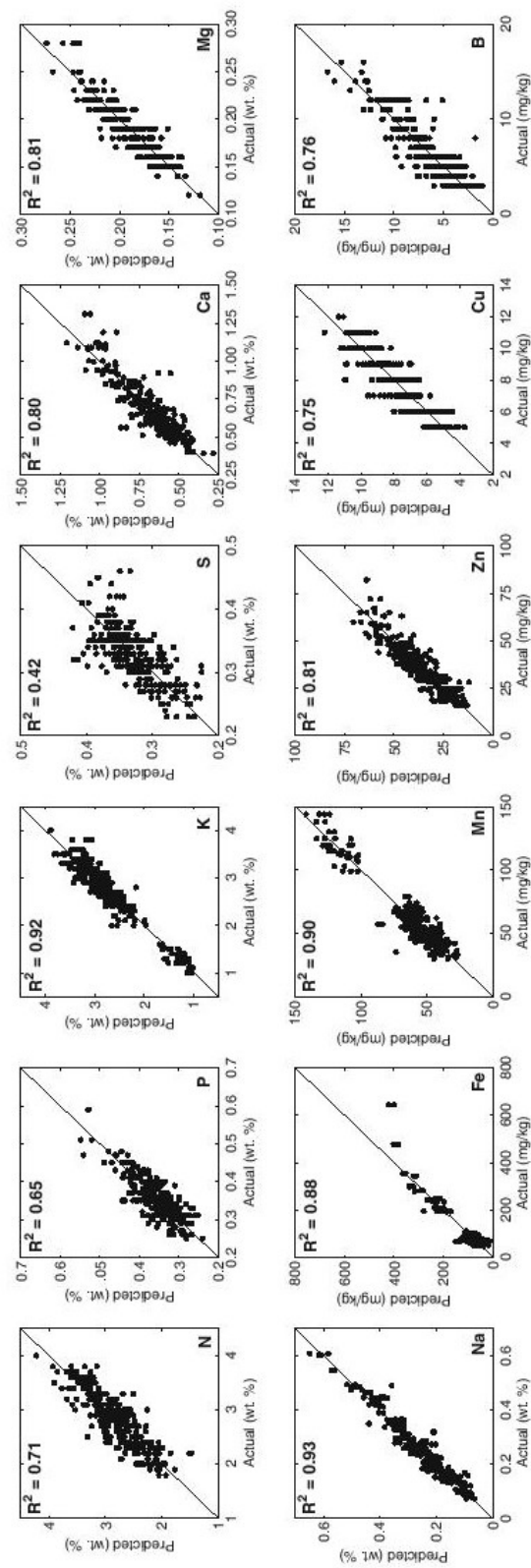


Fig. 3 Predictions created from PLS 10-fold cross-validation on pelletized pasture under argon

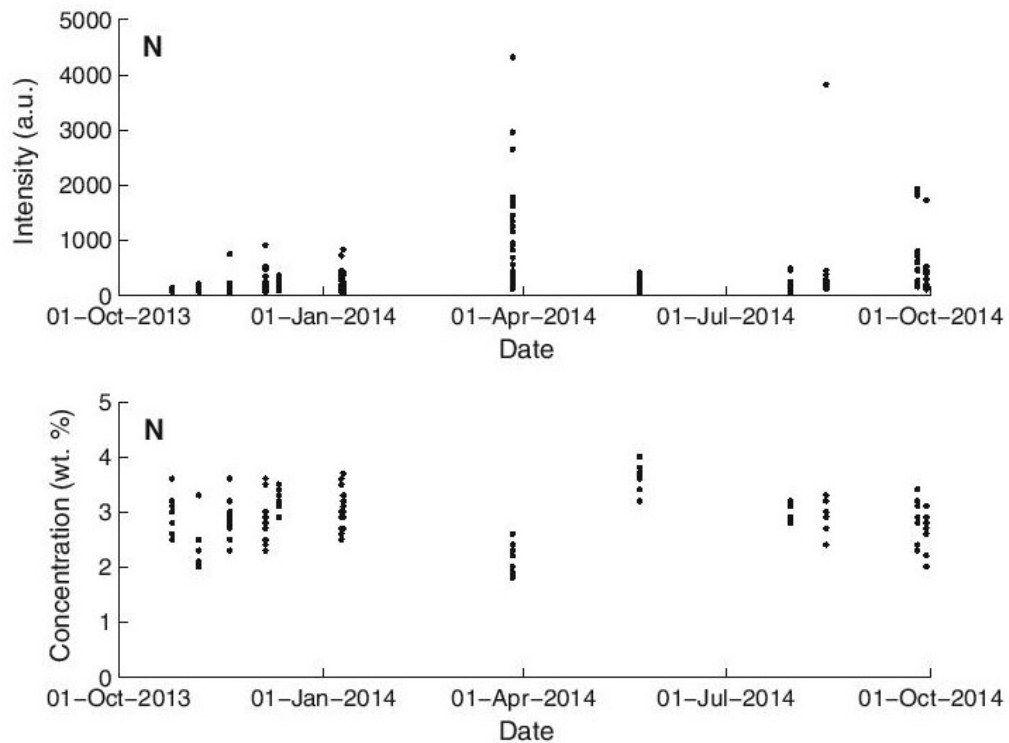


Fig. 4 Moisture effects on the N I 746.83 nm emission line

766.49 nm, K I 769.90 nm, Ca I 422.67 and Na I 589.00 nm respectively. The PLS model built for N may have taken into account the stoichiometric relation between these elements, thus the high VIP scores for K, Ca and Na.

Potassium, sodium and manganese

Besides sodium, the K I 766.49 and K I 769.90 nm lines are the strongest lines in the collected spectra. The cluster of samples with low potassium concentration evident in Fig. 3 is due to pasture harvested during a drought as discussed above. Potassium is the only macro nutrient that gave reasonable results, that is an R^2 greater than 0.9 for pellet samples. The emission lines that received the highest VIP scores for pellets under argon were Na I 589.00 nm, K I 766.49 nm, Na I 589.59 and K I 769.90 nm with scores of 765, 652, 543 and 542. The sodium PLS models performed the best out of all the nutrients studied with a R^2 of 0.93 and a RMSEP of 0.029 wt% for pellets under argon. The large intensities from the sodium D-lines (Na I 589.00 and Na I 589.59 nm) are responsible for the good correlations. The Na I 589.00 nm had the highest VIP score of 842. The strongest manganese line, Mn I 403.08 nm, was weak for fresh pasture, but there are very few spectra that show this emission line. However, the manganese model gives satisfactory results. This is most likely due to the model gaining information from emission lines of other elements that correlate with manganese. This is shown by the Na I 589.00 nm, K I 766.49 nm, K I 769.90 and Na I 589.59 nm receiving the highest VIP scores of 757, 666, 522 and 509 respectively.

Calcium

The Ca II 393.37 and Ca II 396.85 nm lines are the third largest emissions after sodium and potassium. Despite the high intensities from these lines the PLS models do not have high correlations with the actual calcium concentrations. One reason is that the low ionization energy (6.11 eV) for neutral calcium means that there will be emissions from both neutral and ionized calcium. Table 4 lists all the ionization limits of the elements studied in this work. Emission lines from ionized species with ionization energies around 6 eV are commonly observed from LIBS plasmas (Cremers and Radziemski 2013c). The low ionization potential causes large fluctuations in the ratio of neutral to singularly ionized calcium seen between plasmas created on the same sample.

Self-absorption can cause low correlations, but there was no evidence of this in any of the spectra. The resolution of the spectrometer at Ca I 422.727 nm is 0.052 nm and might not be sufficient to show self-absorption. However, this effect usually happens at higher calcium concentrations than the ones discussed in this study (Cremers and Radziemski 2013d).

Potassium and sodium both have ionization potentials lower than calcium. The reason potassium and sodium do not suffer from the same problem as calcium is that the next electron level in the ionized species is so high that it rarely gets populated. This means that the electrons predominantly remain in the ground state, of the ionized species, and very few emissions from ionized potassium or sodium are observed. The emission lines that had a strong influence on the PLS models for pellets under argon were Na I 589.00 nm, K I 766.49 nm, K I 769.90 and Na I 589.59 nm receiving the highest VIP scores of 707, 639, 500 and 490. The calcium lines with the strongest VIP scores were Ca II 393.37 nm, Ca II 396.85 nm, and Ca I 422.67 nm with scores of 308, 213 and 142.

Phosphorus and sulphur

Phosphorus and sulphur do not show any correlations as their strong emission lines are in the ultraviolet region below the measurement range of the spectrometers. The strongest persistent lines are P I 167.97, P I 177.50, S I 142.50, S I 147.40 and S I 180.73 nm. The only phosphorus line that was occasionally observed was a weak P I 253.56 nm line in the

Table 4 Ionization levels of each element's neutral species

Element	Ionization limit (eV)	Next shell (eV)
N	14.53	1.90
P	10.49	1.10
K	4.34	20.15
S	10.36	1.84
Ca	6.11	1.69
Mg	7.65	4.42
Na	5.14	32.85
Fe	7.90	0.23
Mn	7.43	1.17
Zn	9.39	6.01
Cu	7.73	2.72
B	8.30	4.63

The first electron energy level of the singularly ionized element is also listed (Kramida et al. 2017). Each entry is rounded to two decimal places

pellet samples under argon, which had interference with the stronger Fe I 253.56 nm emission line. The VIP score received for this line was 0.067 which means it had very little influence on the model built by PLS. The strongest sulphur line in the region captured by the spectrometers was S I 182.62 nm, which was not visible in any spectra. It had a VIP score of 0.002. The lines that had the strongest VIP scores for both the phosphorus and sulphur were Na I 589.00, K I 766.49, K I 769.90 and Na I 589.59 nm all of which were in the range of 513–796.

Magnesium, copper and iron

The poor calibrations curves for magnesium, copper and iron are due to their weak emission lines. The PLS models are highly influenced by strong lines which is reflected in the VIP scores. The first magnesium line that appears in the VIP scores, for pellets under argon, is 76th with a VIP score of 8.5. The highest VIP score was 755 for a sodium line. The VIPs suggest that sodium, potassium, calcium, argon and hydrogen are more important for the model than the magnesium lines. Copper produces similar results. The Cu I 324.75 nm and Cu I 327.40 nm lines were the strongest copper lines found. The Cu I 324.75 nm line was ranked the 108th variable of importance with a VIP score of 4.9 for pellet samples under argon. Sodium, potassium, calcium and argon displayed the strongest importance in the model, with Na I 589.59 nm having the highest VIP score of 698. The weak VIP scores for copper are evidence for the model's lack of dependence on the copper lines. Calculating the VIPs for the iron model produces no iron lines with a score greater than one. This means the model is not significantly influenced by the iron emissions and is based on secondary correlations with emissions from other elements. The strongest iron line found in the spectra was the Fe II 238.20 nm line. Figure 5 displays a region in the spectra with a few of the strongest iron lines. Each of the 280 spectra for pellets under argon are overlaid on top of each other. These lines are over 100 times smaller than the largest emission lines.

Zinc and boron

Emissions from zinc and boron are not observed consistently on the samples investigated. The strongest zinc line, Zn I 213.86 nm, could only be observed in pellet samples under argon. The strongest boron emission was from B I 249.77 nm which was just above the noise floor and, in some instances, was not observed at all. This produces poor correlations between the models and the actual zinc and boron concentrations. The high R^2 values for both zinc and boron, in pellets sampled under argon, are produced because the lines that influenced the PLS models were Na I 589.00 nm, K I 766.49 nm, K I 769.90 nm and Na I 589.59 nm. The VIP scores for these lines were between 414 and 646. These zinc and boron lines received VIP scores of 0.03 and 0.0009 respectively.

To conclude, the use of an argon purge had mixed results. When used on fresh pasture, there was increased R^2 for all elements except P, better RMSECV for all nutrients except P, Ca and Cu, poorer precision and improved LOD for S, Ca, Mg, Na, Fe, Mn and Zn. An argon purge used on pelletized pasture increased the R^2 for all elements except S, Ca, Mn and B. It reduced the RMSECV and enhanced the precision for N, K, Ca, Mg, Fe, Zn and Cu. It also improved LOD for N, P, Mg, Na, Fe, Zn and Cu. Dried pellets had better R^2 and RMSECV results because there was less between-sample variation caused by the different moisture levels between each fresh sample. The precision for N, P, S, Fe and B were worse in dried pasture. The inability to create high correlating models is due to the shot-to-shot

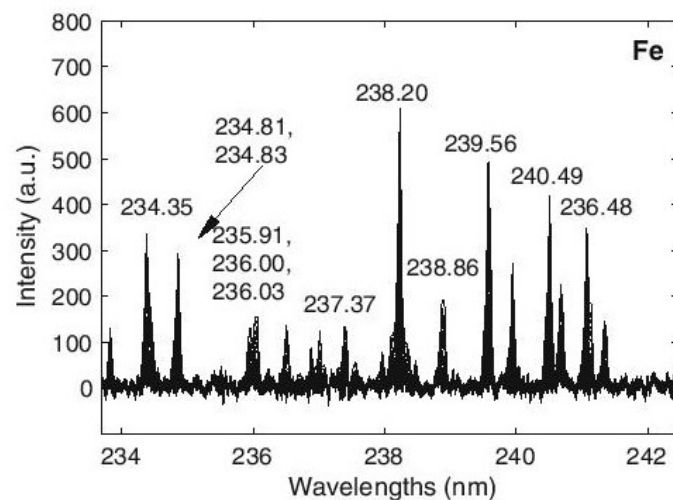


Fig. 5 The strongest iron lines found in the spectral range studied. All spectra are displayed

variation inherent in LIBS. This variation is caused by many factors including sample inhomogeneity, matrix effects, perturbations in experimental parameters, amount of ablated material and the temperature dependence of plasmas (Hahn and Omenetto 2012). The limitation on measuring fresh pasture is the between-sample variation caused by the range of moisture levels existing in pasture which affect emission line intensities.

In field feasibility

Using LIBS to quantitatively measure fresh pasture, under laboratory conditions, had limited success. The nutrient models for fresh pasture were inferior to models created from spectra generated on dried pasture. K, Fe, Mn, Zn and Cu had R^2 values higher than 0.5 with RMSECVs of 0.35, 0.0051, 0.0013, 0.0009 and 0.00011 wt%, respectively. These values are not accurate enough for quantitative measurements but are sufficient to estimate semi-quantitative levels of nutrients. Our laboratory results indicate what might be achievable with an equivalent in-field system although lesser performance should be expected due to greater variability. However, in-field LIBS measurements could be used to identify whether nutrient levels are within a certain range or not. Decisions can then be made in real time as to the type of fertilizer needed in specific areas of a field. The fertilizer application would be sub-optimal but would be an improvement compared to covering an entire field with excess or too little fertilizer.

Implementing an in-field LIBS system to measure herbage would require an autofocus system to mitigate the variability caused by lens-to-sample distance. A successful autofocus system using the setup in this study was reported by Jull et al. (2017). A similar LIBS unit could then be mounted on agricultural machinery or an agricultural robot to perform measurements and give real-time feedback for tailored fertilizer application. Additional mechanical assemblies would be required to reduce vibration and shock caused from navigating uneven terrain, and issues related to laser safety need to be addressed.

Conclusions

Results indicate that flushing pasture samples with argon while obtaining LIBS spectra has mixed effects. R^2 was increased for every element in fresh pasture except P, RMSECV was reduced for pelletized samples, and precision was reduced for every element in fresh pasture. When comparing fresh and dried pasture, there were reductions in RMSECV for all elements in dried pasture but increases in R^2 for all elements. Results for precision and LOD were mixed. The reason that the dried pellets had better RMSECV results were that there is less between-sample variation caused by the different moisture levels between each fresh sample.

Fresh pasture generates weak spectral emissions at the laser energy used in this study. N, P, Mg, Fe and Cu models all suffer from this problem. The N model also has an interfering contribution from the atmosphere, and the P model has interference from Fe spectra. Zn and B have extremely weak emission lines. Zn lines only appeared under argon, and B lines occasionally did not appear at all. Another confounding issue for Ca and Mg is ionization, where the amount of the element in the plasma is split between neutral and ionized states and the amount of ionization taking place is not consistent between shots. A final issue was that the persistent lines for S only appeared in the ultraviolet range, out of the range of the spectrometers. One way to overcome the problem is to increase the temperature in the plasma. This can be achieved through increasing the power of the laser pulse. Increasing the temperature in the plasma would increase the emission line strength, increase the number of emission lines present in the spectrum and produce full ionization of Ca and Mg, all of which will lead to improvements in actual concentration prediction by calibration models.

Using dried pellets under an argon atmosphere provides the most accurate and precise determination of the elements in pasture. This work showed how accurate LIBS is when used on fresh herbage and what performance could be expected in-field. Different laser parameters, such as wavelength, pulse energy and pulse duration, may increase accuracy.

This is the first time LIBS has been used on fresh pasture samples. Successful calibration curves on pasture pellets, all having an R^2 greater than 0.90, were made for K, Na and Mn. The laboratory results suggest that semi quantitative analyses can be made in-field on fresh pasture to create estimates of nutrient levels. The estimates could then be used to influence fertilizer application.

Acknowledgements We would like to acknowledge and offer continuing respect and admiration to deceased colleague Dr. Sadhana Talele, who was not able to see this work completed. Financial assistance from the New Zealand Ministry of Business, Innovation and Employment under contract C11X1209 is gratefully acknowledged.

References

- Allegrini, F., & Olivieri, A. C. (2014). IUPAC-consistent approach to the limit of detection in partial least-squares calibration. *Analytical Chemistry*, 86(15), 7858–7866. <https://doi.org/10.1021/ac501786u>.
- ASTM E1655-05. (2012). *Standard practices for infrared multivariate quantitative analysis*. West Conshohocken, PA, USA: ASTM International.
- Barker, A. V., & Pilbeam, D. J. (2006). *Handbook of plant nutrition* (1st ed.). Boca Raton, FL, USA: CRC Press/Taylor & Francis.
- Barnett, W. B., Fassel, V. A., & Kniseley, R. N. (1968). Theoretical principles of internal standardization in analytical emission spectroscopy. *Spectrochimica Acta, Part B: Atomic Spectroscopy*, 23(10), 643–664.

- Boqué, R., & Rius, F. X. (1996). Multivariate detection limits estimators. *Chemometrics and Intelligent Laboratory Systems*, 32(1), 11–23. [https://doi.org/10.1016/0169-7439\(95\)00049-6](https://doi.org/10.1016/0169-7439(95)00049-6).
- Boyain-Goitia, A. R., Beddows, D. C. S., Griffiths, B. C., & Telle, H. H. (2003). Single-pollen analysis by laser-induced breakdown spectroscopy and Raman microscopy. *Applied Optics*, 42(30), 6119–6132.
- Braga, J. W. B., Trevizan, L. C., Nunes, L. C., Rufini, I. A., Santos, D., Jr., & Krug, F. J. (2010). Comparison of univariate and multivariate calibration for the determination of micronutrients in pellets of plant materials by laser induced breakdown spectrometry. *Spectrochimica Acta—Part B: Atomic Spectroscopy*, 65(1), 66–74. <https://doi.org/10.1016/j.sab.2009.11.007>.
- Chauhan, D. K., Tripathi, D. K., Rai, N. K., & Rai, A. K. (2011). Detection of biogenic silica in leaf blade, leaf sheath, and stem of bermuda grass (*Cynodon dactylon*) using LIBS and phytolith analysis. *Food Biophysics*, 6(3), 416–423. <https://doi.org/10.1007/s11483-011-9219-y>.
- Chong, I. G., & Jun, C. H. (2005). Performance of some variable selection methods when multicollinearity is present. *Chemometrics and Intelligent Laboratory Systems*, 78(1), 103–112. <https://doi.org/10.1016/j.chemolab.2004.12.011>.
- Cremers, D., & Radziemski, L. (2013a). Introduction. In *Handbook of laser-induced breakdown spectroscopy* (2nd ed., p. 3). West Sussex, UK: Wiley.
- Cremers, D., & Radziemski, L. (2013b). Basics of the LIBS plasma. In *Handbook of laser-induced breakdown spectroscopy* (2nd ed., pp. 48–58). West Sussex, UK: Wiley.
- Cremers, D., & Radziemski, L. (2013c). Qualitative LIBS analysis. *Handbook of laser-induced breakdown spectroscopy* (pp. 151–183). West Sussex, UK: Wiley.
- Cremers, D., & Radziemski, L. (2013d). LIBS analytical figures of merit and calibration. In *Handbook of Laser-Induced Breakdown Spectroscopy* (2nd ed., pp. 131–140). West Sussex, UK: Wiley.
- Devey, K., Mucalo, M., Rajendram, G., & Lane, J. (2015). Pasture vegetation elemental analysis by laser-induced breakdown spectroscopy. *Communications in Soil Science and Plant Analysis*, 46, 72–80. <https://doi.org/10.1080/00103624.2014.988578>.
- Fink, H., Panne, U., & Niessner, R. (2002). Process analysis of recycled thermoplasts from consumer electronics by laser-induced plasma spectroscopy. *Analytical Chemistry*, 74(17), 4334–4342. <https://doi.org/10.1021/ac025650v>.
- Gorham, J. (2006). Sodium. In A. V. Barker & D. J. Pilbeam (Eds.), *Handbook of plant nutrition* (1st ed., pp. 573–575). Boca Raton, FL, USA: CRC Press/Taylor & Francis.
- Hahn, D. W., & Omenetto, N. (2012). Laser-induced breakdown spectroscopy (LIBS), part II: Review of instrumental and methodological approaches to material analysis and applications to different fields. *Applied Spectroscopy*, 66(4), 347–419. <https://doi.org/10.1366/11-06574>.
- Jull, H., Ewart, P., Künemeyer, R., & Schaare, P. (2017). Selective surface sintering using a laser-induced breakdown spectroscopy system. *Journal of Spectroscopy*, 2017, 1–11. <https://doi.org/10.1155/2017/1478541>.
- Jull, H., Künemeyer, R., Talele, S., Schaare, P., & Seelye, M. (2015). Laser-induced breakdown spectroscopy analysis of sodium in pelletised pasture samples. In D. Bailey, S. Demidenko, & G. S. Gupta (Eds.), *6th International conference on automation, robotics and applications, ICARA 2015* (pp. 262–268). Danvers, MA, USA: Institute of Electrical and Electronics Engineers Inc. <https://doi.org/10.1109/icara.2015.7081157>.
- Kramida, A., Yu. Ralchenko, Reader, J., & NIST ASD Team. (2017). NIST Atomic Spectra Database (ver. 5.2). Retrieved January 3, 2018, from <http://physics.nist.gov/asd>.
- Lazic, V., Rauschenbach, I., Jovicevic, S., Jessberger, E. K., Fantoni, R., & Di Fino, M. (2007). Laser induced breakdown spectroscopy of soils, rocks and ice at subzero temperatures in simulated Martian conditions. *Spectrochimica Acta—Part B: Atomic Spectroscopy*, 62(12), 1546–1556. <https://doi.org/10.1016/j.sab.2007.10.006>.
- Martin, M. Z., Stewart, A. J., Gwinn, K. D., & Waller, J. C. (2010). Laser-induced breakdown spectroscopy used to detect endophyte-mediated accumulation of metals by tall fescue. *Applied Optics*, 49(13), C161–C167.
- Mehmood, T., Martens, H., Sæbø, S., Warringer, J., & Snipen, L. (2011). A partial least squares based algorithm for parsimonious variable selection. *Algorithms for Molecular Biology*, 6(1), 1–12. <https://doi.org/10.1186/1748-7188-6-27>.
- Nunes, L. C., Batista Braga, J. W., Trevizan, L. C., Florêncio De Souza, P., Arantes De Carvalho, G. G., Júnior, D. S., et al. (2010). Optimization and validation of a LIBS method for the determination of macro and micronutrients in sugar cane leaves. *Journal of Analytical Atomic Spectrometry*, 25(9), 1453–1460.
- Ortiz, M. C., Sarabia, L. A., Herrero, A., Sánchez, M. S., Sanz, M. B., Rueda, M. E., et al. (2003). Capability of detection of an analytical method evaluating false positive and false negative (ISO 11843) with

- partial least squares. *Chemometrics and Intelligent Laboratory Systems*, 69(1), 21–33. [https://doi.org/10.1016/S0169-7439\(03\)00110-2](https://doi.org/10.1016/S0169-7439(03)00110-2).
- Rai, P. K., Jaiswal, D., Rai, N. K., Pandhija, S., Rai, A. K., & Watal, G. (2009). Role of glycemic elements of *Cynodon dactylon* and *Musa paradisiaca* in diabetes management. *Lasers in Medical Science*, 24(5), 761–768.
- Rauschenbach, I., Lazic, V., Pavlov, S. G., Hübers, H. W., & Jessberger, E. K. (2008). Laser induced breakdown spectroscopy on soils and rocks: Influence of the sample temperature, moisture and roughness. *Spectrochimica Acta—Part B: Atomic Spectroscopy*, 63(10), 1205–1215. <https://doi.org/10.1016/j.sab.2008.08.006>.
- Thakur, S. N. (2007). Atomic emission spectroscopy. In J. P. Singh & S. N. Thakur (Eds.), *Laser-induced breakdown spectroscopy* (pp. 29–30). Oxford, UK: Elsevier.
- van Maarschalkerweerd, M., & Husted, S. (2015). Recent developments in fast spectroscopy for plant mineral analysis. *Frontiers in Plant Science*, 6, 169. <https://doi.org/10.3389/fpls.2015.00169>.
- Wold, S., Johansson, E., & Cocchi, M. (1993). PLS—partial least-squares projections to latent structures. In H. Kubinyi (Ed.), *3D QSAR in drug design: Theory, methods and applications* (pp. 523–550). Leiden, The Netherlands: ESCOM.

Chapter 4

Laser-Induced Breakdown Spectroscopy Analysis of Sodium in Pelletised Pasture Samples

a peer-reviewed conference publication
published in

**2015 6th International Conference on Automation, Robotics and
Applications (ICARA)**

by

H. Jull, R. Künnemeyer, S. Talele, P. Schaare, and M. Seelye

Laser-Induced Breakdown Spectroscopy Analysis of Sodium in Pelletised Pasture Samples

Harrisson Jull, Rainer Künnemeyer and Sadhana Talele
School of Engineering
University of Waikato
Hamilton, New Zealand
hj75@students.waikato.ac.nz

Peter Schaare and Mark Seelye
Bioengineering Department
The New Zealand Institute for Plant and Food Research Ltd
Hamilton, New Zealand
peter.schaare@plantandfood.co.nz
mark.seelye@plantandfood.co.nz

Abstract—Sodium concentration in plants inhibit shoot and root growth. Traditional wet-chemical methods of determining elemental concentrations require pre-treatment and leave unwanted by-products. Laser-induced breakdown spectroscopy is a technique that needs very little pre-treatment and produces no secondary waste. Laser-induced breakdown spectroscopy is used in this work to determine sodium concentrations in dried pasture samples. Temperature correction on the gathered spectra was attempted using Boltzmann and Saha-Boltzmann plots. These methods failed to deliver satisfactory results. Different combinations of internal reference standards were used on the Na I 818.326 nm line which resulted in an improved correlation with sodium concentration. Partial least squares regression was used on the gathered spectra to find emission lines that vary with the sodium concentration. Calcium, sodium, potassium and an argon line demonstrated high predictor weights. The Na I 818.326 nm, Na I 819.482 nm, K I 693.876 nm and K I 691.108 nm lines exhibited large dependence on sodium concentration. Building a calibration curve of sodium to potassium emission line intensity versus sodium to potassium concentration in the samples produced a correlation of $R^2 = 0.918$ and an error in prediction of 0.0254.

Keywords—Agriculture; Electron emission; Environmental management; Environmental monitoring; Fertilizers; Lasers; Vegetation mapping.

I. INTRODUCTION

Precision agriculture (PA) generates environmental and financial benefits through application of specific fertilisers, in particular areas and at precise times. This ensures land users obtain maximum yield at minimal expenses while reducing environmental side-effects such as excess run-off caused by over fertilisation. Sodium fertiliser application can stimulate growth in potassium deficient crops. The application of sodium fertiliser is also important in forage crops where grazing herds need certain quantities of sodium for growth and production (see [1] and the references therein). Salinity stress in plants can inhibit root and shoot growth. In pasture salinity reduces cell numbers in leaves [2]. Sodium ions are similar to potassium ions and the potassium ion transporters do not discriminate between them. When excess sodium ions are present in the soil they compete with the potassium ions for uptake in plant roots [3]. This leads to ion-specific stresses resulting from altered

K^+/Na^+ ratios [4]. Salt build up in leaves is evidence of salinity and can be toxic to the plant [2]. This work uses Laser-induced breakdown spectroscopy (LIBS) combined with a range of post processing techniques to determine the sodium concentration in dried pasture pellets. This work can be used as a starting point for diagnosing salinity stress in dried pasture samples. It also serves as a precursor for an infield LIBS sensor that will be mounted on agricultural machinery (e.g. a quad bike) which will be used to sample fresh pasture and generate results in real-time.

A. Literature Review

Few studies have been done using LIBS on pasture. Martin et al. [5] assessed the use of LIBS on pelletised samples to determine whether Tall Fescue Grass (*Festuca arundinacea*) was infected with endophyte. LIBS was found to be more sensitive to cadmium detection than ICP-MS. Due to the lack of samples there was no method found to differentiate between healthy and infected samples. The study detected iron, manganese, magnesium, lead, calcium, zinc, and cadmium in grass samples. Braga et al. [6] studied micronutrients in pelletised plant materials to determine the efficiency of multivariate and univariate calibrations. Grass (*Axonopus obtusifolius*) was used to validate their calibrations. To reduce matrix effects and shot-to-shot variations the C I 193.090 nm emission line was used to normalise all emission lines. The multivariate model for grass followed the expected values but the univariate model did not. They concluded that if a reduction in matrix effects was to be achieved, specific calibrations should be done using material that closely resembles the physical and chemical makeup of the plant species to be studied. Rai et al. [7] examined the usefulness of Bermuda grass (*Cynodon dactylon*) extracts dissolved in distilled water as a treatment for diabetics. The only reference to elemental concentration in their samples was that the concentration was proportional to the emission lines studied. Chauhan et al. [8] studied the distribution of silicon in Bermuda grass (*Cynodon dactylon*). The intensity of the Si I 288.15 nm line was normalised with the concentration of silicon in the samples through phytolith analysis. This technique does not give the actual concentration of silicon in the sample but a relative concentration. No quantitative analysis was performed. Boyain-Goitia et al. [9] used LIBS for the analysis of

bioaerosols, specifically pollen. Pollen spectra and spectra from grass fragments were compared. To reduce matrix effects all spectra were normalised with the CN band heads. They concluded that the grass fragments did not emit the chromium and iron lines observed in pollen, the calcium and aluminium concentrations were similar in both samples, silicon was found in the spectrum of the grass fragments which is likely caused by soil dust on the surface of the sample, the difficulty distinguishing between grass and pollen was due to the lack of spectra and the phenylalanine concentration in grass seems to be significantly lower than in pollen. From these articles a calibration specific for pasture was not established.

B. Theory

LIBS, also known as laser-induced plasma spectroscopy (LIPS), is a type of optical emission spectroscopy. LIBS focuses a high-power, short-pulsed laser onto a sample ablating a small amount of sample material through inverse Bremsstrahlung creating a plasma [10]. The incident LIBS beam can be focused on the sample surface of a solid or liquid or it can be focused inside a liquid or gas. Pulse energies required for breakdown vary between samples but are typically greater than 10^8 W cm^{-2} [11]. During the first several hundred nanoseconds after plasma formation, excited electrons decay from higher energy levels triggering free-free and free-bound transitions. These transitions cause continuum and ion spectral emissions [12, 13]. As the plasma cools the excited electrons decay even more reducing the continuum emission allowing atomic and molecular emissions to dominate. This occurs approximately one microsecond after plasma formation [13]. The spectra generated at this time provide qualitative and quantitative information on the chemical makeup of the sample.

Common chemometric techniques such as Principal Component Analyses (PCA) and Partial Least Squares Regression (PLS) are employed for sample identification and discrimination and for generating calibrations. A calibration made for a specific sample cannot be used on another sample since each matrix responds differently to the same set of parameters [14]. For quantitative analysis calibration curves are usually generated displaying the instrument response as a function of concentration from a particular element [15]. Variations in plasma properties can lead to a decrease in accuracy of the calibration curve, electron temperature being one of the main causes [16]. Assuming local thermodynamic equilibrium (LTE) the dependency of emission line intensity on temperature can be seen in the known intensity equation

$$I = \frac{FC_S A_{ki} g_k e^{\left(\frac{-E_k}{kT}\right)}}{\lambda U_S(T)} \quad (1)$$

where F is a value relating to the plasma parameters and collection system, C_S is the concentration of the species of interest, A_{ki} is the Eisenstein emission coefficient, g_k is the degeneracy of upper level, E_k is the energy the of upper level, k is Boltzmann's constant, T is the electron temperature in the plasma, λ is the wavelength of the emission and $U_S(T)$ is the partition function of the species of interest [17]. The atomic coefficients in (1) can be found in [18]. If the electron

temperature is known for a spectrum the temperature dependant components of (1) can be removed.

1) Boltzmann Plots

Boltzmann plots can be used to find the electron temperature of a plasma from a given spectrum. Taking the natural logarithm of (1) and rearranging produces

$$\ln\left(\frac{I\lambda}{A_{ki}g_k}\right) = \frac{-1}{kT}E_k + \ln\left(\frac{FC_S}{U_S(T)}\right) \quad (2)$$

which is of the form

$$y = mx + c. \quad (3)$$

A linear relationship is produced between the integrated intensity of an emission line and the upper level energy of the emitted photon [17]. The x and y components are then plotted ignoring the x -intercept term giving a linear plot which has a gradient inversely proportional to the temperature [17]. The plotted emission lines must all be from the same species, must not transition to the ground state and have significant signal-to-noise ratio. The full criteria set by [19]. This technique is utilised in Calibration-Free LIBS (CF-LIBS) [17]. CF-LIBS assumes the plasma to be in LTE and combines the Saha equation and Boltzmann plot to determine species concentration in a sample. CF-LIBS can also help in dealing with matrix effects.

2) Saha-Boltzmann Plots

To determine the electron temperature with better precision Saha-Boltzmann plots are used. These plots use the Saha equation to include ionic lines in the Boltzmann plot thus increasing the range of upper level energies. This inclusion improves the accuracy of the slope of the fitted line. The x and y components of (2) are altered to

$$E_k^* = E_k + E_{IP} - \Delta E \quad (4)$$

$$\ln\left(\frac{I\lambda}{A_{ki}g_k}\right)^* = \ln\left(\frac{I\lambda}{A_{ki}g_k}\right) - \ln\left(\frac{2(2\pi m_e kT)^{3/2}}{h^3 n_e}\right) \quad (5)$$

when used for ionic lines. Where m_e is the mass of an electron, h is Plank's constant, n_e is the electron density, E_{IP} is the ionisation potential and ΔE is a correction due to plasma interactions with the ion [20]. The electron density is needed before (5) can be used. The Stark width of the hydrogen-beta line (H_β 486.13 nm) or the hydrogen-gamma (H_γ 434.05 nm) line from the Balmer series are typically used to calculate the electron density [21]. When neither of these is present the hydrogen-alpha line (H_α 656.28 nm) can be used to find the electron density from [22]

$$n_e = 8.02 \times 10^{12} (\Delta\lambda_{1/2}/\alpha_{1/2})^{1.5} \quad (6)$$

where $\Delta\lambda_{1/2}$ is the full width at half maximum (FWHM) of H_α and $\alpha_{1/2}$ is coefficient which is a function of pressure and temperature [23]. The slight dependence on temperature in (5) requires an initial estimate of the electron temperature before a rapidly converging iterative process can be used to determine the correct temperature [20].

3) Internal Reference Standard

Another way to correct for experimental variations is to construct calibration curves using an internal reference standard [21]. The emission lines of interest are normalised to an element that comprises the bulk of the sample, e.g. carbon, essentially making a ratio. This ratio should be more resilient to random fluctuations in plasma emission than a single line since the same variations would affect the reference standard which has a concentration that is consistent between samples.

C. Why LIBS?

LIBS is an attractive method because it has the potential to make rapid multi-elemental stand-off measurements in real-time. There is less sample preparation involved compared to conventional wet-chemical laboratory techniques and no secondary waste. For example precipitation gravimetry, which is based on mass measurement of an analyte, requires the sample to be dissolved and treated so that the reagent only reacts with the species of interest. Once the precipitate is formed from adding the reagent to the sample it is then filtered and washed free of impurities. The precipitate is then heated in a crucible to remove the solvent and any unwanted volatile species. The remnant is then weighed. Using the weight of the crucible with the formed compound, the weight of the empty crucible and the molar mass of the compound the concentration of analyte in the sample can be determined. This process is then repeated for different analytes with their corresponding reagents [24].

For the reasons above LIBS was chosen to investigate sodium concentrations in dried pasture samples. LIBS was also chosen so that future work could be done in infield on fresh pasture working to replicate the results found in this work. This approach would require little (only a few cleaning shoots on the pasture if needed) sample preparation. Once suitable results are found the LIBS system could then be installed on an agricultural robot, autonomously applying fertilisers which mitigate salinity stress (such as calcium [2]) in affected areas.

This paper discusses various methods that correct variations between spectra and the corresponding correlations achieved between the correct emission lines and laboratory-determined elemental concentrations.

II. EXPERIMENTAL

A LIBS-6 system (Applied Photonics Ltd) comprising a Quantel Big Sky laser and six Avantes spectrometers was used in this work. The emitted laser beam is encircled by six lenses and fibres coupled to the spectrometers. The lenses were focused to where plasma initiation occurs, i.e. the ablation site. A Quantel Nd:YAG laser operating at 1064 nm, 100 mJ, 7 ns was used as the ablation source. The plasma emission captured by the spectrometers spanned wavelengths that cover the range 182.26-908.07 nm. The delay and integration times were set to 1.27 μ s and 1.1 ms respectively. These values correspond to the minimum settings available on the spectrometers.

Sample moisture significantly reduces the emission line intensities and the limits of detection [25]. For this reason pasture samples were sent to a commercial analytical laboratory where they were dried and ground to determine

elemental composition. A portion of the powder was returned and pressed into pellets. An accumulation of 100 shots was taken on each pellet under an Argon atmosphere, each shot on a new location on the sample. The resulting spectra were corrected for dark current and background. A Newport quartz-tungsten-halogen reference lamp was used to correct the spectral response of the spectrometers. The reference lamp did not emit at wavelengths lower than 417.14 nm. Only those lines which were corrected were used in this study. A Lorentzian profile was fitted to the lines of interest to find peak and integrated intensities.

Calibration curves were generated for the temperature corrected and uncorrected sodium emission lines using the laboratory-determined elemental concentrations. Calibration curves were also created taking the ratio of the sodium emission lines with an internal reference.

III. RESULTS AND DISCUSSION

Calibration curves were made with the uncorrected peak and integrated emission line intensities of the four identified sodium lines (588.995, 589.592, 818.326 and 819.482 nm). This paper only presents the results for the 818.326 nm line since it showed the best correlation out of the sodium lines analysed. Fig. 1 shows the least squares linear regression between the peak and integrated intensities of the 818.326 nm line and the laboratory-determined concentrations. The correlations were $R^2 = 0.347$ and $R^2 = 0.308$ for the peak and integrated intensities. These poor correlations were attributed

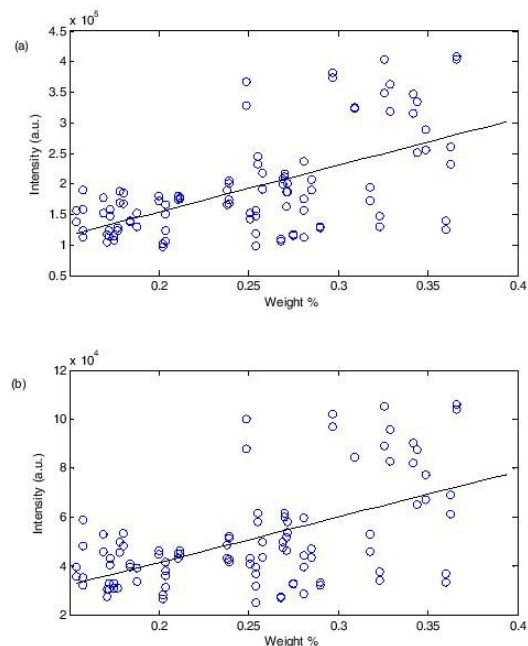


Figure 1. Calibration curves of the Na I 818.326 nm line verse sodium reference concentration in dried pasture pellets using (a) peak intensities and (b) integrated intensities. The solid lines represent a least squares linear regression with (a) $R^2 = 0.347$ and (b) $R^2 = 0.308$.

TABLE 1. NEUTRAL LINES USED IN THE BOLTZMANN PLOT FOR DETERMINING PLASMA TEMPERATURE.

Species	Wavelength (nm)
Ca I	428.3011
Ca I	428.9367
Ca I	429.8988
Ca I	430.2528
Ca I	430.7744
Ca I	431.8652
Ca I	442.5437
Ca I	443.4957
Ca I	445.4779
Ca I	585.7451
Ca I	610.2723
Ca I	612.2217
Ca I	616.2173
Ca I	643.9075
Ca I	646.2567
Ca I	649.3781

to plasma temperature variations between samples. Some sources of temperature variations include lens-to-sample distance (LTSD), the amount of sample ablated, the spectrometers looking at different sites in the plasma which has spatial variations and shots taken from different locations on the sample [16].

A. Boltzmann Plots

Boltzmann plots were constructed using (2) and the criteria described previously to correct for the temperature deviations between plasmas. Table 1 lists the 16 calcium lines used to rectify each spectrum. The spectra displayed a temperature range of ~3400-6700 K. The Boltzmann plot for one spectrum is displayed in Fig. 2. Using these temperatures the partition functions and exponential terms were calculated and the observed emission lines rendered temperature independent. The calibration curves produced correlations of $R^2 = 0.019$ and

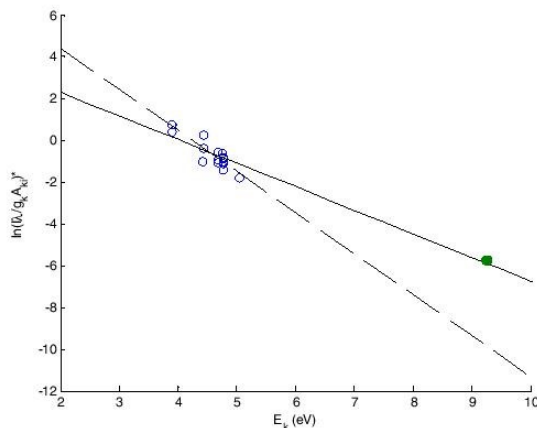


Figure 2. Boltzmann and Saha-Boltzmann plots of calcium for one spectrum. Hollow circles representing neutral lines (Table 1) and solid circles (overlapped) representing ionic lines (Table 2). The dashed line and solid line displaying least squares fits from the Boltzmann and Saha-Boltzmann plots. The temperatures obtained were 5900 K (Boltzmann plot) and 8100 K (Saha-Boltzmann plot).

$R^2 = 0.023$ for peak and integrated intensities. The reduced correlations maybe due to incorrect electron temperatures, the plasma existing in partial-LTE (p-LTE) not LTE, matrix effects, incorrect emission line identification and errors in calculations. The lines were identified correctly but some of the fitted Lorentzian profiles were questionable. Removing the questionable lines did not improve the correlations. The calculations were checked and no flaws were found. Increasing the number of lines in the Boltzmann plot would increase the accuracy in the temperature calculations. Increasing the plasma temperature would increase the intensity of emission lines and lead to more lines available for the Boltzmann plots. A technique known as double-pulse LIBS (DP-LIBS) can be used to increase emission line intensities by utilising a second pulse to reheat the plasma [26]. Instead of increasing the temperature in the plasma the gate delay of the spectrometer can be reduced to look at the plasma at a higher temperature. The integration time can also be reduced to find a pulse energy, gate delay and integration time that will produce an optimal signal-to-background ratio. The validity of LTE can be checked using various methods including the McWhirter criterion and Boltzmann plots of different species. These methods need an accurate value for the electron density or electron temperature [27, 28]. However, none of the approaches mentioned above can be achieved with the current experimental setup.

B. Saha-Boltzmann Plots

Singly ionised calcium lines (Ca II 854.209 nm and Ca II 866.214 nm) were added to the Boltzmann plots using (4), (5) and (6) creating Saha-Boltzmann plots to increase the accuracy of the calculated electron temperature. The H_β and the H_γ were not observed in the spectra, so the H_α line was used to calculate the electron density using equation (6). The calculated electron densities ranged from 3.2×10^{16} to $1.6 \times 10^{17} \text{ cm}^{-3}$. The Saha-Boltzmann plot for one spectrum is displayed in Fig. 2. A range of different $\alpha_{1/2}$ coefficients was used to calculate the Stark widths. The resulting temperatures ranged between ~6800-9500 K, producing correlations of corrected emission line intensities to sodium concentration ranging between $R^2 = 0.344-0.347$. Using the Saha-Boltzmann plots produced better correlations than the Boltzmann plots alone but these correlations are still comparable to the uncorrected emission lines. This may be due to the fact that besides Stark broadening other broadening mechanisms are present in the spectra. Doppler broadening is expected to be negligible since the temperatures of LIBS plasmas usually range between 0.5-1 eV. The dominant form of broadening is assumed to be from the instrument. The inaccurate calculations of Stark broadening in the hydrogen-alpha line cause inaccurate temperature calculations. Measuring the instrument broadening may help in determining the correct temperature of the plasma. p-LTE may be another reason for inaccurate temperatures. The long integration time may also be another cause for the incorrect temperature calculations. The integration time is set to one millisecond which corresponds to the lifetime of the plasma [13]. The spectra would then cover a range of temperatures and depending on the sample it may cover a time when the plasma is not in LTE. The spectra would then display an average temperature resulting from the integration time.

C. Internal Reference Standards

Carbon lines, C₂ swan band and CN violet band heads were investigated as suitable internal references. An oxygen line was also added to account for reactions with C₂ reducing the C₂ emission. Table 2 lists the lines and wavelengths used. Combinations of these lines were used to account for the distribution of carbon in the plasma. The least squares linear regression correlations obtained from these combinations are displayed in Table 3. The integrated profile intensity ratio of Na/(C 833 + C₂ + CN + O) gave the best correlation of R² = 0.665 which is a considerable improvement on the uncorrected emission lines. Possible reasons for the low correlations maybe due to weak carbon emission lines. Another method of combining the carbon contributions in the plasma maybe more effective than using simple addition.

D. Partial Least Squares Analysis

PLS was used to identify which lines influence the sodium emissions. Using four latent variables a PLS regression model

TABLE 2. EMISSION LINES INVESTIGATED FOR SUITABLE INTERNAL REFERENCE STANDARD.

Species	Wavelength (nm)
C I	247.856
C I	833.515
C ₂	516.52
CN	388.34
O I	844.676

TABLE 3. COMBINATIONS OF INTERNAL REFERENCE STANDARDS USED AGAINST THE NA I 818.326 NM PEAK INTENSITY AND INTEGRATED LINE PROFILE.

Internal reference	Correlation (R ²)	
	Peak	Integral
None	0.347	0.308
C 247	0.146	0.080
C 833	0.306	0.211
C ₂	0.555	0.604
CN	0.507	0.467
CN+C ₂	0.562	0.605
C 247+C ₂	0.554	0.606
C 833+C ₂	0.589	0.636
C 833+C ₂ +CN	0.580	0.636
C 247+C ₂ +CN	0.597	0.636
O	0.565	0.181
C 833+C ₂ +CN+O	0.236	0.665

TABLE 4. EMISSION LINES THAT THE CHANGE WITH SODIUM CONCENTRATION. THE ASTERISKED POTASSIUM LINES DID NOT CHANGE SIGNIFICANTLY, SEE TEXT FOR DETAILS.

Species	Wavelength (nm)
Na I	588.995
Na I	589.592
Na I	818.326
Na I	819.482
Ca I	422.673
Ca II	393.366
Ca II	396.847
Ar I	811.531
K I	766.490
K I	769.896
*K I	693.876
*K I	691.108

was created using the collected spectra as the predictor variables and the laboratory-determined elemental concentrations as the response variables. Plotting the fitted against observed response generated a correlation of R² = 0.855 which is significantly better than any correlation from using an internal reference standard. Fig. 3 displays the weightings of the latent variables across the spectra. Significant weightings from the PLS model were produced for sodium, calcium and potassium lines as well as an argon line. These lines are the first ten lines listed in Table 4. The relationship between the peak intensities of these lines and the sodium concentration in the samples were investigated using PLS. The two potassium lines displayed obvious signs of self-absorption so the potassium predictors were replaced with the potassium lines with the asterisk preceding them. PLS on these selected lines produced a correlation between fitted and observed responses of R² = 0.835. The sodium concentration in the samples showed the greatest dependence on the Na I 818.326 nm, Na I 819.482 nm and K I 693.876 nm lines. This is expected since sodium and potassium use the same pathways and the salinity in a plant affects the sodium to potassium ion ratio. This explains the interaction between the sodium and potassium emissions recorded from the plasma.

E. Ratio Method

The ratio of sodium to potassium was evaluated under the assumption that the elemental ratios are not affected by the amount of ablated mass [16]. Different combinations of Na I 818.326 nm, Na I 819.482 nm, K I 693.876 nm and K I 691.108 nm lines were used to produce sodium to potassium ratios. The sodium to potassium ratios gave correlations with the sodium concentrations of R² = 0.584-0.764 and R² = 0.761-0.770 for the peak and integrated line intensities, respectively. The poor correlations are because the results of the ratios are not temperature independent. Also potassium is not suitable for an internal reference standard since it does not make up the bulk of the sample. Using potassium as an internal reference standard makes the ratio dependant on the potassium concentration as well as the sodium concentration.

The sodium to potassium emission ratios were verified against the laboratory-determined sodium to potassium

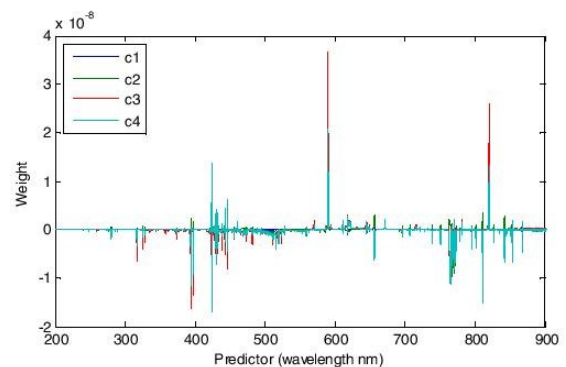


Figure 3. PLS weightings on the entire data set. c1-c4 are the latent variables.

concentration ratio. The correlation from this approach produced the best results, a correlation of $R^2 = 0.918$ for the ratio of peak intensities of Na I 818.326 nm and K I 693.876 nm. The calibration curve for this relationship is displayed in Fig. 4. The root mean squared error of prediction (RMSEP) for this calibration curve was ± 0.0587 which corresponds to an error of ± 0.0085 in the reference sodium to potassium ratio. This allows the comparison of peak intensity ratios to a reference range of 0.11. The RMSEP was calculated using

$$RMSEP = \sqrt{\frac{\sum_{i=1}^N (\hat{y}_i - y_{ref,i})^2}{N}} \quad (8)$$

where N is the number of samples, \hat{y}_i is the prediction concentration and $y_{ref,i}$ is the actual concentration [29].

Examination of equation (1) explains why the Na I 818.326 nm to K I 693.876 nm ratio correlates well with the ratio of concentrations. Taking the ratio of two lines using (1) produces

$$\frac{I^1}{I^2} = \frac{C_s^1 A_{ki}^1 g_k^1 \lambda^2 U_S^2(T)}{C_s^2 A_{ki}^2 g_k^2 \lambda^1 U_S^1(T)} e^{\left(\frac{E_k^2 - E_k^1}{kT}\right)} \quad (9)$$

where the superscript represent the two lines used. The ratio of partition functions are assumed to be rendered temperature independent [16]. The exponential term is now the only temperature dependant function in (9). As the difference in upper level energies decreases the temperature dependency of (9) decreases as well. Using Na I 818.326 nm and K I 693.876 nm lines the energy difference is -0.214 eV. This is the lowest difference attained by all the observed lines in the spectra.

IV. CONCLUSIONS

The present work demonstrates different methods used to determine sodium concentrations in dried pelletised pasture samples. Success was found in finding the sodium to potassium ratio which is important to plant growth. There are many variations in LIBS plasmas. Of importance are the temperature variations between the plasmas. These are caused by LTSD, the amount of sample ablated, the spectrometers looking at different sites in the plasma which has spatial variations, the plasma existing in p-LTE not LTE, matrix effects, etc. These variations cause unsatisfactory correlations when producing calibration curves. There are various methods to overcome these variations. These include using the temperatures found from Boltzmann and Saha-Boltzmann plots to correct the emission lines of interest. The plasma must be in LTE for these methods to work unless the particular species used for the plots is the species of interest. Another method for reducing experimental fluctuations is DP-LIBS. DP-LIBS ablates more sample mass, increases plasma temperature, increases plasma volume, decreases electron density, decreases plasma density and can reduce matrix effects [26, 30].

In this work the Boltzmann plot method was unsatisfactory. Increasing the number of emission lines in the plot would

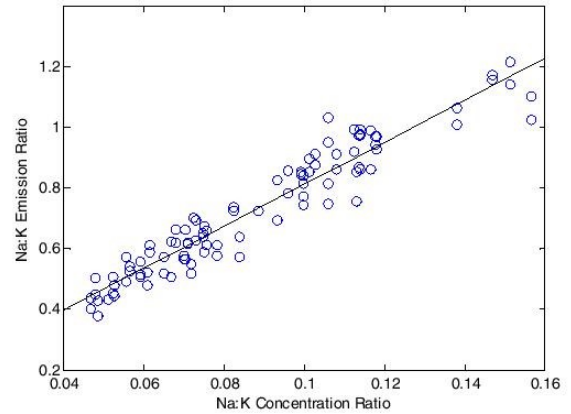


Figure 4. Calibration curve for the sodium to potassium peak intensity ratio versus the sodium to potassium concentration ratio of dried pasture pellets. The solid lines represent the result for a least squares linear regression with $R^2 = 0.918$. The lines used for the intensity ratio are Na I 818.326 nm and K I 693.8764 nm.

increase the accuracy in the temperature calculations. This could be done by increasing the plasma temperature. The methods for increasing plasma temperature cannot be done with the experimental setup in this work. The Saha-Boltzmann plot method was also limited. Finding the contribution of instrument broadening on the emission lines will help in determining the true Stark width which would lead to correct electron density calculations and correct electron temperatures. For the Boltzmann and Saha-Boltzmann plots to work the plasma needs to be in LTE. The existence of LTE in the plasma needs to be confirmed. Finding the optimal experimental parameters for the pelletised samples will help in obtaining improved spectra. This cannot be done with the experimental setup in this work.

The most effective method in this work was that of using the peak intensity ratios compared to the verified concentration ratios of sodium to potassium. That is Na I 818.326 nm / K I 693.876 nm versus Na/K concentrations. The correlation was $R^2 = 0.918$ with an RMSEP of ± 0.0587 . This method outperformed the internal reference method because the upper level electron energy difference between lines was lower than any pair of lines observed. Further work to improve results may mean changing the experimental setup or using other post-processing techniques.

The success in this work serves as a method for finding the sodium to potassium concentration in dried pelletised pasture samples. The results from this work can be used by someone skilled in the art of botany to determine the salinity stress on pasture.

ACKNOWLEDGMENTS

Financial assistance from the Ministry of Business, Innovation and Employment is gratefully acknowledged. This work was supported by The New Zealand Institute for Plant and Food Research Ltd in conjunction with The University of Waikato.

REFERENCES

- [1] J. Gorham, "Sodium," in *Handbook of Plant Nutrition*, A. V. Barker and D. J. Pilbeam, Eds., 1st ed Boca Raton, FL: CRC Press, 2007, pp. 573-575.
- [2] A. Läuchli and S. R. Grattan, "Plant growth and development under salinity stress," in *Advances in Molecular Breeding Toward Drought and Salt Tolerant Crops*, M. Jenks, P. Hasegawa, and S. M. Jain, Eds., 1st ed: Springer Netherlands, 2007, pp. 1-32.
- [3] J. Pardo and F. Quintero, "Plants and sodium ions: keeping company with the enemy," *Genome Biology*, vol. 3, pp. 1-4, 24 May 2002.
- [4] E. Blumwald, "Sodium transport and salt tolerance in plants," *Current Opinion in Cell Biology*, vol. 12, pp. 431-434, 2000.
- [5] M. Z. Martin, A. J. Stewart, K. D. Gwinn, and J. C. Waller, "Laser-induced breakdown spectroscopy used to detect endophyte-mediated accumulation of metals by tall fescue," *Applied Optics*, vol. 49, pp. C161-C167, 2010.
- [6] J. W. B. Braga et al., "Comparison of univariate and multivariate calibration for the determination of micronutrients in pellets of plant materials by laser induced breakdown spectrometry," *Spectrochimica Acta - Part B Atomic Spectroscopy*, vol. 65, pp. 66-74, 2010.
- [7] P. K. Rai et al., "Role of glycemic elements of *Cynodon dactylon* and *Musa paradisiaca* in diabetes management," *Lasers in Medical Science*, vol. 24, pp. 761-768, 2009.
- [8] D. K. Chauhan, D. K. Tripathi, N. K. Rai, and A. K. Rai, "Detection of Biogenic Silica in Leaf Blade, Leaf Sheath, and Stem of *Bermuda Grass* (*Cynodon dactylon*) Using LIBS and Phytolith Analysis," *Food Biophysics*, vol. 6, pp. 416-423, 2011.
- [9] A. R. Boyain-Goitia, D. C. S. Beddows, B. C. Griffiths, and H. H. Telle, "Single-pollen analysis by laser-induced breakdown spectroscopy and raman microscopy," *Applied Optics*, vol. 42, pp. 6119-6132, 2003.
- [10] D. Cremers and L. Radziemski, "Introduction," in *Handbook of Laser-Induced Breakdown Spectroscopy*, 2nd ed West Sussex, UK: John Wiley & Sons Ltd, 2013, p. 3.
- [11] D. Cremers and L. Radziemski, "Basics of the LIBS plasma," in *Handbook of Laser-Induced Breakdown Spectroscopy*, 2nd ed West Sussex, UK: John Wiley & Sons Ltd, 2013, p. 49.
- [12] S. N. Thakur, "Atomic emission spectroscopy," in *Laser-Induced Breakdown Spectroscopy*, J. P. Singh and S. N. Thakur, Eds., 1st ed Oxford, UK: Elsevier, 2007, p. 26.
- [13] R. E. Russo, X. L. Mao, J. H. Yoo, and J. J. Gonzalez, "Laser Ablation," in *Laser-Induced Breakdown Spectroscopy*, J. P. Singh and S. N. Thakur, Eds., 1st ed Oxford, UK: Elsevier, 2007, p. 61.
- [14] J. Moros, J. A. Lorenzo, P. Lucena, L. M. Tobaría, and J. J. Laserna, "Simultaneous Raman spectroscopy-laser-induced breakdown spectroscopy for instant standoff analysis of explosives using a mobile integrated sensor platform," *Analytical Chemistry*, vol. 82, pp. 1389-1400, 2010.
- [15] D. Cremers and L. Radziemski, "LIBS analytical figures of merit and calibration," in *Handbook of Laser-Induced Breakdown Spectroscopy*, 2nd ed West Sussex, UK: John Wiley & Sons Ltd, 2013, pp. 131-140.
- [16] U. Panne, C. Haisch, M. Clara, and R. Niessner, "Analysis of glass and glass melts during the vitrification process of fly and bottom ashes by laser-induced plasma spectroscopy. Part I: Normalization and plasma diagnostics," *Spectrochimica Acta, Part B: Atomic Spectroscopy*, vol. 53, pp. 1957-1968, 1998.
- [17] A. Ciucci et al., "New procedure for quantitative elemental analysis by laser-induced plasma spectroscopy," *Applied Spectroscopy*, vol. 53, pp. 960-964, 1999.
- [18] A. Kramida, Yu. Ralchenko, J. Reader, and NIST ASD Team (2014). *NIST Atomic Spectra Database (ver. 5.2)*. Available: <http://physics.nist.gov/asd>
- [19] A. De Giacomo, M. Dell'Aglio, O. De Pascale, S. Longo, and M. Capitelli, "Laser induced breakdown spectroscopy on meteorites," *Spectrochimica Acta - Part B Atomic Spectroscopy*, vol. 62, pp. 1606-1611, 2007.
- [20] Ş. Yalçın, D. R. Crosley, G. P. Smith, and G. W. Faris, "Influence of ambient conditions on the laser air spark," *Applied Physics B: Lasers and Optics*, vol. 68, pp. 121-130, 1999.
- [21] S. N. Thakur, "Atomic emission spectroscopy," in *Laser-Induced Breakdown Spectroscopy*, J. P. Singh and S. N. Thakur, Eds., 1st ed Oxford, UK: Elsevier, 2007, pp. 44-48.
- [22] H. R. Griem, "Appendix III: Fractional intensity widths of hydrogen and ionized helium lines," in *Spectral Line Broadening by Plasmas*, 1st ed New York: Academic Press, 1974, pp. 314-316.
- [23] D. Cremers and L. Radziemski, "Basics of the LIBS plasma," in *Handbook of Laser-Induced Breakdown Spectroscopy*, 2nd ed West Sussex, UK: John Wiley & Sons Ltd, 2013, pp. 35-36.
- [24] D. A. Skoog, D. M. West, J. F. Holler, and S. R. Crouch, "Gravimetric methods of analysis," in *Fundamentals of analytical chemistry*, 9th ed Belmont, Ca: Brooks/Cole, 2014, pp. 281-291.
- [25] M. Galiová et al., "Utilization of laser-assisted analytical methods for monitoring of lead and nutrition elements distribution in fresh and dried *Capsicum annum* l. leaves," *Microscopy Research and Technique*, vol. 74, pp. 845-852, 2011.
- [26] J. Uebbing, J. Brust, W. Sdorra, F. Leis, and K. Niemax, "Reheating of a laser-produced plasma by a second pulse laser," *Applied Spectroscopy*, vol. 45, pp. 1419-1423, 1991.
- [27] D. Cremers and L. Radziemski, "Basics of the LIBS plasma," in *Handbook of Laser-Induced Breakdown Spectroscopy*, 2nd ed West Sussex, UK: John Wiley & Sons Ltd, 2013, pp. 40-41.
- [28] R. Agrawal et al., "LIBS: A quality control tool for food supplements," *Food Biophysics*, vol. 6, pp. 527-533, 2011.
- [29] R. Bro, Á. Rinman, and N. M. Faber, "Standard error of prediction for multilinear PLS: 2. Practical implementation in fluorescence spectroscopy," *Chemometrics and Intelligent Laboratory Systems*, vol. 75, pp. 69-76, 2005.
- [30] D. Cremers and L. Radziemski, "Basics of the LIBS plasma," in *Handbook of Laser-Induced Breakdown Spectroscopy*, 2nd ed West Sussex, UK: John Wiley & Sons Ltd, 2013, pp. 58-62.

Chapter 5

Considerations needed for sensing mineral nutrient levels in pasture using a benchtop laser-induced breakdown spectroscopy system

a peer-reviewed book chapter

to be submitted in

Smart Sensors for Precision Agriculture

by

H. Jull, R. Künnemeyer, and P. Schaare

Considerations needed for sensing mineral nutrient levels in pasture using a benchtop laser-induced breakdown spectroscopy system

H. Jull^{a*}, R. Künnemeyer^a, and P. Schaare^b

^a The Dodd Walls Centre for Photonic and Quantum Technologies, School of Engineering, University of Waikato, Hamilton 3240, New Zealand

^b Plant and Food Research, Hamilton 3240, New Zealand

*Corresponding author. Email address harrisson.jull@gmail.com

Abstract

Precision agriculture aims to increase yield and profits while reducing costs, waste, and environmental side-effects. This is achieved through a process of measuring, modelling and acting; for example, laser-induced breakdown spectroscopy (LIBS) can be used to measure macro and micro nutrients in crops to determine nutrient requirements. The limiting factor with quantitative LIBS analysis of plant nutrient levels is the variation between shots on the same sample. Following a review of current literature relevant to LIBS for agriculture, this work investigates whether different chemometric methods can mitigate these variations and can create quantitative calibrations for nutrient levels in fresh and dried pelletised pasture under laboratory conditions. The methods explored were Savitzky Golay filtering, multiple linear regression, principal component regression, partial least-squares regression, gaussian process regression, and artificial neural networks. The algorithms that performed best were partial least-squares with gaussian process regression (R^2 of 0.93, 0.95, and 0.92 for K, Na, and Mn, respectively), principal components analysis with artificial neural networks (R^2 of 0.94, 0.83, and 0.80 for Fe, Ca, and Mg, respectively), and partial least-squares with artificial neural networks (R^2 of 0.77 for B). Removing the moisture from the pasture improved model R^2 values by 4-5 % on average. Acquiring spectra under an argon purge produced a small reduction in accuracy for some nutrients compared to models acquired in air. Including categorical data in the principal component regression and the artificial neural networks produced negligible improvements in prediction.

This chapter will give an introduction to using different types of chemometric analyses on spectra generated by LIBS to measure micro and macro nutrients in pasture under laboratory conditions. It discusses the challenges faced when building models for each nutrient.

Keywords: Laser-induced breakdown spectroscopy, Pasture, Chemometrics, Agriculture.

Introduction

Precision agriculture is a farming technique that measures and reacts to site-specific crop variability. One method is to optimise crop yield through precisely timed and tailored fertiliser application and application rates. This not only creates financial benefits, through increased yield and reducing the amount of fertiliser applied, but also reduces the environmental side effects caused by over fertilisation, i.e., leaching and runoff into streams and rivers. Accurate sensor technologies able to give real-time information on the nutritional status of crops are needed to realise precision agriculture [1]. Laser-induced breakdown spectroscopy (LIBS) is a technique that has become popular for its ability to make fast elemental analyses. LIBS uses a high powered pulsed laser to create a plasma on a target material's surface through inverse Bremsstrahlung [2]. As the plasma cools, electrons transition from high energy levels to lower levels and emit photons. Photons are emitted at specific wavelengths corresponding to the particular elements that constitute the plasma and represent the elemental makeup of the sample. The concentration of these elements directly affects the intensities of the emission lines in the spectrum [3]. LIBS is a sensitive technique that needs no sample preparation and has the potential to produce reliable calibrations that determine the nutrient levels in pasture. The essential elements needed for plant growth are the macro (N, P, K, Ca, S, and Mg) and micro nutrients (B, Cl, Mn, Fe, Zn, Cu, Mo, and Ni).

LIBS spectra exhibit strong within- and between-sample variation which reduces the repeatability of measurements [4]. The shot-to-shot variations originate from multiple sources, like sample inhomogeneity, surface roughness, matrix effects,

sample moisture, and differences in experimental parameters. The main cause of variability in spectra is the difference in plasma temperatures. The exponential Boltzmann factor and the partition function in the emission line intensity equation both have strong temperature dependence. Averaging multiple spectra from the same sample, using internal standards, normalisation, and chemometric algorithms can reduce the shot-to-shot variation. Some of the first quantitative chemometric methods that have been used for LIBS include linear or rank correlation [5], multiple linear regression (MLR) [6], principal component regression (PCR) [7], partial least squares regression (PLS) [8], and artificial neural networks (ANN) [9]. Increasing the signal to noise ratio by increasing the emission line intensities can produce additional lines that contain valuable information. This is achieved through increasing the temperature in the plasma by increasing the laser pulse energy or using an argon atmosphere.

LIBS for agriculture

There have been many studies using LIBS on agriculture. A summary of the majority of these studies is presented in Table 1. This table contains studies performed on agricultural material, including all those which are relevant for the following discussion. Various wavelengths, pulse durations, and repetition rates have been used for the lasers in these studies. Nd:YAG lasers are typically used for LIBS because they are reliable, compact, and are easy to use [10]. Most of the studies mentioned below use a 1064 nm Nd:YAG laser. Unfortunately, there are a few studies where there is no information on the spectrometer settings.

Table 1. Laser parameters and spectrometer settings for LIBS on various agricultural samples.

(λ : wavelength, t_p : pulse duration, f : pulse frequency, E : pulse energy, t_d : gate delay, Δt : integration time)

Sample	Laser				Spectrometer		Ref.
	λ [nm]	t_p [ns]	f [Hz]	E [mJ]	t_d [μ s]	Δt [μ s]	
Algae	1,064	7	2	100	6	0.6	[11]
Algae	1,064	5-7	10	30	-	2,000,000	[12]
Apple leaves, pine needles, citrus leaves, tea leaves, rice flour, Cannabis plant leaves and flower tops	1,064	7	10	200	-	-	[13]
Aquatic plant, aquatic moss, bush branches and leaves, cabbage, soya flour, rice flour, wheat flour, spinach leaves, brachiaria, banana leaves coffee leaves, maize leaves, mango leaves, pepper leaves, soya leaves, olive leaves, apple leaves, guava leaves, grass and jackfruit leaves	532	12	10	71	9	1.1	[14]
Bean leaves	1,064	5	10	200	2	5	[15]
Bean leaves, bush branches and leaves, cabbage, soya flour, rice flour, apple leaves, peach leaves, wheat flour and spinach leaves	1,064	5	10	360	2	5	[16]
Bermuda grass	532	4	-	10	-	-	[17]
Bermuda Grass and <i>Musa paradisiaca</i>	-	-	1	175	-	-	[18]
Bitter gourd (<i>Momordica charantia</i> L.)	1,064	-	-	200	-	-	[19]
Bitter Melon	-	-	10	40	-	-	[20]
Black tea (<i>Anxi, Fujian</i>), Huangya tea (<i>Ya'an, Sichuan</i>), Longjing tea and Pu'er tea (<i>Pu'er, Yunnan</i>)	1,064	8	20	20-100	2-30	2	[21]
Boldo leaves (<i>Peumus boldus Molina</i>)	1,064	5	10	110 and 220	2	5	[22]
Bran tissues and wheat grain	193	15	1	-	-	2,000	[23]
Broad bean (<i>Vicia faba</i>)	266	-	1	5	1 (delay)	10	[24]
	1,064	-	1	100	0.5 (interpulse delay)		
Cabbage leaf	532	4	4	20	1.5	-	[25]
Capsicum leaves	532	5	-	10	1	10	[26]
Carrot Root (<i>Daucus carota</i>)	532	8	10	-	-	-	[27]
Cauliflower and broccoli	532	7	2	96	1	5	[28]
Chinese cabbage	1,064	8	2	120	2	2,000	[29]
Chinese tea leaves, Longjing green tea, Mengding Huangya, White tea, Tie Guanyin, Wuyi black tea, and Pu'er tea	1,064	5.82	-	50	1.2	4	[30]
Citrus leaf	355	5	10	5	1	50	[31]
	1,064	5	10	110			
Citrus leaves	1,064	-	10	50	48.5	-	[32]
Citrus leaves	1,064	8	10	50	2.5	2,000	[33]
Coffee	1,064	8	10	50	-	-	[34]
Coffee	266	8	20	31	0.4	-	[35]

Coffee beans	1,064	8	-	50	11	2,100	[36]
Cotton	1,064	5	0.67	-	1.3	4.5	[37]
Cucurbita maxima seeds	532	4	1	100	-	-	[38]
Dallisgrass (<i>Paspalum dilatatum</i>); wheat (<i>Triticum aestivum</i>), soybean (<i>Glycine max</i>); bell pepper (<i>Capsicum annuum</i>)	800	0.000,035	1,000	0.3	-	500,000	[39]
Duckweed (<i>Lemna minor</i>)	266	5	-	10	1	10	[40]
	1,064	5	-	100	1	10	
<i>Emblica officinalis</i>	-	-	2	175	-	-	[41]
<i>Ficus bengalensis</i>	-	-	-	-	-	-	[42]
<i>Folium lycii</i>	1,064	8	-	-	0.8	2,000	[43]
Gannan navel orange	-	-	2	20	1.2	2,000	[44]
Gannan navel orange	1,064	8	0.1-10	110	2	-	[45]
Green herb, tomato leaves and coffee beans	1,064	5	-	-	-	-	[46]
Guava	-	-	2	175	-	-	[47]
Holly leaves	1,064	10	10	45	0.5	2,000	[48]
	266	-	-	45	0.5	2,000	
Holly leaves	1,064	-	-	10-80	-	-	[49]
	266	-	-	10-80	-	-	
<i>Juncus efusus L.</i>	1,064	3-5	2	340	1	1,000	[50]
Lettuce	532	5	-	10	1	10	[51]
<i>Ligusticum wallichii</i>	1,064	5.82	20	26.8	1.5	20	[52]
Maize (<i>Zea mays L.</i>)	-	-	-	-	-	-	[53]
Maize (<i>Zea mays</i>), sunflower (<i>Helianthus annuus</i>) and lettuce (<i>Lactuca sativa</i>)	532	5	-	10	1	10	[54]
Maize and holly (<i>Ilex chinensis Sims</i>)	1,064	-	-	90	-	-	[55]
Maize leaf and Red osier dogwood leaves	795	0.000,16	10	0.1	-	-	[56]
Mustard grass	1,064	-	10	300	-	-	[57]
Navel oranges	1,064	8	10	200	1.28	2,000	[58]
<i>Ocimum sanctum, Ocimum americanum, Ocimum gratissimum, and Ocimum basilicum</i>	532	4	10	-	-	-	[59]
Orange leaves	1,064	10	10	200	1.28	-	[60]
Orange peel	1,064	8	10	200	1.28	2,000	[61]
Orange tree leaves	1,064	8	10	-	1.28	2,000	[62]
Peach, apple, and spinach	1,064	-	-	10-30	-	-	[63]
Perennial ryegrass (<i>Lolium perenne</i>) and white clover (<i>Trifolium repens</i>)	1,064	-	-	200	1	-	[64]
<i>Phaleria Macrocarpa</i> leaves	1,064	10	-	100	-	-	[65]
Pollen	-	10	-	30	1.5	2,000	[66]
Pollen and fresh grass fragments	1,064	-	5	20-30	1	4	[67]
Poplar tree leaves	800	0.000,1	10	25	-	-	[68]
Potato skin	266	5	10	5-20	Various	Various	[69]
Potato skin	1,064	5	-	10	1	1	[70]
Potato skin and flesh	1,064	4	20	10	1	5	[71]
Potato, carrot, celery and aubergine	266	-	10	10	0.1	5	[72]

Powdered rice, starch and seaweed	10,600	200	10	1,500	1	100	[73]
Prickle pears	1064	20	-	300	-	-	[74]
<i>Psoralea corylifolia</i> seed	-	-	2	175	-	-	[75]
<i>Psoralea corylifolia</i> seed	-	-	2	175	-	-	[76]
Red Fuji apples and Hosui pears	1,064	-	20	160	2	-	[77]
Rice	1,064	5	1	-	-	-	[78]
Rice Leaves (<i>Oryza sativa</i> L.)	532	8	1	60	4	20	[79]
Rice seed and milk powder	10,600	200	20	1,500	-	2,000,000	[80]
Saffron (<i>C. sativus</i> L.), safflower (<i>Carthamus tinctorius</i> L.), marigold flower (<i>Calendula officinalis</i> L.), turmeric (<i>Curcuma longa</i> L.)	1,064	-	4	38	0.3	20	[81]
Scented geranium	1,064	8	-	80	5	15	[82]
Scented geranium	1,064	12	1	-	2	2	[83]
Seed kernels of pumpkin (<i>Cucurbita maxima</i>), ash gourd (<i>Benincasa hispida</i>), watermelon (<i>Citrullus lanatus</i>) and muskmelon (<i>Cucumis melo</i>)	532	4	2	40	1	5	[84]
Sophora leaves	800	0.000,15	10	5	-	-	[85]
Soybean leaves	532 1,064	4 6	- -	1, 4, 8, 16 and 32 1, 4, 8, 16 and 32	1 1	- -	[86]
Spinach leaf powder and unpolished rice flour	1,064	7	10	80-140	-	-	[87]
Spinach leaves	532	12	10	70	1.1	9	[88]
spinach, mustard, chenopodium, fenugreek, and chickpea leaves	532	4	10	10	-	-	[89]
Spirulina and chlorella	10,600	100	1.3	Various	-	30,000,000	[90]
Starch powders and rice flour	1,064	7	10	30	-	-	[91]
Sugar cane	1,064	5	10	220	2	4.5	[92]
Sugar cane	-	-	-	50, 75	0.5, 1	-	[93]
Sugar cane (<i>Saccharum officinarum</i>)	532	4	10	10	-	-	[94]
Sugar cane and Boldo leaves	1,064	5	10	365	2	5	[95]
Sugar cane leaves	1,064	5	10	-	2	5	[96]
Sugar cane leaves	1,064	5	10	110	2	4.5	[97]
Sugar cane leaves	1,064	5	10	110	2	5	[98]
Sugar cane, orange tree leaves and soy leaves	1,064	5	10	110	2	4.5	[99]
Sugarcane (<i>Saccharum officinarum</i>), soy (<i>Glycine max</i>), citrus (<i>Citrus sinensis</i>), coffee (<i>Coffea arabica</i>), maize (<i>Zea mays</i>), eucalyptus (<i>Eucalyptus sp.</i>), mango (<i>Mangifera indica</i>), bean (<i>Phaseolus vulgaris</i>), banana (<i>Musa paradisiaca</i>), lettuce (<i>Lactuca sativa</i>), brachiaria (<i>Brachiaria decumbens</i>), pearl millet (<i>Pennisetum americanum</i>), grape (<i>Vitis sp.</i>), rubber tree (<i>Hevea brasiliensis</i>), tomato (<i>Solanum lycopersicum</i>), apple leaves, peach leaves, spinach leaves, tomato leaves, and pine needles	1,064 532 266 800	6 6 6 0.000,6	3.3 3.3 3.3 1,000	70 70 70 1.65	0.75 0.75 0.75 0.35	3 3 3 0.25	[100]
Sunflower (<i>Helianthus annuus</i>), leaves/stem	532	5	-	10	1	10	[101]
Sunflower (<i>Helianthus annuus</i>), leaves/stem	795	0.000,16	10	0.1	-	-	[102]
Sunflower (<i>Helianthus annuus</i>), leaves/stem	532	5	-	10	1	10	[103]

Sunflower (<i>Helianthus annuus</i>), leaves/stem	532	5	-	10	1	10	[104]
Sunflower (<i>Helianthus annuus</i>), leaves/stem	532	5	-	10	1	10	[105]
Sunflower, leaves/stem	355	6	20	-	-	0.50	[106]
	790	0.000,03	20	-	-	0.50	
Tall fescue and apple leaf	532	-	-	23	0.5	10	[107]
Tangerine leaves and Rhododendron leaves	1,064	20	100	1.1	-	100,000	[108]
Tea leaves	1,064	8	4	30	1.5	2	[109]
Tea plants (<i>Sambucus nigra L.</i> , <i>Hypericum perforatum L.</i> , <i>Crataegus oxyacantha auct. non L.</i> , <i>Rubus idaeus L.</i> and <i>Betula species L.</i>)	1,064	8	10	70	1	1,050	[110]
Tobacco	266	6	10	25	0.25	1,050	[111]
Tobacco leaves	532	8	1	60	1.5	10	[112]
Tomato leaves	1,064	6	20	100	2	5	[113]
Tomato leaves, spinach leaves, apple leaves, peach leaves Spanish moss and pine needles	1,064	5	1	100	1	10	[114]
<i>Trichosanthes dioica</i> fruit	532	3-4	2	175	-	-	[115]
<i>Tsumura kackontou</i>	10,600	200	-	1,500	10	100	[116]
<i>Tsumura kackontou</i>	10,600	200	-	1,000-1,500	-	-	[117]
Turmeric	532	4	10	18	-	-	[118]
Wheat and gardenia	800	0.000,035	1,000	0.3	-	-	[119]
Wheat flour	1,064	5	-	-	1-3	1-10	[120]
Wheat flour	1,064	-	4	38	0.3	1,050	[121]
Wheat grain	193	15	1	35	-	-	[122]
Wheat grain	532	5	20	80	0.5	2,000	[123]
	193	15	1	-	-	-	
Wheat leaves, poppy leaves, barley leaves and rape leaves	1,064	12	-	80-150	-	1	[124]
Wheat seedlings (<i>Triticum aestivum L.</i>)	532	4	4	10	-	-	[125]
Wheat seedlings (<i>Triticum aestivum L.</i>)	532	4	4	10	-	-	[126]
White chickpea	1,064	-	8	40	0.650	1,050	[127]
<i>Withania coagulans</i> fruit	-	-	-	-	-	-	[128]
<i>Withania coagulans</i> fruit	-	-	-	-	-	-	[129]
Wood	1,064	5	10	50-70	3	10	[130]
Wood	1,064	8	2	-	17	5,000	[131]
Wood	1,064	10	2	-	-	5,000	[132]
Wood	532	-	-	45	-	10	[133]
Wood	-	10	10	200	-	-	[134]
Wood	532	5	-	-	-	-	[135]
Wood and <i>babassu mesocarp</i>	266	-	5-20	5-25	0-0.4	-	[136]

The extensive literature list of Table 1 shows that there have been many studies on biological material and agricultural products, but there are very few related to pasture. Studying fresh herbage using LIBS has not been explored in-depth. Chauhan et al. [17] used fresh Bermuda grass in their study of Si distribution within leaves. Spectra were averaged and the Si I 288.15 nm emission line was used to analyse the amount of silicon at different locations on the leaves. Jull et al. [137] investigated fresh and dried, pelletized pasture in air and under an argon atmosphere using PLS. The root mean square error of cross-validation (RMSECV) of the models were better for pellets, but the fresh pasture models had better precision. The pellet spectra exhibited less between-sample variation because the moisture was removed from the samples. The moisture reduced the intensity of the fresh pasture emission lines. An explanation of the limiting factors inhibiting calibrations were given for each macro and micro nutrient. The best results were obtained for K, Na, and Mn. Jull et al. [138] studied temperature correction on pasture spectra using Boltzmann plots, Saha-Boltzmann plots, and internal standards. The Boltzmann plot and Saha-Boltzmann plot methods needed additional emission lines, confirmation of local thermodynamic equilibrium, and the degree of instrument broadening to produce better accuracies. PLS models were created using spectra normalised to carbon lines. Violet band and swan band heads produced better results. The best results were generated by taking the ratio of two emission lines with similar upper level electron energies. Boyain-Goitia et al. [67] investigated similarities between fresh grass fragments and pollen using LIBS spectra. The main difference was that the pollen spectra had Cr and Fe emission lines. Concentrations for Ca and Al were similar for the samples. Differentiating between the samples was hard due to the limited number of samples. Si was found in the grass spectra. This was attributed to soil dust on the samples. It was found that normalising the spectra with the CN violet band produced a reduction in matrix effects.

There have been other studies on grass that did not use fresh samples. Bermuda grass (*Cynodon dactylon*) was investigated for a possible treatment for diabetics by Rai et al. [18]. The sap in the samples was removed, and the resulting plant material was crushed and lyophilized into powders which were dissolved in distilled water. The C III 229.6 nm line was used to normalise the emission lines of interest. The resulting ratios identified that certain amounts of K, Na, and Mg in Bermuda grass

have antidiabetic effects. Tall Fescue Grass (*Festuca arundinacea*) was formed into pellets and investigated for endophyte infection by Martin et al. [107]. The small number of samples made it difficult to discriminate between healthy and infected grass. Braga et al. [14] used pelletized grass (*Axonopus obtusifolius*) to validate micronutrient calibration models. The study compared multivariate (PLS) and univariate calibrations. The spectra were normalised by the C I 193.09 nm line to reduce variations. The PLS models performed better than the univariate models. The physical and chemical makeup of the samples used in the calibration should be similar to the intended plant species to be studied. This will produce superior calibrations. Pelletized pasture samples were used to create calibration models for macro and micronutrients by Devey et al. [64]. LIBS was compared to inductively coupled plasma - optical emission spectroscopy (ICP-OES). The spectra were processed using Savitzky Golay (SG) smoothing, vector normalisation, and wavelet smoothing before PLS models were generated on different spectral regions using selected wavelengths only. The best results were found for Na, K, Ca, and P and were similar to those for ICP-OES.

Experimental setup

A LIBS-6 (Applied Photonics, UK) system with a Nd:YAG laser (Big Sky Ultra, Quantel, France) operating at 1064 nm with a pulse width of 7 ns, and pulse energy of 100 mJ was focused perpendicular to the sample surface to generate the plasma. The setup had a fixed distance to the sample. Each spectrum was acquired with six (Avantes, The Netherlands) spectrometers in a LIBS-6 unit covering the range 182.26-908.07 nm. All spectrometers were set to start recording after a delay time of 1.27 μ s with respect to the laser pulse and an integration time of 1 ms. A 3-axis translation stage was employed to move the sample so that each LIBS pulse was on a fresh surface but at the same height.

Fresh pasture (a mix of ryegrass and clover) from 20 different plots was harvested over a 13 month period creating a total of 280 samples. The fresh pasture was pressed flat in a holder. An accumulation of 100 shots under an air atmosphere, and 100 shots under an argon purge were taken for each batch of harvested pasture. Each shot was taken from a new location on the sample. The pasture samples were

sent to a commercial analytical laboratory where they were dried at 62°C overnight and ground to pass through a 1 mm screen. Nitrogen was estimated by Dumas combustion calibrated NIR. All other elements were determined by nitric acid/hydrogen peroxide digestion followed by ICP-OES. Table 2 contains the limits of detection for the qualitative analysis performed by the laboratory. A portion of the powder was returned and pellets were pressed for each batch of harvested pasture. An accumulation of 100 shots under an air atmosphere, and 100 shots under an argon purge were taken for each pellet. Each shot was taken from a new location on the sample. All spectra were corrected for dark current and background.

Data treatment

Building quantitative models on raw spectroscopic data can lead to low correlations. Pre-processing can enhance the data by removing noise and recovering peaks. Regression techniques can then build models on improved data, producing better results. Pre-processing of data includes smoothing, removal of dark current and background, and transformations. After pre-processing, calibrations are produced. Simple univariate linear regression on LIBS spectra can produce poor results due to the variations in the data. These variations include nonlinearities, interferences, and noise. The advantages of using multivariate over univariate models include data compression, reduction of noise, increased tolerance of interferences, instrument selectivity becomes less important, and outliers are easily detected. The multivariate models also provide information on which variables are important in the calibration [139]. Multivariate chemometric methods can build models on the entire spectrum captured by the spectrometers whereas univariate methods only use one wavelength, or more in the case of internal normalisation. The methods used in this study are briefly explained. A detailed explanation can be found in the references quoted.

Table 2. Description of the macro and micro nutrients in the dataset determined by a commercial analytical laboratory.

Element	Range	Mean	Detection limit
N (wt. %)	1.8-4.0	2.8±0.49	0.1
P (wt. %)	0.25-0.59	0.36±0.054	0.02
K (wt. %)	1.0-4.0	2.7±0.68	0.1

S (wt. %)	0.23-0.46	0.33±0.042	0.02
Ca (wt. %)	0.39-1.31	0.68±0.18	0.02
Mg (wt. %)	0.12-0.28	0.19±0.03	0.02
Na (wt. %)	0.0730-0.608	0.26±0.12	0.002
Fe (mg/kg)	48-644	100±82	5
Mn (mg/kg)	30-144	61±25	3
Zn (mg/kg)	16-82	44±57	2
Cu (mg/kg)	5-12	7.5±1.8	1
B (mg/kg)	3-16	6.2±3.0	1

Savitzky Golay

A SG filter is a type of filter that is used for reducing noise, thus smoothing the data [140]. The result is an increase to the signal-to-noise ratio without overly distorting the data. Filtering is done by applying a polynomial function to a windowed set of the data and then adjusting the coefficients of the polynomial to minimise the mean-squared approximation error for the window. The central data point in the window is then replaced with the new value obtained from the polynomial function. The window is propagated through the entire data set until all data points have been processed. SG filtering can be used to calculate the derivatives of a signal.

Multiple Linear Regression

MLR is an extended version of simple linear regression which builds a model between the variables in the predictors and the output responses [141]. The predictor variables are regressed to find constant regression coefficients that minimises the sum of squares on the responses. Problems occur when some of the predictors are strongly correlated with each other (multicollinearity), or with a linear combination of several predictors.

Principal Component Regression

PCR compresses data by creating new variables called Principal Components (PCs) [141]. The PCs are linear combinations of the predictors and are uncorrelated. The first PC contains as much of the variability in the predictors as possible. Each successive PC accounts for the highest amount of variance in an orthogonal direction to the preceding PCs. With a small number of PCs the data set can be reduced but still retains a large portion of the variability. The drawback of PCR is

that the variance caught by some of the PCs does not correspond to the responses. Thus there are various ways to determine which PCs to retain.

Partial Least-Squares Regression

PLS is a chemometric technique that has been employed to overcome the drawbacks of between spectra variability, which is not related to the responses [141]. PLS is used when there are many variables, compared to observations, and when there is high collinearity between variables. This is perfectly suited to LIBS spectra that have thousands of variables, many of which are collinear. PLS maximises the covariance between the predictors and responses by projecting the responses and the predictors to a new space. An underlying relationship can be found that is not easily detected by inspecting the spectra. This relationship is conveyed through the Latent Variables (LVs) which, like PCs, are a compression of the original data. PLS has found great success building calibration models that perform better than simple linear regression of a single emission line [97, 142].

Gaussian Process Regression

Gaussian process regression (GP) generates nonparametric kernel-based probabilistic models [143]. They take a collection of random variables which defines a distribution over functions. This is done by including only those functions that agree with the observations reducing the uncertainty around those data points. A noise function is added to the model that explains how much deviation there is between the response and function values. The function used in this study is the squared exponential covariance function, also known as the radial basis function. Tuning of the noise and length-scale parameters is needed to produce an accurate model.

Artificial Neural Networks

ANN are a group of techniques that based on the workings of biological systems. A feed-forward network is one of the types of ANN that handles nonlinearities in data [141]. The predictors are called the input layer and the responses are called the output layer. Between these layers are hidden layers that are comprised of elements called neurons. Each input to a neuron has an associated weighting which it is multiplied by before being summed and passed on to all the neurons in the next layer. The output layer and neurons are non-linear functions of linear combinations

from the input layer and are commonly a sigmoid function. To train the network back-propagation is commonly used to update the regression coefficients as each observation is processed by the network. This continues until the prediction error is as small as possible.

Chemometric methods can fail when there are a large number of predictors and not enough data in the responses. Dimension reduction is a method of overcoming this problem. Techniques such as PCR and PLS compress the data into a few new variables (PCs and LVs). The scores from these can then be used as inputs for methods like ANN and GP significantly improving results [144, 145].

Figures of merit

To ensure that statistical results generalise for prediction of an independent dataset a model validation technique known as cross-validation may be used [146]. Cross-validation splits the data up into training and test sets. A model is created on the training set and then evaluated on the test set. The process is repeated choosing a new test set which was not a part of the previous test set. This continues until each observation has been included in a test set. The number of iterations and the size of the test and training sets are determined by the split in the dataset. The percentage split is determined by how many folds are specified, this is known as k -fold cross-validation. A moderate number for k reduces the variance, increasing the performance of the method [147]. In this study 10-fold cross-validation is used. The accuracy of a model is determined by the difference between the predicted results and the actual responses.

One measure of accuracy for a cross-validated model is the RMSECV, which is calculated as

$$\text{RMSECV} = \sqrt{\frac{\sum_{i=1}^n (\hat{y}_i - y_i)^2}{n}} \quad (1)$$

where \hat{y} are the predictions from the cross-validation for the i -th sample which was not used in building the model for that fold, y are the actual responses, and n is the number of samples. Normalizing the RMSECV provides a better comparison

between the models created for the different nutrients. The normalized root mean squared error of cross-validation (NRMSECV) is

$$\text{NRMSECV} = \frac{\text{RMSECV}}{y_{\max} - y_{\min}} \quad (2)$$

where y_{\max} and y_{\min} refer to the maximum and minimum concentrations of the particular nutrient the model was built for. The result is expressed as a percentage.

Calibration models for N, P, K, S, Ca, Mg, Na, Fe, Mn, Zn, Cu, and B were generated using multiple chemometric methods. No standardisation was done on the spectra before analyses. SG filtering, SG first derivative, and SG second derivative were performed on the spectra followed by PLS to find out if this form of pre-processing would benefit this particular type of data. The harvest site and date were investigated with PCR to determine whether this information would explain some variations in the data. PCR performed on the spectra alone was used for a comparison. MLR, PCR, PLS, PLS+GP, PCR+ANN, and PLS+ANN performed on the spectra were compared to determine which method would be best for pasture. The results were used to investigate the effects that argon and moisture had on the models. All methods used were investigated using 10-fold cross-validation to tune the parameters (number of latent variables, noise and length-scale, principal components, and neurons) reducing the RMSECV. The software packages that were used were Matlab (MathWorks, US) and Weka (The University of Waikato, NZ) (for a description of the software refer to [148]).

Results and Discussion

Savitzky Golay filtering

SG filtering was investigated to see if improvements could be made through pre-processing the spectra. SG, SG first derivative, and SG second derivative filtering followed by PLS were performed on the four datasets (fresh pasture in air, fresh pasture under argon, pellets in air, and pellets under argon) and compared to PLS with no filtering. A 6th order polynomial fit with a window length of 11 were used for filtering with the number of LVs depending on the element for the model.

SG filtering of LIBS spectra from nitrogen in pellets sampled in air resulted in a reduction in NRMSECV of 1.7 % which was the only model to show a decrease of NRMSECV greater than 1 %. Overall SG was considered ineffective since there was little to no reduction in NRMSECV. For this reason, it was not used in any further analyses.

Categorical data

There may be perturbations between samples caused by site specific environmental effects and date specific events. These are hard to identify through visual inspection, but the influence can be detected and compensated for through chemometric techniques such as PCR and ANN. PCR and PCR+ANN were used to investigate whether including categorical data (date and site of harvest) would increase predictions in the models. There were six neurons in the first hidden layer and three in the second hidden layer for each model. The number of PCs depended on the element analysed.

There was very little change in the results using the categorical data. The biggest change recorded was a 0.2 % decrease in NRMSECV when including the categorical data for potassium in pellet samples in argon. Performing ANN after PCR did not significantly increase the accuracy of the models. The model that had the largest improvement in NRMSECV, using PCR+ANN, was sulphur (0.4 %) in pellets under argon.

Argon and moisture effects

Argon is commonly used in plasma spectroscopy to increase the electron density and temperature in plasmas. The chemometric methods used to investigate the effects of an argon purge were MLR, PCR, PLS, PLS+GP, PCR+ANN, and PLS+ANN. The noise and length-scale parameters were optimised with values of 0.01 and 5.77 respectively for GP and 6 neurons in the first hidden layer and 3 in the second hidden layer for ANN. The number of PCs and LVs were dependant on the element of interest.

Using an argon purge produced small differences. The changes can be seen in Fig. 1. The NRMSECV for these models were averaged to see the overall effect that argon had on fresh and pelletized pasture. Table 3 displays the results. Models created from fresh pasture under argon for N, K, Fe, Mn, Zn, and B produced NRMSECV over 1 % better than models created in air, Mn having the largest increase of 2.1 %. Pelletized pasture models created under argon only produced 1.2 % better NRMSECV for N and Cu. NRMSECV for Ca and B were worse, a decrease of 1.2 % and 1.6 %, respectively.

There is a marked increase in accuracy for models built on pellets compared to models built on fresh samples, due to the reduction in moisture content in the samples. The moisture changes the breakdown threshold of a material which increases both within-sample and between-sample variations [79]. Fig. 1 and Table 3 show that removing the moisture in the pasture leads to an average increase in accuracy of 4-5 % with the highest increase recorded for B, that of 9.6 %. The increase may also be partially attributed to the increased homogenisation produced by grinding the samples. Fresh pasture will have different nutrient distributions in each blade of grass.

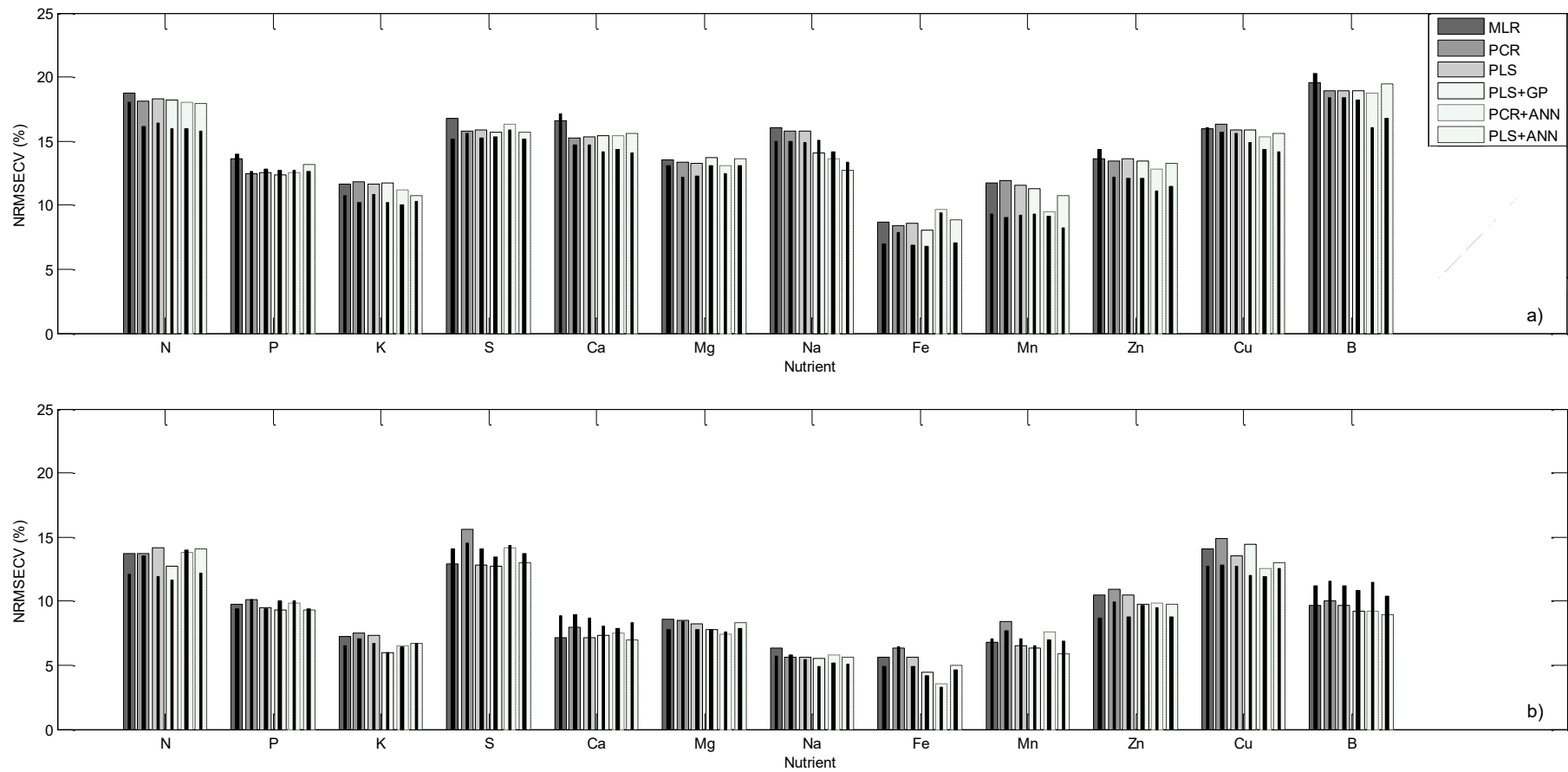


Fig. 1. Accuracy of models created for (a) fresh and (b) pelletized pasture. The bars indicate NRMSECV produced from spectra recorded in air and the solid black lines within the bars represent values created under argon.

Table 3. Average NRMSECV values calculated from MLR, PCR, PLS, PLS+GP, PCR+ANN, and PLS+ANN. The uncertainty is one standard deviation.

Element	Fresh pasture		Pelletized pasture	
	In air	Under argon	In air	Under argon
N (%)	18.2 ±0.3	16.4 ±0.8	13.7 ±0.5	12.5 ±0.9
P (%)	12.8 ±0.5	12.9 ±0.5	9.6 ±0.3	9.7 ±0.4
K (%)	11.5 ±0.4	10.4 ±0.3	6.9 ±0.6	6.5 ±0.4
S (%)	16.0 ±0.4	15.4 ±0.3	13.5 ±1.1	14.0 ±0.4
Ca (%)	15.6 ±0.5	14.9 ±1.2	7.3 ±0.3	8.5 ±0.4
Mg (%)	13.4 ±0.2	12.7 ±0.5	8.1 ±0.5	7.9 ±0.3
Na (%)	14.7 ±1.4	14.6 ±0.7	5.8 ±0.3	5.4 ±0.4
Fe (%)	8.7 ±0.5	7.5 ±1.0	5.1 ±1.0	4.7 ±1.0
Mn (%)	11.1 ±0.9	9.0 ±0.4	6.9 ±0.9	7.0 ±0.4
Zn (%)	13.4 ±0.3	12.2 ±1.1	10.2 ±0.5	9.2 ±0.6
Cu (%)	15.8 ±0.3	15.1 ±0.8	13.7 ±0.9	12.5 ±0.4
B (%)	19.1 ±0.3	18.0 ±1.5	9.5 ±0.4	11.1 ±0.5

Comparison of models

Comparing the different chemometric algorithms, there were mixed results with no single method outperforming the rest. Different techniques worked better on different elements. Fig. 2 and Fig. 3 display the best calibration curves generated for fresh pasture in air and pelletized pasture under argon. Looking at which methods produced the best models for each element in the different datasets (fresh pasture in air, fresh pasture under argon, pelletized pasture in air, and pelletized pasture under argon) can give a general overview of which algorithm performed best overall.

Looking at the best performing models for the 12 nutrients from the 4 data sets showed that PLS+GP, PCR+ANN, and PLS+ANN were the best algorithms producing 19, 15, and 7 of the 48 models respectively. MLR, PCR, and PLS only produced only one, four, and two of the best models. Looking specifically at elements that produce models with R^2 values over 0.8 and NRMSECV under 10 %, the more complex methods, PLS+GP, PCR+ANN, and PLS+ANN produced models with higher accuracy for K, Na, Ca under argon, Mg and Fe in pelletized samples, and Mn in air. The largest improvement was a reduction in NRMSECV of 3.3 % when comparing the PLS+ANN model with the MLR model for Na in fresh

pasture. The time taken to perform ANN is the compromise for increasing the accuracy of the model. Inspection of Fig. 2 and Fig. 3 shows that there are two groupings of concentrations for K and Mn. The low K and high Mn concentrations harvested in March 2014 were caused by a drought in the region. The non-Normal range of concentrations provides added leverage for R^2 and NRMSECV values making them look similar to other elements.

Table 4 displays the RMSECV values to provide a better idea of how the predictions are distributed. The data in Table 4 was made by choosing the best RMSECV with the best R^2 value from all algorithms. K has the second worst RMSECV out of the macronutrients, but because of the range of concentrations in the samples it has one of the best correlation coefficients even without the drought data.

Another way to increase the predictive ability of the models is to build them on better data with stronger, consistent emissions. The spectra in this work had weak emission lines for N, P, Mg, Fe, and Cu. Zn lines only appeared under an argon atmosphere, and B lines were only visible on a few occasions. The major problem with N comes from the N contribution in the atmosphere. Using argon did increase the accuracy of the N models. Emissions for S could not be obtained with the spectrometers used in this work, so the models would have been created on inferred data. The strongest line for P had interferences from Fe which would limit quantitative analysis. Ca and Mg produced some of the better models even though some of the emissions from these elements were not from ionised Ca and Mg. The ratio of neutral calcium to ionised calcium changes from shot to shot producing varying spectra for the same sample. This is the same for magnesium.

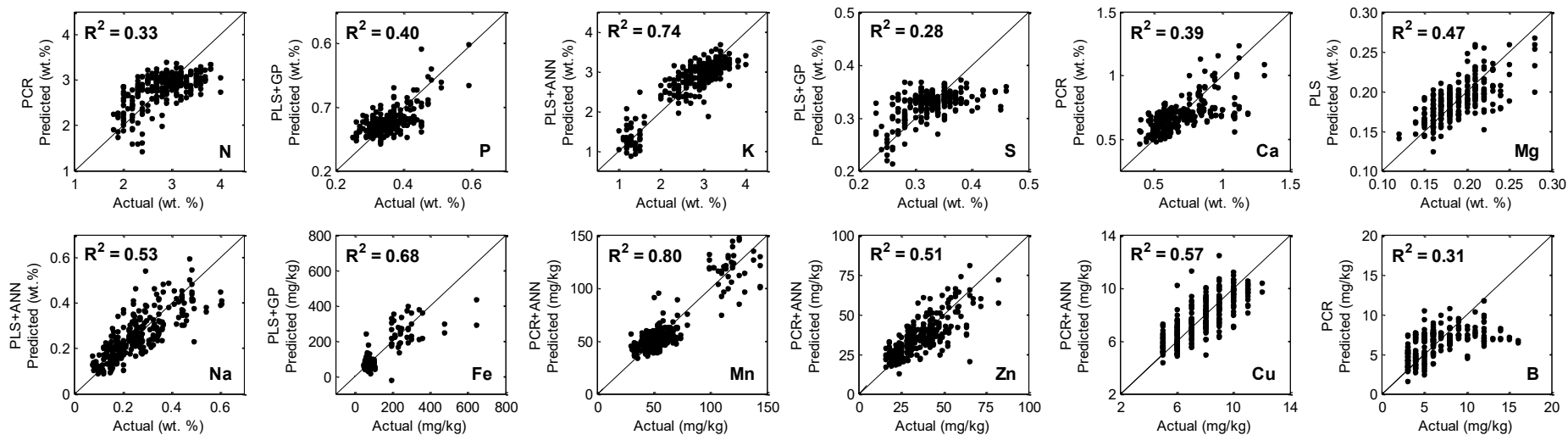


Fig. 2. The best calibrations created for fresh pasture in air.

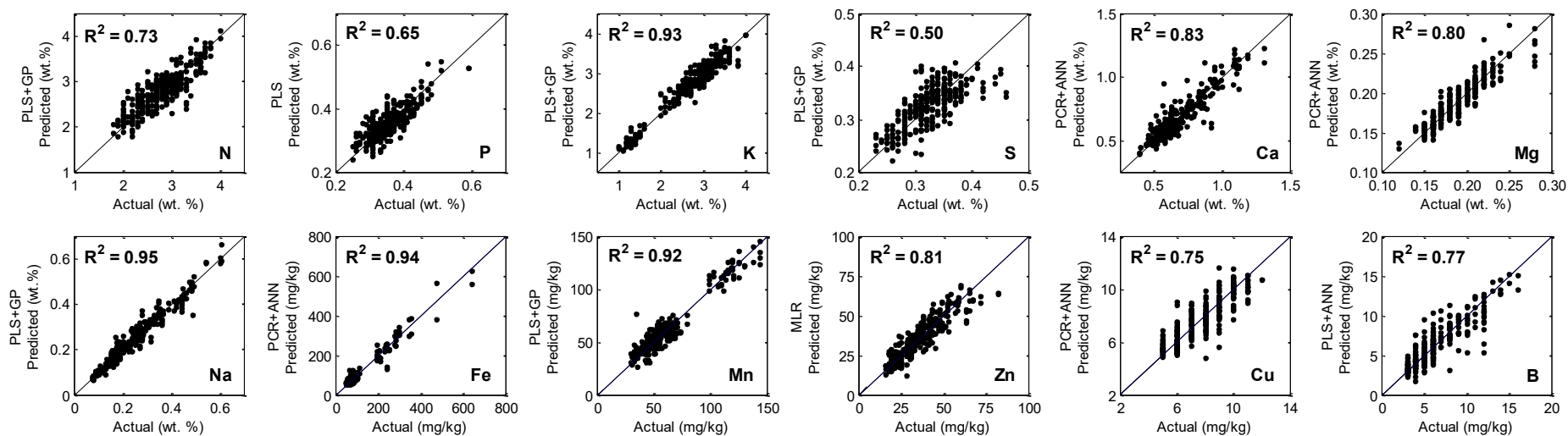


Fig. 3. The best calibrations created for pelletized pasture under argon.

Table 4. The best algorithms for the nutrients in each dataset.

Element	Pasture in air		Pasture under argon		Pellets in air		Pellets under argon	
	Method	RMSECV	Method	RMSECV	Method	RMSECV	Method	RMSECV
N (wt. %)	PCR	0.40	PLS+GP	0.35	PLS+GP	0.28	PLS+GP	0.26
P (wt. %)	PLS+GP	0.042	PLS+GP	0.043	PLS+GP	0.032	PLS	0.032
K (wt. %)	PLS+ANN	0.32	PCR+ANN	0.30	PLS+GP	0.18	PLS+GP	0.18
S (wt. %)	PLS+GP	0.036	PLS+GP	0.035	PLS+GP	0.029	PLS+GP	0.031
Ca (wt. %)	PCR	0.14	PLS+GP	0.13	PLS+ANN	0.064	PCR+ANN	0.073
Mg (wt. %)	PLS	0.021	PCR	0.020	PCR+ANN	0.012	PCR+ANN	0.012
Na (wt. %)	PLS+ANN	0.068	PCR+ANN	0.076	PLS+GP	0.030	PLS+GP	0.026
Fe (mg/kg)	PLS+GP	48	PLS+GP	41	PCR+ANN	21	PCR+ANN	20
Mn (mg/kg)	PCR+ANN	11	PLS+ANN	9.4	PLS+ANN	6.7	PLS+GP	7.4
Zn (mg/kg)	PCR+ANN	8.5	PCR+ANN	7.3	PLS+GP	6.5	MLR	5.7
Cu (mg/kg)	PCR+ANN	1.1	PCR+ANN	1.0	PCR+ANN	0.88	PCR+ANN	0.84
B (mg/kg)	PCR	2.5	PCR+ANN	2.1	PLS+ANN	1.2	PLS+ANN	1.3

In field application

As discussed above, the major issue with LIBS measurements on pasture is variability. The chemometric methods used in this study provide reasonable models to estimate semi-quantitative levels of nutrients. These laboratory results indicate how an in field system would perform minus the added in field variability. For in field use to be realised, improved models from better quality spectra with less shot-to-shot variation are needed [149]. The variations in experimental parameters, surface roughness, and local inhomogeneity may be mitigated by increasing the spot size and ablating more material. Finding a way to normalise the spectra to disregard moisture would help increase predictability of quantitative calibration models. Accurate chemometric models can be produced once these factors are minimised. Infield implementation can then be realised for fresh pasture using a LIBS sensor to determine fertilizer application and rate in real time.

Conclusions

SG filtering was ineffective, there was little to no reduction in NRMSECV since the main source of disparity is shot-to-shot variation, not noise in the spectra. Including categorical data for PCR and PCR+ANN did not produce a significant increase in prediction. The use of an argon purge increased the predictive capability in fresh samples with a reduction of over 1 % in NRMSECV for N, K, Fe, Mn, Zn,

and B. For pelletised samples only N, Cu, and Zn had an improvement over 1 % in NRMSECV with Ca and B producing a decrease of 1.2 % and 1.6 %, respectively. The highest increase in predictive ability was produced by using dried pellets instead of fresh samples. The reduction in moisture led to models having an average increase in accuracy of 4-5 %. No single chemometric method provided improvement for all nutrients. The algorithms that performed the best were PLS+GP, PCR+ANN, and PLS+ANN.

To increase the predictive ability of chemometric models improved spectra are needed and the shot-to-shot variation needs to be reduced. Temperature differences between plasmas is a main factor contributing to the variations. Ca and Mg suffer the most from the temperature difference between plasmas because the temperature changes the amount of Ca and Mg being ionised. This significantly changes the intensities of the neutral and ionised emission lines. Other issues that need resolving are that some of the nutrients displayed weak lines or interferences from other lines and the surrounding atmosphere. The chemometric methods used in this study provide reasonable models. Before infield use is viable, a moisture normalisation method needs to be developed to produce accuracies similar to that of dried pasture.

Acknowledgements

We would like to acknowledge and offer continuing respect and admiration to deceased colleague Dr. Sadhana Talele, who was not able to see this work completed.

This work was supported by New Zealand's Ministry of Business, Innovation and Employment under contract C11X1209

References

- [1] M. van Maarschalkerweerd and S. Husted, "Recent developments in fast spectroscopy for plant mineral analysis," *Frontiers in Plant Science*, vol. 6, p. 169, 2015.
- [2] D. Cremers and L. Radziemski, "Introduction," in *Handbook of Laser-Induced Breakdown Spectroscopy*, 2nd ed West Sussex, UK: John Wiley & Sons Ltd, 2013, p. 3.

- [3] S. N. Thakur, "Atomic emission spectroscopy," in *Laser-Induced Breakdown Spectroscopy*, J. P. Singh and S. N. Thakur, Eds., ed Oxford, UK: Elsevier, 2007, pp. 29-30.
- [4] D. W. Hahn and N. Omenetto, "Laser-induced breakdown spectroscopy (LIBS), part II: Review of instrumental and methodological approaches to material analysis and applications to different fields," *Applied Spectroscopy*, vol. 66, pp. 347-419, 2012.
- [5] G. Galbács, I. B. Gornushkin, B. W. Smith, and J. D. Winefordner, "Semi-quantitative analysis of binary alloys using laser-induced breakdown spectroscopy and a new calibration approach based on linear correlation," *Spectrochimica Acta - Part B Atomic Spectroscopy*, vol. 56, pp. 1159-1173, 2001.
- [6] S. Palanco and J. J. Laserna, "Full automation of a laser-induced breakdown spectrometer for quality assessment in the steel industry with sample handling, surface preparation and quantitative analysis capabilities," *Journal of Analytical Atomic Spectrometry*, vol. 15, pp. 1321-1327, 2000.
- [7] R. Wisbrun, I. Schechter, R. Niessner, H. Schröder, and K. L. Kompa, "Detector for trace elemental analysis of solid environmental samples by laser plasma spectroscopy," *Analytical Chemistry*, vol. 66, pp. 2964-2975, 1994.
- [8] U. Panne, M. Clara, C. Haisch, and R. Niessner, "Analysis of glass and glass melts during the vitrification of fly and bottom ashes by laser-induced plasma spectroscopy. Part II. Process analysis," *Spectrochimica Acta Part B: Atomic Spectroscopy*, vol. 53, pp. 1969-1981, 1998.
- [9] J. B. Sirven, B. Bousquet, L. Canioni, and L. Sarger, "Laser-induced breakdown spectroscopy of composite samples: Comparison of advanced chemometrics methods," *Analytical Chemistry*, vol. 78, pp. 1462-1469, 2006.
- [10] D. Cremers and L. Radziemski, "LIBS apparatus fundamentals," in *Handbook of Laser-Induced Breakdown Spectroscopy*, D. Cremers and L. Radziemski, Eds., 2nd ed West Sussex, UK: John Wiley & Sons Ltd, 2013, pp. 69-121.

- [11] M. Garcimuño, D. M. Díaz Pace, and G. Bertuccelli, "Laser-induced breakdown spectroscopy for quantitative analysis of copper in algae," *Optics and Laser Technology*, vol. 47, pp. 26-30, 2013.
- [12] L. Niu, H. H. Cho, K. S. Song, H. Cha, Y. Kim, and Y. I. Lee, "Direct determination of strontium in marine algae samples by laser-induced breakdown spectrometry," *Applied Spectroscopy*, vol. 56, pp. 1511-1514, 2002.
- [13] M. M. El-Deftar, J. Robertson, S. Foster, and C. Lennard, "Evaluation of elemental profiling methods, including laser-induced breakdown spectroscopy (LIBS), for the differentiation of Cannabis plant material grown in different nutrient solutions," *Forensic Science International*, vol. 251, pp. 95-106, 2015.
- [14] J. W. B. Braga, L. C. Trevizan, L. C. Nunes, I. A. Rufini, D. Santos Jr, and F. J. Krug, "Comparison of univariate and multivariate calibration for the determination of micronutrients in pellets of plant materials by laser induced breakdown spectrometry," *Spectrochimica Acta - Part B Atomic Spectroscopy*, vol. 65, pp. 66-74, 2010.
- [15] L. C. Trevizan, D. Santos Jr, R. E. Samad, N. D. Vieira Jr, L. C. Nunes, I. A. Rufini, and F. J. Krug, "Evaluation of laser induced breakdown spectroscopy for the determination of micronutrients in plant materials," *Spectrochimica Acta - Part B Atomic Spectroscopy*, vol. 64, pp. 369-377, 2009.
- [16] L. C. Trevizan, D. Santos Jr, R. E. Samad, N. D. Vieira Jr, C. S. Nomura, L. C. Nunes, I. A. Rufini, and F. J. Krug, "Evaluation of laser induced breakdown spectroscopy for the determination of macronutrients in plant materials," *Spectrochimica Acta - Part B Atomic Spectroscopy*, vol. 63, pp. 1151-1158, 2008.
- [17] D. K. Chauhan, D. K. Tripathi, N. K. Rai, and A. K. Rai, "Detection of Biogenic Silica in Leaf Blade, Leaf Sheath, and Stem of Bermuda Grass (*Cynodon dactylon*) Using LIBS and Phytolith Analysis," *Food Biophysics*, vol. 6, pp. 416-423, 2011.
- [18] P. K. Rai, D. Jaiswal, N. K. Rai, S. Pandhija, A. K. Rai, and G. Watal, "Role of glycemic elements of *Cynodon dactylon* and *Musa paradisiaca* in

- diabetes management," *Lasers in Medical Science*, vol. 24, pp. 761-768, 2009.
- [19] M. Iqbal, Z. ul Haq, A. Malik, C. M. Ayoub, Y. Jamil, and J. Nisar, "Pre-sowing seed magnetic field stimulation: A good option to enhance bitter gourd germination, seedling growth and yield characteristics," *Biocatalysis and Agricultural Biotechnology*, vol. 5, pp. 30-37, 2016.
- [20] N. K. Rai, P. K. Rai, S. Pandhija, G. Watal, A. K. Rai, and D. Bicanic, "Application of LIBS in detection of antihyperglycemic trace elements in *Momordica charantia*," *Food Biophysics*, vol. 4, pp. 167-171, 2009.
- [21] P. Zheng, M. Shi, J. Wang, and H. Liu, "The spectral emission characteristics of laser induced plasma on tea samples," *Plasma Science and Technology*, vol. 17, pp. 664-670, 2015.
- [22] G. G. A. de Carvalho, D. Santos Jr, M. da Silva Gomes, L. C. Nunes, M. B. B. Guerra, and F. J. Krug, "Influence of particle size distribution on the analysis of pellets of plant materials by laser-induced breakdown spectroscopy," *Spectrochimica Acta Part B: Atomic Spectroscopy*, vol. 105, pp. 130-135, 2015.
- [23] M. R. Martelli, F. Brygo, P. Delaporte, X. Rouau, and C. Barron, "Estimation of Wheat Grain Tissue Cohesion via Laser Induced Breakdown Spectroscopy," *Food Biophysics*, vol. 6, pp. 433-439, 2011.
- [24] L. Krajcarová, K. Novotný, M. Kummerová, J. Dubová, V. Gloser, and J. Kaiser, "Mapping of the spatial distribution of silver nanoparticles in root tissues of *Vicia faba* by laser-induced breakdown spectroscopy (LIBS)," *Talanta*, vol. 173, pp. 28-35, 2017.
- [25] S. Awasthi, R. Kumar, A. Devanathan, R. Acharya, and A. K. Rai, "Multivariate methods for analysis of environmental reference materials using laser-induced breakdown spectroscopy," *Analytical Chemistry Research*, vol. 12, pp. 10-16, 2017.
- [26] M. Galiová, J. Kaiser, K. Novotný, M. Hartl, R. Kizek, and P. Babula, "Utilization of laser-assisted analytical methods for monitoring of lead and nutrition elements distribution in fresh and dried *Capsicum annum* l. leaves," *Microscopy Research and Technique*, vol. 74, pp. 845-852, 2011.

- [27] N. Shukla, A. S. Bharti, S. Srivastava, and K. N. Uttam, "Determination of Elements in Carrot Root by Laser Induced Breakdown Spectroscopy," *National Academy Science Letters*, vol. 40, pp. 47-51, 2017.
- [28] C. R. Bhatt, B. Alfarraj, C. T. Ghany, F. Y. Yueh, and J. P. Singh, "Comparative Study of Elemental Nutrients in Organic and Conventional Vegetables Using Laser-Induced Breakdown Spectroscopy (LIBS)," *Applied Spectroscopy*, vol. 71, pp. 686-698, 2017.
- [29] M. Yao, H. Yang, L. Huang, T. Chen, G. Rao, and M. Liu, "Detection of heavy metal Cd in polluted fresh leafy vegetables by laser-induced breakdown spectroscopy," *Applied Optics*, vol. 56, pp. 4070-4075, 2017.
- [30] J. Wang, P. Zheng, H. Liu, and L. Fang, "Classification of Chinese tea leaves using laser-induced breakdown spectroscopy combined with the discriminant analysis method," *Analytical Methods*, vol. 8, pp. 3204-3209, 2016.
- [31] M. M. Suliyanti, M. Pardede, T. J. Lie, K. H. Kurniawan, A. Khumaeni, K. Kagawa, M. O. Tjia, and Y. I. Lee, "Direct powder analysis by laser-induced breakdown spectroscopy utilizing laser-controlled dust production in a small chamber," *Journal of the Korean Physical Society*, vol. 58, pp. 1129-1134, 2011.
- [32] F. M. V. Pereira, D. M. B. P. Milori, A. L. Venâncio, M. D. S. T. Russo, P. K. Martins, and J. Freitas-Astúa, "Evaluation of the effects of *Candidatus Liberibacter asiaticus* on inoculated citrus plants using laser-induced breakdown spectroscopy (LIBS) and chemometrics tools," *Talanta*, vol. 83, pp. 351-356, 2010.
- [33] A. C. Ranulfi, R. A. Romano, A. Bebechibuli Magalhães, E. J. Ferreira, P. Ribeiro Villas-Boas, and D. Marcondes Bastos Pereira Milori, "Evaluation of the Nutritional Changes Caused by Huanglongbing (HLB) to Citrus Plants Using Laser-Induced Breakdown Spectroscopy," *Applied Spectroscopy*, vol. 71, pp. 1471-1480, 2017.
- [34] E. J. Ferreira, E. C. Ferreira, A. C. B. Delbem, and D. M. B. P. Milori, "Ensemble of predictors and laser induced breakdown spectroscopy for certifying coffee," *Electronics Letters*, vol. 47, pp. 967-969, 2011.
- [35] M. A. Gondal, U. Baig, M. A. Dastageer, and M. Sarwar, "Determination of elemental composition of coffee using UV-pulsed laser induced

- breakdown spectroscopy," in *AIP Conference Proceedings*, Gizan, Saudi Arabia, 2016, p. 030007.
- [36] T. V. Silva, S. Z. Hubinger, J. A. Gomes Neto, D. M. B. P. Milori, E. J. Ferreira, and E. C. Ferreira, "Potential of Laser Induced Breakdown Spectroscopy for analyzing the quality of unroasted and ground coffee," *Spectrochimica Acta - Part B Atomic Spectroscopy*, vol. 135, pp. 29-33, 2017.
- [37] E. R. Schenk and J. R. Almirall, "Elemental analysis of cotton by laser-induced breakdown spectroscopy," *Applied Optics*, vol. 49, pp. C153-C160, 2010.
- [38] D. K. Kushawaha, M. Yadav, S. Chatterji, A. K. Srivastava, and G. Watal, " α -amylase and α -glucosidase inhibitory activity assessment of Cucurbita maxima seeds – A LIBS based study," *International Journal of Phytomedicine*, vol. 8, pp. 312-318, 2016.
- [39] J. N. Kunz, D. V. Voronine, B. A. Ko, H. W. H. Lee, A. Rana, M. V. Bagavathiannan, A. V. Sokolov, and M. O. Scully, "Interaction of femtosecond laser pulses with plants: towards distinguishing weeds and crops using plasma temperature," *Journal of Modern Optics*, vol. 64, pp. 942-947, 2017.
- [40] P. Modlitbová, K. Novotný, P. Pořízka, J. Klus, P. Lubal, H. Zlámalová-Gargošová, and J. Kaiser, "Comparative investigation of toxicity and bioaccumulation of Cd-based quantum dots and Cd salt in freshwater plant Lemna minor L," *Ecotoxicology and Environmental Safety*, vol. 147, pp. 334-341, 2018.
- [41] S. Mehta, P. K. Rai, D. K. Rai, N. K. Rai, A. K. Rai, D. Bicanic, B. Sharma, and G. Watal, "LIBS-based detection of antioxidant elements in seeds of Emblica officinalis," *Food Biophysics*, vol. 5, pp. 186-192, 2010.
- [42] R. K. Singh, S. Mehta, D. Jaiswal, P. K. Rai, and G. Watal, "Antidiabetic effect of Ficus bengalensis aerial roots in experimental animals," *Journal of Ethnopharmacology*, vol. 123, pp. 110-114, 2009.
- [43] D. Sun, M. Su, C. Dong, D. Zhang, and X. Ma, "A semi-quantitative analysis of essential micronutrient in folium lycii using laser-induced breakdown spectroscopy technique," *Plasma Science and Technology*, vol. 12, pp. 478-481, 2010.

- [44] H. Hu, L. Huang, M. Liu, T. Chen, P. Yang, and M. Yao, "Nondestructive determination of Cu residue in orange peel by laser induced breakdown spectroscopy," *Plasma Science and Technology*, vol. 17, pp. 711-715, 2015.
- [45] M. Yao, L. Huang, J. Zheng, S. Fan, and M. Liu, "Assessment of feasibility in determining of Cr in Gannan Navel Orange treated in controlled conditions by laser induced breakdown spectroscopy," *Optics & Laser Technology*, vol. 52, pp. 70-74, 2013.
- [46] A. A. Bol'shakov, J. H. Yoo, C. Liu, J. R. Plumer, and R. E. Russo, "Laser-induced breakdown spectroscopy in industrial and security applications," *Applied Optics*, vol. 49, pp. C132-C142, 2010.
- [47] P. K. Rai, N. K. Rai, A. K. Rai, and G. Watal, "Role of LIBS in elemental analysis of *Psidium guajava* responsible for glycemic potential," *Instrumentation Science and Technology*, vol. 35, pp. 507-522, 2007.
- [48] D. C. Zhang, X. Ma, W. Q. Wen, H. P. Liu, and P. J. Zhang, "Studies of laser induced-breakdown spectroscopy of holly leaves," *Journal of Physics: Conference Series*, vol. 185, p. 012058, 2009.
- [49] D.-C. Zhang, X.-W. Ma, W.-Q. Wen, P.-J. Zhang, X.-L. Zhu, B. Li, and H.-P. Liu, "Influence of Laser Wavelength on Laser-induced Breakdown Spectroscopy Applied to Semi-Quantitative Analysis of Trace-Elements in a Plant Sample," *Chinese Physics Letters*, vol. 27, p. 063202 (4 pp.), 2010.
- [50] X. Liu, J. Huang, Z. Wu, Q. Zhang, X. Shi, N. Zhao, S. Jia, and Y. Qiao, "Microanalysis of multi-element in *Juncus effusus* L. by LIBS technique," *Plasma Science and Technology*, vol. 17, pp. 904-908, 2015.
- [51] V. Diopan, V. Shestivska, O. Zitka, M. Galiova, V. Adam, J. Kaiser, A. Horna, K. Novotny, M. Liska, L. Havel, J. Zehnalek, and R. Kizek, "Determination of plant thiols by liquid chromatography coupled with coulometric and amperometric detection in lettuce treated by lead(II) ions," *Electroanalysis*, vol. 22, pp. 1248-1259, 2010.
- [52] J. Wang, S. Xue, P. Zheng, Y. Chen, and R. Peng, "Determination of Lead and Copper in *Ligusticum wallichii* by Laser-Induced Breakdown Spectroscopy," *Analytical Letters*, vol. 50, pp. 2000-2011, 2017.
- [53] S. Qamar, M. Aslam, and M. A. Javed, "Determination of Proximate Chemical Composition and Detection of Inorganic Nutrients in Maize (*Zea*

- mays L.)," in *Materials Today: Proceedings*, New York, USA, 2016, pp. 715-718.
- [54] O. Krystofova, V. Shestivska, M. Galiova, K. Novotny, J. Kaiser, J. Zehnalek, P. Babula, R. Opatrilova, V. Adam, and R. Kizek, "Sunflower plants as bioindicators of environmental pollution with lead (II) ions," *Sensors*, vol. 9, pp. 5040-5058, 2009.
- [55] C. Zhao, D. Dong, X. Du, and W. Zheng, "In-field, in situ, and in vivo 3-dimensional elemental mapping for plant tissue and soil analysis using laser-induced breakdown spectroscopy," *Sensors (Basel, Switzerland)*, vol. 16, p. 1764, 2016.
- [56] O. Samek, J. Lambert, R. Hergenroder, M. Liska, J. Kaiser, K. Novotny, and S. Kukhlevsky, "Femtosecond laser spectrochemical analysis of plant samples," *Laser Physics Letters*, vol. 3, pp. 21-5, 2006.
- [57] M. Barbaferi, R. Pini, A. Ciucci, and E. Tassi, "Field assessment of Pb in contaminated soils and in leaf mustard (*Brassica juncea*): The LIBS technique," *Chemistry and Ecology*, vol. 27, pp. 161-169, 2011.
- [58] Y. Mingyin, L. Jinlong, L. Muhua, L. Qiulian, and L. Zejian, "Discrimination of Ca, Cu, Fe, and Na in Gannan Navel orange by laser induced breakdown spectroscopy," in *4th Conference on Computer and Computing Technologies in Agriculture (CCTA)*, Nanchang, China, 2011, pp. 608-613.
- [59] D. K. Tripathi, A. K. Pathak, D. K. Chauhan, N. K. Dubey, A. K. Rai, and R. Prasad, "An efficient approach of Laser Induced Breakdown Spectroscopy (LIBS) and ICAP-AES to detect the elemental profile of *Ocimum L.* species," *Biocatalysis and Agricultural Biotechnology*, vol. 4, pp. 471-479, 2015.
- [60] M. Yao, M. Liu, J. Zhao, and L. Huang, "Identification of nutrition elements in orange leaves by laser induced breakdown spectroscopy," in *Intelligent Information Technology and Security Informatics (IITSI), 2010 Third International Symposium on*, Jingtangshan, China, 2010, pp. 398-401.
- [61] Z. Lei, M. Yao, M. Liu, Q. Peng, X. Zhang, T. Chen, and Y. Xu, "Analysis the macronutrients in Gannan navel oranges for three kinds of sample state by laser induced breakdown spectroscopy," in *Image and Signal Processing*

- (CISP), 2011 4th International Congress on, Shanghai, China, 2011, pp. 2464-2466.
- [62] X. Zhang, M. Yao, M. Liu, and Z. Lei, "Analysis of trace elements in leaves using laser-induced breakdown spectroscopy," in *5th International Conference on Computer and Computing Technologies in Agriculture, CCTA*, Beijing, China, 2011, pp. 334-339.
- [63] S. I. Gornushkin, I. B. Gornushkin, J. M. Anzano, B. W. Smith, and J. D. Winefordner, "Effective normalization technique for correction of matrix effects in laser-induced breakdown spectroscopy detection of magnesium in powdered samples," *Applied Spectroscopy*, vol. 56, pp. 433-436, 2002.
- [64] K. Devey, M. Mucalo, G. Rajendram, and J. Lane, "Pasture Vegetation Elemental Analysis by Laser-Induced Breakdown Spectroscopy," *Communications in Soil Science and Plant Analysis*, vol. 46, pp. 72-80, 2015.
- [65] Z. Haider, J. Ali, M. Arab, Y. B. Munajat, S. Roslan, R. Kamarulzman, and N. Bidin, "Plasma Diagnostics and Determination of Lead in Soil and Phaleria Macrocarpa Leaves by Ungated Laser Induced Breakdown Spectroscopy," *Analytical Letters*, vol. 49, pp. 808-817, 2016.
- [66] A. C. Samuels, F. C. DeLucia Jr, K. L. McNesby, and A. W. Miziolek, "Laser-induced breakdown spectroscopy of bacterial spores, molds, pollens, and protein: Initial studies of discrimination potential," *Applied Optics*, vol. 42, pp. 6205-6209, 2003.
- [67] A. R. Boyain-Goitia, D. C. S. Beddows, B. C. Griffiths, and H. H. Telle, "Single-pollen analysis by laser-induced breakdown spectroscopy and raman microscopy," *Applied Optics*, vol. 42, pp. 6119-6132, 2003.
- [68] S. Ma, X. Gao, K. Guo, M. Kahsay, and J. Lin, "Analysis of the element content in poplar tree leaves by femtosecond laser-induced breakdown spectroscopy," *Science China: Physics, Mechanics and Astronomy*, vol. 54, pp. 1953-1957, 2011.
- [69] W. Lei, V. Motto-Ros, M. Boueri, Q. Ma, D. Zhang, L. Zheng, H. Zeng, and J. Yu, "Time-resolved characterization of laser-induced plasma from fresh potatoes," *Spectrochimica Acta - Part B Atomic Spectroscopy*, vol. 64, pp. 891-898, 2009.

- [70] S. Beldjilali, W. L. Yip, J. Hermann, T. Baba-Hamed, and A. Belasri, "Investigation of plasmas produced by laser ablation using single and double pulses for food analysis demonstrated by probing potato skins," *Analytical and Bioanalytical Chemistry*, vol. 400, pp. 2173-2183, 2011.
- [71] S. Beldjilali, D. Borivent, L. Mercadier, E. Mothe, G. Clair, and J. Hermann, "Evaluation of minor element concentrations in potatoes using laser-induced breakdown spectroscopy," *Spectrochimica Acta - Part B Atomic Spectroscopy*, vol. 65, pp. 727-733, 2010.
- [72] V. Juvé, R. Portelli, M. Boueri, M. Baudalet, and J. Yu, "Space-resolved analysis of trace elements in fresh vegetables using ultraviolet nanosecond laser-induced breakdown spectroscopy," *Spectrochimica Acta - Part B Atomic Spectroscopy*, vol. 63, pp. 1047-1053, 2008.
- [73] A. Khumaeni, Z. S. Lie, H. Niki, K. H. Kurniawan, E. Tjoeng, Y. I. Lee, K. Kurihara, Y. Deguchi, and K. Kagawa, "Direct analysis of powder samples using transversely excited atmospheric CO₂ laser-induced gas plasma at 1 atm," *Analytical and Bioanalytical Chemistry*, vol. 400, pp. 3279-3287, 2011.
- [74] T. Flores, L. Ponce, M. Arronte, and E. de Posada, "Free-running and Q:Switched LIBS measurements during the laser ablation of Prickle Pears spines," *Optics and Lasers in Engineering*, vol. 47, pp. 578-583, 2009.
- [75] P. Dhar, I. Gembitsky, P. Rai, N. Rai, A. K. Rai, and G. Watal, "A Possible Connection Between Antidiabetic & Antilipemic Properties of Psoralea corylifolia Seeds and the Trace Elements Present: A LIBS Based Study," *Food Biophysics*, vol. 8, pp. 95-103, 2013/06/01 2013.
- [76] P. Dhar, I. Gembitsky, P. K. Rai, N. K. Rai, A. K. Rai, and G. Watal, "A Possible Connection Between Antidiabetic & Antilipemic Properties of Psoralea corylifolia Seeds and the Trace Elements Present: A LIBS Based Study," *Food Biophysics*, pp. 1-9, 2012.
- [77] X. Du, D. Dong, X. Zhao, L. Jiao, P. Han, and Y. Lang, "Detection of pesticide residues on fruit surfaces using laser induced breakdown spectroscopy," *RSC Advances*, vol. 5, pp. 79956-79963, 2015.
- [78] T. J. Jiang, Z. Guo, M. J. Ma, L. Fang, M. Yang, S. S. Li, J. H. Liu, N. J. Zhao, X. J. Huang, and W. Q. Liu, "Electrochemical laser induced breakdown spectroscopy for enhanced detection of Cd(II) without

- interference in rice on layer-by-layer assembly of graphene oxides," *Electrochimica Acta*, vol. 216, pp. 188-195, 2016.
- [79] J. Peng, Y. He, L. Ye, T. Shen, F. Liu, W. Kong, X. Liu, and Y. Zhao, "Moisture Influence Reducing Method for Heavy Metals Detection in Plant Materials Using Laser-Induced Breakdown Spectroscopy: A Case Study for Chromium Content Detection in Rice Leaves," *Analytical Chemistry*, vol. 89, pp. 7593-7600, 2017.
- [80] A. Khumaeni, M. Ramli, Y. Deguchi, Y. Lee, N. Idris, K. H. Kurniawan, T. J. J. Lie, and K. Kagawa, "New technique for the direct analysis of food powders confined in a small hole using transversely excited atmospheric CO₂ laser-induced gas plasma," *Applied Spectroscopy*, vol. 62, pp. 1344-1348, 2008.
- [81] S. Varliklioz Er, H. Eksi-Kocak, H. Yetim, and I. H. Boyaci, "Novel Spectroscopic Method for Determination and Quantification of Saffron Adulteration," *Food Analytical Methods*, vol. 10, pp. 1547-1555, 2017.
- [82] M. Hassan, M. Sighicelli, A. Lai, F. Colao, A. H. H. Ahmed, R. Fantoni, and M. A. Harith, "Studying the enhanced phytoremediation of lead contaminated soils via laser induced breakdown spectroscopy," *Spectrochimica Acta - Part B Atomic Spectroscopy*, vol. 63, pp. 1225-1229, 2008.
- [83] M. Hassan, M. Abdelhamied, A. H. Hanafy, R. Fantoni, and M. A. Harith, "Laser monitoring of phytoextraction enhancement of lead contaminated soil adopting EDTA and EDDS," in *AIP Conference Proceedings*, Cairo, Egypt, 2011, pp. 93-100.
- [84] J. Singh, R. Kumar, S. Awasthi, V. Singh, and A. K. Rai, "Laser Induced breakdown spectroscopy: A rapid tool for the identification and quantification of minerals in cucurbit seeds," *Food Chemistry*, vol. 221, pp. 1778-1783, 2017.
- [85] M. Bossu, Z. Q. Hao, M. Baudalet, J. Yu, Z. Zhang, and J. Zhang, "Femtosecond laser-induced breakdown spectroscopy for detection of trace elements in sophora leaves," *Chinese Physics Letters*, vol. 24, pp. 3466-3468, 2007.
- [86] G. Nicolodelli, G. S. Senesi, A. C. Ranulfi, B. S. Marangoni, A. Watanabe, V. de Melo Benites, P. P. A. de Oliveira, P. Villas-Boas, and D. M. B. P.

- Milori, "Double-pulse laser induced breakdown spectroscopy in orthogonal beam geometry to enhance line emission intensity from agricultural samples," *Microchemical Journal*, vol. 133, pp. 272-278, 2017.
- [87] G. Kim, J. Kwak, J. Choi, and K. Park, "Detection of nutrient elements and contamination by pesticides in spinach and rice samples using laser-induced breakdown spectroscopy (LIBS)," *Journal of Agricultural and Food Chemistry*, vol. 60, pp. 718-724, 2012.
- [88] L. C. Nunes, G. A. da Silva, L. C. Trevizan, D. Santos Júnior, R. J. Poppi, and F. J. Krug, "Simultaneous optimization by neuro-genetic approach for analysis of plant materials by laser induced breakdown spectroscopy," *Spectrochimica Acta - Part B Atomic Spectroscopy*, vol. 64, pp. 565-572, 2009.
- [89] P. Shukla, R. Kumar, and A. K. Raib, "Detection of Minerals in Green Leafy Vegetables Using Laser Induced Breakdown Spectroscopy," *Journal of Applied Spectroscopy*, vol. 83, pp. 872-877, 2016.
- [90] S. Zivkovic, M. Momcilovic, A. Staicu, J. Mutic, M. Trtica, and J. Savovic, "Spectrochemical analysis of powdered biological samples using transversely excited atmospheric carbon dioxide laser plasma excitation," *Spectrochimica Acta - Part B Atomic Spectroscopy*, vol. 128, pp. 22-29, 2017.
- [91] H. H. Cho, Y. J. Kim, Y. S. Jo, K. Kitagawa, N. Arai, and Y. I. Lee, "Application of laser-induced breakdown spectrometry for direct determination of trace elements in starch-based flours," *Journal of Analytical Atomic Spectrometry*, vol. 16, pp. 622-627, 2001.
- [92] P. F. de Souza, D. Santos, G. G. A. de Carvalho, L. C. Nunes, M. da Silva Gomes, M. B. B. Guerra, and F. J. Krug, "Determination of silicon in plant materials by laser-induced breakdown spectroscopy," *Spectrochimica Acta - Part B Atomic Spectroscopy*, 2013.
- [93] J. P. R. Romera, P. L. Barsanelli, and F. M. V. Pereira, "Expeditious prediction of fiber content in sugar cane: An analytical possibility with LIBS and chemometrics," *Fuel*, vol. 166, pp. 473-476, 2016.
- [94] D. K. Tripathi, R. Kumar, D. K. Chauhan, A. K. Rai, and D. Bicanic, "Laser-induced breakdown spectroscopy for the study of the pattern of silicon

- deposition in leaves of saccharum species," *Instrumentation Science and Technology*, vol. 39, pp. 510-521, 2011.
- [95] G. G. A. De Carvalho, D. Santos Jr, L. C. Nunes, M. D. S. Gomes, F. D. O. Leme, and F. J. Krug, "Effects of laser focusing and fluence on the analysis of pellets of plant materials by laser-induced breakdown spectroscopy," *Spectrochimica Acta - Part B Atomic Spectroscopy*, vol. 74-75, pp. 162-168, 2012.
- [96] M. B. Bueno Guerra, A. Adame, E. De Almeida, G. G. Arantes De Carvalho, M. A. Stolf Brasil, D. Santos, Jr., and F. J. Krug, "Direct analysis of plant leaves by EDXRF and LIBS: microsampling strategies and cross-validation," *Journal of Analytical Atomic Spectrometry*, vol. 30, pp. 1646-1654, 2015.
- [97] L. C. Nunes, J. W. Batista Braga, L. C. Trevizan, P. Florêncio De Souza, G. G. Arantes De Carvalho, D. S. Júnior, R. J. Poppi, and F. J. Krug, "Optimization and validation of a LIBS method for the determination of macro and micronutrients in sugar cane leaves," *Journal of Analytical Atomic Spectrometry*, vol. 25, pp. 1453-1460, 2010.
- [98] M. da Silva Gomes, G. G. A. de Carvalho, D. Santos Junior, and F. J. Krug, "A novel strategy for preparing calibration standards for the analysis of plant materials by laser-induced breakdown spectroscopy: A case study with pellets of sugar cane leaves," *Spectrochimica Acta Part B: Atomic Spectroscopy*, vol. 86, pp. 137-141, 2013.
- [99] M. D. S. Gomes, D. Santos Jr, L. C. Nunes, G. G. A. De Carvalho, F. De Oliveira Leme, and F. J. Krug, "Evaluation of grinding methods for pellets preparation aiming at the analysis of plant materials by laser induced breakdown spectrometry," *Talanta*, vol. 85, pp. 1744-1750, 2011.
- [100] G. G. Arantes de Carvalho, J. Moros, D. Santos, Jr., F. J. Krug, and J. J. Laserna, "Direct determination of the nutrient profile in plant materials by femtosecond laser-induced breakdown spectroscopy," *Analytica Chimica Acta*, vol. 876, pp. 26-38, 2015.
- [101] M. Galiova, J. Kaiser, K. Novotny, O. Samek, L. Reale, R. Malina, K. Palenikova, M. Lika, V. Cudek, V. Kanicky, V. Otruba, A. Poma, and A. Tucci, "Utilization of laser induced breakdown spectroscopy for

- investigation of the metal accumulation in vegetal tissues," *Spectrochimica Acta - Part B Atomic Spectroscopy*, vol. 62, pp. 1597-1605, 2007.
- [102] J. Kaiser, O. Samek, L. Reale, M. Liška, R. Malina, A. Ritucci, A. Poma, A. Tucci, F. Flora, A. Lai, L. Mancini, G. Tromba, F. Zanini, A. Faenov, T. Pikuz, and G. Cinque, "Monitoring of the heavy-metal hyperaccumulation in vegetal tissues by X-ray radiography and by femto-second laser induced breakdown spectroscopy," *Microscopy Research and Technique*, vol. 70, pp. 147-153, 2007.
- [103] M. Galiova, J. Kaiser, K. Novotny, J. Novotny, T. Vaculovic, M. Lika, R. Malina, K. Stejskal, V. Adam, and R. Kizek, "Investigation of heavy-metal accumulation in selected plant samples using laser induced breakdown spectroscopy and laser ablation inductively coupled plasma mass spectrometry," *Applied Physics A: Materials Science and Processing*, vol. 93, pp. 917-922, 2008.
- [104] S. Krizkova, P. Ryant, O. Krystofova, V. Adam, M. Galiova, M. Beklova, P. Babula, J. Kaiser, K. Novotny, J. Novotny, M. Liska, R. Malina, J. Zehnalek, J. Hubalek, L. Havel, and R. Kizek, "Multi-instrumental analysis of tissues of sunflower plants treated with silver(I) ions - Plants as bioindicators of environmental pollution," *Sensors*, vol. 8, pp. 445-463, 2008.
- [105] J. Kaiser, M. Galiova, K. Novotny, R. Cervenka, L. Reale, J. Novotny, M. Lika, O. Samek, V. Kanicky, A. Hrdlicka, K. Stejskal, V. Adam, and R. Kizek, "Mapping of lead, magnesium and copper accumulation in plant tissues by laser-induced breakdown spectroscopy and laser-ablation inductively coupled plasma mass spectrometry," *Spectrochimica Acta - Part B Atomic Spectroscopy*, vol. 64, pp. 67-73, 2009.
- [106] A. Assion, M. Wollenhaupt, L. Haag, F. Mayorov, C. Sarpe-Tudoran, M. Winter, U. Kutschera, and T. Baumert, "Femtosecond laser-induced-breakdown spectroscopy for Ca 2+ analysis of biological samples with high spatial resolution," *Applied Physics B: Lasers and Optics*, vol. 77, pp. 391-397, 2003.
- [107] M. Z. Martin, A. J. Stewart, K. D. Gwinn, and J. C. Waller, "Laser-induced breakdown spectroscopy used to detect endophyte-mediated accumulation of metals by tall fescue," *Applied Optics*, vol. 49, pp. C161-C167, 2010.

- [108] T. Ohta, M. Ito, T. Kotani, and T. Hattori, "Emission enhancement of laser-induced breakdown spectroscopy by localized surface plasmon resonance for analyzing plant nutrients," *Applied Spectroscopy*, vol. 63, pp. 555-558, 2009.
- [109] J. Wang, M. Shi, P. Zheng, and S. Xue, "Quantitative Analysis of Lead in Tea Samples by Laser-Induced Breakdown Spectroscopy," *Journal of Applied Spectroscopy*, vol. 84, pp. 188-193, 2017.
- [110] D. F. Andrade, E. R. Pereira-Filho, and P. Konieczynski, "Comparison of ICP OES and LIBS analysis of medicinal herbs rich in flavonoids from Eastern Europe," *Journal of the Brazilian Chemical Society*, vol. 28, pp. 838-847, 2017.
- [111] D. M. Silvestre, F. de Oliveira Leme, C. S. Nomura, and A. N. do Nascimento, "Direct analysis of barium, calcium, potassium, and manganese concentrations in tobacco by laser-induced breakdown spectroscopy," *Microchemical Journal*, vol. 126, pp. 545-550, 2016.
- [112] J. Peng, K. Song, H. Zhu, W. Kong, F. Liu, T. Shen, and Y. He, "Fast detection of tobacco mosaic virus infected tobacco using laser-induced breakdown spectroscopy," *Scientific Reports*, vol. 7, p. 44551, 2017.
- [113] X. Fang and S. R. Ahmad, "Elemental analysis in environmental land samples by stand-off laser-induced breakdown spectroscopy," *Applied Physics B*, pp. 1-7, 2013/09/07 2013.
- [114] Q. Sun, M. Tran, B. W. Smith, and J. D. Winefordner, "Direct determination of P, Al, Ca, Cu, Mn, Zn, Mg and Fe in plant materials by laser-induced plasma spectroscopy," *Canadian Journal of Analytical Sciences and Spectroscopy*, vol. 44, pp. 164-170, 1999.
- [115] G. Watal, B. Sharma, P. K. Rai, D. Jaiswal, D. K. Rai, N. K. Rai, and A. K. Rai, "LIBS-based detection of antioxidant elements: a new strategy," *Methods in molecular biology (Clifton, N.J.)*, vol. 594, pp. 275-285, 2010.
- [116] A. Khumaeni, H. Niki, K. I. Fukumoto, Y. Deguchi, K. Kurihara, K. Kagawa, and Y. I. Lee, "A unique technique of laser-induced breakdown spectroscopy using transversely excited atmospheric CO₂ laser for the sensitive analysis of powder samples," *Current Applied Physics*, vol. 11, pp. 423-427, 2011.

- [117] A. Khumaeni, H. Niki, Y. Deguchi, K. Kurihara, K. Kagawa, and Y. I. Lee, "Analysis of organic powder samples by using the metal-assisted subtarget effect in a Transversely-Excited Atmospheric (TEA) CO₂ laser-induced he gas plasma at 1 atm," *Journal of the Korean Physical Society*, vol. 55, pp. 2441-2446, 2009.
- [118] M. Tiwari, R. Agrawal, A. K. Pathak, A. K. Rai, and G. K. Rai, "Laser-induced breakdown spectroscopy: An approach to detect adulteration in turmeric," *Spectroscopy Letters*, vol. 46, pp. 155-159, 2013.
- [119] J. N. Kunz, D. V. Voronine, H. W. H. Lee, A. V. Sokolov, and M. O. Scully, "Rapid detection of drought stress in plants using femtosecond laser-induced breakdown spectroscopy," *Optics Express*, vol. 25, pp. 7251-7262, 2017.
- [120] L. C. Peruchi, L. C. Nunes, G. G. A. de Carvalho, M. B. B. Guerra, E. de Almeida, I. A. Rufini, D. Santos Jr, and F. J. Krug, "Determination of inorganic nutrients in wheat flour by laser-induced breakdown spectroscopy and energy dispersive X-ray fluorescence spectrometry," *Spectrochimica Acta Part B: Atomic Spectroscopy*, vol. 100, pp. 129-136, 2014.
- [121] G. Bilge, B. Sezer, K. E. Eseller, H. Berberoğlu, H. Kâşksel, and İ. H. Boyacı, "Determination of Ca addition to the wheat flour by using laser-induced breakdown spectroscopy (LIBS)," *European Food Research and Technology*, vol. 242, pp. 1685-1692, 2016.
- [122] M. R. Martelli, C. Barron, P. Delaporte, G. Viennois, X. Rouau, and A. Sadoudi, "Pulsed laser ablation: A new approach to reveal wheat outer layer properties," *Journal of Cereal Science*, vol. 49, pp. 354-362, 2009.
- [123] M. R. Martelli, F. Brygo, A. Sadoudi, P. Delaporte, and C. Barron, "Laser-induced breakdown spectroscopy and chemometrics: A novel potential method to analyze wheat grains," *Journal of Agricultural and Food Chemistry*, vol. 58, pp. 7126-7134, 2010.
- [124] M. Pouzar, T. Cernohorsky, M. Prusova, P. Prokopcakova, and A. Krejcova, "LIBS analysis of crop plants," *Journal of Analytical Atomic Spectrometry*, vol. 24, pp. 953-957, 2009.
- [125] D. K. Tripathi, V. P. Singh, S. M. Prasad, D. K. Chauhan, N. Kishore Dubey, and A. K. Rai, "Silicon-mediated alleviation of Cr(VI) toxicity in wheat seedlings as evidenced by chlorophyll florescence, laser induced breakdown

- spectroscopy and anatomical changes," *Ecotoxicology and Environmental Safety*, vol. 113, pp. 133-144, 2015.
- [126] D. K. Tripathi, V. P. Singh, S. M. Prasad, N. K. Dubey, D. K. Chauhan, and A. K. Rai, "LIB spectroscopic and biochemical analysis to characterize lead toxicity alleviative nature of silicon in wheat (*Triticum aestivum* L.) seedlings," *Journal of Photochemistry and Photobiology B: Biology*, vol. 154, pp. 89-98, 2016.
- [127] B. Sezer, G. Bilge, A. Berkkan, U. Tamer, and I. Hakki Boyaci, "A rapid tool for determination of titanium dioxide content in white chickpea samples," *Food Chemistry*, vol. 240, pp. 84-89, 2018.
- [128] D. Jaiswal, P. K. Rai, and G. Watal, "Hypoglycemic and antidiabetic effects of withania coagulans fruit ethanolic extract in normal and streptozotocin-induced diabetic rats," *Journal of Food Biochemistry*, vol. 34, pp. 764-778, 2010.
- [129] D. Jaiswal, P. K. Rai, and G. Watal, "Antidiabetic effect of *Withania coagulans* in experimental rats," *Indian Journal of Clinical Biochemistry*, vol. 24, pp. 88-93, 2009.
- [130] A. Uhl, K. Loebe, and L. Kreuchwig, "Fast analysis of wood preservers using laser induced breakdown spectroscopy," *Spectrochimica Acta - Part B Atomic Spectroscopy*, vol. 56, pp. 795-806, 2001.
- [131] T. M. Moskal and D. W. Hahn, "On-line sorting of wood treated with chromated copper arsenate using laser-induced breakdown spectroscopy," *Applied Spectroscopy*, vol. 56, pp. 1337-1344, 2002.
- [132] H. M. Solo-Gabriele, T. G. Townsend, D. W. Hahn, T. M. Moskal, N. Hosein, J. Jambeck, and G. Jacobi, "Evaluation of XRF and LIBS technologies for on-line sorting of CCA-treated wood waste," *Waste Management*, vol. 24, pp. 413-424, 2004.
- [133] M. Z. Martin, N. Labbé, N. André, R. Harris, M. Ebinger, S. D. Wullschleger, and A. A. Vass, "High resolution applications of laser-induced breakdown spectroscopy for environmental and forensic applications," *Spectrochimica Acta - Part B Atomic Spectroscopy*, vol. 62, pp. 1426-1432, 2007.

- [134] B. A. Gething, J. J. Janowiak, and R. H. Falk, "Assessment of laser induced breakdown spectroscopy (LIBS) for classification of preservative in CCA-treated lumber," *Forest Products Journal*, vol. 59, pp. 67-74, 2009.
- [135] M. Z. Martin, N. Labbé, T. G. Rials, and S. D. Wullschleger, "Analysis of preservative-treated wood by multivariate analysis of laser-induced breakdown spectroscopy spectra," *Spectrochimica Acta Part B: Atomic Spectroscopy*, vol. 60, pp. 1179-1185, 2005.
- [136] D. M. Silvestre, F. M. Barbosa, B. T. Aguiar, F. O. Leme, and C. S. Nomura, "Feasibility study of calibration strategy for direct quantitative measurement of K and Mg in plant material by laser-induced breakdown spectrometry," *Analytical Chemistry Research*, vol. 5, pp. 28-33, 2015.
- [137] H. Jull, R. Künnemeyer, and P. Schaare, "Nutrient detection in fresh and dried pasture using laser-induced breakdown spectroscopy," *Precision Agriculture*, accepted January 25 2018.
- [138] H. Jull, R. Künnemeyer, S. Talele, P. Schaare, and M. Seelye, "Laser-induced breakdown spectroscopy analysis of sodium in pelletised pasture samples," in *Automation, Robotics and Applications (ICARA), 2015 6th International Conference on*, 2015, pp. 262-268.
- [139] R. Bro, "Multivariate calibration: What is in chemometrics for the analytical chemist?," *Analytica Chimica Acta*, vol. 500, pp. 185-194, 2003.
- [140] A. Savitzky and M. J. E. Golay, "Smoothing and differentiation of data by simplified least squares procedures," *Analytical Chemistry*, vol. 36, pp. 1627-1639, 1964.
- [141] T. Næs, T. Isaksson, T. Fearn, and T. Davies, *A User-Friendly Guide to Multivariate Calibration and Classification*. Chichester, UK: NIR publications, 2002.
- [142] H. Fink, U. Panne, and R. Niessner, "Process analysis of recycled thermoplasts from consumer electronics by laser-induced plasma spectroscopy," *Analytical Chemistry*, vol. 74, pp. 4334-4342, 2002.
- [143] C. E. Rasmussen and C. K. I. Williams, *Gaussian Processes for Machine Learning*: University Press Group Limited, 2006.
- [144] C. Borggaard and H. H. Thodberg, "Optimal minimal neural interpretation of spectra," *Analytical Chemistry*, vol. 64, pp. 545-551, 1992.

- [145] P. J. Gemperline, J. R. Long, and V. G. Gregoriou, "Nonlinear multivariate calibration using principal components regression and artificial neural networks," *Analytical Chemistry*, vol. 63, pp. 2313-2323, 1991.
- [146] I. H. Witten, E. Frank, and M. A. Hall, "Chapter 5 - Credibility: Evaluating What's Been Learned," in *Data Mining: Practical Machine Learning Tools and Techniques (Third Edition)*, ed Boston: Morgan Kaufmann, 2011, pp. 147-187.
- [147] R. Kohavi, "A study of cross-validation and bootstrap for accuracy estimation and model selection," presented at the Proceedings of the 14th international joint conference on Artificial intelligence - Volume 2, Montreal, Quebec, Canada, 1995.
- [148] I. H. Witten, E. Frank, and M. A. Hall, *Data Mining: Practical Machine Learning Tools and Techniques*, 3 ed. Boston, USA: Morgan Kaufmann, 2011.
- [149] D. Cremers and L. Radziemski, "Chemometric analysis in LIBS," in *Handbook of Laser-Induced Breakdown Spectroscopy*, 2nd ed West Sussex, UK: John Wiley & Sons Ltd, 2013, pp. 223-255.

Chapter 6

Identification of Contamination Levels and the Microstructure of Metal Injection Moulded Titanium

a peer-reviewed publication

published in

Key Engineering Materials

by

P. Ewart, H. Jull, R. Künemeyer, and P. Schaare

Identification of Contamination Levels and the Microstructure of Metal Injection Moulded Titanium

Paul Ewart^{1,2,a*}, Harrison Jull^{2,b}, Rainer Künnemeyer²
and Peter N. Schaare³

¹ Centre of Engineering Industrial Design, Waikato Institute of Technology, Hamilton, New Zealand

² School of Engineering, The University of Waikato, Hamilton, New Zealand

³ The New Zealand Institute for Plant and Food Research, Ruakura, Hamilton, New Zealand

^apewart@fulbrightmail.org, ^bhj75@students.waikato.ac.nz

Keywords: carbide formation, contaminating elements, laser spectroscopy, metal injection moulding, titanium

Abstract. The chemical elements used in the binder system for the injection moulding of titanium metal powders will change the final composition when not adequately controlled. Excess levels of carbon, hydrogen, nitrogen and oxygen adversely effect the mechanical properties by embrittlement. Before sintering debinding is done to remove the maximum possible amount binder thereby ensuring residual carbon levels are minimal. Testing the mechanical properties of samples can acknowledge deficiencies in the final part however, identification of the nature of the deficiencies is not so simple.

In this work titanium-based metal parts were made using the metal injection moulding process and the microstructure was inspected. The investigation used scanning electron microscopy imaging, electron dispersion spectroscopy point and area mapping, LECO trace analysis and X-ray diffraction elemental mapping. Following this samples were ground and polished before immersing their surfaces in an etching solution to further expose the microstructure. Although the data collected from debinding indicated the binder had been removed prior to sintering contamination was still evident. This result showed that the traditional means of reporting binder levels in proportion to part mass after debinding is inaccurate. Subsequently laser induced breakdown spectroscopy was trialed as a method by which to determine the binder levels for parts in the green, grey, brown and sintered form.

Interstitial carbon is a known alpha stabiliser however excess carbon on particle surfaces may impinge on particle coalescence limiting density levels. Comparison of the part mass method of binder determination with the laser induced breakdown spectroscopy results showed that the mass determination method was more accurate for the green and grey parts but the laser induced breakdown spectroscopy results were able to detect the residual binder more accurately for brown and sintered parts.

Introduction

During fabrication by metal injection moulding (MIM) each processing step (feedstock production, moulding, debinding and sintering) is essential to ensuring a successful part is produced. The main deficiencies that affect the feedstock are component uniformity and particle binder interactions [1-6]. For moulding, mould design, rheology and particle loading have shown to be critical [7]. The debinding process requires sufficient strength of the greenpart, greypart and brownpart to enable handling and placement. Sintering results show that, other than shape retention, removal of decomposition products (control of elemental levels) and a clean furnace atmosphere is essential [8].

It is shown from the literature that there is a knowledge gap between metal injection moulding (MIM) as an established manufacturing process and its use for the fabrication of titanium (Ti) parts [9-12]. The moulding process for Ti MIM requires the same rheological considerations as conventional MIM with the tool design having distinct requirements not seen for polymer

processing [13]. One consideration that does stand conventional MIM apart from Ti MIM is the propensity of Ti to have its mechanical properties altered by fractional changes in the elemental composition [14]. The main contributor to this being the thermoplastic components used in feedstock formulation that by necessity, contain the very elements (C, O, N, H) that must be controlled to meet industry standards for Ti metals [3, 6, 14, 15]. Principals of controlling elemental levels identified for Ti but seldom applied to commercial endeavours include, reduction of processing temperatures and accurate measurement of binder levels prior to sintering. In response to this the literature states that thermal processing must ensure residues that introduce impurities are not present during the final stages of the sinter process where the interconnected pores close off [16].

Monitoring the changing binder levels during the MIM processes of solution debinding (SD) and thermal debinding (TD) is by weight measurement. At each stage the greenpart, greypart, brownpart and sintered part are weighed and the values compared and referenced to the theoretical binder levels. While these values can correspond well to complete removal of binder the final metal composition is often still evidence of high amounts of carbon resulting from binder residue.

Laser induced breakdown spectroscopy (LIBS) is an optical technique that can be used to determine surface elemental composition. It employs a high powered, short pulsed laser focused onto a sample. The high power density of the pulse rapidly ablates a small amount of the surface material creating a plasma [17]. The plasma becomes opaque and in the case of nanosecond laser pulses the plasma absorbs the remaining laser pulse and increases the temperature in the plasma [18]. The pressure produced by plasma formation increases the boiling point of the sample surface stopping further vaporisation and spectroscopy then analyses the plasma vapour [19]. Many aspects of plasma are still not fully understood but the author considers the models describing the ablation process may be sufficient for this study.

Experimental

A previously formulated binder system was produced with a mixture of linear low density polyethylene (LLDPE), polypropylene (PP), polyethylene glycol (PEG), carnauba wax (CW) and refined beeswax (RBW) [20]. This was subsequently compounded with pure titanium (TiCP) at a volume fraction of 0.6 using a ThermoLab co-rotating twin screw extruder (TSE, $\omega = 50$ r/min, $T = 170$ °C). The Dr Boy 50T2 injection moulder was used for moulding the sample greenparts (Figure 1) followed by marking and weight measurement.

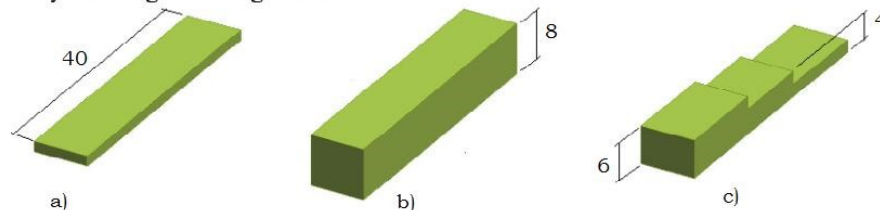


Figure 1: Sample green parts geometries, a) thin part, b) thick part and c) step part.

Solvent debinding (SD) was done by placing the greenparts in circulating water ($T = 50$ °C, $t = (0$ to $100)$ h) to remove the PEG. At specified times parts were removed from the water, dried ($T = 50$ °C, $t = 24$ h) and weighed to measure binder mass loss.

Low temperature thermal debinding (LTTD) involved slow heating rates ($\beta = 1$ °C/min) to control expansion of the waxes ($T = 100$ °C) and polymers ($T = 175$ °C) using the Contherm 2000 series convection oven. This was followed by an isothermal period to remove the wax components ($T = 250$ °C, $t \leq 100$ h).

The ACME vacuum capable high temperature sinter furnace (Model ZSJ-35/35/70), was used for final sintering of the brownparts ($\beta = 5$ °C/min, $T = 1340$ °C, $t = 180$ min). First gas flow using industrial grade argon ($\dot{V} = 10$ L/min, $T = (20$ to $800)$ °C) and then vacuum condition ($T = (800$ to $1340)$ °C, $p = 2 \times 10^{-3}$ mbar) followed by further gas flow during cooling ($\dot{V} = 20$ L/min).

Visual inspection was by optical microscopy methods (Olympus BX60, Wild M3B) as well as imaging by SEM and EDS (ZEISS EVOMA25). The sintered parts were inspected on the outer and inner surfaces as well as being sectioned and analysed using optical microscopy and SEM. EDS was used to confirm elemental composition. The micro-structure was inspected using samples treated with Kroll's reagent (100 mL distilled water, 2 mL HF, 4 mL HNO₃, $t = 60$ s) and optical microscopy.

Sectioned and polished parts were also analysed using the Panalytical Empyrean series 2 XRD with power settings $P = 45$ kV at $I = 40$ mA through a copper electrode. Scanning from position (20 to 100) °2 θ , using a step size of 0.026 °2 θ , scan step time of $t = 17.34$ s in continuous scanning mode. Peak identification was done using the Highscope software.

Subsequent measurement of the parts was done with the Nd:YAG laser (Laser Analysis Technologies, Spectrolaser 4000, pulse width 7 ns). Operating at the fundamental wavelength of 1064 nm and focused perpendicular to the sample surface to generate the plasma. The setup had a fixed distance to the sample. The energies used per pulse were 50, 100, and 200 mJ. Each spectrum was acquired using the four spectrometers of the Spectrolaser unit which cover the range 185.25-948.80 nm. All spectrometers were set to have a delay time of $t = 1.27$ μ s and an integration time of $t = 1$ ms.

Results and discussion

Debinding. In order to determine correlation between SD rate and remaining binder components, long-time solvent debinding with continuing measurement was done. As shown in Figure 2 the dissolution rate decreased with increasing time. It was seen that the binder was removed from the thinparts but it was not possible to totally remove the binder from the thickparts when the duration was short.

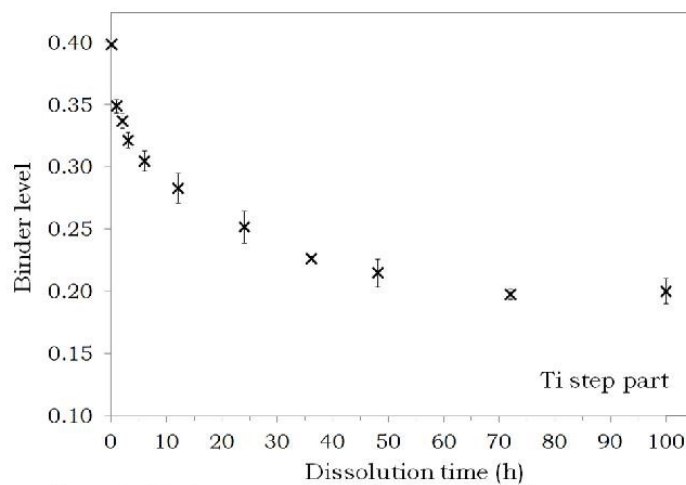


Figure 2: Binder removal by dissolution for the step part.

Irregularities with the debinding system such as loss of particulates or part geometry would be detrimental to the use of mass determination for accurately measuring changes in binder content. The longtime solvent debinding proved to be suitable for the total removal of the water soluble component.

When cracking and surface deformation appeared from TD it was consistent in its form and location; central in the thick parts and central to each step in the step part (Figure 3). Defects in consistent locations indicate causes not related to feedstock inhomogeneity. The cause more likely related to moulding, the location of the gate and the flow behaviour of the feedstock filling the cavity and, was rectified by manipulating the process parameters. However it is reported in literature that similar defects are seen through insufficient binder removal.



Figure 3: TD step parts a) without defects and b) with defects.

As the binder, powder fraction and debinding parameters were kept constant it can be stated that binder removal was a function of sectional thickness and part geometry. Particle loss from the compacts would also have a considerable effect on the final part, especially when the part size is small.

Sintering. The brown parts were sintered under flowing argon, and showed uniform linear shrinkage in all axes ($\epsilon \approx 15\%$, Figure 4c), with no defects, a clean contaminant free surface and density of $\sim 93\%$. Parts with defects that had manifest during debinding retained the defects through sintering (Figure 4 (d)) confirming the often noted fact from literature.

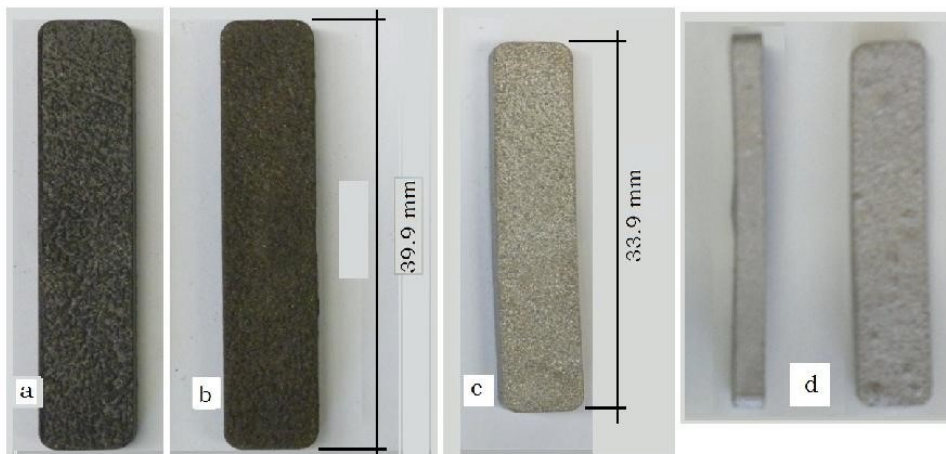


Figure 4: Thin part a) green, b) brown, c) sintered and defects that remained during sintering d) thin part and e) thick part

The step parts were sintered in the ACME vacuum furnace ($\beta = 5 \text{ }^\circ\text{C}/\text{min}$, $T = 1300 \text{ }^\circ\text{C}$, $t = 180 \text{ min}$, $P = 2 \times 10^{-3} \text{ mbar}$) and had good clean surfaces with the distinct titanium lustre (Figure 5). The defects that manifest in the thermal debinding were not able to self-repair therefore accurate density measurement was difficult (Figure 5 b). As above these defects were considered to be due to low powder loading and deficiencies in tool design which promoted separation and non-uniform feedstock flow. This in turn affected debinding with some binder agglomerates creating high internal pressures due to non-uniform expansion during heating.



Figure 5: Sintered Part a) without and b) with defects.

Analysis. Cut and polished samples seen as part of the EDS analysis (Figure 6, Table 1) showed the elemental composition was uniform. The polished outer surface (Figure 6 a) showed silicon traces in the pores and greater consolidation of the particles than the polished inner section. No contaminants were identified in the bulk titanium indicating that carbon diffusion into the bulk may not take place. However levels for carbon within the larger pores (Spectrum 4, Figure 6 b, Table 1) were very high indicating that residue on the particle surfaces, where coalescence was low, was not diffusing out of the part.

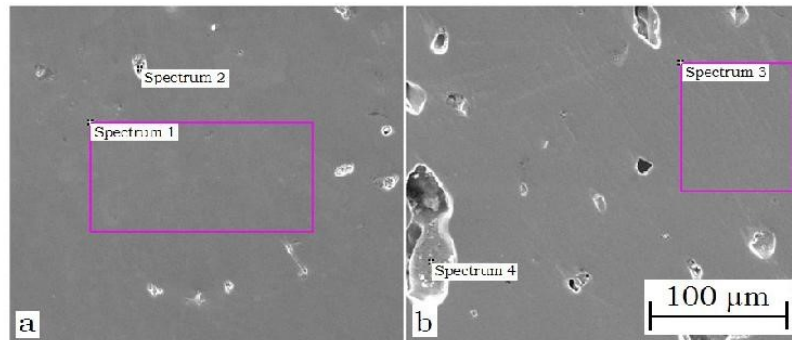


Figure 6: SEM image from the outer surface of thinpart, a) bulk Ti and b) internal porosity.

Table 1: Elemental values from EDS spectrum (w_E (%), Figure 6).

Spectrum	C	Ti	Si
1	0	100.00	0
2	0	99.45	0.55
3	0	100.00	0
4	7.20	92.80	0

The XRD analysis (Figure 7) determined that the residues in the Ti were enough to form carbide compounds although it does not discern any preferential location. Referring to the SEM (Figure 6) and EDS (Table 1) carbon was not present in the bulk material but was seen within the larger pores it is likely the XRD is detecting the carbon within the larger pores. The XRD parameters were only for qualitative elemental determination and not quantitative determination and so peak level may not indicate a definitive ratio of the elements detected. It must also be noted that elemental determination of the compounds was restricted by the limited materials data base available to the Highscope software.

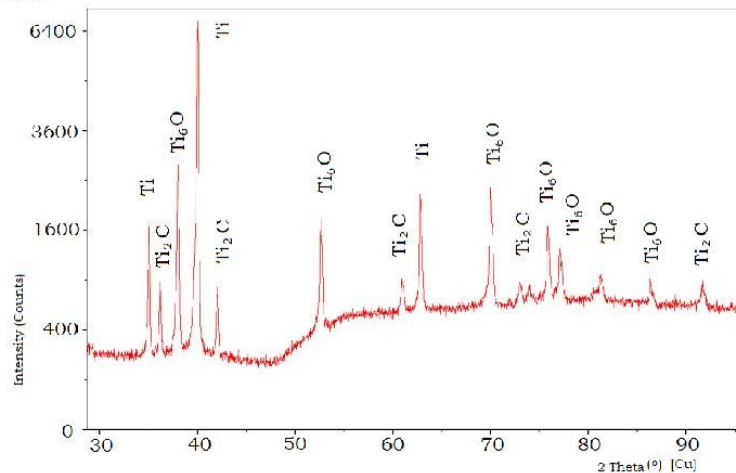


Figure 7: XRD map of the thin titanium part shows high oxygen and carbon levels.

The microstructure of the titanium was highlighted after etching with Kroll reagent to further show evidence of residual binder elements. The images (Figure 8 a) showed some twinning within the mainly alpha grains ($d = (30 \text{ to } 80) \mu\text{m}$) indicative of hydride formation. The formations shown from another area (Figure 8 b) are the alpha grains with contamination likely from the trace carbon identified from EDS.

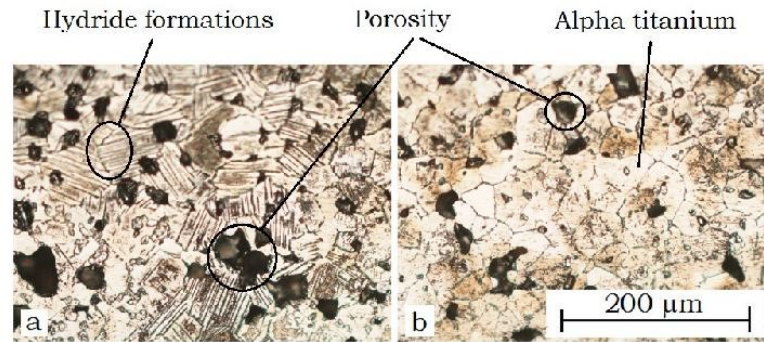


Figure 8: Cross section of thickpart etched with Kroll reagent.

When considering binder removal the generic approach of weighing the parts at each step would typically produce results indicating total removal of the binder and therefore the expectation of zero residue would be valid. However in the final sintering phase evidence of carbon through EDS, carbon compounds through XRD, porosity and contaminating phases via microscopy and the lower than anticipated density levels measured it is evident that the mass determination is highly inaccurate.

To validate this Laser induced breakdown spectroscopy (LIBS) was used to investigate surface elemental composition. The method did not allow a direct measurement of elemental carbon levels but by using the ratio of the Ti II 282.806 nm and the C I 247.856 nm lines the effectiveness of sampling to produce sintering could be monitored. It is important to consider the effects that laser pulses have on the surface of a sample to ensure the resulting values are not obscuring the results by producing new compounds that confuse the instruments detectors [21]. A function of laser pulse parameters including pulse width, pulse energy, fluence and also the penetration of heat into the sample would influence the result [22]. When high power density pulses are used there are differences that an ablation site has compared to the original surface. Inside the ablation crater may be recondensed material from the plasma so it is important to understand how this may be interpreted [23]. The surface properties may have also changed from the heat, stress, and pressure caused by the plasma formation. It is also known that the plasma produced within an inert purge gas such as argon will reduce the oxide layer on the surface of the object. This in turn will ensure that oxide compounds are not reducing the efficacy of the spectrometer.

A problem with LIBS is repeatability. The variability between spectra is caused by fluctuations in experimental parameters and matrix effects. Internal reference standards use a known or constant concentration of a major element to correct inconsistency between shots [24]. Another way to take an internal reference is to spike the sample with a constant concentration of an element that is not present in the sample. The relative intensities obtained from the internal standard removes fluctuations in the spectra caused by experimental conditions. This is not always the case. Plasmas created on the same sample can have different temperatures which affects the exponential part of the emission line equation, and the partition function [25]. An internal standard that has similar upper level electron energy as the emission line of interest reduces temperature effects caused by the exponential function. Choosing species with partition functions that have similar temperature characteristics would also reduce variation. Also common statistics show that if there is noise in the background of a measurement a weaker signal will have a higher percentage variation than that of a strong signal. This means that using a weak line in an internal standard analysis would produce

higher variance than using a stronger line. To ensure this was accounted for during analysis of the MIM samples calibration was attempted.

The LIBS-6 on board camera produced the calibration curve of Figure 9. This linear calibration follows the equation $z = 0.0049x - 1.5359$, where x is the pixel position in the horizontal axis, and z is the position of the translation stage holding the sample. This produces a fit with an R^2 value of 0.997. The line of best fit was made using the central linear region which cover pixels 139-394. The effective depth of this autofocus scheme is determined primarily by the nozzle on the machine. The camera is inside the transparent nozzle which has a small opening where ablation takes place.

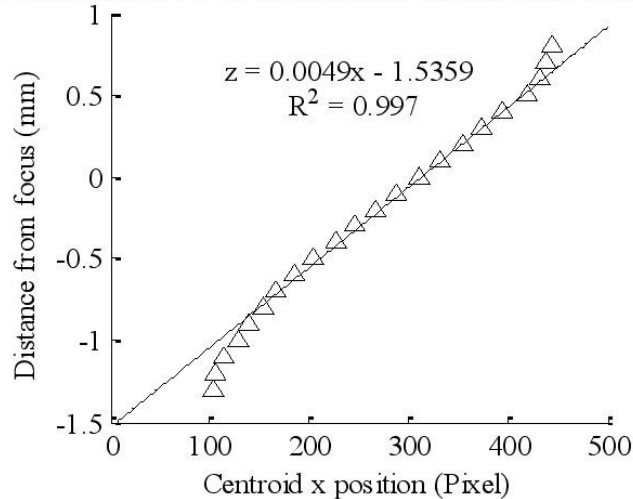


Figure 9: Autofocus performance from the on-board LIBS-6 camera.

With a satisfactory calibration curve the measurement of the samples was done with certainty and the physical effects (Figure 10) seen to produce an increase in the surface density by improving coalescence of the particles and decreasing the porosity.

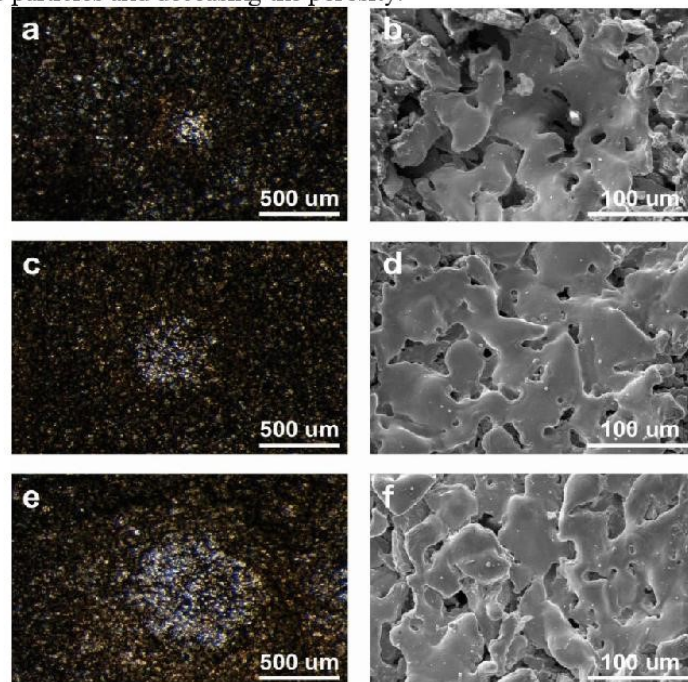


Figure 10: Ablation craters from 20 consecutive laser pulses using 50 mJ (a-b), 100 mJ (c-d) and 200 mJ (e-f). (b), (d), and (f) are SEM images.

Further to this the values determined for the ratio of carbon to titanium peaks was normalised shown in Figure 11 to identify residual binder levels considerably higher than that of both the mass determination method and the theoretical values.

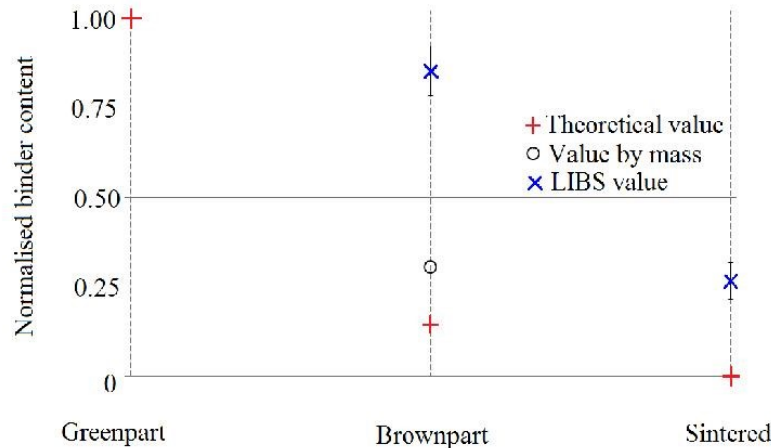


Figure 11: Binder levels as determined by LIBS indicates higher residue level than seen for theoretical or mass determination.

Conclusions

Following the production of titanium parts by injection moulding followed by sintering the microstructure of ground and polished samples showed evidence of excess contamination and low density. Although the data collected from mass determination indicated the binder had been removed prior to sintering and therefore residue should not be present. This result showed that the traditional means of reporting binder levels in proportion to part mass after debinding is inaccurate. Subsequently laser induced breakdown spectroscopy was trialed as a method by which to determine the binder levels for parts in the green, grey, brown and sintered form. Comparison showed that the mass determination method was more accurate for the green and grey parts but the laser induced breakdown spectroscopy results were able to detect residual binder more acutely for brown and sintered parts.

Acknowledgements

Part of this work was supported by New Zealand's Ministry of Business, Innovation and Employment under contract C11X1209.

The authors also wish to acknowledge Dr Seokyoung Ahn and his team for the subsequent moulding, simulation and funding that would otherwise not be possible to achieve.

References

- [1]. Jackson, C., *The Process*, in *Perspectives in Powder Metallurgy. New Methods for the Consolidation of Metal Powders*, H. Hausner, K. Roll, and P. Johnson, Editors. 1967, Plenum Press.
- [2]. Schwartz, S., P. Quirnbach, and M. Kraus, *Solvent Debinding Technology for a Continuous 316L MIM Production*, in *PIM Compilation II. Molding, Debinding, Sintering*, MPIF, Editor. 2007, Metal Powder Industries Federation: Princeton, NJ.
- [3]. Schofalvi, K., *Low Contamination Binders for Reaction Sensitive Alloy Applications*, in *PIM Compilation I. Powders, Binders and Feedstocks*, MPIF, Editor. 2007, Metal Powder Industries Federation: Princeton, NJ.

-
- [4]. Myers, N., R. Baijal, and P. King, *Sintering of PIM Fe-2Ni-0.8C*, in *PIM Compilation II. Molding, Debinding, Sintering*, MPIF, Editor. 2007, Metal Powder Industries Federation: Princeton, NJ.
- [5]. Guha, S., *MER introduces golf clubs using superfine powders*. Metal Powder Report 1997.
- [6]. Gai, G., et al., *Particle shape modification and related property improvements*. Powder Technology 2008. **183**: p. 115-121.
- [7]. Herranz, G., et al., *Development of new feedstock formulation based on high density polyethylene for MIM of M2 high speed steels*. Powder Metallurgy, 2005. **48**(2).
- [8]. Banerjee, S. and C. Joens, *A Comparison of Techniques for Processing Powder Metal Injection Molded 17-4 PH Materials*. 2008.
- [9]. German, R., *Conceptual Optimization of Titanium Powder Injection Molding*, in *Advances in Powder Metallurgy & Particulate Materials*, M. Bulger and B. Stebick, Editors. 2010, Metal Powder Industries Federation: Hollywood, Florida. p. 11.
- [10]. Froes, S., *Getting better: big boost for titanium MIM prospects*. Metal Powder Report, 2006: p. 4.
- [11]. JPMA, *2011 Report for MIM Market*. 2011, Japan Powder Metallurgy Association: Tokyo.
- [12]. Kryachek, V.M., D.A. Levina, and L.I. Chernyshev, *Powder Metallurgy Abroad, Developmental Trends in European Powder Metallurgy*. Powder Metallurgy and Metal Ceramics, 2007. **46**(11-12).
- [13]. Heaney, D. and R. German, *Advances in the Sintering of Titanium Powders*, in *Euro PM2004*. 2004.
- [14]. Li, Y., X.M. Chou, and L.M. Yu, *Dehydrogenation debinding process of MIM titanium alloys by TiH₂ powder*. Powder Metallurgy, 2006. **49**(3).
- [15]. Oberg, E., et al., *Machinery's Handbook*. 29 ed, ed. C. McCauley. 2012, New York, NY: Industrial Press Inc.
- [16]. German, R., *Coarsening in Sintering: Grain Shape Distribution, Grain Size Distribution, and Grain Growth Kinetics in Solid-Pore Systems*. Critical Reviews in Solid State and Materials Sciences, 2010. **35**: p. 43.
- [17]. Cremers, D. and L. Radziemski, *Introduction*, in *Handbook of Laser-Induced Breakdown Spectroscopy*. 2013, John Wiley & Sons Ltd: West Sussex, UK. p. 3.
- [18]. Singh, J.P. and S.N. Thakur, *Fundamentals of Laser Induced Breakdown Spectroscopy*, in *Laser-Induced Breakdown Spectroscopy*, J.P. Singh and S.N. Thakur, Editors. 2007, Elsevier: Oxford, UK. p. 3.
- [19]. Ready, J.F., *Effects Due to Absorption of Laser Radiation*. Journal of Applied Physics, 1965. **36**(2): p. 462-468.
- [20]. Ewart, P., D. Zhang, and S. Ahn, *Injection moulding titanium powders; feedstock compounding, homogeneity and handling strength*. Powder Injection Moulding International, 2011. **5**(2): p. 6.
- [21]. Leme, F.O., et al., *Effect of pulse repetition rate and number of pulses in the analysis of polypropylene and high density polyethylene by nanosecond infrared laser induced breakdown spectroscopy*. Applied Surface Science, 2012. **258**(8): p. 3598-3603.
- [22]. Bogaerts, A., et al., *Laser ablation for analytical sampling: what can we learn from modeling?* Spectrochimica Acta Part B: Atomic Spectroscopy, 2003. **58**(11): p. 1867-1893.
- [23]. Cremers, D. and L. Radziemski, *Basics of the LIBS plasma*, in *Handbook of Laser-Induced Breakdown Spectroscopy*, D. Cremers and L. Radziemski, Editors. 2013, John Wiley & Sons Ltd: West Sussex, UK. p. 29.
- [24]. Thakur, S.N., *Atomic emission spectroscopy*, in *Laser-Induced Breakdown Spectroscopy*, J.P. Singh and S.N. Thakur, Editors. 2007, Elsevier: Oxford, UK. p. 44-48.
- [25]. Panne, U., et al., *Analysis of glass and glass melts during the vitrification process of fly and bottom ashes by laser-induced plasma spectroscopy. Part I: Normalization and plasma diagnostics*. Spectrochimica acta, Part B: Atomic spectroscopy, 1998. **53**(14): p. 1957-1968.

Chapter 7

Selective Surface Sintering Using a Laser-Induced Breakdown Spectroscopy System

a peer-reviewed publication

published in

Journal of Spectroscopy

by

H. Jull, P. Ewart, R. Künnemeyer, and P. Schaare

Research Article

Selective Surface Sintering Using a Laser-Induced Breakdown Spectroscopy System

H. Jull,^{1,2} P. Ewart,^{1,3} R. Künnemeyer,^{1,2} and P. Schaare⁴

¹School of Engineering, University of Waikato, Hamilton 3240, New Zealand

²The Dodd-Walls Centre for Photonic and Quantum Technologies, Hamilton 3240, New Zealand

³Waikato Institute of Technology, Hamilton 3200, New Zealand

⁴The New Zealand Institute for Plant & Food Research Ltd, Hamilton 3240, New Zealand

Correspondence should be addressed to H. Jull; harrison.jull@gmail.com

Received 27 March 2017; Revised 24 May 2017; Accepted 30 May 2017; Published 27 July 2017

Academic Editor: Violeta Lazic

Copyright © 2017 H. Jull et al. This is an open access article distributed under the Creative Commons Attribution License, which permits unrestricted use, distribution, and reproduction in any medium, provided the original work is properly cited.

Titanium metal injection molding allows creation of complex metal parts that are lightweight and biocompatible with reduced cost in comparison with machining titanium. Laser-induced breakdown spectroscopy (LIBS) can be used to create plasma on the surface of a sample to analyze its elemental composition. Repetitive ablation on the same site has been shown to create differences from the original sample. This study investigates the potential of LIBS for selective surface sintering of injection-molded titanium metal. The temperature created throughout the LIBS process on the surface of the injection-molded titanium is high enough to fuse together the titanium particles. Using the ratio of the Ti II 282.81 nm and the C I 247.86 nm lines, the effectiveness of repetitive plasma formation to produce sintering can be monitored during the process. Energy-dispersive X-ray spectroscopy on the ablation craters confirms sintering through the reduction in carbon from 20.29 Wt.% to 2.13 Wt.%. Scanning electron microscope images confirm sintering. A conventional LIBS system, with a fixed distance, investigated laser parameters on injection-molded and injection-sintered titanium. To prove the feasibility of using this technique on a production line, a second LIBS system, with an autofocus and 3-axis translation stage, successfully sintered a sample with a nonplanar surface.

1. Introduction

Metal injection molding (MIM) is a fabrication method that uses the injection molding process and sintering to create metal parts with complex geometry (parts with varying surface heights). This process combines metal powders with a carrier system or binder, containing thermoplastic polymers and waxes to create a feedstock that can be injected into a mold to form a green part [1]. The binder is then gradually removed from the green part by a solvent debinding method, a thermal debinding method, or a combination of both. The part is then referred to as a brown part and is sintered in a furnace at high temperature whereby the particles coalesce or fuse together to form a fully consolidated metal part. Using titanium (Ti) metal in MIM allows parts to be created that are both light in weight and biocompatible [2]. The complex shapes formed offer a reduction in costs associated with titanium parts made by conventional fabrication processes

such as casting or machining and can even form parts not possible to produce by any other means. However, powder metallurgy (PM) is known to produce parts with mechanical properties inferior to those produced from wrought metals due to stress raisers and surface irregularities resulting from incomplete particle coalescence. Incomplete coalescence of titanium PM parts is known to occur due to low-quality starting powders, low sintering time, or temperature and also contaminated furnace atmosphere, all of which affect the outermost surface. These surface defects may be mitigated by optimizing the sinter cycle, secondary processes such as bead blasting and polishing or treatments such as electropolishing and coating.

Titanium MIM has the added problem of contamination through any residual binder components of which carbon and oxygen are the most prevalent and the most difficult to mitigate. The transformation of the titanium lattice structure during sintering is influenced by these impurities, and the

formation of oxides/carbides also impinges on the coalescence. While the saturation levels of interstitial oxygen ($w \leq 5\%$) are high, carbon compounds readily form on powder surfaces above 370°C . The presence of carbon on the titanium particles interferes with heat transfer, the oxide presence means the detection, and quantification of the elemental levels is difficult.

Sintering of metals can also be done with high-powered continuous wave (CW) lasers such as those used in direct metal laser sintering and selective laser sintering. This process requires a high-power density over a short time [3]. Laser-induced breakdown spectroscopy (LIBS) uses a high-power pulsed laser to ablate the surface of a sample and to create a plasma that contains the surface elements. The study presented here investigates whether LIBS can be used for selective surface sintering of injection-molded titanium while simultaneously measuring the amount of sintering that has taken place.

1.1. Laser-Induced Breakdown Spectroscopy. LIBS is a form of optical emission spectroscopy utilizing a high-powered, pulsed laser. The short pulse is focused onto a sample surface where it creates a high-power density in a localized area. A plasma is created from the ablated material [4]. Plasma formation is a complex process, which is still under investigation. The current models for ablation describing the change in thermal properties of the sample material are adequate for this study [5]. The models for nanosecond laser ablation state that when a laser hits a target, with enough high energy, the surface heats up, melts, vaporizes, and ionizes creating a plasma. If there is additional energy in the laser pulse, the plasma absorbs it, increasing the plasma temperature. Further heating of the surface of the target can occur if the plasma is hot enough [6, 7]. For a more detailed discussion on plasma ablation, refer to [8] and the references therein.

Substantial shot-to-shot variation is a problem for quantitative LIBS analysis. Plasmas created on identical samples can have different temperatures which affect emission line intensities [9]. Subtle changes in experimental conditions and surface composition can cause these temperature variations. To improve results, averages are generated by repeatedly measuring the same sample. The average spectra can then provide quantitative information on the composition of the sample.

The use of multiple LIBS pulses has been employed for different purposes. One use is removing surface layers off various materials. The LIBS laser is focused on the same surface position, and multiple pulses are used with spectroscopy feedback to determine when the surface layer has been successfully removed. Costela et al. [10] cleaned graffiti off urban buildings with minimal damage to the surface of the building. Li et al. [11] removed cobalt from tungsten carbide hardmetal. Diego-Vallejo et al. [12] used linear correlation and artificial neural networks to determine when the top layers of solar cells had been removed. Majewski et al. [13] cleaned contaminants from thermal barrier coatings, and Roberts et al. [14] removed rock-covering fossils. Maravelaki et al. [15] cleaned Pentelic marble covered in encrustations. Acquaviva et al. [16] cleaned the bust of St. Gregory the

Armenian of contaminants. Flores et al. [17] removed spines from pricked pears without visible damage to the pear, and Bengtsson et al. [18] cleaned salt off high-voltage insulators.

Another use of multiple LIBS pulses is depth profiling. Martelli et al. [19, 20] determined the different tissues in wheat by looking at the Mg II 279.55 nm to Mg I 285.22 nm intensity ratio as repetitive shots were taken at the same location. Abdelhamid et al. [21] investigated the effects of laser irradiance and working distance of a sample looking at how the intensity of Cu I 465.1 nm and Au I 431.5 nm changed after repetitive shots. Theodorakopoulos and Zafropoulos [22] looked at depth profiles of varnishes using the C_2 swan band. De Bonis et al. [23] observed the change in the ratio formed by Cu I 282.35 nm and Sn I 283.94 nm for an increasing number of shots on a corroded copper tin alloy. Most of the studies mentioned above used more than 100 pulses because of the small amount of surface material removed. The effects of heat propagation on the underlying surface were not addressed because they were irrelevant for the purposes employed. The heat distribution is determined by laser pulse parameters [8] and the optical coupling efficiency of the material. The ablation site can have differences compared to the original surface. These differences include melted and recondensed matter which no longer exhibits the original sample composition. Surface reflectivity and surface breakdown threshold change [7]. This is caused by high-power density pulses, heat, stress, and pressure during the plasma formation [24]. Inside the ablation crater, there is also recondensed material from the plasma [4]. The study presented in this paper utilizes the heat, stress, and pressure created by multiple plasma formations to change the surface properties to a desired state.

LIBS has previously been used as a process-monitoring technique. Boué-Bigne [25] investigated segregation and decarburization using LIBS on polished high-carbon steel. Elemental maps of the surfaces were produced using individual emission lines. One map created using a neutral manganese line was normalized with a neutral iron line removing the baseline gradient. Cabalín and Laserna [26] used pulsed laser deposition to coat silicon with manganin. They produced multielemental maps to monitor the coating constituents. Pedarnig et al. [27] utilized LIBS for in situ monitoring of plasma emission on thin-film deposition. Emission lines of interest were normalized by neutral and ionized yttrium lines and a neutral zinc line. Gruber et al. [28] designed a LIBS system for in situ analysis of solid and molten metals. Chromium, copper, manganese, and nickel were investigated using iron lines as an internal standard. Gruber et al. [29] also performed LIBS analysis on molten metal for chromium, nickel, and manganese but under a vacuum. Lopez-Moreno et al. [30] created a stand-off LIBS system to analyze molten metal as an in-process control. Quantitative analysis of chromium, nickel, and manganese was performed on steel samples at 1000°C . The present work investigates LIBS as a method for real-time monitoring of the amount of sintering taking place as a result of the LIBS process.

1.2. Internal Standards. In theory, taking a ratio of two emission lines can compensate for the fluctuations in the

amplitude of spectra caused by experimental conditions. This is referred to as an internal reference, where all emission lines of interest are normalized using a single emission line. The emission line used as a reference is usually from an element with a constant concentration or of an element that makes up the majority of the plasma [6]. The sample can also be spiked with a foreign element of constant concentration, which can be used as a reference. An important consideration is to choose lines that have similar upper level electron energies (E_k). This will reduce the temperature effects, which cause large deviations in emission intensities. Temperature characteristics of each line need to be considered if variations are to be minimized. The magnitudes of the emission lines are to be comparable to reduce the statistical uncertainties produced by combining the percentage uncertainties of each signal. An example of this problem would be combining a strong line with a weak line. The percentage uncertainty, which is used to compute the resulting variance, would be larger for the weak line producing a high uncertainty.

This study investigates the use of multiple LIBS pulses, for postprocessing, to improve the outer surface of Ti MIM samples with complex geometry. This is achieved by the removal of residual carbon (compounds) from and below the surface thus enabling full coalescence. This process will be controlled by spectral feedback from the carbon and titanium lines. The hypothesis is that the heat caused by the LIBS process, from multiple pulses, is sufficiently high that the amount of surface sintered is relatively large compared to the ablated material. This would allow laser sintering and measurement of surface properties at the same time.

2. Experimental Setup

A commercial Spectrolaser 4000 unit (Laser Analysis Technologies, Australia) containing a Nd:YAG laser operating at 1064 nm with a pulse width of 7 ns and pulse energies of 50, 100, and 200 mJ was focused at a fixed distance perpendicular to the sample surface to generate the plasma. The spot diameter was about 650 μm , which results in an irradiance of about 8.6 GW cm^{-2} at 200 mJ per pulse. The wavelength range of 185.25–948.80 nm was captured by the four spectrometers inside the Spectrolaser unit. The spectrometers were set to integrate for 1 ms after a 1.27 μs delay from the onset of the laser pulse. This system can reach high laser pulse energies but does not allow changing of the lens-to-sample distance. The setup was used to investigate the effect that laser pulse energy has on thermally debound injection-molded titanium samples.

A second commercial system (LIBS-6, Applied Photonics, UK) containing a Nd:YAG laser (Big Sky Ultra, Quantel, France) with the same wavelength, pulse width, delay, and integration time as the Spectrolaser was set to 100 mJ per pulse. The built-in beam expander was focused to produce a spot size on the sample of 450 μm , roughly 80 mm from the beam expander producing an irradiance of 9.0 GW cm^{-2} . Each spectrum was acquired with six spectrometers (Avantes, The Netherlands) covering the range 182.26–908.07 nm. A 3-axis translation stage moved

the sample into the focal position of the LIBS beam. This system produces less laser pulse energy than the previous one but can change the lens-to-sample distance. The setup was used to demonstrate the selective sintering process at different heights using a simple autofocus system.

The Spectrolaser system was used with a fixed distance to the sample to acquire an average of 100 spectra from different locations on a single thermally debound sample and a single-sintered sample (see Section 2.2 for sample descriptions). Different locations were used to avoid the effects of previous pulses on the same site. Spectra were then acquired by sampling 10 different locations, on the thermally debound sample, 20 times at 50, 100, and 200 mJ per pulse. The second LIBS system was used with the autofocus function enabled to evaluate its use in removing surface carbon on a sample with varying surface height.

A commercial field emission scanning electron microscope (SEM) (Hitachi S-4700, Hitachi High Technologies, USA) with an accelerating voltage of 20 kV, emission current of 11,000 nA, and a working distance of 11,200 μm was used to investigate the morphology of the ablation craters. An energy-dispersive X-ray spectroscopy (EDS) attachment to the SEM (Noran System 6, Thermo Fisher Scientific, USA) was used to compare the composition of the craters to that obtained from the LIBS spectra.

2.1. Autofocus. A 635 nm, 4.5 mW, continuous wave laser directed on the ablation site was used in conjunction with a miniature CCD video camera, connected to the LIBS-6 module, to create an autofocus system based on the triangulation method. The laser was aligned so that the axis of the laser beam would intersect with the ablation site. The AForge.NET framework (a library of common computer vision algorithms [31]) was used to filter the image from the camera to only show the beam spot. The centroids of the resulting images (Figures 1(b), 1(d), and 1(f)) were calculated, and a model created to relate the centroid position of the laser spot with the distance from the ablation site. Figure 1(b) corresponds to the sample being too close to the LIBS-6 machine, Figure 1(d) too far from the LIBS-6 system, and Figure 1(f) at a distance where the focus of the LIBS beam is directly on the surface of the sample. This set-up was used in a feedback control system to move the vertical translation stage and hold the sample at the correct height.

2.2. Samples. The samples were made using a binder system comprised of polyethylene glycol 8000, polyethylene glycol 20,000, natural bees wax, linear low-density polyethylene, and polypropylene [32]. The metal powder was commercially pure titanium produced by the hydride-dehydride route with a particle size less than 325 μm (Specialty Metallurgical Products Co. Inc., USA). The binder system was combined with the titanium powder to produce a feedstock with a volume fraction of 30% binder to 70% metal powder. The feedstock was mixed using a corotating twin screw extruder (Thermo-Lab, Lab digital, USA) operating $D = 16$ mm screws, $L/D = 24$, $\omega = 0$ –250 r/min, and $T = 30$ –300°C. Injection molding was done using a fully hydraulic injection-molding machine

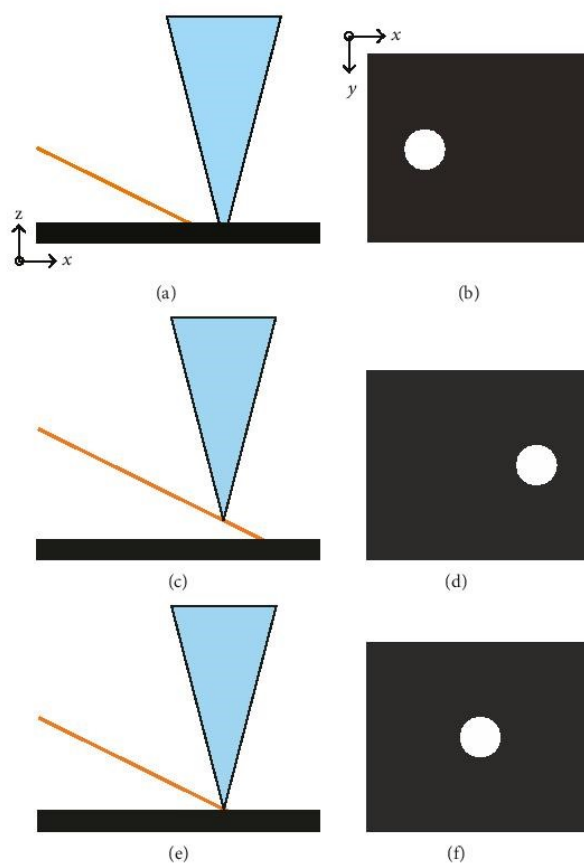


FIGURE 1: Triangulation method using a 635 nm CW laser (beam entering from the left). The vertical beam converging on the sample represents the LIBS beam. (a), (c), and (e) show where the autofocus laser strikes the sample surface. (b), (d), and (f) show the camera images of the filtered autofocus laser spots.

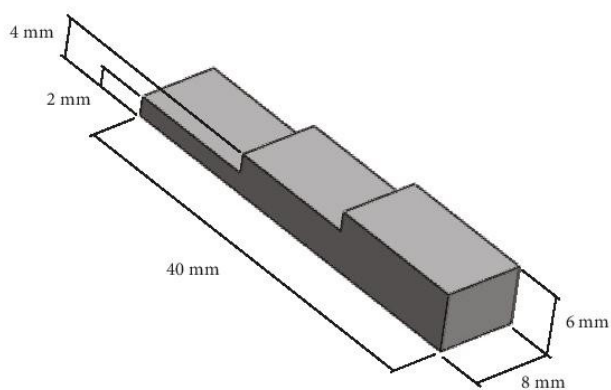


FIGURE 2: Geometry and dimensions for the titanium injection-molded part.

(35 M, Dr Boy, Germany) to create a part shape with complex geometry, that is, with multiple step heights. The dimensions of the part are shown in Figure 2.

Debinding was done using both solvent and thermal processes. A solvent debinding kit (SDK) assembled at the University of Texas-Pan American was used for the test

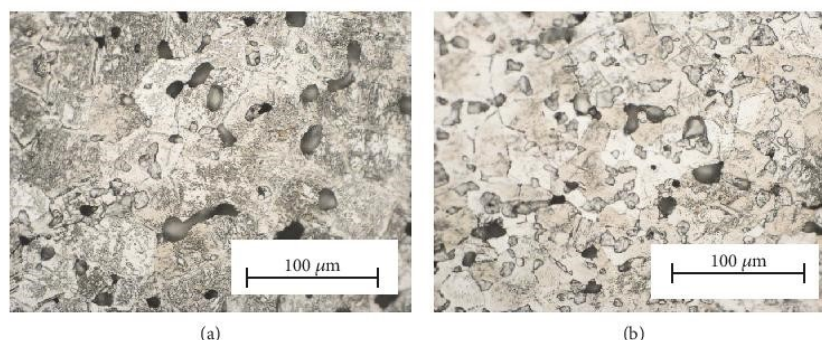


FIGURE 3: Microstructure of thermally sintered Ti part prior to laser sintering (a) polished external surface and (b) sectioned and polished internal microstructure.

samples [32]. Thermal debinding was done in a convective drying oven (FED53, Binder, USA) ($V = 53 \text{ L}$, $T = 30\text{--}300^\circ\text{C}$) with a gas tight chamber and programmable PID temperature control. After parts were solvent debound, the samples were identified using the designation “TD” for thermal debound (brown parts).

The brown parts were sintered in a furnace (ACME, China) by initial heating with an isothermal period at 470°C ($\beta = 5^\circ\text{C}/\text{min}$, $t = 60 \text{ min}$) followed by further heating to 800°C , all under argon sweep gas ($\dot{V} = 10.0 \text{ L}/\text{min}$). This was followed by a further heat increase and a final isothermal period at sinter temperature under vacuum ($5^\circ\text{C}/\text{min}$, $t = 180 \text{ min}$, $T = 1350^\circ\text{C}$, $p = 2.0 \times 10^{-3} \text{ mbar}$). The sintered parts were given the designation “S.” Both TD and S samples were sanded to remove surface coating and finger print residue. Sectioned and polished S samples were analyzed by X-ray diffraction (XRD) (Empyrean, PANalytical, The Netherlands), with power settings 45 kV at 40 mA through a copper electrode, scanning from position 20 to $100^\circ 2\theta$, using a step size of $0.026^\circ 2\theta$, scan step time of 17.340 s in continuous scanning mode. Peak identification was done using the HighScore software (PANalytical, The Netherlands).

3. Results and Discussions

3.1. The TD and S Samples. The conventional means of determining binder level during MIM processing is by weighing each sample and comparing the mass to the theoretical value. This method is accurate for most solvent, and thermal debinding processes carried out under 250°C . However, conventional thermal debinding temperatures are above 420°C , at which point the thermoplastic binders are reduced to the constituent elements (carbon, oxygen, nitrogen, and hydrogen). Also, at these temperatures, titanium preferentially absorbs those elements with no indication from the component mass. Without destructive testing, it is difficult to determine whether binder residue levels are sufficiently low, and the desired mechanical properties are achieved. Higher elemental levels near the external surfaces can be seen (Figure 3(a)) compared to those internally (Figure 3(b)). The difference arises because the rate of elemental diffusion is slower than the rate of surface deposition

once the pores between the particles close during sintering and densities greater than about 94% are reached.

Even where levels of carbon and oxygen meet specified standards, they may still hinder coalescence of the particles during sintering and cause surface porosity. Surface porosity as seen in Figure 3 reduces the mechanical properties of the final part. The XRD analysis confirmed the presence of carbon and oxygen, as carbide formations, near the external surface [33]. The ability to reduce the elemental levels at the surface should therefore enable a decrease in porosity and subsequent increase in overall density leading to improvements in mechanical properties. Using LIBS to selectively sinter parts of the surface, postprocessing may have the ability to do this.

3.2. Difference in Carbon Content between the TD and S Samples. The average spectra of 100 shots on each of the TD and S samples are shown in Figure 4. These spectra were analyzed to find spectral lines that fulfilled the criteria discussed in Section 1.2. Each shot was aimed at different locations on the sample. The emission lines observed in the spectra of the S sample were weaker, and the background continuum was reduced. The Ti II lines were dominant, and the strong lines of Ti I, which are prevalent between 400 and 600 nm , were significantly reduced. These differences are shown in Figure 4. The UV range, where a number of well-identified Ti lines are present, is highlighted in Figure 5.

Lines that were identified as suitable for internal standardization were C I 247.86 nm ($E_k = 7.685 \text{ eV}$) and Ti II 282.81 nm ($E_k = 8.132 \text{ eV}$). Taking the ratio of these lines, over all 100 shots on the S sample are 2.45 . The C I and Ti II line intensity depends on transition probabilities, electron temperature, and electron density of the plasma, which are governed by highly complex processes in a multicomponent plasma. Time profiles of the species differ as well. As the lifetime of the plasma is shorter than the minimum integration time of the spectrometers, the temporal behavior cannot be analyzed. However, the intensity ratio of the C I/Ti II lines can be calibrated against other measurements, like EDS, and should be useful to determine when enough carbon has been removed. A threshold value of 2.45 was used to indicate when the TD sample had been sintered. At this threshold, the

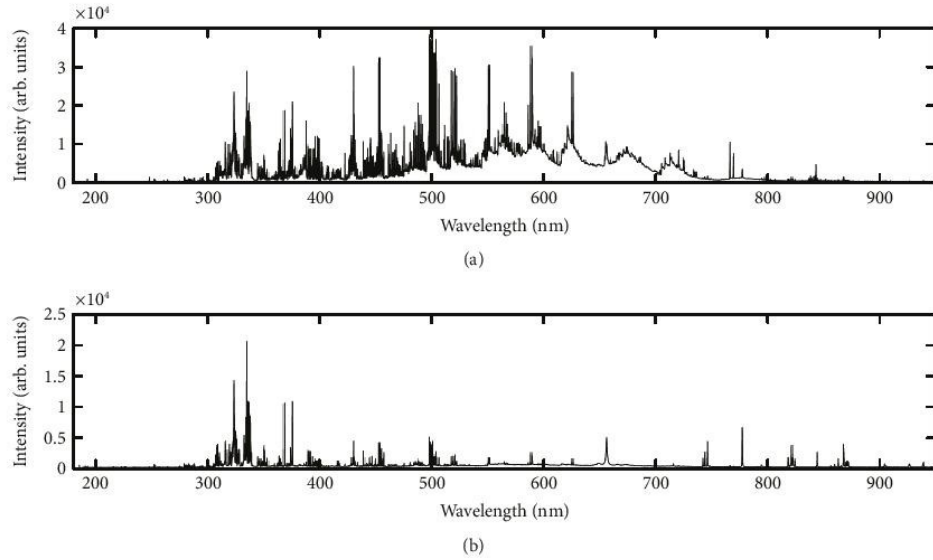


FIGURE 4: Average spectra acquired from 100 shots on the TD (a) and S (b) samples. Each shot was on a fresh surface which had not previously been sampled.

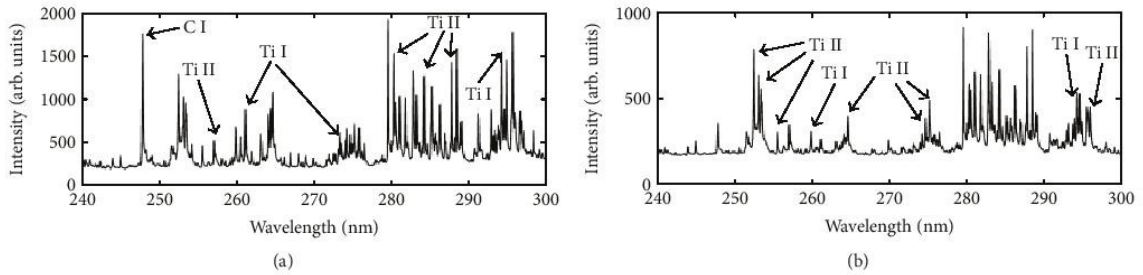


FIGURE 5: Enlarged section of Figure 4 showing some of the differences between the Ti I and Ti II emissions from the TD (a) and S (b) samples.

TABLE 1: Comparison of the Ti and C content.

	LIBS		EDS			
	Peak intensity ratio (Ti/C)	C (Wt.%)	Ti (Wt.%)	V (Wt.%)	O (Wt.%)	Si (Wt.%)
Thermally debound	0.762	20.29 ± 0.32	74.00 ± 0.68	—	5.71 ± 0.56	—
Sintered	2.45	1.79 ± 0.24	96.78 ± 0.69	0.24 ± 0.24	—	1.19 ± 0.08

amount of titanium and carbon in the TD sample surface would resemble that of the S sample.

EDS results show that there is a difference in carbon between the TD sample and the S sample of 18.5 Wt.%. Table 1 displays the results obtained from EDS. When the vanadium content is low, an incorrect concentration for vanadium is determined because of the overlap between the $TiK\beta$ (4.93 keV) and the $VK\alpha$ (4.95 keV) peaks in the EDS spectra [34]. The actual vanadium content was determined to be less than 0.01% V from the supplier (Specialty Metallurgical Products Co. Inc., USA). The silicon content is a residue from sanding the sample. The peak intensity ratio of the

spectral lines is proportional to the amount of Ti II compared with C I present in the plasma. The amount of titanium in the plasma would be split between Ti I and Ti II. Therefore, the actual concentration ratio, which can be calculated from the EDS results, cannot easily be determined from the spectra without full knowledge of all plasma parameters, like electron temperature and electron density.

3.3. *Energy Effects on Multiple Shots.* Irradiating an ablation site multiple times with LIBS pulses and comparing the resulting spectra gives information on the amount of sintering taken place. The TD sample was irradiated in 10 different

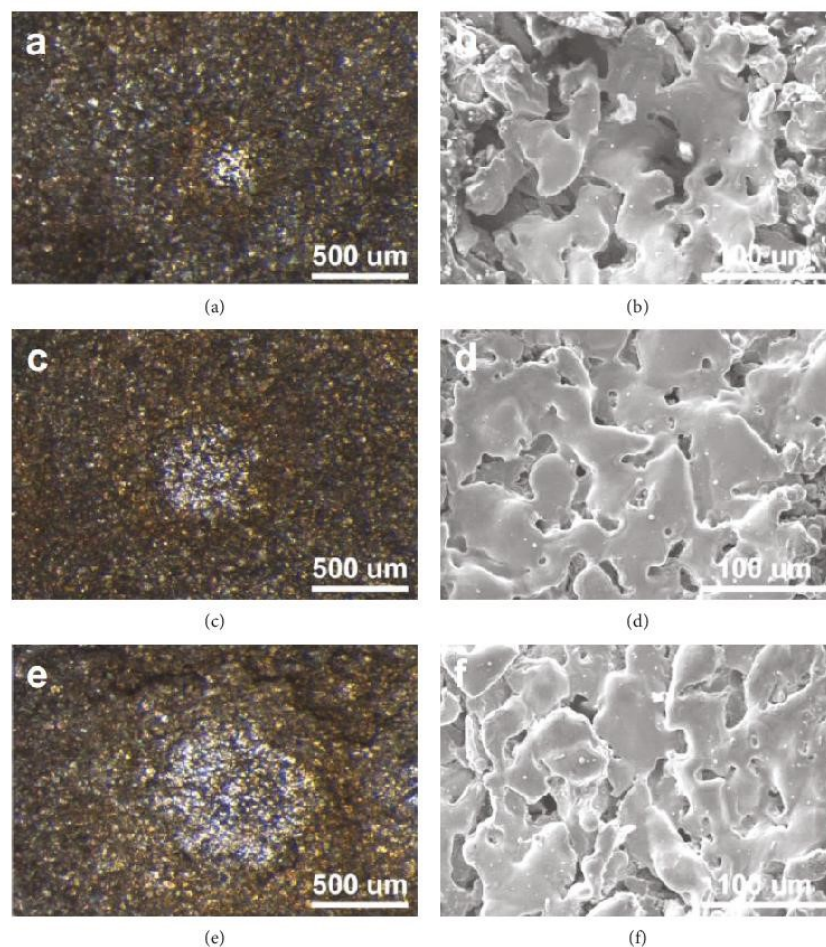


FIGURE 6: Ablation craters from 20 consecutive laser pulses using 50 mJ (a), (b); 100 mJ (c), (d); and 200 mJ (e), (f). (a), (c), and (e) are taken with a SEM (Copyright 2016 Trans Tech Publications Ltd. reprinted with permission [33]).

locations by 20 successive pulses. This process was repeated at different laser pulse energies. The resulting spectra were investigated to determine the effect of laser pulse energy. Figure 6 shows the ablation sites at different laser energies. Figures 6(a), 6(c), and 6(e) are optical microscopy images and Figures 6(b), 6(d), and 6(f) are SEM images. The area being sintered increases as the laser pulse energy increases, as can be seen by the increasing spot in Figures 6(a), 6(c), and 6(e). SEM images of the centers of the ablation craters shown in Figures 6(a), 6(c), and 6(e) are displayed in Figures 6(b), 6(d), and 6(f). These images confirm that sintering has taken place. The edge of the sintered titanium particles are seen in Figure 6(b). The contrast between titanium particles that have and have not been sintered is displayed in Figure 7.

In addition to the line ratio mentioned above, other spectral lines were considered for their suitability to monitor sintering. Sixteen Ti I lines were investigated by calculating the ratio of the Ti I line intensity to the C I 247.86 nm

intensity. These ratios were normalized then scaled so that they could be compared to the above reference threshold value. Successive sampling using different energies is displayed in Figure 8 for the Ti I 398.18 nm/C I 247.86 nm intensity ratio. The error bars in Figure 8 correspond to the standard deviation of the 10 spectra that were used to find the average ratio for each point on the graph. All other emission line ratios exhibit a trend similar to that of Figure 8. The small initial value in the first shot may be due to surface contamination. The large fluctuations and error bars are produced by the large difference in ΔE_k (difference in E_k) between the Ti I lines and C I 247.86 nm which range from 3.26 eV to 5.29 eV. At these high-energy differences, the ratios cannot mitigate the differences in plasma temperature caused by shot-to-shot variations.

Using the same normalizing and scaling procedure as above, 47 Ti II to C I 247.86 nm intensity ratios were analyzed as well. The wavelengths of the Ti II lines were between 252.56 and 457.20 nm and had ΔE_k between -0.39 eV and

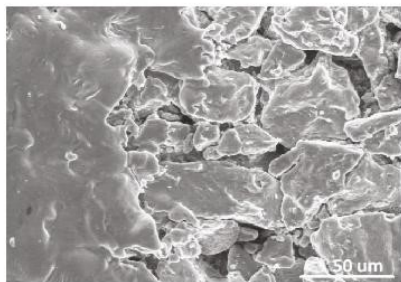


FIGURE 7: SEM showing the edge of sintered titanium. Unsintered particles to the right were not irradiated with the laser beam.

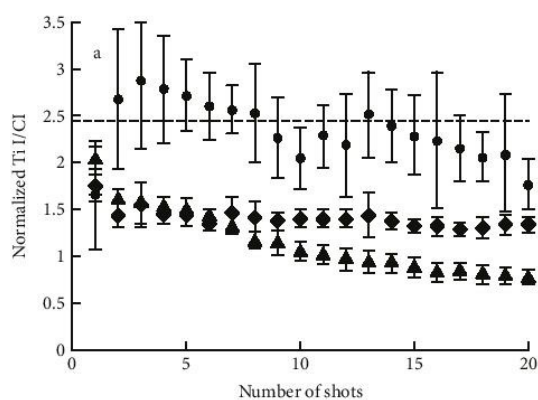


FIGURE 8: Evolution of the normalized Ti I 398.18 nm/C I 247.86 nm intensity ratio of the thermally debound sample. The dashed line shows the sintering threshold. The different energies used were 200 mJ (●), 100 mJ (◆), and 50 mJ (▲) per pulse.

4.02 eV. A selection of these lines is shown in Table 2, and their variation with the number of 200 mJ laser shots in Figure 9. After 10 shots, all line ratios are above the sintering threshold.

Using Ti II rather than Ti I, substantial lines improved the sintering prediction. The Ti II lines that produced the best results were 264.59, 280.48, 281.02, 281.78, and 282.81 nm. Their upper energy level difference to the C I line, ΔE_k , is between -0.397 and -0.881 eV. All lines followed the trend shown in Figure 10 for the 282.81 nm line. However, C I 247.86 nm ($E_k = 7.685$ eV) and Ti II 282.81 nm ($E_k = 8.132$ eV) was identified as the most robust combination for internal standardization.

Figure 10 shows that 50 mJ successive shots bring no increase to the titanium to carbon intensity ratio but instead give a slow, steady decline. At 100 mJ, the ratio of peak intensities increases until the tenth shot where the ratio starts to decrease. It is not clear what causes this behavior. At 200 mJ, the intensity ratio increases until it surpasses the threshold of the S sample obtained from Section 3.2. After 10 shots, the threshold value is surpassed, and the TD surface composition is comparable to the S surface. The reason the

TABLE 2: Ionized titanium emission lines used in Figure 9.

λ (nm)	E_k (eV)	ΔE_k
253.13	5.03	2.65
264.59	8.57	-0.88
281.02	8.10	-0.41
283.22	4.95	2.73
351.08	5.42	2.26
352.03	5.57	2.12
353.54	5.57	2.12
362.48	4.64	3.04
416.36	5.57	2.12
433.79	3.94	3.75
450.13	3.87	3.82

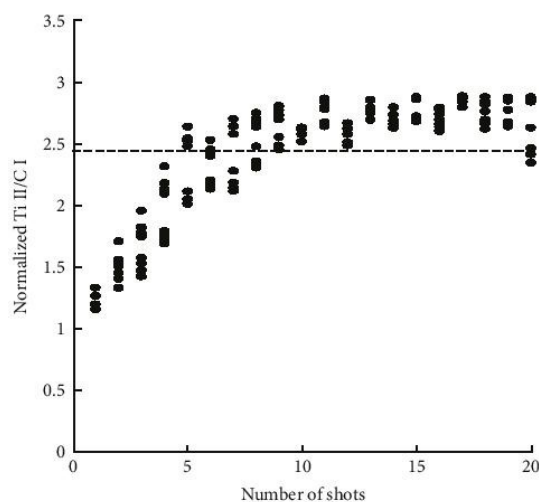


FIGURE 9: Evolution of multiple Ti II lines (Table 2) for a laser pulse energy of 200 mJ. Each point is an average of 10 shots. The dashed line shows the sintering threshold.

ratio continues to increase for 200 mJ is that the high-power density produced by the 200 mJ pulse raises the temperature in the sample through heating from the LIBS beam during plasma formation. The heat on the surface starts the sintering process, removing residual binder and fusing together the titanium particles. As the number of laser pulses increases, particle fusion increases. The particle fusion and necking in Figures 6, 7, and 11 are evidence that the surface has been sintered.

EDS results (Table 3) of the ablation crater created from the 200 mJ treatment (Figure 6(e)) show that the carbon content after 20 shots has reduced from 20.29 Wt.% to 2.13 Wt.% which is comparable to the S sample. The area examined by EDS is presented in Figure 6(f). This confirms the reduction in carbon seen in the titanium to carbon intensity ratio obtained from the LIBS spectra. These results show that there is enough heat penetrating into the sample

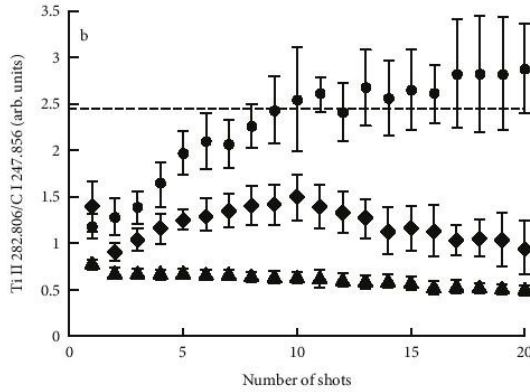


FIGURE 10: Evolution of the peak intensity ratio for Ti II 282.81 nm/ C I 247.86 nm on the thermally debound sample. The dashed line shows the sintering threshold. The different energies used were 200 mJ (●), 100 mJ (◆), and 50 mJ (▲).

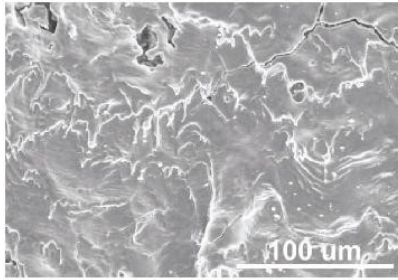


FIGURE 11: SEM image of sintering resulting from slowly moving the LIBS-6 beam after 10 shots.

creating sintering with very small removal of surface material due to plasma formation.

3.4. Reduction of Carbon Signal in LIBS Spectra. The focal position of the LIBS beam was positioned on the surface of the TD sample. The spot size of the laser, determined from the ablation crater, is approximately $650\ \mu\text{m}$ in diameter. When successive shots are fired, sintering expands until it fills the entire spot size of the incident laser. The high-carbon content correlates to the unsintered part of the surface being sampled and is reduced as the area being sampled fuses together. When the entire area under the laser spot is sintered, the Ti/C ratio resembles that of sintered titanium.

It can be seen from the SEM images in Figure 6 that there has been sintering in all ablation craters from 50, 100, and 200 mJ laser pulses even though the LIBS intensity ratio does not reach the threshold value of the S sample. After 20 shots at 50 mJ, there is a sintered spot in the middle of the ablation crater which is about $250\ \mu\text{m}$ in diameter. Because of the low laser energy, there is not enough heat generated on the surface of the sample to produce particle fusion over the

TABLE 3: Sample composition after repetitive shots compared to traditional sintering. Results obtained from EDS.

	C (Wt.%)	Ti (Wt.%)	V (Wt.%)	Si (Wt.%)
Ablation crater	2.13 ± 0.26	97.27 ± 0.84	0.59 ± 0.32	—
Sintered	1.79 ± 0.24	96.78 ± 0.69	0.24 ± 0.24	1.19 ± 0.08

entire spot size of the laser. Subsequent shots would still be sampling the carbon in the unsintered part of the ablation crater, and the Ti/C ratio does not reach the threshold value. The 100 mJ crater shows similar results with a slightly bigger sintered spot.

3.5. Implementation. The LIBS-6 system, coupled with the autofocus unit and 3-axis translation stage, was used to produce sintering on the surface of the sample steps at heights of 2, 4, and 6 mm (see Figure 12). The Spectrolaser system produced sintering at 200 mJ per pulse, with an irradiance of $8.6\ \text{GW cm}^{-2}$. Using the LIBS 6 system, which has a smaller spot size, increases irradiance on the sample causing higher temperatures and increased localized heating on the surface of the sample. With a pulse energy of 100 mJ, an irradiance of $9.0\ \text{GW cm}^{-2}$ is produced which is comparable to the Spectrolaser system. Therefore, the LIBS-6 system will provide the same heat that the Spectrolaser system produces, entirely sintering the spot area after 10 shots.

The results of sintering a line on the TD sample using the LIBS-6 system and the ratio threshold of 2.45 to control the process are displayed in Figures 11 and 12. The LIBS-6 system had a spot diameter of $450\ \mu\text{m}$ and a repetition rate of 20 Hz with the sample stage moving at a speed of roughly $0.4\ \text{mm/s}^{-1}$. It can be seen that the titanium particles have fused together forming a solid mass. After sintering had taken place, on an ablation site, the LIBS beam was moved to a new surface which overlapped the previous spot. Sintering was then repeated on the new surface. The liquid titanium formed on the new spot flowed over the previously sintered spot and has fused together. These regions are seen in Figure 11. This process was repeated until a sintered line was produced across the sample. Figure 12 shows the effectiveness of pulsed laser sintering a line across injection-molded titanium at step heights of 6, 4, and 2 mm using autofocus. The effect of heat propagation through the part can be seen by the titanium bluing.

4. Conclusions

LIBS has been proven useful for sintering-selected surfaces of injection-molded titanium. The LIBS beam, plasma, and residual heat of the sample surface all contribute to the heating of the injection-molded titanium causing sintering. By observing the C I 247.856 nm and the Ti II 282.806 nm lines and then comparing the intensity ratio to that of a conventionally sintered sample, the amount of sintering taking place can be determined. Repetitive shots continue heating the surface and provide spectral feedback to monitor whether the sintering process is complete. The effectiveness

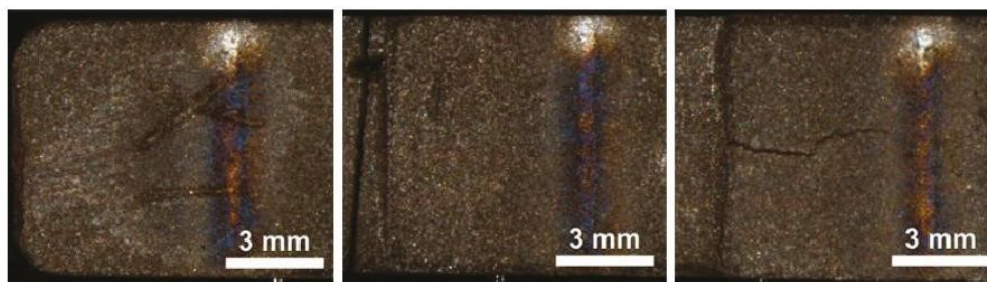


FIGURE 12: Optical micrograph of line sintering at different step heights. Left to right: 2, 4, and 6 mm step heights.

of using LIBS to determine when the sample has been sintered has been verified using EDS and SEM images. EDS results show a 18.5 Wt.% reduction in carbon content. It was found that 10 shots at an irradiance between 8.6 and 9.0 GW cm⁻² is sufficient to sinter the spot produced by the LIBS beam.

Using the triangulation method described, an autofocus mechanism was produced and calibrated to the LIBS-6 system. This system was used on an injection-molded grey part with varying step heights to prove the viability of using LIBS in a production process on metal parts with complex geometry. Sintered lines were produced on different step heights of an injection-molded sample. The heat from repetitive plasma formations has colored the previously sintered titanium.

Additional Points

Highlights. The amount of sintering under a laser spot is evaluated using LIBS. Spectral measurements determine the relative titanium to carbon content. LIBS and Energy-dispersive X-ray Spectroscopy results display a reduction in carbon contents on the sintered surface.

Conflicts of Interest

The authors declare that they have no conflicts of interest.

Acknowledgments

The authors would like to acknowledge and offer continuing respect and admiration to deceased colleague Dr. Sadhana Talele, who was not able to see this work completed. This work was supported by New Zealand's Ministry of Business, Innovation and Employment under contract C11X1209.

References

- [1] J. Beddoes and M. J. Bibby, "6 - powder metallurgy," in *Principles of Metal Manufacturing Processes*, J. Beddoes and M. J. Bibby, Eds., pp. 173–189, Butterworth-Heinemann, Oxford, 1999.
- [2] T. Ebel, "17 - metal injection molding (MIM) of titanium and titanium alloys," in *Handbook of Metal Injection Molding*, D. F. Heaney, Ed., pp. 415–445, Woodhead Publishing, Cambridge, United Kingdom, 2012.
- [3] A. Simchi, "Direct laser sintering of metal powders: mechanism, kinetics and microstructural features," *Materials Science and Engineering A*, vol. 428, pp. 148–158, 2006.
- [4] D. Cremers and L. Radziemski, "Introduction," in *Handbook of Laser-Induced Breakdown Spectroscopy*, p. 3, John Wiley & Sons Ltd, West Sussex, UK, 2013.
- [5] J. F. Ready, "Effects due to absorption of laser radiation," *Journal of Applied Physics*, vol. 36, pp. 462–468, 1965.
- [6] J. P. Singh and S. N. Thakur, "Fundamentals of laser induced breakdown spectroscopy," in *Laser-Induced Breakdown Spectroscopy*, J. P. Singh and S. N. Thakur, Eds., p. 3, Elsevier, Oxford, UK, 2007.
- [7] D. Cremers and L. Radziemski, "Basics of the LIBS plasma," in *Handbook of Laser-Induced Breakdown Spectroscopy*, D. Cremers and L. Radziemski, Eds., p. 29, John Wiley & Sons Ltd, West Sussex, UK, 2013.
- [8] A. Bogaerts, Z. Chen, R. Gijbels, and A. Vertes, "Laser ablation for analytical sampling: what can we learn from modeling?" *Spectrochimica Acta Part B: Atomic Spectroscopy*, vol. 58, pp. 1867–1893, 2003.
- [9] U. Panne, C. Haisch, M. Clara, and R. Niessner, "Analysis of glass and glass melts during the vitrification process of fly and bottom ashes by laser-induced plasma spectroscopy. Part I: normalization and plasma diagnostics," *Spectrochimica Acta Part B: Atomic Spectroscopy*, vol. 53, pp. 1957–1968, 1998.
- [10] A. Costela, I. García-Moreno, C. Gómez, O. Caballero, and R. Sastre, "Cleaning graffiti on urban buildings by use of second and third harmonic wavelength of a Nd:YAG laser: a comparative study," *Applied Surface Science*, vol. 207, pp. 86–99, 2003.
- [11] T. Li, Q. Lou, Y. Wei, F. Huang, J. Dong, and J. Liu, "Laser-induced breakdown spectroscopy for on-line control of selective removal of cobalt binder from tungsten carbide hard-metal by pulsed UV laser surface ablation," *Applied Surface Science*, vol. 181, pp. 225–233, 2001.
- [12] D. Diego-Vallejo, D. Ashkenasi, A. Lemke, and H. J. Eichler, "Selective ablation of Copper-Indium-Diselenide solar cells monitored by laser-induced breakdown spectroscopy and classification methods," *Spectrochimica Acta Part B: Atomic Spectroscopy*, vol. 87, pp. 92–99, 2013.
- [13] M. S. Majewski, C. Kelley, W. Hassan, W. Brindley, E. H. Jordan, and M. W. Renfro, "Laser induced breakdown spectroscopy for contamination removal on engine-run thermal barrier coatings," *Surface and Coatings Technology*, vol. 205, pp. 4614–4619, 2011.
- [14] D. E. Roberts, A. du Plessis, J. Steyn, L. R. Botha, S. Pityana, and L. R. Berger, "An investigation of Laser Induced Breakdown Spectroscopy for use as a control in the laser removal

- of rock from fossils found at the Malapa hominin site, South Africa," *Spectrochimica Acta Part B: Atomic Spectroscopy*, vol. 73, pp. 48–54, 2012.
- [15] P. V. Maravelaki, V. Zafropoulos, V. Kilikoglou, M. Kalaitzaki, and C. Fotakis, "Laser-induced breakdown spectroscopy as a diagnostic technique for the laser cleaning of marble," *Spectrochimica Acta Part B: Atomic Spectroscopy*, vol. 52, pp. 41–53, 1997.
- [16] S. Acquaviva, M. L. De Giorgi, C. Marini, and R. Poso, "A support of restoration intervention of the bust of St. Gregory the Armenian: compositional investigations by laser induced breakdown spectroscopy," *Applied Surface Science*, vol. 248, pp. 218–223, 2005.
- [17] T. Flores, L. Ponce, M. Arronte, and E. de Posada, "Free-running and Q: switched LIBS measurements during the laser ablation of Prickle Pears spines," *Optics and Lasers in Engineering*, vol. 47, pp. 578–583, 2009.
- [18] M. Bengtsson, R. Grönlund, M. Lundqvist, A. Larsson, S. Kroöll, and S. Svanberg, "Remote laser-induced breakdown spectroscopy for the detection and removal of salt on metal and polymeric surfaces," *Applied Spectroscopy*, vol. 60, pp. 1188–1191, 2006.
- [19] M. R. Martelli, C. Barron, P. Delaporte, G. Viennois, X. Rouau, and A. Sadoudi, "Pulsed laser ablation: a new approach to reveal wheat outer layer properties," *Journal of Cereal Science*, vol. 49, pp. 354–362, 2009.
- [20] M. R. Martelli, F. Brygo, P. Delaporte, X. Rouau, and C. Barron, "Estimation of wheat grain tissue cohesion via laser induced breakdown spectroscopy," *Food Biophysics*, vol. 6, pp. 433–439, 2011.
- [21] M. Abdelhamid, S. Grassini, E. Angelini, G. M. Ingo, and M. A. Hariith, "Depth profiling of coated metallic artifacts adopting laser-induced breakdown spectrometry," *Spectrochimica Acta Part B: Atomic Spectroscopy*, vol. 65, pp. 695–701, 2010.
- [22] C. Theodorakopoulos and V. Zafropoulos, "Depth-profile investigations of triterpenoid varnishes by KrF excimer laser ablation and laser-induced breakdown spectroscopy," *Applied Surface Science*, vol. 255, pp. 8520–8526, 2009.
- [23] A. De Bonis, B. De Filippo, A. Galasso, A. Santagata, A. Smaldone, and R. Teghil, "Comparison of the performances of nanosecond and femtosecond Laser Induced Breakdown Spectroscopy for depth profiling of an artificially corroded bronze," *Applied Surface Science*, vol. 302, pp. 275–279, 2014.
- [24] F. O. Leme, Q. Godoi, P. H. M. Kiyataka, D. Santos, J. A. M. Agnelli, and F. J. Krug, "Effect of pulse repetition rate and number of pulses in the analysis of polypropylene and high density polyethylene by nanosecond infrared laser induced breakdown spectroscopy," *Applied Surface Science*, vol. 258, pp. 3598–3603, 2012.
- [25] F. Boué-Bigne, "Laser-induced breakdown spectroscopy applications in the steel industry: rapid analysis of segregation and decarburization," *Spectrochimica Acta Part B: Atomic Spectroscopy*, vol. 63, pp. 1122–1129, 2008.
- [26] L. M. Cabalin and J. J. Laserna, "Surface stoichiometry of manganin coatings prepared by pulsed laser deposition as described by laser-induced breakdown spectrometry," *Analytical Chemistry*, vol. 73, pp. 1120–1125, 2001.
- [27] J. D. Pedarnig, J. Heitz, T. Stehrer et al., "Characterization of nano-composite oxide ceramics and monitoring of oxide thin film growth by laser-induced breakdown spectroscopy," *Spectrochimica Acta Part B: Atomic Spectroscopy*, vol. 63, pp. 1117–1121, 2008.
- [28] J. Gruber, J. Heitz, H. Strasser, D. Bäuerle, and N. Ramaseder, "Rapid in-situ analysis of liquid steel by laser-induced breakdown spectroscopy," *Spectrochimica Acta - Part B Atomic Spectroscopy*, vol. 56, pp. 685–693, 2001.
- [29] J. Gruber, J. Heitz, N. Arnold et al., "In situ analysis of metal melts in metallurgic vacuum devices by laser-induced breakdown spectroscopy," *Applied Spectroscopy*, vol. 58, pp. 457–462, 2004.
- [30] C. Lopez-Moreno, S. Palanco, and J. J. Laserna, "Calibration transfer method for the quantitative analysis of high-temperature materials with stand-off laser-induced breakdown spectroscopy," *Journal of Analytical Atomic Spectrometry*, vol. 20, pp. 1275–1279, 2005.
- [31] aforgenet.com, "AForge.NET framework," 2012, <http://www.aforgenet.com/framework/>.
- [32] P. Ewart, S. Ahn, and D. Zhang, "Mixing titanium MIM feedstock: homogeneity, debinding and handling strength," *Powder Injection Moulding International*, vol. 5, pp. 54–59, 2011.
- [33] P. Ewart, H. Jull, R. Künemeyer, and P. N. Schaare, "Identification of contamination levels and the microstructure of metal injection moulded titanium," in *Key Engineering Materials*, T. Ebel and F. Pyczak, Eds., vol. 704, pp. 161–169, Trans Tech Publications Ltd, Zurich, Switzerland, 2016.
- [34] J. C. Russ, "Chapter 3 - energy dispersive spectrometers," in *Fundamentals of Energy Dispersive X-ray Analysis*, J. C. Russ, Ed., pp. 17–41, Butterworth-Heinemann, Oxford, United Kingdom, 1984.

Chapter 8

Classification of recyclables using laser- induced breakdown spectroscopy for waste management

a peer-reviewed publication

in review by

Spectroscopy Letters

by

H. Jull, J. Bier, R. Künemeyer, and P. Schaare

Classification of recyclables using laser-induced breakdown spectroscopy for waste management

H. Jull^{a*}, J. Bier^{a, b}, R. Künnemeyer^{a, c}, and P. Schaare^d

^a School of Engineering, University of Waikato, Hamilton 3240, New Zealand

^b Aduro Biopolymers, Hamilton 3240, New Zealand

^c Dodd Walls Centre for Photonic and Quantum Technologies, New Zealand

^d Plant and Food Research, Hamilton 3240, New Zealand

* Corresponding author. Email address harrison.jull@gmail.com

Abstract

With the ever-increasing amount of generated waste governments around the world are looking for, and implementing, ways to minimise waste output and maximise waste recovery. The main difficulties are sorting waste items, identifying the different types of plastics, and the time taken to sort them manually. Bioplastics such as polylactic acid and Novatein thermoplastic protein can be incorporated into the recycling stream to minimise waste. Laser-induced breakdown spectroscopy spectra analysed by k -nearest neighbour and soft independent modelling by class analogy were investigated as methods that can rapidly identify recyclables. Raw, peak normalised, and total intensity normalised spectra were used to identify which would improve classification. Laser-induced breakdown spectroscopy spectra were generated by single laser shots to different locations on nine samples, glass (brown, green, and clear), tin, aluminium, polylactic acid, Novatein, polyethylene terephthalate, and high-density polyethylene. To prove that the system has the potential to be used on a waste sorting stream an autofocus unit was developed to move the laser-induced breakdown spectroscopy beam into focus on the different sample geometries. Two classification methods were investigated, soft independent modelling by class analogy and the k -nearest neighbours algorithm. k -nearest neighbours on raw spectra produced the best results. Discrimination between bioplastics and plastics were 100 %. Glass samples could not be reliably distinguished from each other. Surface contamination produced 3 misclassifications

from 405 spectra in the training data. The same results were obtained when the spectral range was reduced from 182.26 - 908.07 nm to 313.20 - 908.07 nm.

Keywords: Laser induced breakdown spectroscopy, LIBS, Polylactic acid, Novatein Thermoplastic Protein, Recycling.

Highlights: Waste management, Laser-induced breakdown spectroscopy, bioplastic, recycling.

8.1 Introduction

With large amounts of waste being generated around the world, countries and industries are implementing strategies to recycle as much of this waste as possible. New Zealand government and local councils are implementing safeguards such as legislation, initiatives, and accords to minimise waste and increase recycling [1-3]. The Waste Minimisation Act [1] requires local councils to promote waste management and minimisation, and create a waste management and minimisation plan. Local government and industry have adhered to the act to improve the sustainability of packaging used in New Zealand through greater material and energy efficiency in the production, use, and recovery of packaging materials [3]. There has been great success thus far with 73 % of New Zealanders having access to kerbside recycling, and a further 24 % having access to drop-off centres in 2006 [2]. Kerbside recycling accepts aluminium and tin cans, paper, glass, and various plastics depending on location. All local councils recycle polyethylene terephthalate (PET) and high-density polyethylene (HDPE) [4].

Currently material recovery facilities in New Zealand sort plastics manually by product. Around the world different sorting methods are used. The difficulties with these methods include separating and identifying plastics, and the time taken to perform these processes. For example, near-infrared spectroscopy is not applicable to black samples, mid-infrared spectroscopy takes several seconds to acquire a measurement and has difficulty identifying heavy metals [5-7]. An automated process using laser-induced breakdown spectroscopy (LIBS) would greatly mitigate these difficulties, if not eliminate them. Plastic packaging contains

additives such as fillers, colorants, and plasticisers all of which can be disposed of or recycled in various ways. These additives reduce the reliability and quality of sorted materials because they introduce impurities within the sorted plastic types, which is one of the main shortfalls of recycling [8].

8.1.1 Bioplastics

Another way to minimise waste would be to use bioplastics, which may be biodegradable and compostable under appropriate conditions. Packaging industries have become increasingly interested in developing bioplastics to replace food packaging [9]. Global production of bioplastics has an estimated annual growth rate of up to 30 % and will reach an expected capacity of 3.5 million tonnes in 2020 [10, 11]. Not all plastics produced from bio-mass feedstocks are necessarily biodegradable and compostable [10]. Some, for example bio-based polyethylene, are chemically identical to conventionally derived plastics which are recycled [11].

A major concern with recycling bio-based plastics, that are biodegradable, is that they may be mistaken for, and combined with, regular plastics contaminating plastic waste streams. Thus, they may need removal and separation from existing recycling streams if found in kerbside collection. Polylactic acid (PLA) is a commonly known biodegradable bioplastic which is derived from corn or other carbohydrate sources [9]. PLA has the potential to replace PET, HDPE, low-density polyethylene (LDPE), and polystyrene (PS) for many applications ([9, 10, 12] and the references therein) because it has similar properties. These properties include high versatility, thermoplasticity, good resistance against grease and oil, low permeability to aromas, and low temperature sealability [11, 13, 14]. A few items made from PLA are blow moulded bottles, dinnerware, food packaging, food wrap, deli trays, and injection moulded food containers [12, 14, 15]. Novatein[®] Thermoplastic Protein [16] is an up-and-coming thermoplastic currently being developed by Aduro Biopolymers LP. Novatein is derived from blood meal, which is a by-product of the meat processing industry. Using the by-products not only maximises the value from co-products from the meat processing, but it also minimises waste by creating biodegradable plastics which can replace plastics going into landfills. Novatein has mechanical properties comparable to LDPE [17].

8.1.2 Laser induced breakdown spectroscopy

LIBS is a type of optical emission spectroscopy which focuses a high-power, short-pulsed laser onto the surface of a sample, ablating a tiny amount of sample material, and creating a plasma [18]. During the early lifetime of the plasma excited electrons decay from high energy levels triggering free-free and free-bound transitions. The spectrum produced is dominated by a continuum background [19, 20]. As the plasma continues to cool the excited electrons decay even more allowing atomic and molecular emissions to dominate. The spectra generated at this time provide qualitative and quantitative information on the chemical makeup of the sample. LIBS measurements can be done in situ, at varying distances, and can provide results in real time. These advantages make LIBS very attractive for use in the recycling industry.

LIBS has been used for classification, identification, recycling, and sorting of plastics and other waste. Applications include determining the manufacturer and origin of mobile phones from polymer fragments [21], sorting cement, brick, gypsum block, wood, polyvinyl chloride (PVC), glass (white, green and brown), sandstone, gabbro, and steel rebar in waste streams from demolished build sites [22]. Some of the plastics that have been investigated for recycling are PET [7, 23-30], HDPE [7, 23-30], LDPE [7, 23, 24, 26-30], polyethylene (PE) [26, 27, 31, 32], polypropylene [7, 23-32], PS [23-33], PVC [7, 22, 26-31, 33], polyoxymethylene, [31], polytetrafluoroethylene [31], polyoxyethylene [31], polyamide [31-33], polybutylene terephthalate [31], acrylonitrile butadiene styrene [31-33], polycarbonate [31-33], styrene-butadiene [33], polyphenylene oxide [33], and thermoplastic polyester [33].

A recycling technique should have very little, if any, pre-processing to make the method as efficient as possible. Aquino and Pereira-Filho [21] fired a single, low energy pulse with a 250 μm spot diameter to clean the surfaces of the samples. The spot area was reduced and the pulse energy increased before analysing the samples. Xia and Bakker [22] used compressed air to clean the dust off of their samples. The samples were then placed on a rotating plate in a way so that they were all level. The setup simulated the intended application where the waste would have the surface scraped off to provide a flat surface for analysis, removing the need for an

autofocus unit. Despite efforts to flatten the sample surface a problem encountered was that shot-to-shot variation was caused mostly by the LIBS pulses missing the samples. Gondal and Siddiqui [28] formed pellets out of plastics granules and powder. Sattmann et al. [7] washed, dried, and shredded plastic bottles into flakes. The flakes were then pressed into a mould.

Sorting is not a trivial task, which can be attested to by the many post processing techniques that have been employed on LIBS spectra for recycling. These include using specific emission lines [7, 21, 23, 31], emission line ratios [7, 23, 26, 28, 29, 31, 33], specific regions of wavelengths [23, 25], the entire range of wavelengths [21, 22, 24, 27, 30, 33], and spectra have been normalised by different methods [21, 22, 32, 33]. Many chemometric methods have been used [7, 21, 24, 25, 27, 29, 30].

The work presented here explores LIBS' suitability for sorting recycling waste streams. Principal component analysis (PCA) [21-23, 25, 31, 33], soft independent modelling by class analogy (SIMCA) [21], and k -nearest neighbour (k -NN) [21] are compared for spectral analysis. Peak normalisation and total intensity normalisation are investigated as possible spectral pre-treatment methods [34, 35]. In addition to identifying materials that are common to all sorting facilities around New Zealand the possibility of distinguishing PLA and Novatein from regular plastic waste is also investigated.

8.2 Experimental setup

A LIBS-6 system (Applied Photonics, UK) containing a Nd:YAG laser (Big Sky Ultra, Quantel, France) operating at the fundamental wavelength of 1064 nm, with a pulse width of 7 ns, was focused perpendicular to the sample surface to generate the plasma. The pulse energy was 100 mJ. Each spectrum was acquired with the six spectrometers in the LIBS-6 unit covering the range 182.26 - 908.07 nm. All spectrometers were set to start recording after a delay time of 1.27 μ s with respect to the laser pulse and an integration time of 1.1 ms. A 3-axis translation stage moved the sample along the axis of the LIBS beam.

8.2.1 Autofocus

Two 635 nm, 5 mW, continuous wave lasers directed on the ablation site were used in conjunction with a miniature CCD video camera to create an autofocus system based on the laser triangulation [36]. The CCD video camera was part of the LIBS-6 system. The lasers were mounted on the LIBS-6 nozzle opposite each other as in Fig. 1. The lasers were aligned so that the axis of each laser beam would intersect with the ablation site. One of the lasers was turned on, illuminating the site to be ablated, and an image was taken using the CCD camera. The distance to the sample was then found using triangulation. The laser was then turned off and the process was repeated for the remaining laser. The two 635 nm lasers were used to overcome the geometric limitations of using the triangulation method from one angle. If one of the lasers has its beam blocked then the other laser will still acquire a valid distance. The AForge.NET framework (a library of common computer vision algorithms [37]) filtered the beam spot from the image. The centroid of the spot was used to find the distance to the sample surface and the 3-axis translation stage was moved into place.

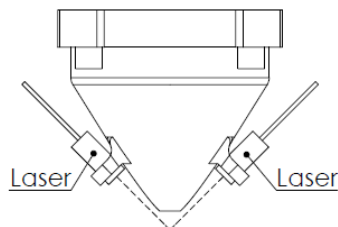


Fig. 1. Autofocus setup on the LIBS-6 nozzle. The charge-coupled device camera is located inside the nozzle.

8.2.2 Samples

The samples consisted of the common items collected in kerb-side recycling, glass bottles (clear, green, and brown), plastics bottles (PET and HDPE), a tin can, and an aluminium can. Two bioplastics (PLA and Novatein) were also included to determine whether they can be distinguished from the other recycled plastics. The bioplastic grades used were NatureWorks® PLA Polymer 3051D (Natureworks, LLC) and Novatein® IR3020 (Aduro Biopolymers, Hamilton, New Zealand). Both

are suitable for injection moulding and could mistakenly be discarded in curb-side recycling.

To resemble the intended implementation of LIBS in a sorting facility, where possibly only one shot will be taken of an item, the spectra gathered from the samples were not averaged. A total of 50 spectra was collected for each sample. Each spectrum corresponding to a single shot in a new location on the surface of the sample. Dark current and background removal was performed on the spectra.

8.2.3 Statistical analysis

The spectrum from each sample was mean centered before processing. PCA was then performed on the spectra. PCA transforms a set of variables into a new set of orthogonal variables called principal components (PCs) that capture as much of the variability in the original data as possible. The first PC contains the largest variance in the data. The next PC accounts for the maximum possible variance in an orthogonal direction compared to the previous PC. The number of PCs range from one to the number of variables in the data set. By applying PCA to the spectra the dimensions are reduced while retaining as much of the variability as possible. Leave-one-out cross-validation (LOO-CV) was used on the PCA model to reduce the effects of overfitting. The PCs were used as inputs for k -NN classification [38]. k -NN is a classification algorithm that uses a distance measure, the Euclidean distance in this study, to determine how far away the investigated sample is away from the k closest samples surrounding it. The classifications of the k samples are averaged to classify the unknown sample. The optimal k number of neighbours was determined by minimising the loss function, which in this case was taken to be the percentage of misclassifications.

Individual PCA models were made for each class and LOO-CV was used to find the optimal number of PCs for each class. These models were used as inputs for SIMCA. SIMCA is a classification algorithm that calculates the orthogonal distance and scores distance from each model to the sample under investigation [39]. In the PLS_Toolbox [40] version of SIMCA, called alternative SIMCA, the Mahalanobis distance and the squared residuals are used to calculate the reduced distance. The

class boundaries determined by the PCA models of each class are used with the calculated reduced distance to classify the new sample as belonging to a single class, more than one class, or not belonging to any class. The samples belonging to multiple classes, or not assigned to any classes, can be forced into the class that it is closest to.

The above analyses were repeated for two types of normalisation. The first type was dividing each spectrum by its highest intensity. The second type was dividing each spectrum by the accumulated total of emission line intensities. The results of the normalisations were compared to results on raw spectra without normalisations. The data were split, using 45 spectra from each sample for training and validation in the cross-validation, and 5 spectra from each sample for testing. Analysis was done using the PLS_Toolbox (Eigenvector Research Inc, US) in Matlab (MathWorks, US).

8.3 Results and Discussions

By averaging the bioplastic and plastic spectra visual differences can be seen between PLA, Novatein, PET, and HDPE. Fig. 2 displays the averaged spectra. The Sodium D-lines at around 589 nm were very strong in the spectrum for Novatein (NTP) with intensities of roughly 52,000 and 40,000. Because of that the y-axis of the Novatein plot in Fig. 2 has been limited to 10,000 a.u. so spectra could be more easily compared. One major difference seen is that the CN violet band emissions at 388.34 nm were weaker for bioplastics. However, these results are misleading. Visual classification cannot be relied on because of the shot-to-shot variation seen in LIBS spectra. The variation can produce similar spectra from different samples. The purpose of this study is to have one-shot classification regardless of variation.

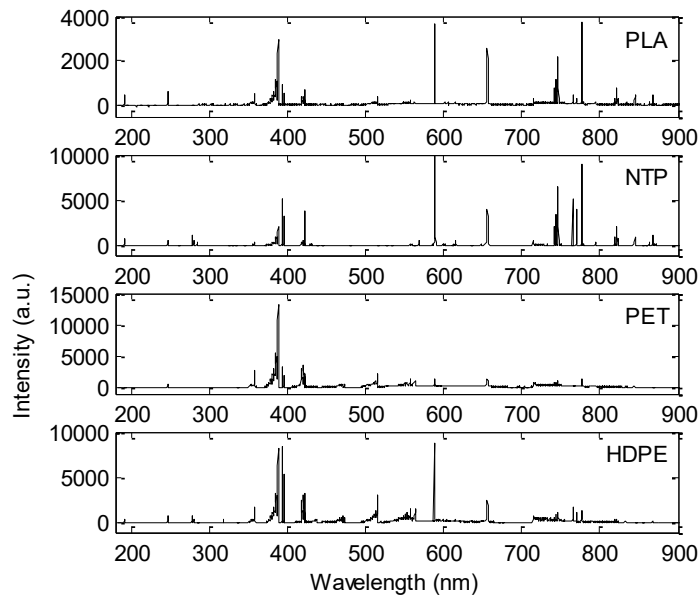


Fig. 2. Average spectra from different plastics and bio plastics. The y-axis for Novatein has been reduced cutting off the sodium D lines which are five times larger than the next strongest lines.

The spectra from glass bottles, plastics, tins, and aluminium cans are also distinguishable from each other by visual inspection. It is harder to classify items that are similar, such as the different types of glass bottles, because there is less variation in the spectra. Separating the glass bottles into three categories (clear, green, and brown) and performing the statistical analysis on the spectra produced a lot of misclassifications. For this reason, the different coloured glass bottles were combined to make a single category of glass bottles. PCA was done on the spectra, and the variability captured by the first two PCs, which accounts for 69 % of the variation, is displayed in Fig. 3 and Fig. 4.

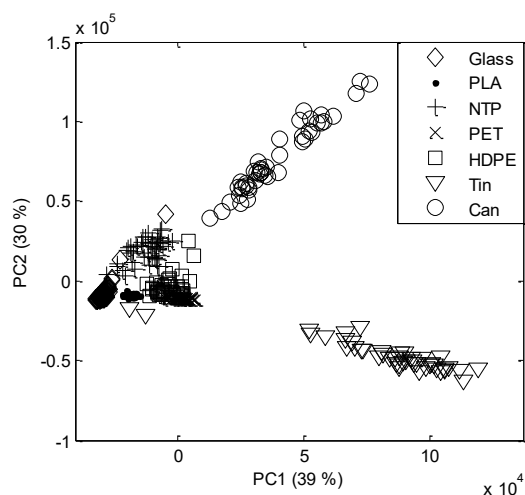


Fig. 3. Scores plot of the first two principal components of the principal component analysis on the different items in recycled waste.

It can be seen that the main variation separates the tin can and the aluminium can from the rest of the items. Fig. 4 shows that PLA is separated by only two PCs and that there are clear overlaps between PET and HDPE, and between glass and Novatein. The overlap between PET and HDPE was not unexpected since Anzano et al. [23] had similar misclassifications using PCA on PET and HDPE.

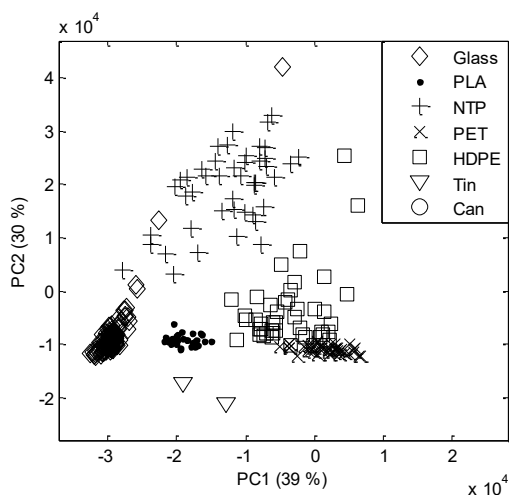


Fig. 4. Closer view of the first two principal components from principal component analysis showing the clustering of samples.

The results from LOO-CV suggested that the optimum number of PCs for the entire dataset was nine and the optimum number of neighbours was two. The optimal number of PCs for each class is shown in Table 1. The number of misclassifications

for k -NN and SIMCA, over the entire dataset (training and test set), are displayed in Table 2. The confusion matrices for the spectra without normalisation are shown in Table 3-5. Neither type of normalisation increases performance for classification. This could be due to contaminants on the sample surface and temperature fluctuations in the plasma changing emission line intensities.

SIMCA classifies a lot of samples as not belonging to any class which is why there are so many misclassifications. Class assignment can be forced by assigning the closest class to the sample. This increases the classifications of SIMCA for all methods of normalisation and by 4 % for the non-normalised spectra. The best classification algorithm is k -NN without normalisation which produces 0.89 % misclassification. The reason SIMCA did not work well is that the models created for each class maximises the within class variation whereas the model created for k -NN maximises the variation over all classes.

Table 1. Optimum number of principal components used for soft independent modelling by class analogy. Determined by leave-one-out cross-validation.

Class	PCs
Glass	3
PLA	2
NTP	2
PET	6
HDPE	5
Tin can	7
Aluminium can	2

Table 2. Performance of the different normalisations and algorithms.

Normalisation	Misclassification (%)		
	k -NN	SIMCA	SIMCA (forced)
None	0.89	5.11	1.11
Maximum intensity	1.78	9.78	6.67
Total intensity	1.56	8.44	1.78

Table 3. Confusion matrix for *k*-nearest neighbours classification on spectra with no normalisation.

		Actual Class						
		Glass	PLA	NTP	PET	HDPE	Tin	Aluminium
Predicted Class	Glass	148	0	0	0	0	0	0
	PLA	0	49	0	0	0	0	0
	NTP	2	1	50	0	0	0	0
	PET	0	0	0	50	1	0	0
	HDPE	0	0	0	0	49	0	0
	Tin	0	0	0	0	0	50	0
	Aluminium	0	0	0	0	0	0	50

Table 4. Confusion matrix for soft independent modelling by class analogy classification on spectra with no normalisation.

		Actual Class						
		Glass	PLA	NTP	PET	HDPE	Tin	Aluminium
Predicted Class	Glass	141	0	0	0	0	0	0
	PLA	0	48	0	0	0	0	0
	NTP	0	0	49	0	0	0	0
	PET	0	0	0	47	0	0	0
	HDPE	0	0	0	1	48	0	0
	Tin	0	0	0	0	0	48	0
	Aluminium	0	0	0	0	0	0	48
	No class	9	2	1	2	2	2	2

Table 5. Confusion matrix for soft independent modelling by class analogy classification on spectra with no normalisation. Samples that were classified as belonging to multiple classes, or to no class, were assigned to the class closest to them.

		Actual Class						
		Glass	PLA	NTP	PET	HDPE	Tin	Aluminium
Predicted Class	Glass	148	0	0	0	0	0	0
	PLA	0	49	0	0	0	0	0
	NTP	2	0	50	0	0	0	0
	PET	0	0	0	48	0	0	0
	HDPE	0	1	0	2	50	0	0
	Tin	0	0	0	0	0	50	0
	Aluminium	0	0	0	0	0	0	50

There were three samples that were misclassified in every analysis. Two were glass spectra from the training dataset and one was a PLA spectrum from the test dataset. Inspection of the spectra from the two glass instances revealed that the Sodium D-lines (Na I 589.00 nm and Na I 589.59 nm) are larger than usual for glass. This is due to the large sodium contribution from fingerprints and the sweat in fingerprint residue on the glass [41, 42]. Fig. 5 shows the dependence of the PCA model on the Sodium D-lines, which has some of the highest loadings. Comparing the misclassified PLA spectrum to the other PLA spectra revealed that there were unusually high emissions for Ca II 393.37 nm, Ca II 396.85 nm, Ca I 422.67 nm, Sodium D-lines (Na I 589.00 nm and Na I 589.59 nm), K I 766.49 nm, and K I 769.90 nm. These lines all correspond to the strongest constituents in sweat which makes up a lot of the residue in fingerprints [42].

The results for the best performing method (*k*-NN without normalisation) shows a misclassification error of 0.79 % which is equivalent to 4 errors. Three of the errors have been discussed above. The two glass spectra and the PLA spectrum were categorised as Novatein. The remaining error was from assigning a HDPE sample to PET. Inspection of the misclassified HDPE spectra revealed a lot of deviations from the typical HDPE spectra. These include no emissions from C I 247.86 nm, K I 766.49 nm, and K I 769.90 nm, lower than usual emissions from

Ca II 393.37 nm, Ca II 396.85 nm, Na I 589.00 nm, Na I 589.59 nm, H α 656.28 nm, N triplet (742, 744, and 746 nm), and the O 777 nm triplet. These differences are possibly from sample contamination. The spectra showed typical emissions from the CN violet bands (388.29, 387.08, 386.14, 385.44 and 385.03 nm) and the C₂ swan bands (516.42 and 512.80 nm). Even with the misclassifications, bioplastics were distinguishable from plastics using single shot LIBS spectra.

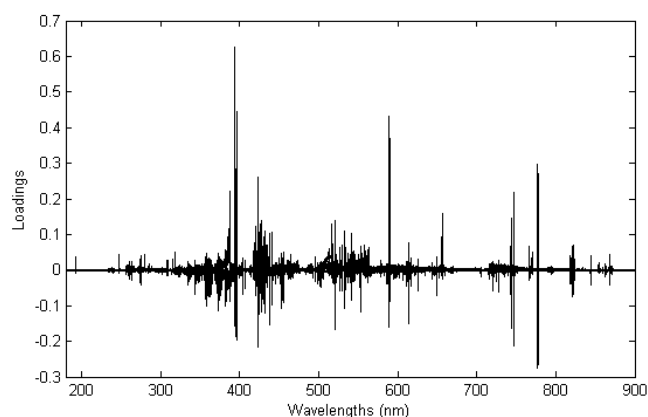


Fig. 5. Principal component analysis loadings plot of the nine principal components.

Ideally a recycling system would have to be as inexpensive as possible. The major cost of a LIBS system is the number of spectrometers used to capture a large range of wavelengths. LOO-CV on k -NN was performed on the spectra from each individual spectrometer to see if a single spectrometer could be used thus reducing the cost of the system. The results presented in Table 6 are of the k -NN models that have been tuned using LOO-CV. Spectrometers 3-6 produced the best results which agrees with the loadings seen in Fig. 5. The accuracy arises from the CN violet bands, C₂ swan bands, calcium, sodium, oxygen, nitrogen, potassium, and H α lines covered in this spectral range.

Different combinations of two different spectrometers were used to see if they would give classification errors close to that of using all six spectrometers. Table 7 displays the results. Combinations of spectrometers 3 with 4, 3 with 5, 4 with 6, and 5 with 6 produce only four misclassifications, one more than using six spectrometers. Using combinations of three different spectrometers produced similar results with a minimum of four misclassifications. This was for spectrometer combinations 3, 4,

5 (6 PCs) and 3, 5, 6 (7 PCs) setting k equal to 2. The misclassifications from the different combinations were not all from the same spectra. Combining four spectrometers (3, 4, 5, and 6) produces the same results as using all spectrometers, that of 3 misclassifications using 8 PCs and setting k to 2. Increasing the number of PCs to 18 produces only two errors, the same as using 19 PCs on the entire spectrum. These two errors are from the two glass spectra discussed earlier.

Table 6. Parameters and performance of using a single spectrometer for classification.

Spectrometer	Spectral range (nm)	Resolution (nm)	PCs	k	Misclassified (%)
1	182.26 - 256.27	0.037	12	2	12.8
2	256.28 - 313.19	0.031	5	2	25.2
3	313.20 - 417.13	0.052	19	2	2.47
4	417.14 - 495.12	0.043	11	2	2.22
5	495.15 - 715.63	0.11	18	2	2.22
6	715.64 - 908.07	0.096	6	2	2.96

Table 7. Misclassification errors using different combinations of spectrometers. The numbers in the brackets are the numbers used for principal components and k .

Spectrometer	Misclassification (%)					
	1	2	3	4	5	6
1	12.8 (12,2)	10.4 (18,2)	1.98 (20,2)	1.73 (18,2)	1.98 (19,2)	2.72 (20,2)
2		25.2 (5,2)	2.72 (4,2)	2.96 (13,2)	2.72 (16,2)	2.22 (8,2)
3			2.47 (19,2)	0.99 (12,2)	0.99 (5,2)	1.23 (15,2)
4				2.22 (11,2)	2.22 (8,2)	0.99 (10,1)
5					2.22 (18,2)	0.99 (6,2)
6						2.96 (6,2)

To use LIBS in practical recycling systems problems caused by surface contamination need to be overcome. Many types of contaminants can obstruct sampling of the actual sample surface and cause errors. These would include labels, water, fingerprints, and residue from consumables. Cleaning shots could be used to overcome this problem but at the cost of the speed of sorting the waste. Each sample would also need to be subjected to multiple shots in different locations to increase the chance of avoiding labels.

8.4 Conclusions

A comparison between k -NN and SIMCA was performed with no data pre-treatment, peak normalisation, and total intensity normalisation. The best results were generated by k -NN with no normalisation. Using k -NN 100 % discrimination between bioplastics and plastics using single shot LIBS spectra was achieved. One HDPE spectrum was misclassified as PET in the cross-validation and one PLA spectrum was misclassified as Novatein from the test set. Fingerprint residue is the main reason for misclassifications, adding extra sodium, potassium, and calcium emissions. The different colours of glass samples could not be distinguished from each other. Tin and aluminium cans had 100 % success rate of correct classification. Reducing the number of spectrometers will significantly reduce the cost of a LIBS system. Using four spectrometers covering the range 313.20-908.07 nm produces the same results as using six spectrometers. Alternative chemometric methods may be able to reduce the number of spectrometers further. In real waste streams samples have coatings on their surfaces, some in the form of labels, which will cause problems with classification. This would mean that the same item would need to have multiple points on the surface investigated by LIBS to avoid thick parts of the coatings. Cleaning shots would also need to be applied. Using LIBS would eliminate the need for roadside and manual sorting, increasing efficiency and minimising costs. It would also increase the reliability and quality of sorted materials. This work demonstrates the ability of LIBS as a one-shot sorting system for recycling waste streams and the viability of incorporating bioplastics in kerbside collection within New Zealand. This is the first time LIBS has been used to differentiate between bioplastics and plastics.

Acknowledgements

We would like to acknowledge and offer continuing respect and admiration to deceased colleague Dr. Sadhana Talele, who was not able to see this work completed.

Financial assistance from the New Zealand Ministry of Business, Innovation and Employment under contract C11X1209 is gratefully acknowledged. This work was supported by The New Zealand institute for Plant and Food Research Ltd, Aduro Biopolymers LP, and the University of Waikato.

References

- [1] New Zealand Government, *Waste Minimisation Act*, Wellington, 2008.
- [2] New Zealand Ministry for the Environment, *The New Zealand Waste Strategy*, Wellington, 2010.
- [3] New Zealand Ministry for the Environment, *New Zealand packaging accord*, Wellington, 2004.
- [4] Recycle.co.nz. *Council Guides*. Available: <http://www.recycle.co.nz/page.php?ref=Regional%20Solutions>
- [5] R. Noll, *Laser-Induced Breakdown Spectroscopy: Fundamentals and Applications*. Heidelberg, Berlin: Springer-Verlag, 2012.
- [6] N. Eisenreich and T. Rohe, "Infrared Spectroscopy in Analysis of Plastics Recycling," in *Encyclopedia of Analytical Chemistry*, ed: John Wiley & Sons, Ltd, 2006.
- [7] R. Sattmann, I. Mönch, H. Krause, R. Noll, S. Couris, A. Hatzia Apostolou, A. Mavromanolakis, C. Fotakis, E. Larrauri, and R. Miguel, "Laser-induced breakdown spectroscopy for polymer identification," *Applied Spectroscopy*, vol. 52, pp. 456-461, 1998.
- [8] G. Davis and J. H. Song, "Biodegradable packaging based on raw materials from crops and their impact on waste management," *Industrial Crops and Products*, vol. 23, pp. 147-161, 2006.
- [9] N. Peelman, P. Ragaert, B. De Meulenaer, D. Adons, R. Peeters, L. Cardon, F. Van Impe, and F. Devlieghere, "Application of bioplastics for food packaging," *Trends in Food Science and Technology*, vol. 32, pp. 128-141, 2013.
- [10] T. Mekonnen, P. Mussone, H. Khalil, and D. Bressler, "Progress in bio-based plastics and plasticizing modifications," *Journal of Materials Chemistry A*, vol. 1, pp. 13379-13398, 2013.
- [11] L. Shen, E. Worrell, and M. Patel, "Present and future development in plastics from biomass," *Biofuels, Bioproducts and Biorefining*, vol. 4, pp. 25-40, 2010.
- [12] M. Jamshidian, E. A. Tehrany, M. Imran, M. Jacquot, and S. Desobry, "Poly-Lactic Acid: Production, applications, nanocomposites, and release studies," *Comprehensive Reviews in Food Science and Food Safety*, vol. 9, pp. 552-571, 2010.

- [13] R. E. Drumright, P. R. Gruber, and D. E. Henton, "Polylactic acid technology," *Advanced Materials*, vol. 12, pp. 1841-1846, 2000.
- [14] J. C. Bogaert and P. Coszach, "Poly(lactic acids): A potential solution to plastic waste dilemma," *Macromolecular Symposia*, vol. 153, pp. 287-303, 2000.
- [15] E. T. H. Vink, K. R. Rábago, D. A. Glassner, and P. R. Gruber, "Applications of life cycle assessment to NatureWorks™ polylactide (PLA) production," *Polymer Degradation and Stability*, vol. 80, pp. 403-419, 2003.
- [16] J. M. Bier, C. J. R. Verbeek, and M. C. Lay, "An eco-profile of thermoplastic protein derived from blood meal Part 1: Allocation issues," *International Journal of Life Cycle Assessment*, vol. 17, pp. 208-219, 2012.
- [17] C. J. R. Verbeek and L. E. Van Den Berg, "Mechanical properties and water absorption of thermoplastic bloodmeal," *Macromolecular Materials and Engineering*, vol. 296, pp. 524-534, 2011.
- [18] D. Cremers and L. Radziemski, "Introduction," in *Handbook of Laser-Induced Breakdown Spectroscopy*, 2nd ed West Sussex, UK: John Wiley & Sons Ltd, 2013, p. 3.
- [19] S. N. Thakur, "Atomic emission spectroscopy," in *Laser-Induced Breakdown Spectroscopy*, J. P. Singh and S. N. Thakur, Eds., 1st ed Oxford, UK: Elsevier, 2007, p. 26.
- [20] R. E. Russo, X. L. Mao, J. H. Yoo, and J. J. Gonzalez, "Laser Ablation," in *Laser-Induced Breakdown Spectroscopy*, J. P. Singh and S. N. Thakur, Eds., 1st ed Oxford, UK: Elsevier, 2007, p. 61.
- [21] F. W. B. Aquino and E. R. Pereira-Filho, "Analysis of the polymeric fractions of scrap from mobile phones using laser-induced breakdown spectroscopy: Chemometric applications for better data interpretation," *Talanta*, vol. 134, pp. 65-73, 2015.
- [22] H. Xia and M. C. M. Bakker, "Reliable classification of moving waste materials with LIBS in concrete recycling," *Talanta*, vol. 120, pp. 239-247, 2014.
- [23] J. Anzano, B. Bonilla, B. Montull-Ibor, and J. Casas-González, "Plastic identification and comparison by multivariate techniques with laser-induced breakdown spectroscopy," *Journal of Applied Polymer Science*, vol. 121, pp. 2710-2716, 2011.

- [24] J. Anzano, B. Bonilla, B. Montull-Ibor, R. J. Lasheras, and J. Casas-Gonzalez, "Classifications of plastic polymers based on spectral data analysis with laser induced breakdown spectroscopy," *Journal of Polymer Engineering*, vol. 30, pp. 177-187, 2010.
- [25] V. K. Unnikrishnan, K. S. Choudhari, S. D. Kulkarni, R. Nayak, V. B. Kartha, and C. Santhosh, "Analytical predictive capabilities of Laser Induced Breakdown Spectroscopy (LIBS) with Principal Component Analysis (PCA) for plastic classification," *RSC Advances*, vol. 3, pp. 25872-25880, 2013.
- [26] J. Anzano, R. J. Lasheras, B. Bonilla, and J. Casas, "Classification of polymers by determining of C1:C2:CN:H:N:O ratios by laser-induced plasma spectroscopy (LIPS)," *Polymer Testing*, vol. 27, pp. 705-710, 2008.
- [27] J. Anzano, M. E. Casanova, M. S. Bermúdez, and R. J. Lasheras, "Rapid characterization of plastics using laser-induced plasma spectroscopy (LIPS)," *Polymer Testing*, vol. 25, pp. 623-627, 2006.
- [28] M. A. Gondal and M. N. Siddiqui, "Identification of different kinds of plastics using laser-induced breakdown spectroscopy for waste management," *Journal of Environmental Science and Health - Part A Toxic/Hazardous Substances and Environmental Engineering*, vol. 42, pp. 1989-1997, 2007.
- [29] I. Moench, R. Sattmann, and R. Noll, "High-speed identification of polymers by laser-induced breakdown spectroscopy," in *Sensors, Sensor Systems, and Sensor Data Processing*, Munich, Ger, 1997, pp. 64-74.
- [30] J. M. Anzano, I. B. Gornushkin, B. W. Smith, and J. D. Winefordner, "Laser-induced plasma spectroscopy for plastic identification," *Polymer Engineering & Science*, vol. 40, pp. 2423-2429, 2000.
- [31] S. Grégoire, M. Boudinet, F. Pelascini, F. Surma, V. Detalle, and Y. Holl, "Laser-induced breakdown spectroscopy for polymer identification," *Analytical and Bioanalytical Chemistry*, vol. 400, pp. 3331-3340, 2011.
- [32] V. C. Costa, F. W. B. Aquino, C. M. Paranhos, and E. R. Pereira-Filho, "Identification and classification of polymer e-waste using laser-induced breakdown spectroscopy (LIBS) and chemometric tools," *Polymer Testing*, vol. 59, pp. 390-395, 2017/05/01/ 2017.
- [33] H. Fink, U. Panne, and R. Niessner, "Process analysis of recycled thermoplasts from consumer electronics by laser-induced plasma spectroscopy," *Analytical Chemistry*, vol. 74, pp. 4334-4342, 2002.

- [34] J. P. Castro and E. R. Pereira-Filho, "Twelve different types of data normalization for the proposition of classification, univariate and multivariate regression models for the direct analyses of alloys by laser-induced breakdown spectroscopy (LIBS)," *Journal of Analytical Atomic Spectrometry*, vol. 31, pp. 2005-2014, 2016.
- [35] P. Porizka, J. Klus, A. Hrdlicka, J. Vrabel, P. Skarkova, D. Prochazka, J. Novotny, K. Novotny, and J. Kaiser, "Impact of Laser-Induced Breakdown Spectroscopy data normalization on multivariate classification accuracy," *Journal of Analytical Atomic Spectrometry*, vol. 32, pp. 277-288, 2017.
- [36] A. Donges and R. Noll, *Laser Measurement Technology Fundamentals and Applications*. Heidelberg, Berlin: Springer-Verlag, 2015.
- [37] aforgenet.com. (2012). *AForge.NET Framework*. Available: <http://www.aforgenet.com/framework/>
- [38] R. O. Duda, P. E. Hart, and D. G. Stork, *Pattern Classification (2nd Edition)*: Wiley-Interscience, 2000.
- [39] S. Wold and M. SjÖStrÖM, "SIMCA: A Method for Analyzing Chemical Data in Terms of Similarity and Analogy," in *Chemometrics: Theory and Application*. vol. 52, ed: AMERICAN CHEMICAL SOCIETY, 1977, pp. 243-282.
- [40] B. M. Wise, J. M. Shaver, N. B. Gallagher, W. Windig, R. Bro, and R. S. Koch, *PLS-Toolbox Manual 4.0 for use with MATLAB™*. Wenatchee, WA: Eigenvector Research, Inc. , 2006.
- [41] M. T. Taschuk, Y. Y. Tsui, and R. Fedosejevs, "Detection and mapping of latent fingerprints by laser-induced breakdown spectroscopy," *Applied Spectroscopy*, vol. 60, pp. 1322-1327, 2006.
- [42] S. J. Montain, S. N. Chevront, and H. C. Lukaski, "Sweat mineral-element responses during 7 h of exercise-heat stress," *International Journal of Sport Nutrition and Exercise Metabolism*, vol. 17, pp. 574-582, 2007.

Chapter 9

Process monitoring using LIBS

Process monitoring using LIBS

The primary aim of this thesis was to develop a LIBS system that could be used on agricultural vehicles, or on a robotic platform. Appendix B discusses the work done on designing a robotic platform that a micro-LIBS unit could be mounted on for autonomous nutritional surveying of a field. Pasture was investigated and variations caused by moisture, and temperature differences, limited the accuracy of the calibrations. Non-aqueous inorganic samples of injection moulded titanium were then investigated to see if removing the complexities of the sample would generate improved results. With success in measuring non-aqueous inorganic material, the focus was turned to non-aqueous organic samples of bio-plastics. This chapter discusses the synthesis of this thesis, combining the works done in chapter 3 through to chapter 8. It gives a summary of the studies and explains the rationale of progression from one study to the next.

Chapter 3 investigated the viability of using LIBS in-field to measure micro and macro nutrients in fresh untreated pasture. Comparisons were made between PLS models created on spectra acquired in air and under an argon atmosphere and between PLS models created on spectra from fresh and dried pasture. The only pre-processing on the spectra was dark current and background subtraction. The coefficient of determination (R^2), root mean squared error of cross-validation (RMSECV), limits of detection (LOD), precision, and variables importance on PLS projections (VIP) were used as figures of merit. The effect of using argon on samples increased the performance of the figures of merit for most nutrient models, some only slightly. This could be due to the increased temperature in the plasma. Fresh pasture samples had higher RMSECV and lower R^2 for all nutrients compared to dried samples.

Comparing the LOD of fresh pasture and dried samples showed that the fresh samples were worse. The change in precision between fresh and dried samples was mixed. The reduction of moisture in the samples causes an increased performance in the PLS modelling, which is seen in Table 3 of Chapter 3. This may be due to an increase in emission line intensity caused by the reduction in moisture in the samples [84-86]. It can also be seen in the increased emissions of nitrogen for the

fresh samples collected during the drought period (Fig. 4, Chapter 3). K, Mg, and Fe concentrations were also affected by the drought. The concentration of K decreased whereas the concentrations of Mg and Fe were higher than normal. The increase in Fe is in agreement with a study performed on detecting drought stress in gardenia and wheat [87]. Fe was found in drought-stressed samples but not in non-stressed samples and K was only found in stressed wheat. This shows that the effects of drought are plant specific.

The extremely weak emission lines for P, Zn and B are a concern since P is only observed in dried samples under argon, Zn only appears under argon, and B lines were not consistently present. Accurate quantitative calibrations cannot be created on spectra that do not have the emission lines of the analysed nutrient. The accuracy would be reliant on the stoichiometric relationships within the matrix. This is also the case for S, which does not have any persistent emission lines in the wavelength range of the spectrometers used in this work. The weak emission lines for N, Mn, Mg, Cu, and Fe should produce accurate models if the lines have sufficient S/B. Variation between spectra acquired from the same sample was the reason why the models for these nutrients are not accurate. Averages were taken from multiple spectra to try to mitigate these variations. The problem with this is that the plasmas formed on each sample are dependent on laser-sample interaction which is affected by the level of moisture present. There is no way to know that the averaged value is representative of the actual concentration in the sample since the variance produced from averaging is quite large. N also has additional problems associated with atmospheric N contribution to the emissions.

Ca and Mg share the problem of their low ionization potentials causing fluctuations between the intensities of both neutral and ionized emission lines. This is because of the different temperatures in each plasma. These temperatures cause the ratio of neutral to ionised emission in the plasma to change between plasmas created on the same sample. The concentrations in the plasma are split between the two species for both Ca and Mg. Figure 1 shows an example of this with two spectra on the same sample.

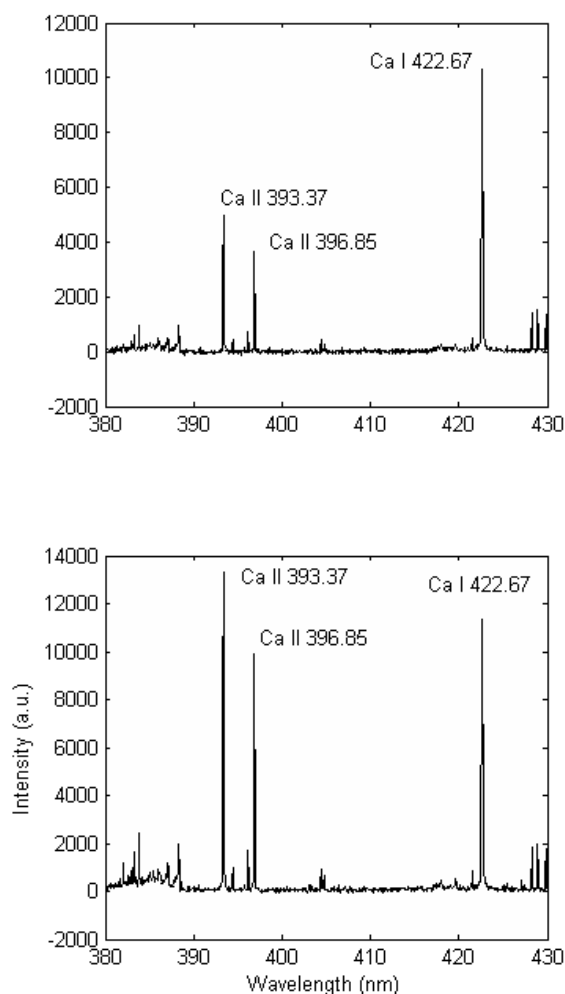


Figure 1. Ionisation effects causing changes in the Ca II and Ca I intensities on the same sample.

The nutrients with successful calibration curves on pasture pellets, having an R^2 greater than 0.90, were K with 0.92, Na with 0.93, and Mn with 0.90. The RMSECV for K, Na, and Mn were 0.2 wt.%, 0.029 wt.%, and 0.0008 wt.% respectively. Most nutrients exhibit weak emissions which affect the accuracy of their PLS models. If the temperature was increased in the plasma this may increase the intensities of emission lines and the number of lines observed. The current setup will not allow for this. Weak lines, ionization effects, and sample moisture contribute to the variations in the spectra as do sample inhomogeneity, matrix effects, perturbations in experimental parameters, amount of ablated material, and the temperature dependence of the plasma [88]. The shot-to-shot variation is the limiting factor in creating accurate models. Pre-processing the spectra and using chemometric methods may increase the accuracy of calibration curves [89-91]. With higher

accuracies, implementation of LIBS systems on agricultural vehicles or robots could be realised infield.

Chapter 4 considers using temperature correction to minimize variations in spectra used to determine sodium concentration in dried pasture. Boltzmann and Saha-Boltzmann plots were used to determine the temperature of the plasmas. The sodium emission lines were corrected using the acquired temperatures and models were created for sodium. These models were compared to models created on the peak intensity and peak area of the sodium emission lines 588.995, 589.592, 818.326 and 819.482 nm. The best R^2 values using peak intensities with and without temperature correction using Boltzmann plots were 0.347 and 0.019. When using the integrated peak area, the best values were 0.308 and 0.023. Figure 2 in Chapter 5 shows an example of the Boltzmann plot used. Finding the temperature using Boltzmann plots was not very accurate since the emission lines used had similar upper-level electron energies (E_k). There needs to be a range of E_k to increase the accuracy of the fitted line. Using the Saha-Boltzmann plots ionised species can be used, increasing the range of E_k . The R^2 values, using the Saha-Boltzmann plots, ranged between 0.344-0.347. Figure 2 in Chapter 5 shows an example of the Saha-Boltzmann plot used. The low correlations may be due to inaccurate calculations of Stark width, electron density, and plasma temperature. Finding the contribution of instrument broadening will increase the accuracy of the Stark width calculation. The inaccuracies may also occur because the plasma may not be in local thermodynamic equilibrium (LTE). A condition called partial-LTE exists when parts of the plasma have different temperatures. LTE needs to be confirmed before calculating the temperature in the plasma. Matrix effects may also cause inaccuracies.

Internal references of C, C₂ swan band head, CN violet band head, O, and combinations of these were used on the Na I 818.326 nm line to investigate reducing variations. Using a combination of a carbon line added with the C₂ swan band head, CN violet band head, and an oxygen line performed the best with an R^2 of 0.665. The reason the internal references did not produce good correlations was that of the large difference in E_k between the lines. Using PLS on the whole spectra

increased the accuracy of the sodium models with an R^2 of 0.855. Performing PLS on particular lines with significant latent variable weights produced an R^2 of 0.835.

The ratio of Na/K is important in identifying salinity stress which is important to plant growth. Similar to using an internal reference, different ratios of Na and K lines were used to minimise the effects of between-plasma temperature variations and experimental variations. The best results were an R^2 of 0.918 and an error in prediction of 0.0587 for the peak intensity ratio of Na I 818.326 nm/ K I 693.876 nm compared to the concentration ratio of Na/K. This ratio produced good correlations because the difference in E_k is small. The small change in E_k reduces the effect of temperature and the ratio itself mitigates other experimental parameter variations.

Chapter 5 investigates using different chemometric methods to mitigate the shot-to-shot variations and create quantitative calibrations on fresh pasture and dried pelletised pasture. The methods explored were Savitzky Golay filtering (SG), multiple linear regression (MLR), principal component regression (PCR), partial least-squares (PLS) regression, Gaussian process regression (GP), and artificial neural network (ANN). R^2 , RMSECV, and normalised root mean squared error of cross-validation (NRMSECV) were the figures of merit used. The NRMSECV was used so that the different nutrients models could be compared. It takes into consideration the range of concentrations used to build the models.

Overall, using different chemometric methods only slightly increased the accuracy of the nutrient models. SG filtering was ineffective since there is minimal noise in the spectra. Introducing categorical data of the plot location and date also did not significantly increase the accuracy of the models. The algorithms that had better performances were PLS+GP with R^2 of 0.93, 0.95, and 0.92 for K, Na, and Mn respectively, PCR+ANN with R^2 of 0.94, 0.83, and 0.80 for Fe, Ca, and Mg respectively, and PLS+ANN with R^2 of 0.77 for B (Table 2, Table 3, Fig 2, and Fig. 3 in Chapter 4). As in Chapter 3, we see that the removal of moisture increases the predictive ability of the models by 4-5 %. For dried samples, some nutrients models still need a higher increase in accuracy to be useful.

A temperature correction on the spectra needs to be made to reduce the shot-to-shot variation. This will be the best way to mitigate the moisture and temperature effects. To determine the temperature in the plasma Boltzmann plots and Saha-Boltzmann plots can be used. The temperature can then be used to correct the spectroscopic emissions. Using internal standards or ratios can mitigate the temperature effect if correct lines are chosen [89]. Lines for internal standards need to have similar upper-level electron energies to minimise temperature effects, have comparable ionization energies, have similar intensities, must not transition to a ground state to avoid self-absorption effects, must not have relatively high intensities because the population is over-estimated, and among other criteria they must have sufficient S/B [54, 92-95].

To further increase the accuracy of nutrient models for pasture, the shot-to-shot variations need to be minimized. These variations are caused by changes in LTSD [15, 96, 97], the amount of sample ablated [36], particle size [36, 98], the microheterogeneity in the pellets [36, 98], matrix effects [99], spectrometer gate delay [25, 100], integration time [101], different laser parameters such as wavelength [102, 103], pulse energy [96, 97, 100], and pulse duration [101]. Many experimental conditions are influenced by the choice of laser wavelength including material ablation and laser penetration depth [104]. Shorter wavelengths have been shown to be more effective at reducing plasma shielding and increasing sample ablation ([105] and the references therein). Studies have found that reducing the particle size in pellets increases the accuracy of models [36, 98], using a femtosecond laser lowers the continuum background producing accurate results for plant material [87], and increasing the fluence by lowering the wavelength of the LIBS laser also increases prediction [36]. Before LIBS can be realised infield, for precision agriculture, a method needs to be developed to produce an accurate quantitative analysis of fresh pasture with minimal variation. This may mean changing the experimental setup or using other post-processing techniques.

With the limitations found in measuring agricultural samples, studies were performed to assess the effectiveness of LIBS on inorganic non-aqueous samples. Many studies using LIBS have been performed on metals and they have found good accuracies [71]. This could be because the metal samples have very few elements

in them which would reduce matrix effects, they have smoother surfaces increasing the consistency of ablated material, and there is no moisture in the samples.

Chapter 6 uses LIBS to identify the contamination levels of carbon in injection moulded titanium. The elements in the binder used for injection moulding of titanium powders needs to be controlled so that the sintered composition is not changed too much. The residual amounts of carbon change the mechanical properties of the sintered titanium. To minimize the carbon levels, debinding removes as much of the binder as possible. An autofocus system, based on the triangulation method, was created to minimise the shot-to-shot variations caused by changes in the LTSD. The on-board LIBS-6 camera and a CW diode laser were used for implementation. The dynamic range of the autofocus system was limited by the LIBS-6 nozzle obstructing the laser spot on the sample from the laser diode.

The LIBS measurements on the surface of the parts at different stages of the injection moulding process give a relative indication of how much carbon is present. The ratio of Ti II 282.806 nm to C I 247.856 nm was used which reduces the temperature variations. The traditional method of mass determination was more accurate for green and grey parts, but LIBS was able to detect residual carbon in brown and sintered parts.

Chapter 7 investigates using LIBS for selective surface sintering of injection moulded titanium. Sintered titanium parts have high elemental levels of residual carbon near the external surface. Reducing the carbon will decrease porosity, increase density, and improve the mechanical properties of the injection moulded parts. Multiple LIBS shots were used on the same spot of the surface of solvent and thermally debound injection moulded titanium. The temperature from the LIBS process was sufficient to remove the carbon and sinter the titanium particles.

Multiple lines were investigated to find a line ratio that would reduce the temperature variations. The ratio of Ti II 282.81 nm to C I 247.86 nm performed the best because of the small change in E_k . This ratio was used to determine when sintering was achieved. This ratio gives a relative indication of the amount of carbon on the surface of the part but can be calibrated to Energy-dispersive X-ray

Spectroscopy (EDS) to determine when sintering is complete. The resultant sintered spot was compared to traditional sintered titanium using EDS on the ablation craters. The LIBS sintered spot had a carbon concentration of 2.13 wt.% which is comparable to the traditionally sintered carbon concentration of 1.79 wt.% and confirms that LIBS can be used to selectively sinter the surface of the injection moulded titanium.

A LIBS system, with the same autofocus system as in chapter 6, was used to prove that this process could be performed on a production line. Lines were sintered in rebound injection moulded titanium parts at varying heights. The autofocus system reduces variations caused by LTSD. The accuracy of the autofocus system is determined by the displacement caused by a single step of the motor which was 1.5 μm , not including hysteresis.

With the success of using LIBS on inorganic non-aqueous samples, studies were performed to assess the effectiveness of LIBS on organic non-aqueous samples. The inorganic non-aqueous samples of titanium were only comprised of a few elements whereas organic non-aqueous samples will have multiple elements which will increase matrix effects and possibly increase variations.

Chapter 8 uses LIBS to distinguish bio-plastics from regular plastics. This study was performed to determine whether bio-plastics could be incorporated into regular recycling streams. Using LIBS to automatically sort the recyclables would reduce the processing time in recycling factories. Identifying bio-plastics would also reduce the contamination that bio-plastics would produce if present in regular plastic recycling. Single shot LIBS was performed on glass, tin, aluminium, polylactic acid (PLA), Novatein thermoplastic protein (NTP), polyethylene terephthalate (PET), and high-density polyethylene (HDPE). Different spectral normalisations and two classification methods were investigated. These were peak and total intensity normalisations with k -nearest neighbour (k -NN) and soft independent modelling by class analogy on the principal components of principal component analysis (SIMCA).

An autofocus system was used to keep the LTSD consistent. The system consisted of two CW lasers directed on the ablation site from opposite sides of the LIBS nozzle and a CCD camera. Each laser coupled with the CCD camera resembles the triangulation method of autofocus. The reason there were two CW lasers is that one laser beam can be obstructed and the reflection would not be acquired by the CCD camera. Having two lasers at different angles reduced this effect.

Single LIBS shots were used so that one-shot classification, regardless of variation, could be investigated. The normalisations did not increase the accuracy of the classification. This may be because of contaminants on the surfaces of samples, temperature fluctuations, or other difficulties. k -NN was more accurate than SIMCA at classifying the recyclables with 100 % discrimination between bioplastics and regular plastics and 0.89 % misclassifications for all recyclables. The success is because k -NN maximises the variation over all classes but SIMCA maximises the variation within each class.

To realise LIBS in a recycling plant, the cost of the system needs to be reduced. This can be done by reducing the number of spectrometers required for classification. The LIBS-6 system used is comprised of six spectrometers. Using combinations of spectrometers 3 with 4, 3 with 5, 4 with 6, and 5 with 6 produces only four misclassifications, one more than using six spectrometers. This would give similar performance at a fraction of the cost of the whole unit. Also, surface contamination from labels, water, fingerprints, and residue is a major drawback that would need to be addressed before adopting LIBS for recycling.

Chapter 10

Conclusion

Conclusion

The aim of this thesis is that a LIBS system can provide detailed, real-time information on the nutritional status of pasture and can be used to tailor fertiliser application rates. This will provide savings to New Zealand farmers, and to the country as a whole. LIBS investigations of fresh and dried pasture were performed in this work. It was established that the difference in moisture between pasture samples hinders accurate prediction of macro and micro nutrients. Removing the moisture in the samples lead to an increase in accuracy of NRMSECV by 4-5 % on average. Moisture, among other factors, contributes to between-spectra variation caused by temperature variations which is difficult to overcome. Multiple chemometric methods and temperature corrections have been performed on the pasture spectra to mitigate these disadvantages.

The work on pasture has found that emission lines from N, P, Mg, Fe, Cu, Zn, and B have weak lines which make it difficult to create a quantitative model. N also has atmospheric interferences. S lines did not appear in the spectral range investigated so the stoichiometric relation between elements is relied upon to create the model. With these disadvantages, success was achieved using PLS+GP (for K, Na, and Mn), PCR+ANN (for Ca, Mg, and Fe), MLR (for Zn), and line ratios (for Na/K).

To increase the performance and accuracy of quantitative models on pasture, repeatable spectra are needed or alternative postprocessing schemes need to be investigated. This may mean that the experimental parameters and setup need to be changed. Once adequate models are created for fresh pasture a LIBS system can be mounted on an agricultural vehicle or robot for infield use.

With the limitations found in measuring agricultural samples, studies were performed on inorganic non-aqueous samples of injection moulded titanium. LIBS was able to acutely detect residual binder for brown and sintered parts better than the traditional mass determination method. A new technique called selective surface sintering using LIBS was also developed for injection moulded titanium. The technique takes advantage of the residual heat, from multiple LIBS shots, to sinter the surface of the samples. At the same time, the spectra produced by LIBS was

used as feedback to monitor the amount of sintering achieved. The results were verified using EDS and SEM images. An autofocus method was developed, based on the triangulation method, to prove the viability of using this technique on metal parts with complex shapes. The autofocus system was verified by sintering injection moulded titanium with varying step heights.

With the success of using LIBS on inorganic non-aqueous samples, studies were performed on organic non-aqueous samples of bio-plastics PLA and NTP. Discriminating HDPE and PET from PLA and NTP was 100 % successful using PCA and *k*-NN. This result proves that bio-plastics can be included in regular curbside collection within New Zealand if LIBS is used in sorting factories. Street sorting would be eliminated if LIBS was implemented and the reliability and quality of sorted materials would increase. To minimise the cost of such systems the number of spectrometers needed can be reduced. Problems may arise with misclassifications generated by surface coatings and contaminants. An autofocus system with two CW lasers, based on the triangulation method, was developed to minimise the obstruction problem inherent to the triangulation method. The autofocus system was validated, in conjunction with LIBS, on classifying recyclables of differing heights.

The work presented in this thesis of quantitative models on fresh pasture, chemometric analyses on pasture, discussion on the leading factors contributing to poor models, and temperature correction and line ratios with regards to pasture are all original works. LIBS for detecting residual carbon in sintered injection moulded titanium, LIBS for selective surface sintering injection moulded titanium, and LIBS for distinguishing bio-plastics from regular plastics are also original works. The success of the work performed is evident by the papers and book chapter under peer review, the peer reviewed papers published in Precision Agriculture, Key Engineering Materials, and the Journal of Spectroscopy, and the peer reviewed paper published in the IEEE conference proceedings of the 6th International Conference on Automation, Robotics and Applications (ICARA). Success is also evident from the presentations in the Eleventh International Conference on Sensing Technology (ICST) 2017, Waikato Young Research Engineers Symposium (WYRES) 2017, IEEE Instrument & Measurement Society Workshop 2016, New

Zealand Institute of Physics Conference (NZIP) 2015, 6th IEEE International Conference on Automation, Robotics and Applications (ICARA), IEEE Instrument & Measurement Society Workshop 2014, and Electronics New Zealand Conference (ENZCon) 2014.

References

References

- [1] C. Mackenzie. (2010, 22 May). *GreenSeeker* [Online]. Available: <http://www.agrioptics.co.nz/products/greenseeker/>
- [2] X. Hou and B. T. Jones, "Field instrumentation in atomic spectroscopy," *Microchemical Journal*, vol. 66, pp. 115-145, 2000.
- [3] J. Moros, J. A. Lorenzo, P. Lucena, L. M. Tobaría, and J. J. Laserna, "Simultaneous Raman spectroscopy-laser-induced breakdown spectroscopy for instant standoff analysis of explosives using a mobile integrated sensor platform," *Analytical Chemistry*, vol. 82, pp. 1389-1400, 2010.
- [4] T. Ahmido, A. Ting, and P. Misra, "Femtosecond laser-induced breakdown spectroscopy of surface nitrate chemicals," *Applied Optics*, vol. 52, pp. 3048-3057, 2013.
- [5] G. Abdellatif and H. Imam, "A study of the laser plasma parameters at different laser wavelengths," *Spectrochimica Acta Part B: Atomic Spectroscopy*, vol. 57, pp. 1155-1165, 2002.
- [6] B. Le Drogoff, J. Margot, M. Chaker, M. Sabsabi, O. Barthélemy, T. W. Johnston, S. Laville, F. Vidal, and Y. Von Kaenel, "Temporal characterization of femtosecond laser pulses induced plasma for spectrochemical analysis of aluminum alloys," *Spectrochimica Acta - Part B Atomic Spectroscopy*, vol. 56, pp. 987-1002, 2001.
- [7] A. K. Knight, N. L. Scherbarth, D. A. Cremers, and M. J. Ferris, "Characterization of laser-induced breakdown spectroscopy (LIBS) for application to space exploration," *Applied Spectroscopy*, vol. 54, pp. 331-340, Mar 2000.
- [8] H. C. Liu, X. L. Mao, J. H. Yoo, and R. E. Russo, "Nonlinear changes in plasma and crater properties during laser ablation of Si," *Applied Physics Letters*, vol. 75, pp. 1216-1218, 1999.
- [9] D. A. Cremers and L. J. Radziemski, "Detection of chlorine and fluorine in air by laser-induced breakdown spectrometry," *Analytical Chemistry*, vol. 55, pp. 1252-1256, 1983.
- [10] R. Wisbrun, I. Schechter, R. Niessner, H. Schröder, and K. L. Kompa, "Detector for trace elemental analysis of solid environmental samples by

- laser plasma spectroscopy," *Analytical Chemistry*, vol. 66, pp. 2964-2975, 1994.
- [11] S. Palanco, J. M. Baena, and J. J. Laserna, "Open-path laser-induced plasma spectrometry for remote analytical measurements on solid surfaces," *Spectrochimica Acta - Part B Atomic Spectroscopy*, vol. 57, pp. 591-599, 2002.
- [12] C. Lopez-Moreno, S. Palanco, and J. J. Laserna, "Stand-off analysis of moving targets using laser-induced breakdown spectroscopy," *Journal of Analytical Atomic Spectrometry*, vol. 22, pp. 84-87, 2007.
- [13] R. A. Multari, L. E. Foster, D. A. Cremers, and M. J. Ferris, "Effect of sampling geometry on elemental emissions in laser-induced breakdown spectroscopy," *Applied Spectroscopy*, vol. 50, pp. 1483-1499, 1996.
- [14] D. A. Cremers, "ANALYSIS OF METALS AT A DISTANCE USING LASER-INDUCED BREAKDOWN SPECTROSCOPY," *Applied Spectroscopy*, vol. 41, pp. 572-579, 1987.
- [15] H. H. Cho, Y. J. Kim, Y. S. Jo, K. Kitagawa, N. Arai, and Y. I. Lee, "Application of laser-induced breakdown spectrometry for direct determination of trace elements in starch-based flours," *Journal of Analytical Atomic Spectrometry*, vol. 16, pp. 622-627, 2001.
- [16] R. Brennetot, J. L. Lacour, E. Vors, A. Rivoallan, D. Vailhen, and S. Maurice, "Mars Analysis by Laser-Induced breakdown Spectroscopy (MALIS): Influence of mars atmosphere on plasma emission and study of factors influencing plasma emission with the use of Doehlert designs," *Applied Spectroscopy*, vol. 57, pp. 744-752, 2003.
- [17] M. D. S. Gomes, D. Santos Jr, L. C. Nunes, G. G. A. De Carvalho, F. De Oliveira Leme, and F. J. Krug, "Evaluation of grinding methods for pellets preparation aiming at the analysis of plant materials by laser induced breakdown spectrometry," *Talanta*, vol. 85, pp. 1744-1750, 2011.
- [18] S. I. Gornushkin, I. B. Gornushkin, J. M. Anzano, B. W. Smith, and J. D. Winefordner, "Effective normalization technique for correction of matrix effects in laser-induced breakdown spectroscopy detection of magnesium in powdered samples," *Applied Spectroscopy*, vol. 56, pp. 433-436, 2002.
- [19] C. Chaléard, P. Mauchien, N. Andre, J. Uebbing, J. L. Lacour, and C. Geertsen, "Correction of matrix effects in quantitative elemental analysis

- with laser ablation optical emission spectrometry," *Journal of Analytical Atomic Spectrometry*, vol. 12, pp. 183-188, 1997.
- [20] A. S. Eppler, D. A. Cremers, D. D. Hickmott, M. J. Ferris, and A. C. Koskelo, "Matrix effects in the detection of Pb and Ba in soils using laser-induced breakdown spectroscopy," *Applied Spectroscopy*, vol. 50, pp. 1175-1181, 1996.
- [21] H. J. Häkkinen and J. E. I. Korppi-Tommola, "Laser-induced plasma emission spectrometric study of pigments and binders in paper coatings: Matrix effects," *Analytical Chemistry*, vol. 70, pp. 4724-4729, 1998.
- [22] B. C. Windom and D. W. Hahn, "Laser ablation - Laser induced breakdown spectroscopy (LA-LIBS): A means for overcoming matrix effects leading to improved analyte response," *Journal of Analytical Atomic Spectrometry*, vol. 24, pp. 1665-1675, 2009.
- [23] J. P. Singh and S. N. Thakur, *Laser-Induced Breakdown Spectroscopy*. Oxford, UK: Elsevier, 2007.
- [24] A. Ciucci, M. Corsi, V. Palleschi, S. Rastelli, A. Salvetti, and E. Tognoni, "New procedure for quantitative elemental analysis by laser-induced plasma spectroscopy," *Applied Spectroscopy*, vol. 53, pp. 960-964, 1999.
- [25] W. Lei, V. Motto-Ros, M. Boueri, Q. Ma, D. Zhang, L. Zheng, H. Zeng, and J. Yu, "Time-resolved characterization of laser-induced plasma from fresh potatoes," *Spectrochimica Acta - Part B Atomic Spectroscopy*, vol. 64, pp. 891-898, 2009.
- [26] M. L. Shah, A. K. Pulhani, G. P. Gupta, and B. M. Suri, "Quantitative elemental analysis of steel using calibration-free laser-induced breakdown spectroscopy," *Applied Optics*, vol. 51, pp. 4612-4621, 2012.
- [27] D. Sun, M. Su, C. Dong, D. Zhang, and X. Ma, "A semi-quantitative analysis of essential micronutrient in folium lycii using laser-induced breakdown spectroscopy technique," *Plasma Science and Technology*, vol. 12, pp. 478-481, 2010.
- [28] M. Tran, Q. Sun, B. W. Smith, and J. D. Winefordner, "Determination of C : H : O : N ratios in solid organic compounds by laser-induced plasma spectroscopy," *Journal of Analytical Atomic Spectrometry*, vol. 16, pp. 628-632, 2001.

- [29] A. Uhl, K. Loebe, and L. Kreuchwig, "Fast analysis of wood preservers using laser induced breakdown spectroscopy," *Spectrochimica Acta - Part B Atomic Spectroscopy*, vol. 56, pp. 795-806, 2001.
- [30] L. Niu, H. H. Cho, K. S. Song, H. Cha, Y. Kim, and Y. I. Lee, "Direct determination of strontium in marine algae samples by laser-induced breakdown spectrometry," *Applied Spectroscopy*, vol. 56, pp. 1511-1514, 2002.
- [31] P. K. Rai, N. K. Rai, A. K. Rai, and G. Watal, "Role of LIBS in elemental analysis of Psidium guajava responsible for glycemic potential," *Instrumentation Science and Technology*, vol. 35, pp. 507-522, 2007.
- [32] A. Khumaeni, M. Ramli, Y. Deguchi, Y. Lee, N. Idris, K. H. Kurniawan, T. J. J. Lie, and K. Kagawa, "New technique for the direct analysis of food powders confined in a small hole using transversely excited atmospheric CO₂ laser-induced gas plasma," *Applied Spectroscopy*, vol. 62, pp. 1344-1348, 2008.
- [33] B. A. Gething, J. J. Janowiak, and R. H. Falk, "Assessment of laser induced breakdown spectroscopy (LIBS) for classification of preservative in CCA-treated lumber," *Forest Products Journal*, vol. 59, pp. 67-74, 2009.
- [34] A. Khumaeni, H. Niki, Y. Deguchi, K. Kurihara, K. Kagawa, and Y. I. Lee, "Analysis of organic powder samples by using the metal-assisted subtarget effect in a Transversely-Excited Atmospheric (TEA) CO₂ laser-induced he gas plasma at 1 atm," *Journal of the Korean Physical Society*, vol. 55, pp. 2441-2446, 2009.
- [35] P. K. Rai, D. Jaiswal, N. K. Rai, S. Pandhija, A. K. Rai, and G. Watal, "Role of glycemic elements of Cynodon dactylon and Musa paradisiaca in diabetes management," *Lasers in Medical Science*, vol. 24, pp. 761-768, 2009.
- [36] J. W. B. Braga, L. C. Trevizan, L. C. Nunes, I. A. Rufini, D. Santos Jr, and F. J. Krug, "Comparison of univariate and multivariate calibration for the determination of micronutrients in pellets of plant materials by laser induced breakdown spectrometry," *Spectrochimica Acta - Part B Atomic Spectroscopy*, vol. 65, pp. 66-74, 2010.

- [37] E. R. Schenk and J. R. Almirall, "Elemental analysis of cotton by laser-induced breakdown spectroscopy," *Applied Optics*, vol. 49, pp. C153-C160, 2010.
- [38] M. Hassan, M. Abdelhamied, A. H. Hanafy, R. Fantoni, and M. A. Harith, "Laser monitoring of phytoextraction enhancement of lead contaminated soil adopting EDTA and EDDS," in *AIP Conference Proceedings*, Cairo, Egypt, 2011, pp. 93-100.
- [39] A. Khumaeni, H. Niki, K. I. Fukumoto, Y. Deguchi, K. Kurihara, K. Kagawa, and Y. I. Lee, "A unique technique of laser-induced breakdown spectroscopy using transversely excited atmospheric CO₂ laser for the sensitive analysis of powder samples," *Current Applied Physics*, vol. 11, pp. 423-427, 2011.
- [40] A. Khumaeni, Z. S. Lie, H. Niki, K. H. Kurniawan, E. Tjoeng, Y. I. Lee, K. Kurihara, Y. Deguchi, and K. Kagawa, "Direct analysis of powder samples using transversely excited atmospheric CO₂ laser-induced gas plasma at 1 atm," *Analytical and Bioanalytical Chemistry*, vol. 400, pp. 3279-3287, 2011.
- [41] M. R. Martelli, F. Brygo, P. Delaporte, X. Rouau, and C. Barron, "Estimation of Wheat Grain Tissue Cohesion via Laser Induced Breakdown Spectroscopy," *Food Biophysics*, vol. 6, pp. 433-439, 2011.
- [42] G. Kim, J. Kwak, J. Choi, and K. Park, "Detection of nutrient elements and contamination by pesticides in spinach and rice samples using laser-induced breakdown spectroscopy (LIBS)," *Journal of Agricultural and Food Chemistry*, vol. 60, pp. 718-724, 2012.
- [43] M. da Silva Gomes, G. G. A. de Carvalho, D. Santos Junior, and F. J. Krug, "A novel strategy for preparing calibration standards for the analysis of plant materials by laser-induced breakdown spectroscopy: A case study with pellets of sugar cane leaves," *Spectrochimica Acta Part B: Atomic Spectroscopy*, vol. 86, pp. 137-141, 2013.
- [44] D. Cremers and L. Radziemski, *Handbook of Laser-Induced Breakdown Spectroscopy*. West Sussex, UK: John Wiley & Sons Ltd, 2013.
- [45] R. C. Wiens, S. Maurice, J. Lasue, O. Forni, R. B. Anderson, S. Clegg, S. Bender, D. Blaney, B. L. Barraclough, A. Cousin, L. Deflores, D. Delapp, M. D. Dyar, C. Fabre, O. Gasnault, N. Lanza, J. Mazoyer, N. Melikechi, P.

- Y. Meslin, H. Newsom, A. Ollila, R. Perez, R. L. Tokar, and D. Vaniman, "Pre-flight calibration and initial data processing for the ChemCam laser-induced breakdown spectroscopy instrument on the Mars Science Laboratory rover," *Spectrochimica Acta Part B: Atomic Spectroscopy*, vol. 82, pp. 1-27, 2013.
- [46] J. Handke, F. Duschek, K. Gruenewald, and C. Pargmann, "Standoff detection applying laser-induced breakdown spectroscopy at the DLR laser test range," 2011.
- [47] H. Jull, R. Künnemeyer, and P. Schaare, "Nutrient detection in fresh and dried pasture using laser-induced breakdown spectroscopy," *Precision Agriculture*, accepted January 25 2018.
- [48] H. Jull, R. Künnemeyer, and P. Schaare, "Considerations needed for sensing mineral nutrient levels in pasture using a benchtop laser-induced breakdown spectroscopy system," Unpublished.
- [49] H. Jull, R. Künnemeyer, S. Talele, P. Schaare, and M. Seelye, "Laser-induced breakdown spectroscopy analysis of sodium in pelletised pasture samples," in *Automation, Robotics and Applications (ICARA), 2015 6th International Conference on*, 2015, pp. 262-268.
- [50] P. Ewart, H. Jull, R. Künnemeyer, and P. N. Schaare, "Identification of contamination levels and the microstructure of metal injection moulded titanium," in *Key Engineering Materials* vol. 704, T. Ebel and F. Pyczak, Eds., ed: Trans Tech Publications Ltd, 2016, pp. 161-169.
- [51] H. Jull, P. Ewart, R. Künnemeyer, and P. Schaare, "Selective Surface Sintering Using a Laser-Induced Breakdown Spectroscopy System," *Journal of Spectroscopy*, vol. 2017, p. 11, 2017.
- [52] H. Jull, J. Bier, R. Künnemeyer, and P. Schaare, "Classification of recyclables using laser-induced breakdown spectroscopy for waste management," submitted for publication.
- [53] D. K. Chauhan, D. K. Tripathi, N. K. Rai, and A. K. Rai, "Detection of Biogenic Silica in Leaf Blade, Leaf Sheath, and Stem of Bermuda Grass (*Cynodon dactylon*) Using LIBS and Phytolith Analysis," *Food Biophysics*, vol. 6, pp. 416-423, 2011.

- [54] A. R. Boyain-Goitia, D. C. S. Beddows, B. C. Griffiths, and H. H. Telle, "Single-pollen analysis by laser-induced breakdown spectroscopy and raman microscopy," *Applied Optics*, vol. 42, pp. 6119-6132, 2003.
- [55] M. Z. Martin, A. J. Stewart, K. D. Gwinn, and J. C. Waller, "Laser-induced breakdown spectroscopy used to detect endophyte-mediated accumulation of metals by tall fescue," *Applied Optics*, vol. 49, pp. C161-C167, 2010.
- [56] K. Devey, M. Mucalo, G. Rajendram, and J. Lane, "Pasture Vegetation Elemental Analysis by Laser-Induced Breakdown Spectroscopy," *Communications in Soil Science and Plant Analysis*, vol. 46, pp. 72-80, 2015.
- [57] J. N. Kunz, D. V. Voronine, B. A. Ko, H. W. H. Lee, A. Rana, M. V. Bagavathiannan, A. V. Sokolov, and M. O. Scully, "Interaction of femtosecond laser pulses with plants: towards distinguishing weeds and crops using plasma temperature," *Journal of Modern Optics*, vol. 64, pp. 942-947, 2017.
- [58] B. Sallé, D. A. Cremers, S. Maurice, R. C. Wiens, and P. Fichet, "Evaluation of a compact spectrograph for in-situ and stand-off Laser-Induced Breakdown Spectroscopy analyses of geological samples on Mars missions," *Spectrochimica Acta Part B: Atomic Spectroscopy*, vol. 60, pp. 805-815, 2005.
- [59] I. Gaona, J. Moros, and J. J. Laserna, "New insights into the potential factors affecting the emission spectra variability in standoff LIBS," *Journal of Analytical Atomic Spectrometry*, vol. 28, pp. 1750-1759, 2013.
- [60] S. Palanco, C. López-Moreno, and J. J. Laserna, "Design, construction and assessment of a field-deployable laser-induced breakdown spectrometer for remote elemental sensing," *Spectrochimica Acta - Part B Atomic Spectroscopy*, vol. 61, pp. 88-95, 2006.
- [61] J. M. Vadillo, P. L. García, S. Palanco, D. Romero, J. M. Baena, and J. J. Laserna, "Remote, real-time, on-line monitoring of high-temperature samples by noninvasive open-path laser plasma spectrometry," *Analytical and Bioanalytical Chemistry*, vol. 375, pp. 1144-1147, 2003.
- [62] R. C. Wiens, R. E. Arvidson, D. A. Cremers, M. J. Ferris, J. D. Blacic, F. P. Seelos IV, and K. S. Deal, "Combined remote mineralogical and elemental identification from rovers: Field and laboratory tests using reflectance and

- laser-induced breakdown spectroscopy," *Journal of Geophysical Research E: Planets*, vol. 107, pp. F10301 - F10304, 2002.
- [63] M. Stepputat and R. Noll, "On-line detection of heavy metals and brominated flame retardants in technical polymers with laser-induced breakdown spectrometry," *Applied Optics*, vol. 42, pp. 6210-6220, 2003.
- [64] I. Gaona, P. Lucena, J. Moros, F. J. Fortes, S. Guirado, J. Serrano, and J. J. Laserna, "Evaluating the use of standoff LIBS in architectural heritage: Surveying the Cathedral of Málaga," *Journal of Analytical Atomic Spectrometry*, vol. 28, pp. 810-820, 2013.
- [65] P. Lucena, I. Gaona, J. Moros, and J. J. Laserna, "Location and detection of explosive-contaminated human fingerprints on distant targets using standoff laser-induced breakdown spectroscopy," *Spectrochimica Acta Part B: Atomic Spectroscopy*, vol. 85, pp. 71-77, 2013.
- [66] J. L. Gottfried, F. C. De Lucia Jr, C. A. Munson, and A. W. Miziolek, "Double-pulse standoff laser-induced breakdown spectroscopy for versatile hazardous materials detection," *Spectrochimica Acta - Part B Atomic Spectroscopy*, vol. 62, pp. 1405-1411, 2007.
- [67] J. L. Gottfried, F. C. De Lucia Jr, and A. W. Miziolek, "Discrimination of explosive residues on organic and inorganic substrates using laser-induced breakdown spectroscopy," *Journal of Analytical Atomic Spectrometry*, vol. 24, pp. 288-296, 2009.
- [68] J. L. Gottfried, F. C. De Lucia Jr, C. A. Munson, and A. W. Miziolek, "Standoff detection of chemical and biological threats using laser-induced breakdown spectroscopy," *Applied Spectroscopy*, vol. 62, pp. 353-363, 2008.
- [69] J. L. Gottfried, R. S. Harmon, F. C. De Lucia Jr, and A. W. Miziolek, "Multivariate analysis of laser-induced breakdown spectroscopy chemical signatures for geomaterial classification," *Spectrochimica Acta - Part B Atomic Spectroscopy*, vol. 64, pp. 1009-1019, 2009.
- [70] C. Frank, L. De Jr, L. Jennifer, C. A. Gottfried, M. Andrzej, and W. Miziolek, "Current status of standoff libs security applications at the united states army research laboratory," *Spectroscopy*, vol. 24, 2009.
- [71] R. Noll, *Laser-Induced Breakdown Spectroscopy: Fundamentals and Applications*. Heidelberg, Berlin: Springer-Verlag, 2012.

- [72] R. Noll and C. Fricke-Begemann, "Stand-off detection of surface contaminations with explosives residues using laser-spectroscopic methods," in *Stand-Off Detection of Suicide Bombers and Mobile Subjects*, H. Schurbert and A. RimskiKorsakov, Eds., ed Dordrecht: Springer, 2006, pp. 89-99.
- [73] P. Werheit, C. Fricke-Begemann, M. Gesing, and R. Noll, "Fast single piece identification with a 3D scanning LIBS for aluminium cast and wrought alloys recycling," *Journal of Analytical Atomic Spectrometry*, vol. 26, pp. 2166-2174, 2011.
- [74] R. Noll, I. Mönch, O. Klein, and A. Lamott, "Concept and operating performance of inspection machines for industrial use based on laser-induced breakdown spectroscopy," *Spectrochimica Acta - Part B Atomic Spectroscopy*, vol. 60, pp. 1070-1075, 2005.
- [75] H. Balzer, M. Hoehne, R. Noll, and V. Sturm, "New approach to online monitoring of the Al depth profile of the hot-dip galvanised sheet steel using LIBS," *Analytical and Bioanalytical Chemistry*, vol. 385, pp. 225-233, 2006.
- [76] A. M. Cousin, S.; Parot, Y.; Michel, Y.; Le Roch, N.; Dalmau, J.; Parès, L.; Perez, R.; Cros, A.; Wiens, R., "ChemCam (MSL) Autofocus Capabilities," in *40th Lunar and Planetary Science Conference*, The Woodlands, Texas, 2009.
- [77] S. Maurice, R. C. Wiens, M. Saccoccio, B. Barraclough, O. Gasnault, O. Forni, N. Mangold, D. Baratoux, S. Bender, G. Berger, J. Bernardin, M. Berthé, N. Bridges, D. Blaney, M. Bouyé, P. Caïs, B. Clark, S. Clegg, A. Cousin, D. Cremers, A. Cros, L. Deflores, C. Derycke, B. Dingler, G. Dromart, B. Dubois, M. Dupieux, E. Durand, L. D'Uston, C. Fabre, B. Faure, A. Gaboriaud, T. Gharsa, K. Herkenhoff, E. Kan, L. Kirkland, D. Kouach, J. L. Lacour, Y. Langevin, J. Lasue, S. Le Mouélic, M. Lescure, E. Lewin, D. Limonadi, G. Manhès, P. Mauchien, C. McKay, P. Y. Meslin, Y. Michel, E. Miller, H. E. Newsom, G. Orttner, A. Paillet, L. Parès, Y. Parot, R. Pérez, P. Pinet, F. Poitrasson, B. Quertier, B. Sallé, C. Sotin, V. Sautter, H. Séran, J. J. Simmonds, J. B. Sirven, R. Stiglich, N. Striebig, J. J. Thocaven, M. J. Toplis, and D. Vaniman, "The ChemCam instrument suite on the Mars Science Laboratory (MSL) rover: Science objectives and mast unit description," *Space Science Reviews*, vol. 170, pp. 95-166, 2012.

- [78] A. Cousin, O. Forni, S. Maurice, O. Gasnault, C. Fabre, V. Sautter, R. C. Wiens, and J. Mazoyer, "Laser induced breakdown spectroscopy library for the Martian environment," *Spectrochimica Acta - Part B Atomic Spectroscopy*, vol. 66, pp. 805-814, 2011.
- [79] Y. Michel, E. Conde, D. Kouach, M. Simpfendorfer, Y. Parot, G. R. Ortner, M. Saccoccio, and S. Maurice, "Chemcam screw/nut autofocus mechanism: Qualification data and guidelines for space-use of ground equipments," Vienna, 2009.
- [80] P. D. Barnett, N. Lamsal, and S. M. Angel, "Standoff Laser-Induced Breakdown Spectroscopy (LIBS) Using a Miniature Wide Field of View Spatial Heterodyne Spectrometer with Sub-Microsteradian Collection Optics," *Applied Spectroscopy*, vol. 71, pp. 583-590, 2017.
- [81] R. Grönlund, M. Lundqvist, and S. Svanberg, "Remote imaging laser-induced breakdown spectroscopy and remote cultural heritage ablative cleaning," *Optics Letters*, vol. 30, pp. 2882-2884, 2005.
- [82] J. Novotný, R. Malina, J. Kaiser, M. Liška, M. Galiová, and K. Novotný, "Implementation of an autofocus algorithm based on searching the best in-focus image into a table-top laser-induced breakdown spectroscopy setup," *Optical Engineering*, vol. 48, 2009.
- [83] B. Ashrafkhani, M. Bahreini, and S. H. Tavassoli, "Repeatability improvement of laser-induced breakdown spectroscopy using an auto-focus system," *Optics and Spectroscopy (English translation of Optika i Spektroskopiya)*, vol. 118, pp. 841-846, 2015.
- [84] M. Galiová, J. Kaiser, K. Novotný, M. Hartl, R. Kizek, and P. Babula, "Utilization of laser-assisted analytical methods for monitoring of lead and nutrition elements distribution in fresh and dried *Capsicum annum* l. leaves," *Microscopy Research and Technique*, vol. 74, pp. 845-852, 2011.
- [85] J. Peng, Y. He, L. Ye, T. Shen, F. Liu, W. Kong, X. Liu, and Y. Zhao, "Moisture Influence Reducing Method for Heavy Metals Detection in Plant Materials Using Laser-Induced Breakdown Spectroscopy: A Case Study for Chromium Content Detection in Rice Leaves," *Analytical Chemistry*, vol. 89, pp. 7593-7600, 2017.
- [86] M. Chen, T. Yuan, Z. Hou, Z. Wang, and Y. Wang, "Effects of moisture content on coal analysis using laser-induced breakdown spectroscopy,"

- Spectrochimica Acta Part B: Atomic Spectroscopy*, vol. 112, pp. 23-33, 2015/10/01/ 2015.
- [87] J. N. Kunz, D. V. Voronine, H. W. H. Lee, A. V. Sokolov, and M. O. Scully, "Rapid detection of drought stress in plants using femtosecond laser-induced breakdown spectroscopy," *Optics Express*, vol. 25, pp. 7251-7262, 2017.
- [88] D. W. Hahn and N. Omenetto, "Laser-induced breakdown spectroscopy (LIBS), part II: Review of instrumental and methodological approaches to material analysis and applications to different fields," *Applied Spectroscopy*, vol. 66, pp. 347-419, 2012.
- [89] J. Peng, F. Liu, F. Zhou, K. Song, C. Zhang, L. Ye, and Y. He, "Challenging applications for multi-element analysis by laser-induced breakdown spectroscopy in agriculture: A review," *TrAC - Trends in Analytical Chemistry*, vol. 85, pp. 260-272, 2016.
- [90] D. Cremers and L. Radziemski, "Chemometric analysis in LIBS," in *Handbook of Laser-Induced Breakdown Spectroscopy*, 2nd ed West Sussex, UK: John Wiley & Sons Ltd, 2013, pp. 223-255.
- [91] F. C. De Lucia, Jr., J. L. Gottfried, C. A. Munson, and A. W. Miziolek, "Multivariate analysis of standoff laser-induced breakdown spectroscopy spectra for classification of explosive-containing residues," *Applied Optics*, vol. 47, pp. 112-21, 2008.
- [92] D. Choi, Y. Gong, S.-H. Nam, S.-H. Han, J. Yoo, and Y. Lee, "Laser-Induced Breakdown Spectroscopy (LIBS) Analysis of Calcium Ions Dissolved in Water Using Filter Paper Substrates: An Ideal Internal Standard for Precision Improvement," *Applied Spectroscopy*, vol. 68, pp. 198-212, 2014.
- [93] R. Gaudiuso, M. Dell'Aglio, O. de Pascale, G. S. Senesi, and A. de Giacomo, "Laser induced breakdown spectroscopy for elemental analysis in environmental, cultural heritage and space applications: A review of methods and results," *Sensors*, vol. 10, pp. 7434-7468, 2010.
- [94] A. De Giacomo, M. Dell'Aglio, O. De Pascale, S. Longo, and M. Capitelli, "Laser induced breakdown spectroscopy on meteorites," *Spectrochimica Acta - Part B Atomic Spectroscopy*, vol. 62, pp. 1606-1611, 2007.

- [95] W. B. Barnett, V. A. Fassel, and R. N. Kniseley, "Theoretical principles of internal standardization in analytical emission spectroscopy," *Spectrochimica Acta Part B: Atomic Spectroscopy*, vol. 23, pp. 643-664, 1968.
- [96] L. C. Trevizan, D. Santos Jr, R. E. Samad, N. D. Vieira Jr, C. S. Nomura, L. C. Nunes, I. A. Rufini, and F. J. Krug, "Evaluation of laser induced breakdown spectroscopy for the determination of macronutrients in plant materials," *Spectrochimica Acta - Part B Atomic Spectroscopy*, vol. 63, pp. 1151-1158, 2008.
- [97] C. Aragon, J. A. Aguilera, and F. Penalba, "Improvements in Quantitative Analysis of Steel Composition by Laser-Induced Breakdown Spectroscopy at Atmospheric Pressure Using an Infrared Nd:YAG Laser," *Applied Spectroscopy*, vol. 53, pp. 1259-1267, 1999/10/01 1999.
- [98] G. G. A. de Carvalho, D. Santos Jr, M. da Silva Gomes, L. C. Nunes, M. B. B. Guerra, and F. J. Krug, "Influence of particle size distribution on the analysis of pellets of plant materials by laser-induced breakdown spectroscopy," *Spectrochimica Acta Part B: Atomic Spectroscopy*, vol. 105, pp. 130-135, 2015.
- [99] D. Cremers and L. Radziemski, "Quantitative LIBS Analysis," in *Handbook of Laser-Induced Breakdown Spectroscopy*. vol. 185-222, 2nd ed West Sussex, UK: John Wiley & Sons Ltd, 2013.
- [100] P. Zheng, M. Shi, J. Wang, and H. Liu, "The spectral emission characteristics of laser induced plasma on tea samples," *Plasma Science and Technology*, vol. 17, pp. 664-670, 2015.
- [101] V. N. Rai and S. N. Thakur, "Physics of Plasma in LIBS," in *Laser-Induced Breakdown Spectroscopy*, J. P. Singh and S. N. Thakur, Eds., ed Oxford, UK: Elsevier, 2007, pp. 83-112.
- [102] G. G. Arantes de Carvalho, J. Moros, D. Santos, Jr., F. J. Krug, and J. J. Laserna, "Direct determination of the nutrient profile in plant materials by femtosecond laser-induced breakdown spectroscopy," *Analytica Chimica Acta*, vol. 876, pp. 26-38, 2015.
- [103] R. E. Russo, X. L. Mao, J. H. Yoo, and J. J. Gonzalez, "Laser Ablation," in *Laser-Induced Breakdown Spectroscopy*, J. P. Singh and S. N. Thakur, Eds., ed Oxford, UK: Elsevier, 2007, pp. 49-82.

- [104] J. L. Gottfried, F. C. De Lucia Jr, C. A. Munson, and A. W. Miziolek, "Laser-induced breakdown spectroscopy for detection of explosives residues: A review of recent advances, challenges, and future prospects," *Analytical and Bioanalytical Chemistry*, vol. 395, pp. 283-300, 2009.
- [105] G. Nicolodelli, G. S. Senesi, A. C. Ranulfi, B. S. Marangoni, A. Watanabe, V. de Melo Benites, P. P. A. de Oliveira, P. Villas-Boas, and D. M. B. P. Milori, "Double-pulse laser induced breakdown spectroscopy in orthogonal beam geometry to enhance line emission intensity from agricultural samples," *Microchemical Journal*, vol. 133, pp. 272-278, 2017.
- [106] M. T. Taschuk, I. V. Cravetchi, Y. Y. Tsui, and R. Fedosejevs, "Micro-LIBS," in *Laser-Induced Breakdown Spectroscopy*, J. P. Singh and S. N. Thakur, Eds., ed Oxford, UK: Elsevier, 2007, pp. 173-196.
- [107] Lynxmotion. (2018, Jan.). *BotBoarduino*. Available: <http://www.lynxmotion.com/c-153-botboarduino.aspx>

Appendix A

**Summary of LIBS analysis of plant material
including various parameters for
experimental setup, as well as emission lines
investigated**

The following is comprehensive list of the plant material used in LIBS studies with a detailed description of experimental parameters in each. This covers the majority of literature and all studies performed on pasture.

Sample	Laser	E (mJ)	Shots	Spot size (µm)	LTSD (mm)	I (GW cm ⁻²)	t _d	t _b	Analysed lines λ (nm)	LOD	Analysis method	Ref.
Tomato leaves, spinach leaves, apple leaves, peach leaves Spanish moss and pine needles, dried and ground	1064 nm	100	20	700,	-	-	1 us	10 us	Al I 308.215	192±6 ppm	Univariate	[1]
	5 ns			100					Ca I 428.301	-		
	1 Hz								Cu I 324.754	3.3±0.3 ppm		
									Fe I 404.582	227±21 ppm		
									Mg I 277.983	-		
									Mn I 403.076	32±3 ppm		
									P I 213.618	0.1±0.01%		
Starch powders and rice flour	1064 nm	30	5x20	-	100	-	-	-	Zn I 213.856	56±5 ppm	Univariate, Boltzmann plot	[2]
	7 ns								Al I 396.153	2 µg/g		
	10 Hz								Cd II 226.502	8 µg/g		
									Cr I 425.435	1 µg/g		
									Cu I 324.754	1 µg/g		
									K I 766.49	3 µg/g		
									Mg II 279.553	0.4 µg/g		
									Mn II 257.61	0.7 µg/g		
									Pb I 405.782	18 µg/g		
									Rb I 780.023	1 µg/g		
Wood	1064 nm	50-	10-20	300-	250	5.1-19.8	3 us	10 us	Sr II 421.552	0.3 µg/g	Univariate, normalised with C I 247.857	[3]
	5 ns	70		500					Al	18, 3.3 ppm		
	10 Hz								As	15, 2.7 ppm		
									B 249.773	1.5, 0.3 ppm		
									C 247	-		
									Cd	1.6, 0.5 ppm		
									Cr	<1 ppm		
									Cu	1.8, 0.3 ppm		
									Hg	19, 4.6 ppm		
									K	3.5, 0.7 ppm		
									Mg	<1 ppm		
									Na	<1 ppm		
									Pb	8.4, 0.6 ppm		
									Si 288.158	5.3, 1 ppm		
								Sn	8.2, 2.2 ppm			

Sample	Laser	E (mJ)	Shots	Spot size (µm)	LTSD (mm)	I (GW cm ⁻²)	t _a	t _b	Analysed lines λ (nm)	LOD	Analysis method	Ref.
Peach, apple, spinach, powdered	1064 nm - -	10-30	5-10	200	100	0.025	-	-	Mg 285.213	-	Univariate	[4]
Wood	1064 nm 8 ns 2 Hz	-	1, 5, 10, 25	-	200	-	17 us	5 ms	Cr I 425.4 Cr I 427.5 Cr I 428.9	-	Depth profiling	[5]
Algae, fried powder	1064 nm 5-7 ns 10 Hz	30	5	-	4-5	-	-	2 s	Sr II 421.55	39.4±3, 1011±42 µg/g	Univariate, normalised with Ca	[6]
Sunflower (leaves/stem)	355, 790 nm 6 ns, 30 fs 20 Hz	-	200	30, 2	15, 10	-	-	50 ns	Ca+Ca2+ 391-398	-	-	[7]
Pollen and fresh grass fragments	1064 nm - 5 Hz	20-30	1	150	300	-	1 us	4 us	Ca II 396.847 Ca 422.673 Ca 430.252 Al 396.152 Cr 396.618 Cr 425.433 Fe 388.628 Fe 427.176 Si 390.552	-	Intensity ratios	[8]
Pollen	- 10 ns -	30	5	-	-	-	1.5 us	2 ms	Mg II 279.55 Mg II 280.27 Mg II 285.21 Mg II 385.04 Ca II 500.14 Ca I 616.21 H I 656.29 N I 744.23 N I 746.83 N I 821.63 N I 868.03 O I 777.19	-	PCA	[9]

Sample	Laser	E (mJ)	Shots	Spot size (μm)	LTSD (mm)	I (GW cm ⁻²)	t _a	t _b	Analysed lines λ (nm)	LOD	Analysis method	Ref.
Wood	1064 nm 10 ns 2 Hz	-	10-15	-	200	-	-	5 ms	Ca, Cr	-	Peak-to-base ratio	[10]
Maize leaf and Red osier dogwood leaves	795 nm 160 fs 10 Hz	0.1	-	10-300	-	-	-	-	Fe	-	Two-dimensional maps	[11]
Sophora leaves	800 nm 150 fs 10 Hz	5	5x3	-	30	-	-	-	Ca	-	Classification	[12]
Sunflower (Helianthus annuus), leaves/stem	532 nm 5 ns -	10	-	350	16	-	1 us	10 us	K Mn Pb I 405.76	-	Normalized peak areas	[13]
Sunflower (Helianthus annuus), leaves/stem	795 nm 160 fs 10 Hz	0.1	-	100	100	-	-	-	Pb Cd	-	Qualitative	[14]
Wood	532 nm - -	45	10	-	-	-	-	10 us	C 247.856	-	Univariate, PCA, PLS	[15]
Guava peel	- - 2 Hz	175	100	-	300	-	-	-	C II 247.88 Na 589.89 Na 891.12 K 766.88 H 656.77 O 777.79 O 845.10 N 868.39 Mg II 279.48 Mg II 280.20	-	Line ratios	[16]
Wood, pelletized powered	532 nm 5 ns -	-	-	-	-	-	-	-	Cu Zn As Cr	-	PCA, PLS	[17]

Sample	Laser	E (mJ)	Shots	Spot size (μm)	LTSD (mm)	I (GW cm ⁻²)	t _a	t _b	Analysed lines λ (nm)	LOD	Analysis method	Ref.
Sunflower (<i>Helianthus annuus</i>), leaves/stem	532 nm 5 ns -	10	-	250	16	-	1 us	10 us	Ag I 328.07 Cu I 324.75	-	Two-dimensional maps	[18]
Scented geranium	1064 nm 8 ns -	80	20	300	250	max 70	5 us	15 us	Pb 405.78	54-2291 mg/kg	Univariate	[19]
Potato, carrot, celery and aubergine	266 nm - 10 Hz	10	5x1000	100	50	-	100 ns	5 us	Mg Al Ca Ti Mn Fe	-	Normalized with C 247.86 nm	[20]
Rice seed and milk powder	10600 nm 200 ns 20 Hz	1500	5x20	1	100	0.75	-	2 s	Ca II 393.3	-	Ratio	[21]
Sunflower (<i>Helianthus annuus</i>), leaves/stem	532 nm 5 ns -	10	1	-	16	-	1 us	10 us	Ag I 328.07 Cu I 324.75	-	Normalized intensity	[22]
Bean leaves, bush branches and leaves, cabbage, soya flour, rice flour, apple leaves, peach leaves, wheat flour and spinach leaves, ground and pelletized	1064 nm 5 ns 10 Hz	360	8	1050	200	8.3	2 us	5 us	K I 404.721 P I 214.911 Fe Ca II 315.901 P I 214.911 Mg I 277.993 Ca II 315.901 Ca I 422.677 K I 404.721 K I 404.420 Mg I 280.224 Mg I 277.993 P I 214.911 P I 255.329	Various Various Various Various Various 0.03 g/kg 0.01 g/kg 3.2 g/kg 2.5 g/kg 0.02 g/kg 0.06 g/kg 0.08 g/kg 0.3 g/kg	Boltzmann plot, LTSD, univariate	[23]

Sample	Laser	E (mJ)	Shots	Spot size (μm)	LTSD (mm)	I (GW cm ⁻²)	t _a	t _b	Analysed lines λ (nm)	LOD	Analysis method	Ref.
Prickle pears	1064 nm 20 ns -	300	-	1000	50	0.6	-	-	Na I 589.5	-	Observation	[24]
Wood	- 10 ns 10 Hz	200	15x5	-	-	-	-	-	Cr 425.4 C 247.85	-	Univariate	[25]
Withania coagulans fruit, ground	- - -	-	-	-	-	-	-	-	-	-	-	[26]
Sunflower (Helianthus annuus), leaves/stem	532 nm 5 ns -	10	-	-	30	-	1 us	10 us	Pb I 283.31 Mg I 277.98	-	Two-dimensional maps	[27]
Tsumura kackontou (herb medicine), paste	10600 nm 200 ns -	1000 - 1500	-	2	200	0.18	-	-	Cr I 425.4 Pb I 405.8	1 mg/kg 5 mg/kg	Ratio, univariate	[28]
Maize (Zea mays), sunflower (Helianthus annuus) and lettuce (Lactuca sativa)	532 nm 5 ns -	10	-	-	30	-	1 us	10 us	Pb I 283.31	-	Two-dimensional maps	[29]
Potato skin	266 nm 5 ns 10 Hz	5-20	4x500	100	50	-	Various	Various	Hα 656.27 Ca II 393.37 C I 247.86 Na I 588.75 Mg I 285.21 Si I 288.16 Al I 308.22 Sr II 407.77 Fe I 383.04 Ti	-	Boltzmann plots, Saha-boltzmann plots, temporal evolution	[30]
Wheat grain	193 nm 15 ns 1 Hz	35	1-100	-	-	-	-	-	-	-	Depth profiling	[31]

Sample	Laser	E (mJ)	Shots	Spot size (μm)	LTSD (mm)	I (GW cm ⁻²)	t _a	t _b	Analysed lines λ (nm)	LOD	Analysis method	Ref.
Spinach leaves	532 nm 12 ns 10 Hz	70	-	-	400	-	1.1	9 us	Al I 309.271 B I 249.773 Ca I 422.544 Cu I 327.395 Fe I :259.940 Mg I 285.213 Mn II 259.375 P I 214.914 Si I 251.611 Zn I 213.861	-	ANOVA, BRANN	[32]
Wheat leaves, poppy leaves, barley leaves and rape leaves	1064 nm 12 ns -	80- 150	30	200	-	-	-	1 us	K 404.72 P 213.61 Mg 277.98 Ca 428.94	30-66 g/kg 2.8-6.6 g/kg 1-5.6 g/kg 6-24 g/kg	Univariate	[33]
Tangerine leaves and Rhododendron leaves	1064 nm 20 ns 100 Hz	1.1	-	-	25	-	-	100 ms	Ca I 558.876 Ca I 616.217 Ca I 643.907 Ca I 714.815 Ca I 422.673 Ca I 657.278 Ca II 501.997 Fe I 373.713 Na I 588.995 K I 766.490 Mo I 317.035	-	Observations	[34]
Bitter Melon	- - 10 Hz	40	-	-	300	-	-	-	K Mg Na Fe Ca Al	-	CF-LIBS	[35]

Sample	Laser	E (mJ)	Shots	Spot size (μm)	LTSD (mm)	I (GW cm ⁻²)	t _a	t _b	Analysed lines λ (nm)	LOD	Analysis method	Ref.
Bean leaves	1064 nm 5 ns 10 Hz	200	10x8	-	165	-	2 us	5 us	B I 249.773 Cu I 324.754 Cu I 327.396 Fe II 275.573 Fe II 259.940 Mn II 257.610 Mn II 294.920 Zn II 206.200 Zn I 213.865	2.2, 1.4 mg/kg 3, 2.5 mg/kg 5, 4 mg/kg 5.6, 4.6 mg/kg 3.6, 2.8 mg/kg 1.8, 1.1 mg/kg 5.5, 4.2 mg/kg 1.2, 1 mg/kg 3.2, 2.9 mg/kg	Univariate	[36]
Bermuda Grass and Musa paradisiaca	- - 1 Hz	175	-	-	300	-	-	-	C III 229.6 C 247.8 Mg II 279.4 Mg II 280.2 N II 567.9 Na II 589.4 N I 593.9 H 656.7 N 744.5 N 747.1 O 777.8 K 766.4 K 770.3 Na 819.1 N 868.4 O 845.1	-	Ratios	[37]
Ficus bengalensis aerial roots	- - -	-	-	-	-	-	-	-	Mg Ca	-	-	[38]
Holly leaves	1064, 266 nm 10 ns 10 Hz	45	3000	-	100	-	500 ns	2 ms	Spectra	-	Observations	[39]

Sample	Laser	E (mJ)	Shots	Spot size (μm)	LTSD (mm)	I (GW cm ⁻²)	t _a	t _b	Analysed lines λ (nm)	LOD	Analysis method	Ref.
Potato skin and flesh	1064 nm 4 ns 20 Hz	10	50	120	150	-	1 us	5 us	H C O N Mg Al Ca Fe Na Mn Ti Li Si K Cu	10 % ppm 9.10 % ppm 79 % ppm 0.30 % ppm 1300 ppm - 170 ppm 20 ppm 34 ppm - - - - 15000 ppm 30 ppm	Plasma temperature calculations, quantitative calculations	[40]
Lettuce	532 nm 5 ns -	10	1	-	16	-	1 us	10 us	Pb I 283.31	-	2D elemental map	[41]
Green herb, tomato leaves and coffee beans	1064 nm 5 ns -	-	-	-	-	-	-	-	-	-	PCA	[42]
Withania coagulans fruit	- - -	-	-	-	300	-	-	-	Mg Na K Zn Ca N	-	Observations	[43]
Wheat grain	532, 193 nm 5, 15 ns 20, 1 Hz	80, -	10	120, -	-	-	500 ns	2 ms	Ca II 396.85 Mg II 279.55	-	Normalised to Swan band, Moving-Window Two-Dimensional Correlation, PLS-DA	[44]

Sample	Laser	E (mJ)	Shots	Spot size (µm)	LTSD (mm)	I (GW cm ⁻²)	t _a	t _b	Analysed lines λ (nm)	LOD	Analysis method	Ref.
Tall fescue and apple leaf, ground and pelletised	532 nm - -	23	10	-	-	-	0.5 us	10 us	Cd 276.47	6 µg/kg	One-way ANOVA, univariate	[45]
Aquatic plant, aquatic moss, bush branches and leaves, cabbage, soya flour, rice flour, wheat flour, spinach leaves, brachiaria, banana leaves, coffee leaves, maize leaves, mango leaves, pepper leaves, soya leaves, olive leaves, apple leaves, guava leaves, grass and jackfruit leaves	532 nm 12 ns 10 Hz	71	30	600	-	2	9 us	1.1 us	B 249.773 Cu 327.395 Fe 275.578 Mn 257.610 Zn 206.200	5, 3 mg/kg 10, 5 mg/kg 7, 7 mg/kg 9, 4 mg/kg 4, 12 mg/kg	Univariate, PLS	[46]
Emblica officinalis seeds	- - 2 Hz	175	100	-	300	-	-	-	O 844.62 H 656.27 N 746.83 N 868.02 O 777.41 Cl 822.17 Na 819.47 C 247.8 Mg II 279.553 Mg II 280.271 Ca II 393.366 Ca II 396.847 Ca 422.673	-	Line ratios	[47]
Bermuda grass	532 nm 4 ns -	10	-	-	-	-	-	-	Si 288.1	-	Normalised intensity	[48]

Sample	Laser	E (mJ)	Shots	Spot size (μm)	LTSD (mm)	I (GW cm ⁻²)	t _a	t _b	Analysed lines λ (nm)	LOD	Analysis method	Ref.
Mustard grass	1064 nm - 10 Hz	300	-	-	-	-	-	-	Pb 217 Pb 220	-	Comparison of resonant lines with trace elements	[49]
Sugar cane leaves, ground and pelletised	1064 nm 5 ns 10 Hz	110	30x25	-	175	-	2 us	4.5 us	P I 214.914 K I 404.414 Ca I 315.895 Ca I 422.673 Mg I 277.983, II 257.611 Fe II 259.940 Zn I 213.861, II 206.200 B I 249.773	0.03, 0.02 g/kg 0.21, 0.35 g/kg 0.08, 0.08 g/kg 0.12, 0.03 g/kg 6.6, 0.5 mg/kg 9.5, 1.3 mg/kg 1.2, 1.9 mg/kg 0.8, 0.5 mg/kg	Univariate, PLS, BRANN	[50]
Cotton (unprocessed), ground and pelletised	1064 nm 5 ns 0.67 Hz	-	5x90	125	-	55	1.3 us	4.5 us	Al I 396.1 Ba II 493.4 Ca II 315.8 Cr I 428.9 Cu I 327.4 Fe I 748.4 Mg II 279.5 Mg II 280.2 Sr II 421.5	12 ppm 8 ppm 51 ppm >12 ppm >19 ppm 2 ppm 2 ppm 2 ppm 0.9 ppm	PCA, LDA	[51]
Holly leaves	1064, 266 nm 10 ns -	10- 80	-	-	100	-	-	-	Mn 279.82 Mg 280.28 Si 288.19 Al 309.31 Ti 334.92 Fe 372.03 Ca 422.63	-	Observations	[52]
Capsicum leaves	532 nm 5 ns -	10	-	200	-	-	1 us	10 us	Pb I 405.78 Mn I 403.07 Mn I 403.31 K I 404.41 K I 404.72	-	2D elemental maps	[53]

Sample	Laser	E (mJ)	Shots	Spot size (μm)	LTSD (mm)	I (GW cm ⁻²)	t _a	t _b	Analysed lines λ (nm)	LOD	Analysis method	Ref.
Folium lycii	1064 nm 8 ns -	-	-	150	300	10	800 ns	2 ms	Ca I 335.02 Ca I 336.19 Ca I 422.67 Ca I 428.30 Ca I 428.94 Ca I 429.90 Ca I 430.77 Ca I 431.87 Ca II 373.69 Ca II 370.60 Ca II 393.37 Al Si Mg Ti Na K Li	-	Plasma temperature calculation, ratios	[54]
Orange leaves	1064 nm 10ns 10 Hz	200	20x100	-	200	-	1.28 us	-	N P Ca Mg S Fe Cu Mn Zn Cl	-	Observations	[55]

Sample	Laser	E (mJ)	Shots	Spot size (μm)	LTSD (mm)	I (GW cm ⁻²)	t _a	t _b	Analysed lines λ (nm)	LOD	Analysis method	Ref.
Citrus leaves, dried	1064 nm - 10 Hz	50	10x1	-	-	-	48.5 us	-	C I 193.027 C I 247.856 C II 426.726 Fe I 229.817 Fe I 251.428 Fe I 399.739 Mn I 279.482 Mn I 279.827 Mn II 270.845 Mn II 344.199 H I 656.279 S I 744.335 N I 746.831 N II 567.602 N I 818.802 K I 766.490 K I 769.896 O I 777.417 O I 844.636 O II 868.609 O II 328.747 Zn I 328.233 Ni II 334.924 Ca I 863.395 Ca II 393.366 Ca II 396.847 Cl II 478.132 Mg I 516.732 Mg I 517.268 Mg I 552.840 Mg I 821.303 Na I 588.995 Na I 589.592	-	PCA, SIMCA	[56]

Sample	Laser	E (mJ)	Shots	Spot size (μm)	LTSD (mm)	I (GW cm ⁻²)	t _a	t _b	Analysed lines λ (nm)	LOD	Analysis method	Ref.
Trichosanthes dioica fruit	532 nm 3-4 ns 2 Hz	175	100	-	300	-	-	-	Mg 285.2 Mg II 279.5 Mg II 280.2 Fe II 234.3 Fe II 238.2 Fe II 239.5 Fe II 240.4 Fe II 249.3 Fe II 258.5 Fe II 259.8 Fe II 260.7 Fe II 261.1 Fe II 273.9 Fe II 274.9 Fe II 275.5 K 766.4 K769.9 Ca II 315.8 Ca II 317.9 Ca II 393.3 Ca II 396.8 Ca II 422.6 C 247.8 C III 229.62 Zn 202.5 Zn 206.2 O 777.2 O 844.6 H 656.2 Na 818.3 Na 589.5 N 744.2 N 746.8 N 868.3	-	One-way ANOVA, ratios	[57]

Sample	Laser	E (mJ)	Shots	Spot size (μm)	LTSD (mm)	I (GW cm ⁻²)	t _a	t _b	Analysed lines λ (nm)	LOD	Analysis method	Ref.
Coffee	1064 nm 8 ns 10 Hz	50	20	-	-	-	-	-	Spectra	-	Decision tree, Rotation Based Method, random subspace method	[58]
Potato skin	1064 nm 5 ns -	10	20x20	100	150	-	1 us	1 us	Mg Al Ca Fe Na Mn Ti Li Si K Cu Sr Ba	50, 20 ppm 10, 5 ppm 2, 1 ppm 100, 50 ppm 2, 1 ppm 7, 3 ppm 9, 4 ppm 0.05, 0.02 ppm 5, 2 ppm 20, 10 ppm 2, 1 ppm 3, 1 ppm 3, 1 ppm	Plasma temperature calculations, compare spectra with plasma model	[59]
Sugar cane, orange tree leaves and soy leaves, ground and pelletised	1064 nm 5 ns 10 Hz	110	30x25	-	175	-	2 us	4.5 us	B Mn P Mg Cu Zn Fe Ca K	-	STD	[60]
Scented geranium, ground and pelletised	1064 nm 12 ns 1 Hz	-	5x5	-	95	-	2 us	2 us	Pb 405.78	-	Ratio	[61]
Tsumura kackontou	10600 nm 200 ns -	1500	-	-	200	0.18	10 us	100 us	Mg I 333.6 Zn 334.5	-	Ratio	[62]

Sample	Laser	E (mJ)	Shots	Spot size (µm)	LTSD (mm)	I (GW cm ⁻²)	t _a	t _b	Analysed lines λ (nm)	LOD	Analysis method	Ref.
Powdered rice, starch and seaweed	10600 nm 200 ns 10 Hz	1500	-	-	200	-	10 us	100 us	Cr N II 399.5 Ca II 393 Cu I 521.8 Cu I 510.5 Cu I 324.7 Cu I 327.4	0.55 mg/kg - - - 0.22 mg/kg 0.22 mg/kg	Ratio	[63]
Orange peel, fresh and ground and pelletised	1064 nm 8 ns 10 Hz	200	30x20	-	200	-	1.28 us	2 ms	Na I 588.866 Na I 589.449 Ca I 616.795 Ca I 643.799 K I 766.441 K I 769.860	-	Relative intensity	[64]
Poplar tree leaves, dried	800 nm 100 fs 10 Hz	25	-	-	35	-	-	-	Fe Ca N P	-	CF-LIBS	[65]
Bran tissues and wheat grain	193 nm 15 ns 1 Hz	-	-	-	-	-	-	2 ms	Ca I 422.67 Ca II 396.85 Mg I 285.22 Mg II 279.55	-	Ratio, ANOVA, Duncan mean test	[66]
Navel Oranges	1064 nm 8 ns 10 Hz	200	10	-	200	-	1.28 us	2 ms	Cu 939.0176 Ca 926.5298 Fe 656.2375 Na 588.995	-	Line intensities	[67]
Citrus leaf	355, 1064 nm 5 ns 10 Hz	5, 110	5x20	-	70, 100	-	1 us	50 us	Ca II 393.3, 396.8	10 mg/kg	Ratios	[68]
Sugar cane (Saccharum officinarum)	532 nm 4 ns 10 Hz	10	5	50	150	1000	-	-	Si 288.1	-	Plasma temperature calculation, normalised intensity, PCA	[69]

Sample	Laser	E (mJ)	Shots	Spot size (µm)	LTSD (mm)	I (GW cm ⁻²)	t _a	t _b	Analysed lines λ (nm)	LOD	Analysis method	Ref.
Sugar cane and Boldo leaves, ground and pelletised	1064 nm 5 ns 10 Hz	365	30x20	180, 450, 600, 750, 1050	200	-	2 us	5 us	Mg I 277.983	-	Univariate	[70]
									Mg II 279.553	0.01 mg/kg		
									Mn II 257.610	0.3 mg/kg		
									P I 213.618	1 mg/kg		
									Mn II 294.920	-		
									Zn II 206.200	0.2 mg/kg		
									Cu I 324.755	0.4 mg/kg		
									Fe II 261.187	-		
									Fe II 259.940	0.4 mg/kg		
									Ca II 393.366	0.1 mg/kg		
									B I 249.773	0.5 mg/kg		
									Al I 309.271	3.9 mg/kg		
									Cd II 214.441	0.2 mg/kg		
Pb II 220.353	0.4 mg/kg											
Spinach leaf powder and unpolished rice flour, pelletised	1064 nm 7 ns 10 Hz	80- 140	50	-	90	-	-	-	Mg II 279.6	29.63 mg/kg	PLS-DA, univariate	[71]
									Ca I 643.9	102.65 mg/kg		
									Na I 819.5	36.36 mg/kg		
									K I 766.5	44.46 mg/kg		
									K I 404.414	2 g/kg		
Orange tree leaves	1064 nm 8 ns 10 Hz	-	-	-	200	-	1.28 us	2 ms	Fe 422.743	-	Ratio	[72]
									K 234.212			
									Al 237.218			
									Mg 263.008			
									Na 588.977			
									Ca 643.895			
Mn 870.169												
Sugar cane leaves, ground and pelletised	1064 nm 5 ns 10 Hz	110	25	-	175	-	2 us	5 us	Mg I 277.669	0.01 g kg ⁻¹	Univariate	[73]
									Mn II 257.610	0.8 mg kg ⁻¹		
									Ca	0.01 g kg ⁻¹		
									K	1.4 g kg ⁻¹		
									P	0.03 g kg ⁻¹		
									Cu	0.6 mg kg ⁻¹		
									Zn	1.0 mg kg ⁻¹		

Sample	Laser	E (mJ)	Shots	Spot size (μm)	LTSD (mm)	I (GW cm ⁻²)	t _a	t _b	Analysed lines λ (nm)	LOD	Analysis method	Ref.
Psoralea corylifolia seeds, solution	- - 2 Hz	175	100	-	300	-	-	-	Mg 285.213 Mg 279.078 Mg 279.553 Mg 279.8 Mg 280.271 C 247.856 C 229.689 Ca 393.366 Ca 396.847 Ca 422.673 Si 250.69 Si 251.611 Si 251.92 Si 252.411 Si 252.851 Si 288.158 Zn 434.97 Zn 445.1 H 656.27 N 746.83 N 868.02 K 766.49 K 769.89 O 777.41 O 844.62 Cl 822.17 Na 819.47	-	Ratios	[74]
Sugar cane	1064 nm 5 ns 10 Hz	220	25	750	200	-	2 us	4.5 us	Si I 212.412	-	Univariate	[75]
Gannan navel orange skin	1064 nm 8 ns 0.1-10 Hz	110	15	-	100	-	2 us	-	Cr I 425.43	-	Univariate using intensity	[76]

Sample	Laser	E (mJ)	Shots	Spot size (μm)	LTSD (mm)	I (GW cm ⁻²)	t _a	t _b	Analysed lines λ (nm)	LOD	Analysis method	Ref.
Psoralea corylifolia seed extract dissolved in distilled water	- - 2 Hz	175	100	-	300	-	-	-	Mg 285.213 Mg 279.078 Mg 279.553 Mg 280.271 C 247.856 C 229.689 Ca 393.366 Ca 396.847 Ca 422.673 Si 250.69 Si 251.611 Si 251.92 Si 252.411 Si 252.851 Si 288.158 Zn 434.97 Zn 445.1 H 656.27 N 746.83 N 868.02 K 766.49 K 769.89 O 777.41 O 844.62 Cl 822.17 Na 819.47	-	Intensity ratios	[77]
Turmeric	532 nm 4 ns 10 Hz	18	10	-	300	-	-	-	C 247.8 Mg 279.6 Ca 422.5 Pb 220.3 Cr 357.8 Si 288.2	-	PCA	[78]

Sample	Laser	E (mJ)	Shots	Spot size (μm)	LTSD (mm)	I (GW cm ⁻²)	t _a	t _b	Analysed lines λ (nm)	LOD	Analysis method	Ref.
Algae	1064 nm 7 ns 2 Hz	100	-	-	100	-	6 us	0.6 us	Mg II 279.55 Mg I 324.75 Mg I 327.39 Mg I 465.11 Mg I 510.55 Mg I 515.32 Mg I 521.82 Mg I 578.21	-	Plasma temperature calculation, ratio, univariate	[79]
Tomato leaves, ground and pelletized	1064 nm 6 ns 20 Hz	100	200	-	100	-	2 us	5 us	Zn 213.86 Pb 405.78 Cr 425.43 Cd 228.8 As 234.98 Hg 253.65	2.8 ppm 1.3 ppm 0.5 ppm 1.6 ppm 20 ppm	Qualitative	[80]
Boldo leaves (Peumus boldus Molina), ground, pelletized	1064 nm 5 ns 10 Hz	110 and 220	20 per spot	750	175	5 and 10	2 us	5 us	Ca I 442.544 K I 404.414 P I 213.618 Mg I 277.983 B I 249.773	-	Measured peak area as particle size changed	[81]
Wheat flour, pellets	1064 nm 5 ns -	-	30x10	750	-	4-10	1-3 us	1-10 us	Ca II 315.887 Ca II 393.366 P I 213.618 Mg I 285.213 Mg II 279.553 K I 404.414 Fe II 259.940 Mn II 257.610 Cu I 324.755 Zn II 202.548	17 mgkg ⁻¹ 1 mgkg ⁻¹ 0.04 mgkg ⁻¹ 10 mgkg ⁻¹ 0.2 mgkg ⁻¹ 1.2 mgkg ⁻¹ 0.7 mgkg ⁻¹ 0.5 mgkg ⁻¹ 0.5 mgkg ⁻¹ 1 mgkg ⁻¹	Univariate using peak area	[82]
White chickpea, ground and pelletized	1064 nm - 8 Hz	40	3x100	-	100	-	650 ns	1.05 ms	Ti 390.11	33.9 ppm (Univariate) 60.9 ppm (PLS)	Univariate and PLS	[83]

Sample	Laser	E (mJ)	Shots	Spot size (μm)	LTSD (mm)	I (GW cm ⁻²)	t _a	t _b	Analysed lines λ (nm)	LOD	Analysis method	Ref.
Bitter gourd (Momordica charantia L.), ground	1064 nm - -	200	-	-	-	-	-	-	Fe 393.33475 Ca 422.63925 Ca 558.92704 Ca 616.21483 Ca 643.92843 Mg 518.35337 Na 588.96954	-	Reported intensities being higher with higher elemental concentrations.	[84]
Wheat seedlings (Triticum aestivum L.)	532 nm 4 ns 4 Hz	10	10	-	150	1000	-	-	Si 532 Ca II 315.8 Ca II 317.9 Cr	-	Emission line intensity equation. Optically thin plasma criteria.	[85]
Sugar cane leaves, dried	1064 nm 5 ns 10 Hz	-	100x5	750	-	-	2 us	5 us	P I 213.618 K I 404.414 Ca II 315.887 Mg I 277.983 Fe II 259.940 Cu I 324.754 Mn II 259.373 Zn B I 249.772 Si I 212.412	-	Elemental mapping. EDXRF vs LIBS.	[86]
Perennial ryegrass (Lolium perenne) and white clover (Trifolium repens), ground and pelletized	1064 nm - -	200	8 shots on new site after 1 cleaning shot	-	-	-	1 us	-	Na 819.4 K 696.4 Mg 882.4 Ca 212.3 Mn 257.6 Fe 248.5 Zn 213.8 B 249.7 P 214.9 Cu 324.7 S 921.3	-	PLS	[87]

Sample	Laser	E (mJ)	Shots	Spot size (µm)	LTSD (mm)	I (GW cm ⁻²)	t _a	t _b	Analysed lines λ (nm)	LOD	Analysis method	Ref.
Wheat seedlings (Triticum aestivum L.)	532 nm 4 ns 4 Hz	10	-	-	150	-	-	-	Si Pb	-	Compared spectra	[88]
Ligusticum wallichii, powdered and pelletized	1064 nm 5.82 ns 20 Hz	26.8	20	-	-	-	1.5 us	20 us	Pb I 405.8 Cu I 324.46	15.7 µg g ⁻¹ 6.3 µg g ⁻¹	Different pressures, investigation of delay times and energy, MLR.	[89]
Duckweed (Lemna minor), dried	266 nm 5 ns 1064 nm 5 ns	10 100	-	-	80.5	-	1000 ns (delay) 500 ns (interpulse delay)	10 us	Cd I 508.58	-	Two-dimensional maps	[90]
Broad bean (Vicia faba) roots, cross sections	266 nm 1 Hz 1064 nm 1 Hz	5 100	-	-	80.5	-	1 us (delay) 500 ns (interpulse delay)	10 us	Cu I 324.754 Ag I 328.068	4 pg 18 pg	Spatial distribution mapping	[91]
Coffee beans, ground and pelletized	1064 nm 8 ns -	50	200	-	-	1000	11 us	2.1 ms	C I 193.0 CN 0.0 387.0 CN 1.1 388.5 C2 0.0 516.6 H 656.2 N I 742.3 N I 744.2 N I 746.8 O I 777.4	-	ANOVA and PCA	[92]
Soybean leaves, dried, ground, and pelletised	532 nm 4 ns - 1064 nm 6 ns -	1, 4, 8, 16 and 32	10	-	-	-	1 us	-	C I 247.856 Mg II 280.27 Mg I 285.213 Si 288.158 Mg I 285.21 Mg II 280.27 Ca II 315.887 Ca II 393.366	-	Individual lines and ratios	[95]

Sample	Laser	E (mJ)	Shots	Spot size (μm)	LTSD (mm)	I (GW cm ⁻²)	t _a	t _b	Analysed lines λ (nm)	LOD	Analysis method	Ref.
Rice Leaves (<i>Oryza sativa</i> L.), fresh and dried	532 nm 8 ns 1 Hz	60	25	-	-	-	4 us	20 us	CN 388.29	-	Univariate and PLS calibration, moisture decreases intensities, plasma parameter analysis.	[93]
									Cr 425.44	4.4665 mg/kg		
									Cr 427.48	5.2346 mg/kg		
									Cr 425.44	4.1505 mg/kg		
									Cr 427.48	4.8613 mg/kg		
									Cr 425.44	4.7078 mg/kg		
									Cr 427.48	5.5340 mg/kg		
									Cr 425.44	4.3856 mg/kg		
Citrus leaves, fresh	1064 nm 8 ns 10 Hz	50	-	-	7	-	2.5 us	2 ms	Mg II 279.55	-	Student's t-test, one-way ANOVA, PCA, PLS with classification via regression	[94]
									Mg II 280.27			
									Mg I 285.21			
									Si I 288.16			
									Al I 308.22			
									Na II 309.27			
									Ca II 315.89			
									Ca II 317.93			
									Cu I 324.75			
									Cu I 327.40			
									Ti II 334.94			
									Ca II 370.60			
									Fe I 373.71			
									Ca II 393.37			
									Ca II 396.85			
									Ca I 422.63			
									Ca I 445.48			
									Ca I 526.56			
									Ca I 527.03			
									Ca I 558.88			
									Ca I 559.45			
									Ca I 559.85			
Ca I 610.27												
Ca I 612.22												

Sample	Laser	E (mJ)	Shots	Spot size (µm)	LTSD (mm)	I (GW cm ⁻²)	t _a	t _b	Analysed lines λ (nm)	LOD	Analysis method	Ref.
									(cont.) Ca I 646.26 Ca I 732.61 K I 766.49 K I 769.90 Ca I 854.21			
Cabbage leaf, pellets	532 nm 4 ns 4 Hz	20	Various	-	-	-	1.5 us	-	-	-	PLSDA and PLSR	[96]
Dallisgrass (<i>Paspalum dilatatum</i>); wheat (<i>Triticum aestivum</i>), soybean (<i>Glycine max</i>); bell pepper (<i>Capsicum annuum</i>), dried leaves	800 nm 35 fs 1 kHz	0.3	10x100	100	-	3.8x10 ⁻⁶	-	0.5 s	Ca I 422.874 Ca I 518.542 Ca I 559.849	-	Plasma temperature calculation	[97]
Chinese cabbage, fresh leaves	1064 nm 8 ns 2 Hz	120	3 cleaning 50	-	-	-	2 us	2 ms	Cd II 214.43 Cd II 226.50 Cd I 228.80	-	Univariate, Savitzky–Golay smoothing, standard normal variate, and PLSR	[98]
Saffron (<i>C. sativus</i> L.), safflower (<i>Carthamus tinctorius</i> L.), marigold flower (<i>Calendula officinalis</i> L.), turmeric (<i>Curcuma longa</i> L.), ground and pelletised	1064 nm - 4 Hz	38	10x15	-	-	-	300 ns	20 us	-	-	PCA and PLS	[99]
Tea plants (<i>Sambucus nigra</i> L., <i>Hypericum perforatum</i> L., <i>Crataegus oxyacantha</i> auct. non L., <i>Rubus idaeus</i> L. and <i>Betula</i> species L.), pellets	1064 nm 8 ns 10 Hz	70	-	100	-	--	1 us	1.05 ms	Ca I 527.027 K I 693.878 Mg I 517.268 C I 193.090 C I 247.856	-	PCA and PLS	[100]

Sample	Laser	E (mJ)	Shots	Spot size (μm)	LTSD (mm)	I (GW cm ⁻²)	t _a	t _b	Analysed lines λ (nm)	LOD	Analysis method	Ref.
Seed kernels of pumpkin (Cucurbita maxima), ash gourd (Benincasa hispida), watermelon (Citrullus lanatus) and muskmelon (Cucumis melo), dried, ground, and pelletised	532 nm 4 ns 2 Hz	40	20	-	-	-	1 us	5 us	Mg II 279.5 Ca II 393.3 Na I 588.9 K I 766.4	0.32-1.20 mg/100 g 1.81-3.58 mg/100 g 3.68 -4.79 mg/100 g 2.11-3.79 mg/100 g	Univariate, PCA	[101]
Wheat and gardenia, fresh leaves	800 nm 35 fs 1 kHz	0.3	20	-	-	-	-	-	Fe I 383.92556 Ca II 393.366 Ca II 396.847 K I 404.7208 Ca I 422.673 O II 430.8999 Na II 445.5224 Ca I 518.885 Ca I 559.849 Na I 588.995	-	Plasma temperature calculation,	[102]
Cauliflower and broccoli, ground	532 nm 7 ns 2 Hz	96	10x10	-	-	-	1 us	5 us	Ca I 422.67 Ca I 558.87 Ca I 643.90 Ca I 646.25 Ca II 315.88 Ca II 370.60 Ca II 393.36 Ca II 396.84 Ca II 396.84 Mg II 279.55 K I 769.89 Na I 588.99 Ca II 396.84 Mg II 279.55	-	Plasma temperature calculation, PCA, ratios	[103]

Sample	Laser	E (mJ)	Shots	Spot size (μm)	LTSD (mm)	I (GW cm ⁻²)	t _a	t _b	Analysed lines λ (nm)	LOD	Analysis method	Ref.
Tobacco leaves, fresh and dried pellets	532 nm 8 ns 1 Hz	60	-	-	-	-	1.5 us	10 us	C I 247.86 Si I 251.61 Si I 288.16 Fe I 293.69 Fe I 385.99 Fe II 253.54 Mg I 277.98 Mg I 285.21 Mg I 382.94 Mg I 383.23 Mg I 383.83 Mg I 389.19 Mg I 516.73 Mg I 517.27 Mg I 518.36 Mg II 279.08 Mg II 279.55 Mg II 279.80 Mg II 280.27 Ca I 422.67 Ca I 428.30 Ca I 428.94 Ca I 429.90 Ca I 430.25 Ca I 430.77 Ca I 431.87 Ca I 442.54 Ca I 443.57 Ca I 457.86 Ca I 458.15 Ca I 458.60 Ca I 487.81 Ca I 504.16 Ca I 518.88	-	Plasma temperature calculation, PCA, PLSDA, SVM	[104]

Sample	Laser	E (mJ)	Shots	Spot size (μm)	LTSD (mm)	I (GW cm ⁻²)	t _a	t _b	Analysed lines λ (nm)	LOD	Analysis method	Ref.
									(cont.)			
									Ca I 526.22			
									Ca I 526.56			
									Ca I 527.03			
									Ca I 558.20			
									Ca I 558.87			
									Ca I 559.45			
									Ca I 559.85			
									Ca I 560.13			
									Ca I 585.75			
									Ca I 610.27			
									Ca I 612.22			
									Ca I 616.22			
									Ca I 616.64			
									Ca I 643.91			
									Ca I 644.98			
									Ca I 646.26			
									Ca I 647.17			
									Ca I 649.38			
									Ca I 671.77			
									Ca I 714.82			
									Ca I 720.22			
									Ca I 854.21			
									Ca II 315.89			
									Ca II 317.93			
									Ca II 370.60			
									Ca II 373.69			
									Ca II 393.37			
									Ca II 396.85			
									Ca II 849.80			
									Ca II 866.21			
									Mn II 292.87			
									Sc II 364.38			
									CN 387.12			

Sample	Laser	E (mJ)	Shots	Spot size (μm)	LTSD (mm)	I (GW cm^{-2})	t_a	t_b	Analysed lines λ (nm)	LOD	Analysis method	Ref.
									(cont.) CN 388.29 Al I 394.40 Al I 396.15 K I 404.41 K I 404.72 K I 693.88 K I 766.49 K I 769.90 Sr I 460.73 Sr II 407.77 4 Sr II 21.55 Na I 589.00 Na I 589.59 Ba I 649.88 H α 656.28 Li I 670.79 N I 742.36 N I 744.23 N I 746.83 N I 818.49 N I 821.63 N I 824.39 N I 862.92 N I 868.03 O I 777.42 O I 844.68			
Tea leaves, dried and pelletised	1064 nm 8 ns 4 Hz	30	10x20	-	-	-	1.5 μs	2 μs	Pb I 405.78 C I 247.856 Mn I 403.076 Mn I 403.307 Mn I 403.449	-	External and internal standards, MLR	[105]

Sample	Laser	E (mJ)	Shots	Spot size (μm)	LTSD (mm)	I (GW cm ⁻²)	t _a	t _b	Analysed lines λ (nm)	LOD	Analysis method	Ref.
spinach, mustard, chenopodium, fenugreek, and chickpea leaves, fresh and pellets	532 nm 4 ns 10 Hz	10	5	-	-	1000	-	-	Si 288.1 Si 251.4 Mg 285.1 Mg 279.5 Mg 279.8 Ti 334.9 Ti 336.1 Ti 337.2 Fe 344.1 Fe 238.3 Fe 240.4 Ca 422.6 Ca 393.3 Ca 396.8 Ca 443.5 Ca 445.5 C 247.8 C 229.6 Al 308.2 Al 309.2	-	RSD of individual lines	[106]
Rice, ground and pelletised	1064 nm 5 ns 1 Hz	-	-	-	-	-	-	-	Cd Ca Cu Mg Mn Na Zn Ni K	5.6 ppb	Univariate	[107]

Sample	Laser	E (mJ)	Shots	Spot size (μm)	LTSD (mm)	I (GW cm ⁻²)	t _a	t _b	Analysed lines λ (nm)	LOD	Analysis method	Ref.
Carrot Root (Daucus carota), fresh and pelletised	532 nm 8 ns 10 Hz	-	-	-	-	-	-	-	Cu 203.5	-	CF-LIBS	[108]
									Cu 218.1			
									Co 228.6			
									Fe 238.2			
									Fe 261.1			
									Fe 358.1			
									Fe 385.9			
									Mg 279.5			
									Mg 285.2			
									Ca 317.9			
									Ca 393.3			
									Ca 396.8			
									Ca 422.6			
									Ca 445.5			
									Ca 643.9			
									Ti 323.4			
									Ti 430.5			
									Zn 330.2			
									Zn 468.0			
									K 404.4			
									K 766.4			
K 769.8												
Sr 460.7												
Na 589.5												
Na 819.4												
Hg 794.4												
C 283.6												
H 434.0												
H 486.1												
H 656.2												
N 444.7												
N 463.0												
N 500.5												
N 594.1												

Sample	Laser	E (mJ)	Shots	Spot size (µm)	LTSD (mm)	I (GW cm ⁻²)	t _a	t _b	Analysed lines λ (nm)	LOD	Analysis method	Ref.
									(cont.) N 746.8 N 868.3 O 777.5 O 844.6			
Spirulina and chlorella, pellets	10.6 µm 100 ns 1.3 Hz	Vari ous	-	-	-	-	-	30 s	Ba 455.40 Sr 460.73 Mn 403.45 Fe 259.94 Mg 285.21	0.96 ppm 0.10 ppm 0.50 ppm 7.08 ppm 3.51 ppm	Univariate	[109]
Wheat flour, pellets	1064 nm - 4 Hz	38	7x15	-	-	-	300 ns	1.05 ms	Ca K	-	PLS	[110]
Maize and holly (Ilex chinensis Sims)	1064 nm - -	90	-	75	-	-	-	-	Mg K P I 213.62 P I 214.91 P I 253.56 P I 255.33 Cl I 827.59 Si 288.16	-	Elemental Mapping, MLR, ratios	[111]
Coffee, ground and pelletised	266 nm 8 ns 20 Hz	31	-	-	-	-	400 ns	-	Al 618.45 Mn I 358.65 Ce II 466 Cu II 780.76 Cr I 286.09 N II 567.95 Na I 588.99 Na I 589.59	-	Univariate	[112]
Phaleria Macrocarpa leaves, ground and pelletised	1064 nm 10 ns -	100	-	-	-	-	-	-	Ca I 422.67 Ca I 445.48 Pb I 363.95	-	Plasma temperature calculation, univariate	[115]

Sample	Laser	E (mJ)	Shots	Spot size (µm)	LTSD (mm)	I (GW cm ⁻²)	t _a	t _b	Analysed lines λ (nm)	LOD	Analysis method	Ref.
Tobacco, ground pelletised	266 nm 6 ns 10 Hz	25	100	50	-	-	0.25 us	1.05 ms	Ba II 493.409 Ca I 422.673 K I 766.490 Mn II 259.373 C I 247.856	25 ug g ⁻¹ 488 ug g ⁻¹ 197 ug g ⁻¹ 32 ug g ⁻¹ -	Univariate	[113]
Chinese tea leaves, Longjing green tea, Mengding Huangya, White tea, Tie Guanyin, Wuyi black tea, and Pu'er tea	1064 nm 5.82 ns -	50	-	-	-	-	1.2 us	4 us	Mg 279.55 Mn 279.83 CN (0-0) 388.34 Ca 393.37 Al 396.15 C2 (0-0) 516.45 Fe 517.46 K 766.49 C I 247.86	-	Fisher Discriminant Analysis, Bayes discriminant analysis	[114]
Sugar cane	- - -	50, 75		75, 125			0.5, 1		C I 193.1		PCA, PLS	[116]
Maize (<i>Zea mays</i> L.), pellets	- - -	-	30	-	-	-	-	-	Na 588.99 Ca 445.49 Mg 285.22 K 404.39 Fe 239.54	-	Qualitative	[117]
Cucurbita maxima seeds, powder	532 nm 4 ns 1 Hz	100	-	-	-	-	-	-	C 247.856 O 777.417 Ca 393.366 Mg 279.553 P 253.561 Na 589.592 K 766.49 N 567.956 H 656.271	-	one-way ANOVA, followed by a post hoc Scheffe's test, ratio	[118]

Sample	Laser	E (mJ)	Shots	Spot size (μm)	LTSD (mm)	I (GW cm ⁻²)	t _a	t _b	Analysed lines λ (nm)	LOD	Analysis method	Ref.
Ocimum sanctum, Ocimum americanum, Ocimum gratissimum, and Ocimum basilicum, ground and pelletised	532 nm 4 ns 10 Hz	-	10	-	-	-	-	-	C 229.6 C 247.8 Si 251.4 Si 288.1 Mg 277.9 Mg 279.7 Mg 279.5 Mg 280.2 Mg 285.2 Mg 382.9 Mg 383.2 Mg 383.8 Ca 315.8 Ca 317.9 Ca 370.6 Ca 373.6 Ca 393.3 Ca 396.8 Ca 422.6 Ca 428.3 Ca 443.5 Ca 445.4 Ca 714.8 Ca 854.2 Fe 258.5 Fe 259.9 Na 330.2 Na 589.6 K 766.4 K 769.8 N 463.0 N 744.2 N 868.0 H 656.2	-	PCA	[119]

Sample	Laser	E (mJ)	Shots	Spot size (µm)	LTSD (mm)	I (GW cm ⁻²)	t _a	t _b	Analysed lines λ (nm)	LOD	Analysis method	Ref.
									(cont.) O 777.4 O 844.6			
Gannan Navel Orange peels	- - 2 Hz	20	10x10	-	-	-	1.2 us	2 ms	Cu I 324.754 Cu I 327.396	-	Univariate	[120]
Red Fuji apples and Hosui pears	1064 nm - 20 Hz	160	-	-	-	-	2 us	-	P 213.62 P 214.91 P 253.56 P 255.33 Cl 837.59	4.3 mg kg ⁻¹ 2.1 mg kg ⁻¹ 1.5 mg kg ⁻¹ 6.9 mg kg ⁻¹ 3.0 mg kg ⁻¹	Univariate	[121]
Wood and babassu mesocarp, ground and pelletised	266 nm - 5-20 Hz	5-25	5-200	35-140	-	-	0-0.4 us	-	K I 766.49 K I 769.896 Mg II 279.553 Mg II 280.27 C I 247.856	12-30 ug g ⁻¹ 36-72 ug g ⁻¹ 14-27 ug g ⁻¹ 6-10 ug g ⁻¹ -	Univariate	[122]
Apple leaves, pine needles, citrus leaves, tea leaves, rice flour, Cannabis plant leaves and flower tops, ground and pelletised	1064 nm 7 ns 10 Hz	200	30	-	-	5.2	-	-	Al I 394.4 Ba I 649.88 Ca I 643.91 Br I 751.3 Cu I 324.75 Fe II 238.2 K I 766.49 Mg I 285.21 Mn II 257.61 Na I 330.3 P II 458.8 Rb I 794.76 Sr I 460.73	4.71 13.80 0.22 69.40 0.11 0.12 1.65 158.00 14.87 3.01 1.39 21.92 0.09 0.77	Quantitative, ANOVA and Tukey's HSD test	[123]

Sample	Laser	E (mJ)	Shots	Spot size (µm)	LTSD (mm)	I (GW cm ⁻²)	t _a	t _b	Analysed lines λ (nm)	LOD	Analysis method	Ref.
Black tea (Anxi, Fujian), Huangya tea (Ya'an, Sichuan), Longjing tea and Pu'er tea (Pu'er, Yunnan), ground and pelletised	1064 nm 8 ns 20 Hz	20- 100	10x20	-	-	-	2-30 us	2 us	C I 247.86 Mg II 279.55 Mn I 279.83 Ca II 393.37 Al I 396.15 CN (0-0) 388.34 Na I 589.59 H I 656.28 K I 766.49 Ca II 317.93 Ca II 370.60 Ca II 373.69 Ca II 396.85	-	Plasma temperature calculation, ratios	[124]
Sugarcane (Saccharum officinarum), soy (Glycine max), citrus (Citrus sinensis), coffee (Coffea arabica), maize (Zea mays), eucalyptus (Eucalyptus sp.), mango (Mangifera indica), bean (Phaseolus vulgaris), banana (Musa paradisiaca), lettuce (Lactuca sativa), brachiaria (Brachiaria decumbens), pearl millet (Pennisetum americanum),	1064 nm 532 nm 266 nm 6 ns 800 nm 60 fs 1 kHz	70 1.65	15	500 150	-	6 1.6x10 ⁵	0.75 us 35 ns	3 us 250 ns	Ca II 315.887 Mg I 285.212 P I 213.618 Cu I 324.755 Fe II 238.204 Mn II 257.610 Zn II 202.548	0.005-0.01 g kg ⁻¹ 0.01-0.05 g kg ⁻¹ 0.1-0.4 g kg ⁻¹ 1-7 mg kg ⁻¹ 3-12 mg kg ⁻¹ 1-2 mg kg ⁻¹ 4-80 mg kg ⁻¹	Hierarchical clustering, dendrogram classification using Euclidean distance, univariate, PLS	[125]

Sample	Laser	E (mJ)	Shots	Spot size (μm)	LTSD (mm)	I (GW cm^{-2})	t_a	t_b	Analysed lines λ (nm)	LOD	Analysis method	Ref.
(cont.)												
grape (<i>Vitis</i> sp.), rubber tree (<i>Hevea brasiliensis</i>), tomato (<i>Solanum lycopersicum</i>), apple leaves, peach leaves, spinach leaves, tomato leaves, and pine needles, dried and pelletised												
Juncus efusus L.	1064 nm 3-5 ns 2 Hz	340	-	-	-	-	1 μs	1 ms	C 192.77 C 247.725 Na 588.952 Na 589.554 Mg 279.418 Mg 280.123 H 656.315 H 777.492 Ca 393.375 Ca 396.816 Li 670.754 C-N 383.522 C-N 386.105 C-N 387.08 C-N 388.296 K 766.52 K 769.96 Al 394.417 Al 396.097 O 777.212 O 777.492 Ba 455.358 Ba 493.388	-	Relative standard deviation	[126]

Sample	Laser	E (mJ)	Shots	Spot size (μm)	LTSD (mm)	I (GW cm ⁻²)	t _a	t _b	Analysed lines λ (nm)	LOD	Analysis method	Ref.
									(cont.)			
									Ba 553.52			
									N 715.709			
									N 744.306			
									N 746.918			
									N 843.762			
									N 869.367			
									N 870.256			
									N 870.947			
									Mg 517.245			
									Mg 518.316			

- [1] Q. Sun, M. Tran, B. W. Smith *et al.*, "Direct determination of P, Al, Ca, Cu, Mn, Zn, Mg and Fe in plant materials by laser-induced plasma spectroscopy," *Canadian Journal of Analytical Sciences and Spectroscopy*, vol. 44, no. 6, pp. 164-170, 1999.
- [2] H. H. Cho, Y. J. Kim, Y. S. Jo *et al.*, "Application of laser-induced breakdown spectrometry for direct determination of trace elements in starch-based flours," *Journal of Analytical Atomic Spectrometry*, vol. 16, no. 6, pp. 622-627, 2001.
- [3] A. Uhl, K. Loebe, and L. Kreuchwig, "Fast analysis of wood preservers using laser induced breakdown spectroscopy," *Spectrochimica Acta - Part B Atomic Spectroscopy*, vol. 56, no. 6, pp. 795-806, 2001.
- [4] S. I. Gornushkin, I. B. Gornushkin, J. M. Anzano *et al.*, "Effective normalization technique for correction of matrix effects in laser-induced breakdown spectroscopy detection of magnesium in powdered samples," *Applied Spectroscopy*, vol. 56, no. 4, pp. 433-436, 2002.
- [5] T. M. Moskal, and D. W. Hahn, "On-line sorting of wood treated with chromated copper arsenate using laser-induced breakdown spectroscopy," *Applied Spectroscopy*, vol. 56, no. 10, pp. 1337-1344, 2002.
- [6] L. Niu, H. H. Cho, K. S. Song *et al.*, "Direct determination of strontium in marine algae samples by laser-induced breakdown spectrometry," *Applied Spectroscopy*, vol. 56, no. 11, pp. 1511-1514, 2002.
- [7] A. Assion, M. Wollenhaupt, L. Haag *et al.*, "Femtosecond laser-induced-breakdown spectrometry for Ca 2+ analysis of biological samples with high spatial resolution," *Applied Physics B: Lasers and Optics*, vol. 77, no. 4, pp. 391-397, 2003.
- [8] A. R. Boyain-Goitia, D. C. S. Beddows, B. C. Griffiths *et al.*, "Single-pollen analysis by laser-induced breakdown spectroscopy and raman microscopy," *Applied Optics*, vol. 42, no. 30, pp. 6119-6132, 2003.
- [9] A. C. Samuels, F. C. DeLucia Jr, K. L. McNesby *et al.*, "Laser-induced breakdown spectroscopy of bacterial spores, molds, pollens, and protein: Initial studies of discrimination potential," *Applied Optics*, vol. 42, no. 30, pp. 6205-6209, 2003.
- [10] H. M. Solo-Gabriele, T. G. Townsend, D. W. Hahn *et al.*, "Evaluation of XRF and LIBS technologies for on-line sorting of CCA-treated wood waste," *Waste Management*, vol. 24, no. 4, pp. 413-424, 2004.
- [11] O. Samek, J. Lambert, R. Hergenroder *et al.*, "Femtosecond laser spectrochemical analysis of plant samples," *Laser Physics Letters*, vol. 3, no. 1, pp. 21-5, 2006.
- [12] M. Bossu, Z. Q. Hao, M. Baudelet *et al.*, "Femtosecond laser-induced breakdown spectroscopy for detection of trace elements in sophora leaves," *Chinese Physics Letters*, vol. 24, no. 12, pp. 3466-3468, 2007.
- [13] M. Galiova, J. Kaiser, K. Novotny *et al.*, "Utilization of laser induced breakdown spectroscopy for investigation of the metal accumulation in vegetal tissues," *Spectrochimica Acta - Part B Atomic Spectroscopy*, vol. 62, no. 12, pp. 1597-1605, 2007.
- [14] J. Kaiser, O. Samek, L. Reale *et al.*, "Monitoring of the heavy-metal hyperaccumulation in vegetal tissues by X-ray radiography and by femto-second laser induced breakdown spectroscopy," *Microscopy Research and Technique*, vol. 70, no. 2, pp. 147-153, 2007.
- [15] M. Z. Martin, N. Labbé, N. André *et al.*, "High resolution applications of laser-induced breakdown spectroscopy for environmental and forensic applications," *Spectrochimica Acta - Part B Atomic Spectroscopy*, vol. 62, no. 12, pp. 1426-1432, 2007.
- [16] P. K. Rai, N. K. Rai, A. K. Rai *et al.*, "Role of LIBS in elemental analysis of Psidium guajava responsible for glycemic potential," *Instrumentation Science and Technology*, vol. 35, no. 5, pp. 507-522, 2007.
- [17] M. Z. Martin, N. Labbé, T. G. Rials *et al.*, "Analysis of preservative-treated wood by multivariate analysis of laser-induced breakdown spectroscopy spectra," *Spectrochimica Acta Part B: Atomic Spectroscopy*, vol. 60, no. 7-8, pp. 1179-1185, 2005.

- [18] M. Galiova, J. Kaiser, K. Novotny *et al.*, "Investigation of heavy-metal accumulation in selected plant samples using laser induced breakdown spectroscopy and laser ablation inductively coupled plasma mass spectrometry," *Applied Physics A: Materials Science and Processing*, vol. 93, no. 4, pp. 917-922, 2008.
- [19] M. Hassan, M. Sighicelli, A. Lai *et al.*, "Studying the enhanced phytoremediation of lead contaminated soils via laser induced breakdown spectroscopy," *Spectrochimica Acta - Part B Atomic Spectroscopy*, vol. 63, no. 10, pp. 1225-1229, 2008.
- [20] V. Juvé, R. Portelli, M. Boueri *et al.*, "Space-resolved analysis of trace elements in fresh vegetables using ultraviolet nanosecond laser-induced breakdown spectroscopy," *Spectrochimica Acta - Part B Atomic Spectroscopy*, vol. 63, no. 10, pp. 1047-1053, 2008.
- [21] A. Khumaeni, M. Ramli, Y. Deguchi *et al.*, "New technique for the direct analysis of food powders confined in a small hole using transversely excited atmospheric CO₂ laser-induced gas plasma," *Applied Spectroscopy*, vol. 62, no. 12, pp. 1344-1348, 2008.
- [22] S. Krizkova, P. Ryant, O. Krystofova *et al.*, "Multi-instrumental analysis of tissues of sunflower plants treated with silver(I) ions - Plants as bioindicators of environmental pollution," *Sensors*, vol. 8, no. 1, pp. 445-463, 2008.
- [23] L. C. Trevizan, D. Santos Jr, R. E. Samad *et al.*, "Evaluation of laser induced breakdown spectroscopy for the determination of macronutrients in plant materials," *Spectrochimica Acta - Part B Atomic Spectroscopy*, vol. 63, no. 10, pp. 1151-1158, 2008.
- [24] T. Flores, L. Ponce, M. Arronte *et al.*, "Free-running and Q:Switched LIBS measurements during the laser ablation of Prickle Pears spines," *Optics and Lasers in Engineering*, vol. 47, no. 5, pp. 578-583, 2009.
- [25] B. A. Gething, J. J. Janowiak, and R. H. Falk, "Assessment of laser induced breakdown spectroscopy (LIBS) for classification of preservative in CCA-treated lumber," *Forest Products Journal*, vol. 59, no. 3, pp. 67-74, 2009.
- [26] D. Jaiswal, P. K. Rai, and G. Watal, "Antidiabetic effect of Withania coagulans in experimental rats," *Indian Journal of Clinical Biochemistry*, vol. 24, no. 1, pp. 88-93, 2009.
- [27] J. Kaiser, M. Galiova, K. Novotny *et al.*, "Mapping of lead, magnesium and copper accumulation in plant tissues by laser-induced breakdown spectroscopy and laser-ablation inductively coupled plasma mass spectrometry," *Spectrochimica Acta - Part B Atomic Spectroscopy*, vol. 64, no. 1, pp. 67-73, 2009.
- [28] A. Khumaeni, H. Niki, Y. Deguchi *et al.*, "Analysis of organic powder samples by using the metal-assisted subtarget effect in a Transversely-Excited Atmospheric (TEA) CO₂ laser-induced he gas plasma at 1 atm," *Journal of the Korean Physical Society*, vol. 55, no. 6, pp. 2441-2446, 2009.
- [29] O. Krystofova, V. Shestivska, M. Galiova *et al.*, "Sunflower plants as bioindicators of environmental pollution with lead (II) ions," *Sensors*, vol. 9, no. 7, pp. 5040-5058, 2009.
- [30] W. Lei, V. Motto-Ros, M. Boueri *et al.*, "Time-resolved characterization of laser-induced plasma from fresh potatoes," *Spectrochimica Acta - Part B Atomic Spectroscopy*, vol. 64, no. 9, pp. 891-898, 2009.
- [31] M. R. Martelli, C. Barron, P. Delaporte *et al.*, "Pulsed laser ablation: A new approach to reveal wheat outer layer properties," *Journal of Cereal Science*, vol. 49, no. 3, pp. 354-362, 2009.
- [32] L. C. Nunes, G. A. da Silva, L. C. Trevizan *et al.*, "Simultaneous optimization by neuro-genetic approach for analysis of plant materials by laser induced breakdown spectroscopy," *Spectrochimica Acta - Part B Atomic Spectroscopy*, vol. 64, no. 6, pp. 565-572, 2009.
- [33] M. Pouzar, T. Cernohorsky, M. Prusova *et al.*, "LIBS analysis of crop plants," *Journal of Analytical Atomic Spectrometry*, vol. 24, no. 7, pp. 953-957, 2009.

- [34] T. Ohta, M. Ito, T. Kotani *et al.*, “Emission enhancement of laser-induced breakdown spectroscopy by localized surface plasmon resonance for analyzing plant nutrients,” *Applied Spectroscopy*, vol. 63, no. 5, pp. 555-558, 2009.
- [35] N. K. Rai, P. K. Rai, S. Pandhija *et al.*, “Application of LIBS in detection of antihyperglycemic trace elements in *Momordica charantia*,” *Food Biophysics*, vol. 4, no. 3, pp. 167-171, 2009.
- [36] L. C. Trevizan, D. Santos Jr, R. E. Samad *et al.*, “Evaluation of laser induced breakdown spectroscopy for the determination of micronutrients in plant materials,” *Spectrochimica Acta - Part B Atomic Spectroscopy*, vol. 64, no. 5, pp. 369-377, 2009.
- [37] P. K. Rai, D. Jaiswal, N. K. Rai *et al.*, “Role of glycemic elements of *Cynodon dactylon* and *Musa paradisiaca* in diabetes management,” *Lasers in Medical Science*, vol. 24, no. 5, pp. 761-768, 2009.
- [38] R. K. Singh, S. Mehta, D. Jaiswal *et al.*, “Antidiabetic effect of *Ficus bengalensis* aerial roots in experimental animals,” *Journal of Ethnopharmacology*, vol. 123, no. 1, pp. 110-114, 2009.
- [39] D. C. Zhang, X. Ma, W. Q. Wen *et al.*, “Studies of laser induced-breakdown spectroscopy of holly leaves,” *Journal of Physics: Conference Series*, vol. 185, 2009.
- [40] S. Beldjilali, D. Borivent, L. Mercadier *et al.*, “Evaluation of minor element concentrations in potatoes using laser-induced breakdown spectroscopy,” *Spectrochimica Acta - Part B Atomic Spectroscopy*, vol. 65, no. 8, pp. 727-733, 2010.
- [41] V. Diopan, V. Shestivska, O. Zitka *et al.*, “Determination of plant thiols by liquid chromatography coupled with coulometric and amperometric detection in lettuce treated by lead(II) ions,” *Electroanalysis*, vol. 22, no. 11, pp. 1248-1259, 2010.
- [42] A. A. Bol'shakov, J. H. Yoo, C. Liu *et al.*, “Laser-induced breakdown spectroscopy in industrial and security applications,” *Applied Optics*, vol. 49, no. 13, pp. C132-C142, 2010.
- [43] D. Jaiswal, P. K. Rai, and G. Watal, “Hypoglycemic and antidiabetic effects of *withania coagulans* fruit ethanolic extract in normal and streptozotocin-induced diabetic rats,” *Journal of Food Biochemistry*, vol. 34, no. 4, pp. 764-778, 2010.
- [44] M. R. Martelli, F. Brygo, A. Sadoudi *et al.*, “Laser-induced breakdown spectroscopy and chemometrics: A novel potential method to analyze wheat grains,” *Journal of Agricultural and Food Chemistry*, vol. 58, no. 12, pp. 7126-7134, 2010.
- [45] M. Z. Martin, A. J. Stewart, K. D. Gwinn *et al.*, “Laser-induced breakdown spectroscopy used to detect endophyte-mediated accumulation of metals by tall fescue,” *Applied Optics*, vol. 49, no. 13, pp. C161-C167, 2010.
- [46] J. W. B. Braga, L. C. Trevizan, L. C. Nunes *et al.*, “Comparison of univariate and multivariate calibration for the determination of micronutrients in pellets of plant materials by laser induced breakdown spectrometry,” *Spectrochimica Acta - Part B Atomic Spectroscopy*, vol. 65, no. 1, pp. 66-74, 2010.
- [47] S. Mehta, P. K. Rai, D. K. Rai *et al.*, “LIBS-based detection of antioxidant elements in seeds of *Emblica officinalis*,” *Food Biophysics*, vol. 5, no. 3, pp. 186-192, 2010.
- [48] D. K. Chauhan, D. K. Tripathi, N. K. Rai *et al.*, “Detection of Biogenic Silica in Leaf Blade, Leaf Sheath, and Stem of Bermuda Grass (*Cynodon dactylon*) Using LIBS and Phytolith Analysis,” *Food Biophysics*, vol. 6, no. 3, pp. 416-423, 2011.
- [49] M. Barbafieri, R. Pini, A. Ciucci *et al.*, “Field assessment of Pb in contaminated soils and in leaf mustard (*Brassica juncea*): The LIBS technique,” *Chemistry and Ecology*, vol. 27, no. SUPPL. 1, pp. 161-169, 2011.
- [50] L. C. Nunes, J. W. Batista Braga, L. C. Trevizan *et al.*, “Optimization and validation of a LIBS method for the determination of macro and micronutrients in sugar cane leaves,” *Journal of Analytical Atomic Spectrometry*, vol. 25, no. 9, pp. 1453-1460, 2010.
- [51] E. R. Schenk, and J. R. Almirall, “Elemental analysis of cotton by laser-induced breakdown spectroscopy,” *Applied Optics*, vol. 49, no. 13, pp. C153-C160, 2010.

- [52] D.-C. Zhang, X.-W. Ma, W.-Q. Wen *et al.*, "Influence of Laser Wavelength on Laser-induced Breakdown Spectroscopy Applied to Semi-Quantitative Analysis of Trace-Elements in a Plant Sample," *Chinese Physics Letters*, vol. 27, no. 6, pp. 063202 (4 pp.), 2010.
- [53] M. Galiová, J. Kaiser, K. Novotný *et al.*, "Utilization of laser-assisted analytical methods for monitoring of lead and nutrition elements distribution in fresh and dried *Capsicum annuum* l. leaves," *Microscopy Research and Technique*, vol. 74, no. 9, pp. 845-852, 2011.
- [54] D. Sun, M. Su, C. Dong *et al.*, "A semi-quantitative analysis of essential micronutrient in folium lycii using laser-induced breakdown spectroscopy technique," *Plasma Science and Technology*, vol. 12, no. 4, pp. 478-481, 2010.
- [55] M. Yao, M. Liu, J. Zhao *et al.*, "Identification of nutrition elements in orange leaves by laser induced breakdown spectroscopy," *2010 International Symposium on Intelligent Information Technology and Security Informatics, IITSI 2010*. pp. 398-401.
- [56] F. M. V. Pereira, D. M. B. P. Milori, A. L. Venâncio *et al.*, "Evaluation of the effects of *Candidatus Liberibacter asiaticus* on inoculated citrus plants using laser-induced breakdown spectroscopy (LIBS) and chemometrics tools," *Talanta*, vol. 83, no. 2, pp. 351-356, 2010.
- [57] G. Watal, B. Sharma, P. K. Rai *et al.*, "LIBS-based detection of antioxidant elements: a new strategy," *Methods in molecular biology (Clifton, N.J.)*, vol. 594, pp. 275-285, 2010.
- [58] E. J. Ferreira, E. C. Ferreira, A. C. B. Delbem *et al.*, "Ensemble of predictors and laser induced breakdown spectroscopy for certifying coffee," *Electronics Letters*, vol. 47, no. 17, pp. 967-969, 2011.
- [59] S. Beldjilali, W. L. Yip, J. Hermann *et al.*, "Investigation of plasmas produced by laser ablation using single and double pulses for food analysis demonstrated by probing potato skins," *Analytical and Bioanalytical Chemistry*, vol. 400, no. 7, pp. 2173-2183, 2011.
- [60] M. D. S. Gomes, D. Santos Jr, L. C. Nunes *et al.*, "Evaluation of grinding methods for pellets preparation aiming at the analysis of plant materials by laser induced breakdown spectrometry," *Talanta*, vol. 85, no. 4, pp. 1744-1750, 2011.
- [61] M. Hassan, M. Abdelhamied, A. H. Hanafy *et al.*, "Laser monitoring of phytoextraction enhancement of lead contaminated soil adopting EDTA and EDDS," *8th International Conference on Laser Applications, ICLA 2011*. pp. 93-100.
- [62] A. Khumaeni, H. Niki, K. I. Fukumoto *et al.*, "A unique technique of laser-induced breakdown spectroscopy using transversely excited atmospheric CO₂ laser for the sensitive analysis of powder samples," *Current Applied Physics*, vol. 11, no. 3, pp. 423-427, 2011.
- [63] A. Khumaeni, Z. S. Lie, H. Niki *et al.*, "Direct analysis of powder samples using transversely excited atmospheric CO₂ laser-induced gas plasma at 1 atm," *Analytical and Bioanalytical Chemistry*, vol. 400, no. 10, pp. 3279-3287, 2011.
- [64] Z. Lei, M. Yao, M. Liu *et al.*, "Analysis the macronutrients in Gannan navel oranges for three kinds of sample state by laser induced breakdown spectroscopy," *4th International Congress on Image and Signal Processing, CISP 2011*. pp. 2464-2466.
- [65] S. Ma, X. Gao, K. Guo *et al.*, "Analysis of the element content in poplar tree leaves by femtosecond laser-induced breakdown spectroscopy," *Science China: Physics, Mechanics and Astronomy*, vol. 54, no. 11, pp. 1953-1957, 2011.
- [66] M. R. Martelli, F. Brygo, P. Delaporte *et al.*, "Estimation of Wheat Grain Tissue Cohesion via Laser Induced Breakdown Spectroscopy," *Food Biophysics*, vol. 6, no. 4, pp. 433-439, 2011.
- [67] Y. Mingyin, L. Jinlong, L. Muhua *et al.*, "Discrimination of Ca, Cu, Fe, and Na in Gannan Navel orange by laser induced breakdown spectroscopy," *4th IFIP International Conference on Computer and Computing Technologies in*

- Agriculture and the 4th Symposium on Development of Rural Information, CCTA 2010, 2011, pp. 608-613.
- [68] M. M. Suliyanti, M. Pardede, T. J. Lie *et al.*, "Direct powder analysis by laser-induced breakdown spectroscopy utilizing laser-controlled dust production in a small chamber," *Journal of the Korean Physical Society*, vol. 58, no. 5, pp. 1129-1134, 2011.
- [69] D. K. Tripathi, R. Kumar, D. K. Chauhan *et al.*, "Laser-induced breakdown spectroscopy for the study of the pattern of silicon deposition in leaves of saccharum species," *Instrumentation Science and Technology*, vol. 39, no. 6, pp. 510-521, 2011.
- [70] G. G. A. De Carvalho, D. Santos Jr, L. C. Nunes *et al.*, "Effects of laser focusing and fluence on the analysis of pellets of plant materials by laser-induced breakdown spectroscopy," *Spectrochimica Acta - Part B Atomic Spectroscopy*, vol. 74-75, pp. 162-168, 2012.
- [71] G. Kim, J. Kwak, J. Choi *et al.*, "Detection of nutrient elements and contamination by pesticides in spinach and rice samples using laser-induced breakdown spectroscopy (LIBS)," *Journal of Agricultural and Food Chemistry*, vol. 60, no. 3, pp. 718-724, 2012.
- [72] X. Zhang, M. Yao, M. Liu *et al.*, "Analysis of trace elements in leaves using laser-induced breakdown spectroscopy," 5th International Conference on Computer and Computing Technologies in Agriculture, CCTA 2011, 2012, pp. 334-339.
- [73] M. da Silva Gomes, G. G. A. de Carvalho, D. Santos Junior *et al.*, "A novel strategy for preparing calibration standards for the analysis of plant materials by laser-induced breakdown spectroscopy: A case study with pellets of sugar cane leaves," *Spectrochimica Acta Part B: Atomic Spectroscopy*, vol. 86, no. 0, pp. 137-141, 2013.
- [74] P. Dhar, I. Gembitsky, P. K. Rai *et al.*, "A Possible Connection Between Antidiabetic & Antilipemic Properties of Psoralea corylifolia Seeds and the Trace Elements Present: A LIBS Based Study," *Food Biophysics*, pp. 1-9, 2012.
- [75] P. F. de Souza, D. Santos, G. G. A. de Carvalho *et al.*, "Determination of silicon in plant materials by laser-induced breakdown spectroscopy," *Spectrochimica Acta - Part B Atomic Spectroscopy*, 2013.
- [76] M. Yao, L. Huang, J. Zheng *et al.*, "Assessment of feasibility in determining of Cr in Gannan Navel Orange treated in controlled conditions by laser induced breakdown spectroscopy," *Optics & Laser Technology*, vol. 52, no. 0, pp. 70-74, 2013.
- [77] P. Dhar, I. Gembitsky, P. Rai *et al.*, "A Possible Connection Between Antidiabetic & Antilipemic Properties of Psoralea corylifolia Seeds and the Trace Elements Present: A LIBS Based Study," *Food Biophysics*, vol. 8, no. 2, pp. 95-103, 2013/06/01, 2013.
- [78] M. Tiwari, R. Agrawal, A. K. Pathak *et al.*, "Laser-induced breakdown spectroscopy: An approach to detect adulteration in turmeric," *Spectroscopy Letters*, vol. 46, no. 3, pp. 155-159, 2013.
- [79] M. Garcimuño, D. M. Díaz Pace, and G. Bertuccelli, "Laser-induced breakdown spectroscopy for quantitative analysis of copper in algae," *Optics and Laser Technology*, vol. 47, pp. 26-30, 2013.
- [80] X. Fang, and S. R. Ahmad, "Elemental analysis in environmental land samples by stand-off laser-induced breakdown spectroscopy," *Applied Physics B*, pp. 1-7, 2013/09/07, 2013.
- [81] G. G. A. de Carvalho, D. Santos Jr, M. da Silva Gomes *et al.*, "Influence of particle size distribution on the analysis of pellets of plant materials by laser-induced breakdown spectroscopy," *Spectrochimica Acta Part B: Atomic Spectroscopy*, vol. 105, no. 0, pp. 130-135, 2015.
- [82] L. C. Peruchi, L. C. Nunes, G. G. A. de Carvalho *et al.*, "Determination of inorganic nutrients in wheat flour by laser-induced breakdown spectroscopy and energy dispersive X-ray fluorescence spectrometry," *Spectrochimica Acta Part B:*

- Atomic Spectroscopy*, vol. 100, no. 0, pp. 129-136, 2014.
- [83] B. Sezer, G. Bilge, A. Berkkan *et al.*, "A rapid tool for determination of titanium dioxide content in white chickpea samples," *Food Chemistry*, vol. 240, pp. 84-89, 2018.
- [84] M. Iqbal, Z. ul Haq, A. Malik *et al.*, "Pre-sowing seed magnetic field stimulation: A good option to enhance bitter melon germination, seedling growth and yield characteristics," *Biocatalysis and Agricultural Biotechnology*, vol. 5, pp. 30-37, 2016.
- [85] D. K. Tripathi, V. P. Singh, S. M. Prasad *et al.*, "Silicon-mediated alleviation of Cr(VI) toxicity in wheat seedlings as evidenced by chlorophyll fluorescence, laser induced breakdown spectroscopy and anatomical changes," *Ecotoxicology and Environmental Safety*, vol. 113, pp. 133-144, 2015.
- [86] M. B. Bueno Guerra, A. Adame, E. De Almeida *et al.*, "Direct analysis of plant leaves by EDXRF and LIBS: microsampling strategies and cross-validation," *Journal of Analytical Atomic Spectrometry*, vol. 30, no. 7, pp. 1646-1654, 2015.
- [87] K. Devey, M. Mucalo, G. Rajendram *et al.*, "Pasture Vegetation Elemental Analysis by Laser-Induced Breakdown Spectroscopy," *Communications in Soil Science and Plant Analysis*, vol. 46, pp. 72-80, 2015.
- [88] D. K. Tripathi, V. P. Singh, S. M. Prasad *et al.*, "LIB spectroscopic and biochemical analysis to characterize lead toxicity alleviative nature of silicon in wheat (*Triticum aestivum* L.) seedlings," *Journal of Photochemistry and Photobiology B: Biology*, vol. 154, pp. 89-98, 2016.
- [89] J. Wang, S. Xue, P. Zheng *et al.*, "Determination of Lead and Copper in *Ligusticum wallichii* by Laser-Induced Breakdown Spectroscopy," *Analytical Letters*, vol. 50, no. 12, pp. 2000-2011, 2017.
- [90] P. Modlitbová, K. Novotný, P. Pořízka *et al.*, "Comparative investigation of toxicity and bioaccumulation of Cd-based quantum dots and Cd salt in freshwater plant *Lemna minor* L.," *Ecotoxicology and Environmental Safety*, vol. 147, pp. 334-341, 2018.
- [91] L. Krajcarová, K. Novotný, M. Kummerová *et al.*, "Mapping of the spatial distribution of silver nanoparticles in root tissues of *Vicia faba* by laser-induced breakdown spectroscopy (LIBS)," *Talanta*, vol. 173, pp. 28-35, 2017.
- [92] T. V. Silva, S. Z. Hubinger, J. A. Gomes Neto *et al.*, "Potential of Laser Induced Breakdown Spectroscopy for analyzing the quality of unroasted and ground coffee," *Spectrochimica Acta - Part B Atomic Spectroscopy*, vol. 135, pp. 29-33, 2017.
- [93] J. Peng, Y. He, L. Ye *et al.*, "Moisture Influence Reducing Method for Heavy Metals Detection in Plant Materials Using Laser-Induced Breakdown Spectroscopy: A Case Study for Chromium Content Detection in Rice Leaves," *Analytical Chemistry*, vol. 89, no. 14, pp. 7593-7600, 2017.
- [94] A. C. Ranulfi, R. A. Romano, A. Bebechibuli Magalhães *et al.*, "Evaluation of the Nutritional Changes Caused by Huanglongbing (HLB) to Citrus Plants Using Laser-Induced Breakdown Spectroscopy," *Applied Spectroscopy*, vol. 71, no. 7, pp. 1471-1480, 2017.
- [95] G. Nicolodelli, G. S. Senesi, A. C. Ranulfi *et al.*, "Double-pulse laser induced breakdown spectroscopy in orthogonal beam geometry to enhance line emission intensity from agricultural samples," *Microchemical Journal*, vol. 133, pp. 272-278, 2017.
- [96] S. Awasthi, R. Kumar, A. Devanathan *et al.*, "Multivariate methods for analysis of environmental reference materials using laser-induced breakdown spectroscopy," *Analytical Chemistry Research*, vol. 12, pp. 10-16, 2017.
- [97] J. N. Kunz, D. V. Voronine, B. A. Ko *et al.*, "Interaction of femtosecond laser pulses with plants: towards distinguishing weeds and crops using plasma temperature," *Journal of Modern Optics*, vol. 64, no. 9, pp. 942-947, 2017.
- [98] M. Yao, H. Yang, L. Huang *et al.*, "Detection of heavy metal Cd in polluted fresh leafy vegetables by laser-induced breakdown spectroscopy," *Applied Optics*, vol. 56, no. 14, pp. 4070-4075, 2017.

- [99] S. Varliklioz Er, H. Eksi-Kocak, H. Yetim *et al.*, "Novel Spectroscopic Method for Determination and Quantification of Saffron Adulteration," *Food Analytical Methods*, vol. 10, no. 5, pp. 1547-1555, 2017.
- [100] D. F. Andrade, E. R. Pereira-Filho, and P. Konieczynski, "Comparison of ICP OES and LIBS analysis of medicinal herbs rich in flavonoids from Eastern Europe," *Journal of the Brazilian Chemical Society*, vol. 28, no. 5, pp. 838-847, 2017.
- [101] J. Singh, R. Kumar, S. Awasthi *et al.*, "Laser Induced breakdown spectroscopy: A rapid tool for the identification and quantification of minerals in cucurbit seeds," *Food Chemistry*, vol. 221, pp. 1778-1783, 2017.
- [102] J. N. Kunz, D. V. Voronine, H. W. H. Lee *et al.*, "Rapid detection of drought stress in plants using femtosecond laser-induced breakdown spectroscopy," *Optics Express*, vol. 25, no. 7, pp. 7251-7262, 2017.
- [103] C. R. Bhatt, B. Alfarraj, C. T. Ghany *et al.*, "Comparative Study of Elemental Nutrients in Organic and Conventional Vegetables Using Laser-Induced Breakdown Spectroscopy (LIBS)," *Applied Spectroscopy*, vol. 71, no. 4, pp. 686-698, 2017.
- [104] J. Peng, K. Song, H. Zhu *et al.*, "Fast detection of tobacco mosaic virus infected tobacco using laser-induced breakdown spectroscopy," *Scientific Reports*, vol. 7, 2017.
- [105] J. Wang, M. Shi, P. Zheng *et al.*, "Quantitative Analysis of Lead in Tea Samples by Laser-Induced Breakdown Spectroscopy," *Journal of Applied Spectroscopy*, vol. 84, no. 1, pp. 188-193, 2017.
- [106] P. Shukla, R. Kumar, and A. K. Raib, "Detection of Minerals in Green Leafy Vegetables Using Laser Induced Breakdown Spectroscopy," *Journal of Applied Spectroscopy*, vol. 83, no. 5, pp. 872-877, 2016.
- [107] T. J. Jiang, Z. Guo, M. J. Ma *et al.*, "Electrochemical laser induced breakdown spectroscopy for enhanced detection of Cd(II) without interference in rice on layer-by-layer assembly of graphene oxides," *Electrochimica Acta*, vol. 216, pp. 188-195, 2016.
- [108] N. Shukla, A. S. Bharti, S. Srivastava *et al.*, "Determination of Elements in Carrot Root by Laser Induced Breakdown Spectroscopy," *National Academy Science Letters*, vol. 40, no. 1, pp. 47-51, 2017.
- [109] S. Zivkovic, M. Momcilovic, A. Staicu *et al.*, "Spectrochemical analysis of powdered biological samples using transversely excited atmospheric carbon dioxide laser plasma excitation," *Spectrochimica Acta - Part B Atomic Spectroscopy*, vol. 128, pp. 22-29, 2017.
- [110] G. Bilge, B. Sezer, K. E. Eseller *et al.*, "Determination of Ca addition to the wheat flour by using laser-induced breakdown spectroscopy (LIBS)," *European Food Research and Technology*, vol. 242, no. 10, pp. 1685-1692, 2016.
- [111] C. Zhao, D. Dong, X. Du *et al.*, "In-field, in situ, and in vivo 3-dimensional elemental mapping for plant tissue and soil analysis using laser-induced breakdown spectroscopy," *Sensors (Switzerland)*, vol. 16, no. 10, 2016.
- [112] M. A. Gondal, U. Baig, M. A. Dastageer *et al.*, "Determination of elemental composition of coffee using UV-pulsed laser induced breakdown spectroscopy."
- [113] D. M. Silvestre, F. de Oliveira Leme, C. S. Nomura *et al.*, "Direct analysis of barium, calcium, potassium, and manganese concentrations in tobacco by laser-induced breakdown spectroscopy," *Microchemical Journal*, vol. 126, pp. 545-550, 2016.
- [114] J. Wang, P. Zheng, H. Liu *et al.*, "Classification of Chinese tea leaves using laser-induced breakdown spectroscopy combined with the discriminant analysis method," *Analytical Methods*, vol. 8, no. 15, pp. 3204-3209, 2016.
- [115] Z. Haider, J. Ali, M. Arab *et al.*, "Plasma Diagnostics and Determination of Lead in Soil and Phaleria Macrocarpa Leaves by Ungated Laser Induced Breakdown Spectroscopy," *Analytical Letters*, vol. 49, no. 6, pp. 808-817, 2016.
- [116] J. P. R. Romera, P. L. Barsanelli, and F. M. V. Pereira, "Expeditious prediction of fiber content in sugar cane: An analytical possibility with LIBS and chemometrics,"

- Fuel*, vol. 166, pp. 473-476, 2016.
- [117] S. Qamar, M. Aslam, and M. A. Javed, "Determination of Proximate Chemical Composition and Detection of Inorganic Nutrients in Maize (*Zea mays* L.)." pp. 715-718.
- [118] D. K. Kushawaha, M. Yadav, S. Chatterji *et al.*, " α -amylase and α -glucosidase inhibitory activity assessment of *Cucurbita maxima* seeds – A LIBS based study," *International Journal of Phytomedicine*, vol. 8, no. 3, pp. 312-318, 2016.
- [119] D. K. Tripathi, A. K. Pathak, D. K. Chauhan *et al.*, "An efficient approach of Laser Induced Breakdown Spectroscopy (LIBS) and ICAP-AES to detect the elemental profile of *Ocimum* L. species," *Biocatalysis and Agricultural Biotechnology*, vol. 4, no. 4, pp. 471-479, 2015.
- [120] H. Hu, L. Huang, M. Liu *et al.*, "Nondestructive determination of Cu residue in orange peel by laser induced breakdown spectroscopy," *Plasma Science and Technology*, vol. 17, no. 8, pp. 711-715, 2015.
- [121] X. Du, D. Dong, X. Zhao *et al.*, "Detection of pesticide residues on fruit surfaces using laser induced breakdown spectroscopy," *RSC Advances*, vol. 5, no. 97, pp. 79956-79963, 2015.
- [122] D. M. Silvestre, F. M. Barbosa, B. T. Aguiar *et al.*, "Feasibility study of calibration strategy for direct quantitative measurement of K and Mg in plant material by laser-induced breakdown spectrometry," *Analytical Chemistry Research*, vol. 5, pp. 28-33, 2015.
- [123] M. M. El-Defdar, J. Robertson, S. Foster *et al.*, "Evaluation of elemental profiling methods, including laser-induced breakdown spectroscopy (LIBS), for the differentiation of Cannabis plant material grown in different nutrient solutions," *Forensic Science International*, vol. 251, pp. 95-106, 2015.
- [124] P. Zheng, M. Shi, J. Wang *et al.*, "The spectral emission characteristics of laser induced plasma on tea samples," *Plasma Science and Technology*, vol. 17, no. 8, pp. 664-670, 2015.
- [125] G. G. Arantes de Carvalho, J. Moros, D. Santos, Jr. *et al.*, "Direct determination of the nutrient profile in plant materials by femtosecond laser-induced breakdown spectroscopy," *Analytica Chimica Acta*, vol. 876, pp. 26-38, 2015.
- [126] X. Liu, J. Huang, Z. Wu *et al.*, "Microanalysis of multi-element in *Juncus effusus* L. by LIBS technique," *Plasma Science and Technology*, vol. 17, no. 11, pp. 904-908, 2015.

Appendix B

Agricultural robot platform

B. 1 Agricultural robot platform

The purpose of this thesis was to determine if LIBS was suitable for precision agriculture. The LIBS system would have to be attached to an agricultural vehicle because of the size of the laser unit. With the emergence of smaller lasers, LIBS systems have been created that are now a fraction of the size we have used. An example is the micro-LIBS unit [106]. With such small units, placing a LIBS system on a small autonomous robot is achievable. For this reason, a prototype agricultural robot was developed that could theoretically carry an onboard micro-LIBS unit. This appendix discusses how the robot functions and the equipment used. This robot would serve as a starting point for a LIBS agricultural rover.

B. 2 Setup and connections

A Botboardunio (Lynxmotion, USA), shown in Figure 1, which is based on the Duemilanove (Arduino), is the central board controlling the robot. All communication and control go through this microcontroller. The Botboardunio communicates to an Uno (Arduino) and an HC-05 Bluetooth transmitter via serial protocol.



Figure 1. Botboardunio microcontroller [107].

The Uno listens to the transmission line (Tx) of the Botbaordunio. It takes the encoded motor commands out of the serial stream and transmits them to the

Sabretooth motor controller using servo commands. The reason the Uno was used is that when a second serial line is used on the Botboarduino it fills the buffer up and slows down the entire programme. This effects the feedback timing on the PI controller for the motors, producing slower corrections.

A Sabretooth Motor Controller (Lynxmotion, USA) takes servo commands from the Uno through the cables intended for the remote-control receiver and controls the four HN-GHIZ-1634T (Lynxmotion, USA) 12V DC gear motors for the robot's wheels.

An optical encoder (E4P OEM Miniature Optical Kit, US Digital, USA) is used to implement PID control in the motors. It is attached to the shaft of one of the motors. The downside of having only one encoder is that if one of the wheels without the encoder slips it will not be picked up.

A magnetometer (GY-273 HMC5883L, Honeywell, USA) determines the current bearing of the robot. It was placed on top of the robot via a cardboard box since metal surfaces disturb the magnetic field around the magnetometer causing it to give false readings.

The GPS (NEO-6M, u-blox, Switzerland) gets the current coordinates of the robot. The U Center (u-blox, Switzerland) software was used to change the default settings on the GPS module to increase accuracy.

The Bluetooth (HC-05) module is used to send data to a computer. This can be used for debugging. It sends longitude, latitude, bearing, heading, and the current state of the robot. The Bluetooth module is connected to a Logic Level Converter to change the communication voltages.

B. 3 System Identification and PID Control

The robot must navigate different terrain where extra effort is needed so that the robot stays at a constant speed. PID control can achieve this with the correct gains. The transfer function of the robot wheels looks like

$$G(s) = \frac{Ae^{-Ls}}{\tau s + 1}$$

and the parameters are acquired by measuring the step response at the output (rpm). The servo input for the Sabretooth motor driver takes inputs from 1500-2000. Shifting the input index from 1500-2000 to 0-500, for simplicity, places the median effort at 250 which allows for more effort when using PI control. The rpm was measured by setting the input of the servo to 250 and then the gain (A) was calculated.

$$A = 154 \text{ [rpm]} / 250 \text{ [servo]} = 0.616 \text{ [rpm/servo]}$$

The steady state (K) of the step response and the delay (L) was determined from Figure 2, calculated as 154 rpm and 37.5 ms.

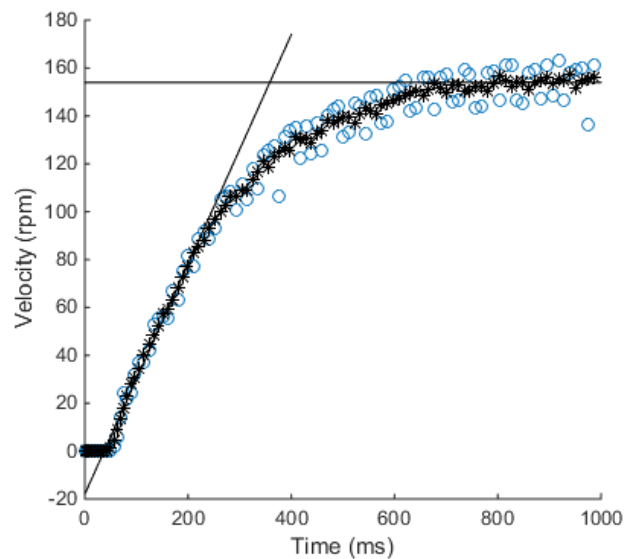


Figure 2. Step response of the robot. Circles are the raw data, stars are the average of the raw data. Steady state is determined from the horizontal line and the delay is found from where the line of the slope crosses the x-axis.

A slope (R) of 0.48 rpm/ms was calculated for the step response by fitting a slope to the initial part of the curve as seen in Figure 3.

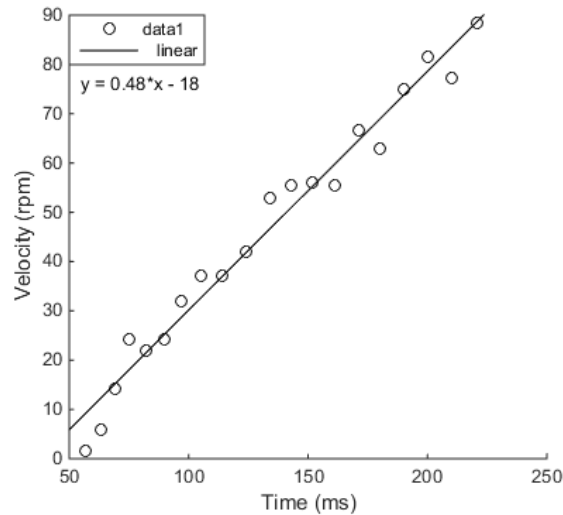


Figure 3. The fitted line to find the slope (R) of the step response.

The time constant (τ) can then be found

$$\tau = K/R = 154 / 0.48 = 321 \text{ ms (3 s.f.)}$$

Using these parameters, the plant transfer function is

$$G(s) = \frac{0.616e^{-37.5s}}{321s + 1}$$

Using this transfer function the Ziegler Nichols tuning parameters were calculated and used as a starting point for PID tuning.

$$K_p = 0.9/RL = 0.9 / (0.48 \times 37.5) = 0.05 \text{ rpm}^{-1}$$

$$K_i = 0.9 \times 0.3/RL^2 = 0.3K_p/L = 0.0004 \text{ rpm}^{-1} \text{ ms}^{-1}$$

The parameters were varied to get the response in Figure 4. Only proportional and integral control were needed to give a faster response with no overshoot and no oscillations. The proportional (K_p) and integral (K_i) gains were 2.5 and 0.008 respectively. The timing of the controller was a problem. It caused oscillations and incorrect RPM readings. This is caused by reading the RPM too quickly and a time delay caused by serial communications. Waiting for a period before updating the controller fixes both this problem and the incorrect RPM readings.

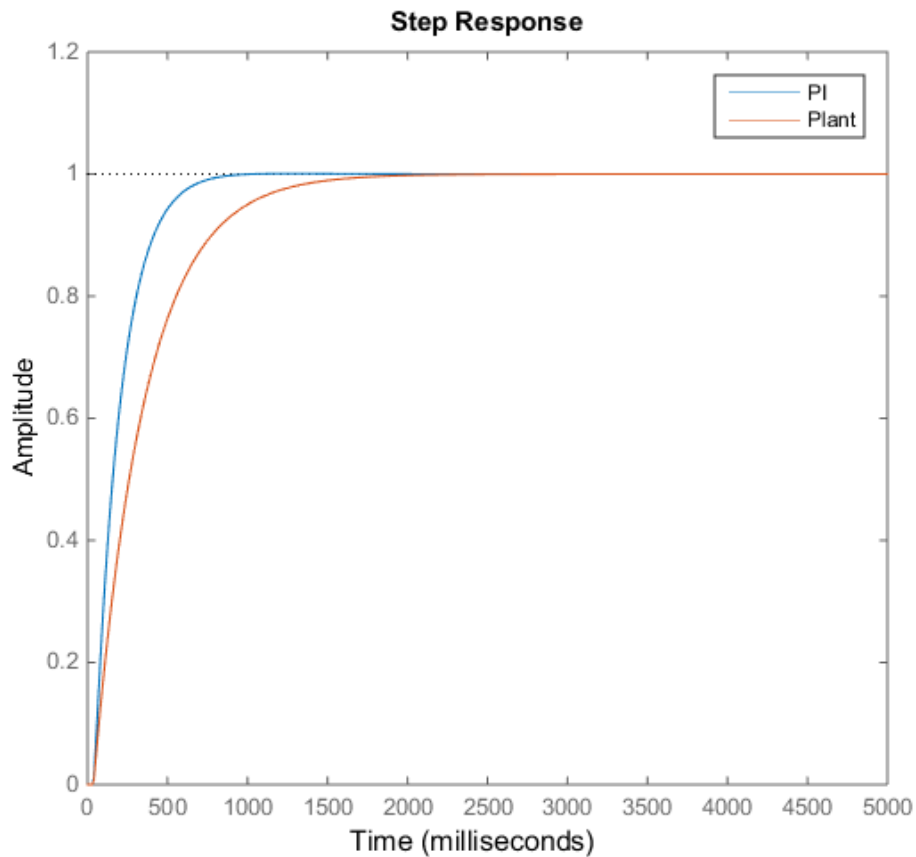


Figure 4. Tuned PI controller in blue compared to the plant in red.

B. 4 GPS navigation

To have a fully autonomous system for precision agriculture the robot needs to be able to navigate given coordinates without assistance from an operator. Along the path, the LIBS laser would take spectra of the pasture and use its current location to store the results. This would allow real-time 2D elemental mapping of a field.

Four waypoints were programmed into the Botboarduino for the robot to navigate around. A state machine was used to implement navigation. The five states were INIT (initialize), CD (change direction), GTG (go to goal), RW (reached waypoint), and STOP (stop). The robot starts off in the INIT state which initializes the position of the robot. The robot stays in this state reading the GPS position and magnetometer heading until the GPS has acquired enough satellites to function

accurately. It then moves to the CD state which compares the heading from the magnetometer to the bearing of the next waypoint. The robot then rotates until it is within a $\pm 5^\circ$ window of the correct heading. The robot then changes to the GTG state which makes the robot drive in a straight line. If the heading exceeds $\pm 5^\circ$ of the bearing the robot goes back into the CD which decreases the speed of the wheels on one side of the robot to slowly change direction. Once the heading is within $\pm 5^\circ$ of the bearing the robot goes back into the GTG state. When the robot is within 1.5 m of the current waypoint the state changes to RW. The next waypoint is then set and the robot is placed in the CD state to rotate so that it is heading in the right direction. This continues until the last waypoint is reached which triggers the STOP state which stops the robot from moving. Figure 8 and Figure 9 show the optimal route (red) if the robot was to go straight to each waypoint and the actual route (blue).

The actual route is not very smooth because of the algorithm used in the CD state. Using PID control, or more elegant methods, for steering the robot would produce smoother navigation. The last leg of the journey had a large deviation from the optimal route. This is due to an antenna (Figure 7) on the stairwell of the parking building causing interference with the magnetometer. To prove this the robot was programmed to drive in a straight line past the antenna and the heading from the magnetometer was recorded. Figure 5 shows the journey of the robot. The curve in the path was caused by the wheels not having the same distance from the robot and from an unbalanced load on top of the robot. Figure 6 shows the disturbance caused by the antenna as the robot passed by. Comparing Figure 5 and Figure 6 it can be seen that just after the robot passed by the antenna is where the maximum interference is located. This may cause a problem for farms with power pylons. GPS could find the heading of the robot by calculating the difference between two points along the journey. The downfall is this is not as accurate for small distances.



Figure 5. The route taken by the robot next to stairwell with the antenna.

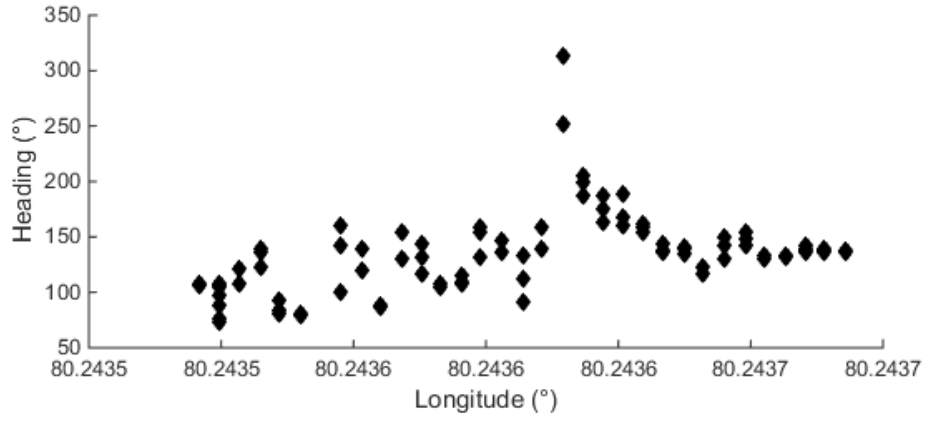


Figure 6. Magnetometer readings as the robot passed by the antenna.



Figure 7. The antenna on the stairwell creating interference.

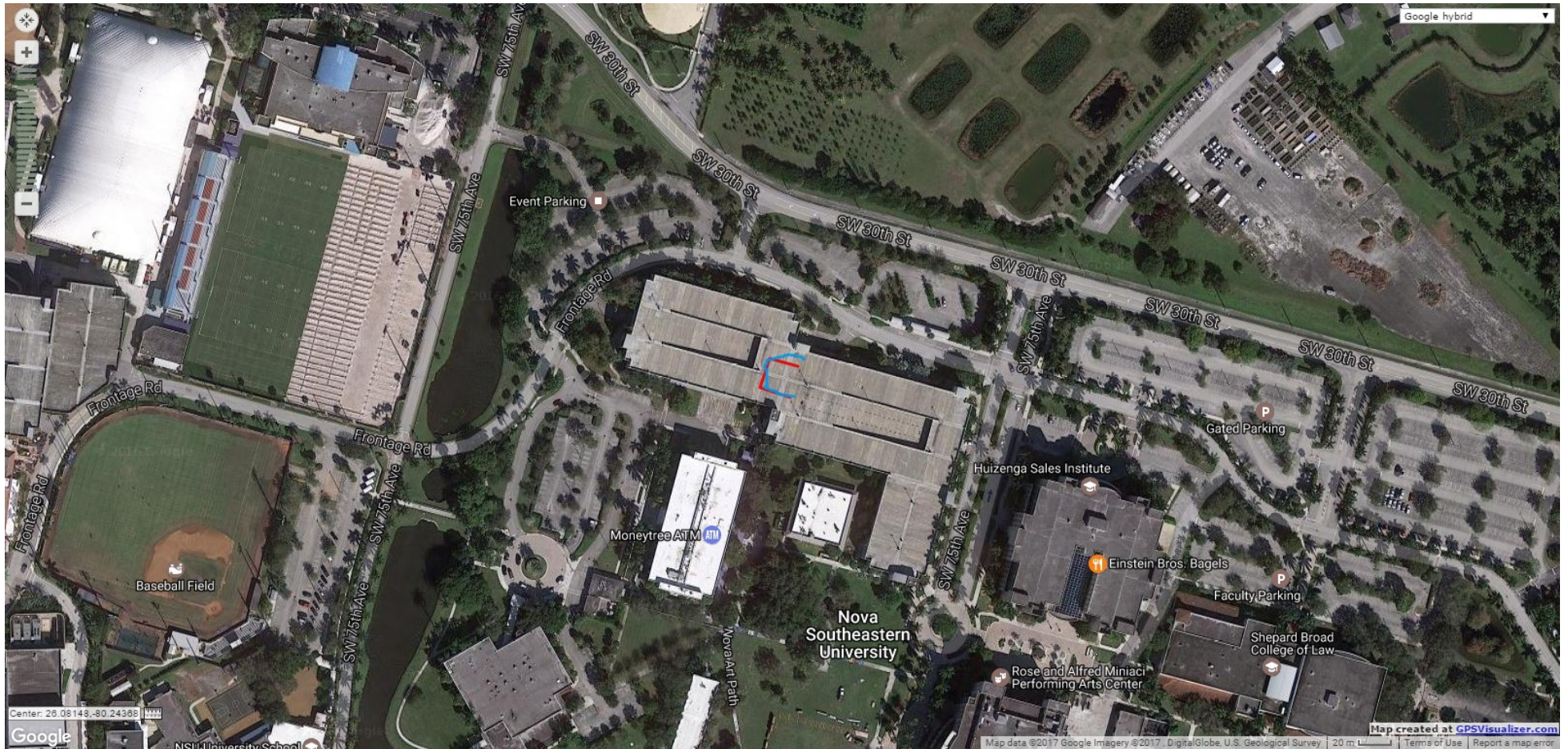


Figure 8. Google maps view of the NOVA Southeastern University campus. Optimal route for the robot in red and actual route in blue.

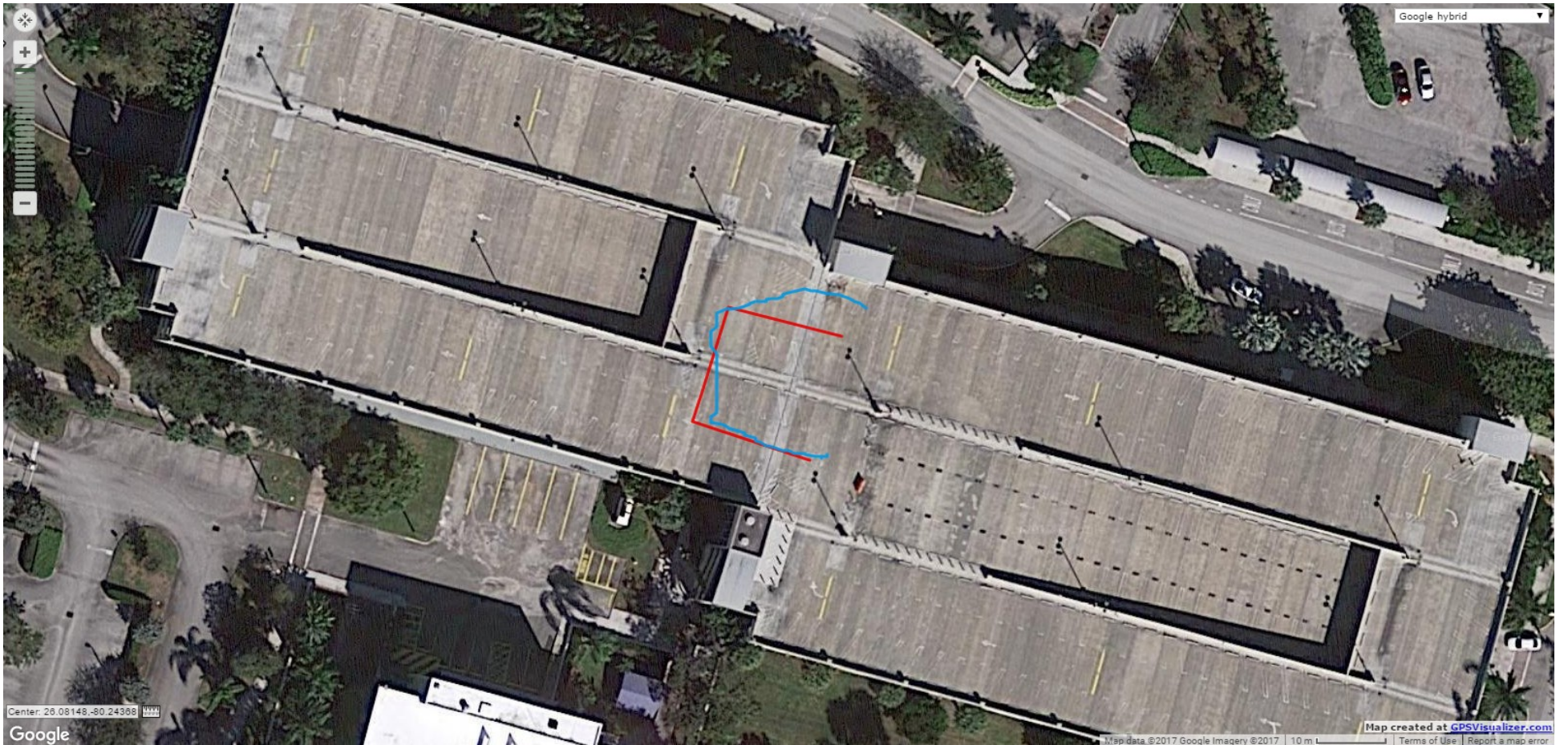


Figure 9. Zoomed in view of Figure 8. Optimal route (red), actual route (blue).

B. 5 Image modelling of grass

A webcam (HD C310, Logitech, USA) was attached to the robot, as can be seen in Figure 10, to determine if the LIBS sensor would be sampling pasture. 50 photos (480x640) were taken of pure grass, 50 photos were taken of pure dirt, and 50 photos were taken of scenes with both grass and dirt. The angle of the camera was fixed for all images. The purpose was to find a model that would suggest that there is enough grass in the image that a sample should be taken. If there is not enough grass then a sample would not be taken.



Figure 10. Prototype Robot.

C.5.1 Classification by fitting Gaussian profiles to each channel of the image

45 photos were taken from each set and converted from RGB (red, green, blue) colour space to the HSI (hue, saturation, intensity) colour space. A histogram was created for each channel of each photo. The histograms for each channel were averaged and a Gaussian profile was fitted to the Hue (Figure) and Intensity

(Figure) channels. The values of the hue and intensity were normalised. The intensity histogram was a summation of two Gaussian profiles which can be seen in Figure . Considering the broader curve as a baseline it can be ignored and the parameters of the thinner curve can be used. The mean of the fitted profiles for the hue and intensity curves were 0.206 ± 0.0552 and 0.515 ± 0.137 respectively. Using these values all images were filtered using a binary threshold where one was for values within the range of plus or minus one standard deviation and zero elsewhere. The percentage of black pixels to white pixels was then calculated and the averages for each set are presented in Table 1.

Table 1. Percentage of black pixels to white pixels in each photo.

	Mean (%)	Standard deviation (%)
Grass	55.1	6.40
Dirt	87.1	5.91
Combo	85.1	2.88

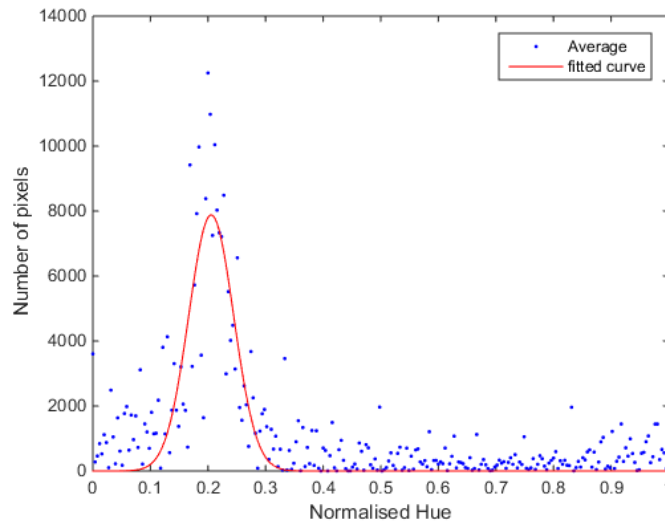


Figure 11. Fitted Gaussian profile for the averaged histograms for the hue channel of each photo.

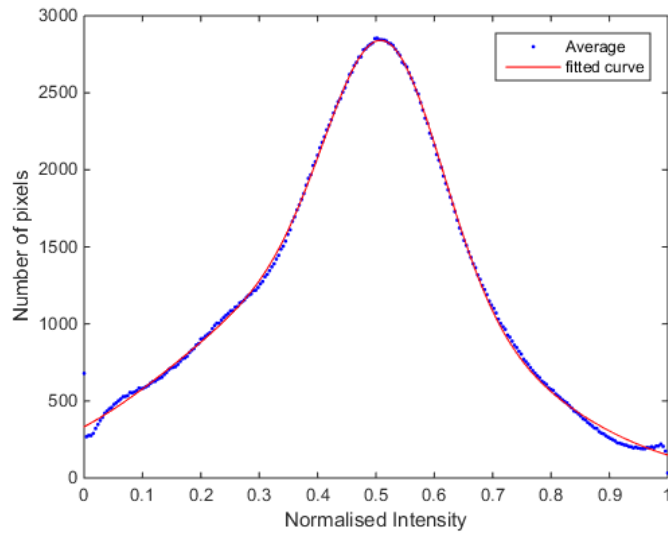


Figure 12. Fitted Gaussian profile for the averaged histograms for the intensity channel of each photo.

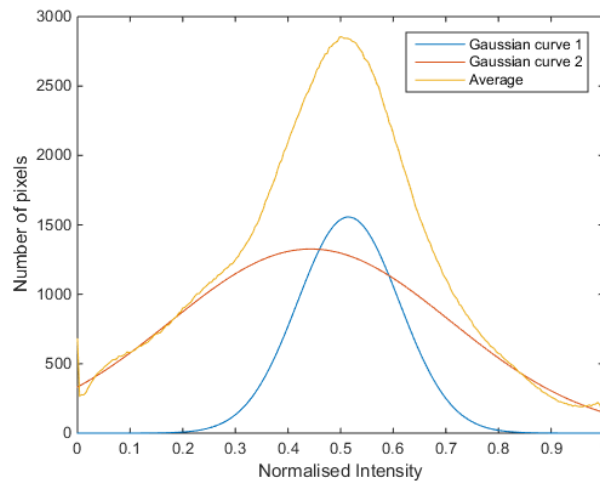


Figure 13. Average intensity histogram decomposed into two Gaussian profiles.

To confirm that the results from the dirt and combination sets are different from the grass set a T-Test was performed. The T-Test result between dirt and grass was $P = 2.46 \cdot 10^{-41}$ and between combination and grass was $P = 1.65 \cdot 10^{-46}$ which proves that they are not from the same distribution. Figure shows the results of calculating the percentages of black to white pixels.

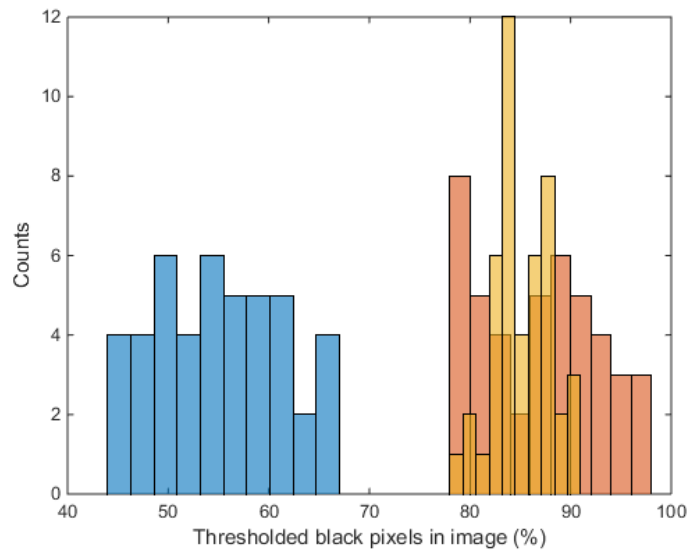


Figure 14. Histograms of the grass (blue), dirt (red), and combination (orange) sets.

Since the standard deviations of the grass and dirt distributions are comparable the threshold can be placed between the means of these distributions which is 71.1 %. The five samples that were left out of each set were then used to test the model. All photos were classified correctly. Figure displays the classifications.

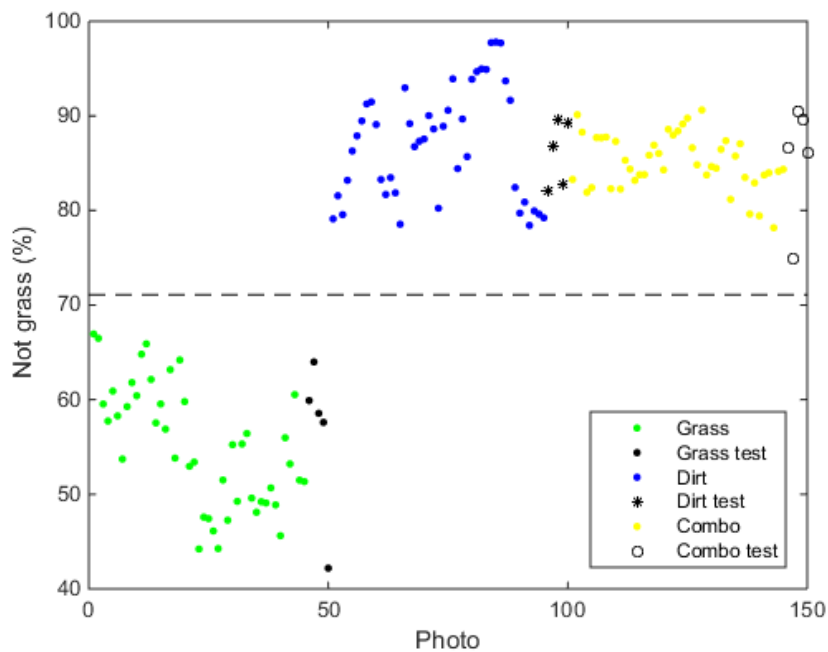


Figure 15. Results of classifying all photos. The dashed line is the threshold.

C.5.2 Classification using a Euclidean rectangle with PCA

A single image of grass which was not from the original 50 photos was taken and the RGB channels were converted to HSI channels. PCA was performed using each pixel as an observation and the HSI channels as the variables for each observation. Because of the noise (pixels not of grass, or grass pixels to bright or dark), the mean of the density of points is not in the centre of the scores plot. The mean and standard deviations of the three scores were taken and used as a threshold to define if a pixel was grass. This produces a 3D rectangle with width 2σ and with the planes of the rectangle in the directions of the eigenvectors. Any pixel within this boundary was considered grass. 45 photos from each set were filtered using this rectangle and the percentage of black to white pixels were determined. Table 1 shows the means and standard deviations for each set. The difference between the grass and dirt means was taken as the threshold. The five remaining photos from each set was then used to test the threshold of 71.9 %. This produced 100 % classification as seen in Figure .

C.5.3 Classification using PCA and the Mahalanobis distance

The same procedure in C.5.2 was used except the Mahalanobis distance was used instead of the Euclidean distance. The Mahalanobis distance creates an elliptical sphere around the dense cluster of pixels that are classed as grass. This reduces the pixels that may get misclassified by using the Euclidean rectangle. The Mahalanobis distance was varied to find the greatest separation between the grass and dirt sets. Table 2 shows the results. Using a Mahalanobis distance of 1.35 gave the greatest separation of 41.3 %, as seen in Table 3, between the means of the grass and dirt sets. The threshold was set to 64.9 % to separate grass from dirt. Figure shows 100 % classification of grass, dirt, and the grass and dirt combination photos.

Table 1. Percentage of black pixels to white pixels in each photo using the Euclidean distance.

	Mean	Standard deviation
Grass	53.8	5.94
Dirt	90.0	2.80
Combo	82.5	3.89

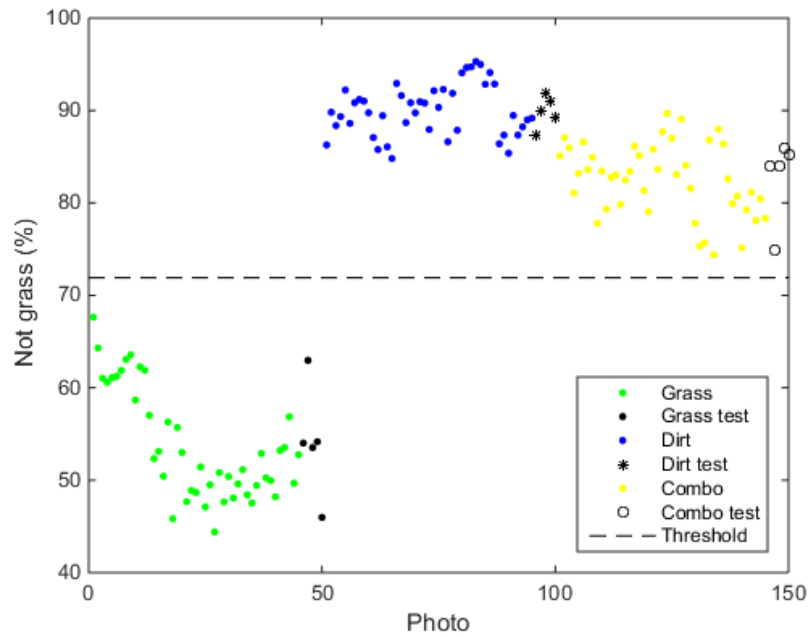


Figure 16. Results of classifying all photos using the Euclidean distance.

Table 2. Separation caused by different Mahalanobis distances.

Mahalanobis		1.20	1.25	1.30	1.35	1.40	1.45	1.50	1.55
Grass	μ (%)	53.3	50.0	47.0	44.3	41.7	39.2	37.0	34.9
	σ (%)	6.15	6.49	6.74	6.94	7.07	7.15	7.16	7.14
Dirt	μ (%)	92.8	90.4	88.1	85.5	82.8	79.9	76.9	73.7
	σ (%)	2.73	3.37	4.12	4.93	5.77	6.59	7.34	8.09
Diff		39.5	40.4	41.1	41.3	41.1	40.7	39.9	38.8

Table 3. Percentage of black pixels to white pixels in each photo using the Mahalanobis distance.

	Mean	Standard deviation
Grass	44.3	6.94
Dirt	85.5	4.93
Combo	77.9	4.49

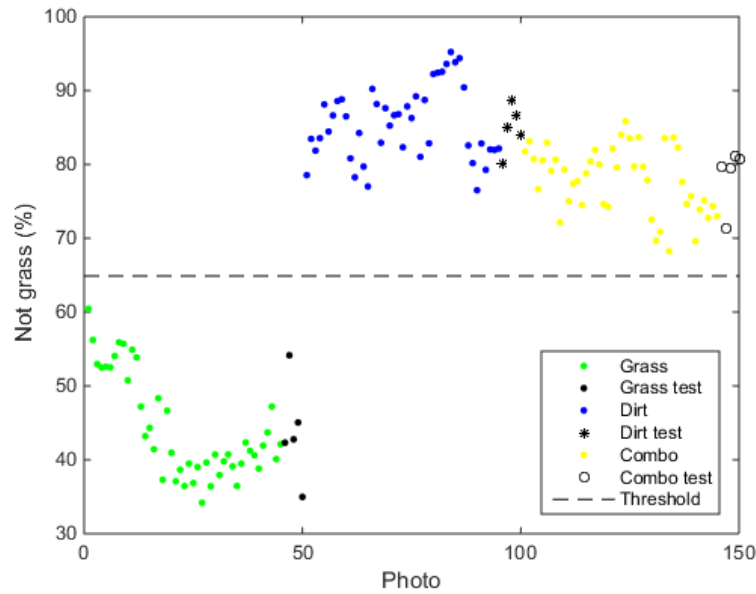


Figure 17. Results of classifying all photos using the Mahalanobis distance.

C.5.5 PCA with a Euclidean rectangle using a Box-cox transformation

Some of the channels in the HSI space were skewed. A box-cox transformation was performed on all channels to make them more Gaussian-like before PCA was performed. The rest of the procedure is the same as C.5.2, creating a Euclidean rectangle to differentiate grass from dirt. The threshold was set to 71.2 % and it had 100 % success at classifying grass. Table 4 and Figure show the results. Using the box-cox transformation did not improve the classification. The photos closest to the threshold on either side had a separation of 4.88 % using the box-cox transformation and 6.75 % without the transformation.

Table 4. Percentage of black pixels to white pixels in each photo using a box-cox transformation.

	Mean	Standard deviation
Grass	52.9	6.89
Dirt	89.5	4.92
Combo	81.8	3.83

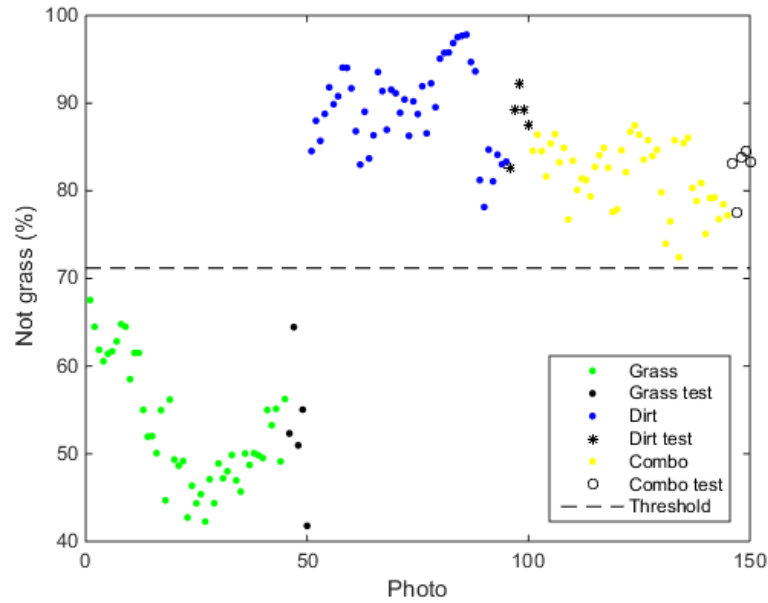


Figure 18. Results of classifying all photos using a box-cox transformation.

B. 6 Summary

Using PCA and the Mahalanobis distance produced 41.3 % separation which was the greatest separation between the grass and dirt samples. The raspberry pi toolbox in Simulink does not allow the Mahalanobis calculation to be uploaded to the raspberry pi. For this reason, PCA with the Euclidean rectangle would have to be used for implementation. Figure shows an example of the PCA-Euclidean rectangle thresholding for an image from each set of data. The percentage of black to white pixels in the figure are 57.2 %, 89.7 %, and 92.6 % for the grass, dirt, and combination images respectively.

This could not be implemented on the robot because power could not be supplied to the raspberry pi without additional batteries. It was tested by using power supplied by a computer and by connecting the web camera to the raspberry pi. It was slow but could be used to sample every few seconds. Using some code optimization may reduce the computation time of the algorithm.



a)



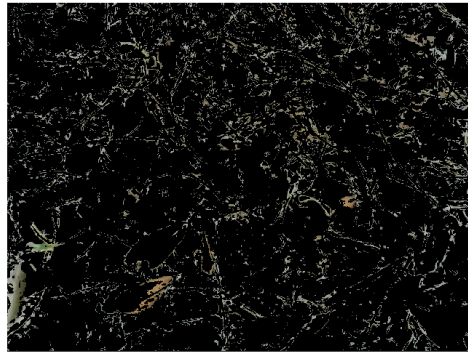
b)



c)



d)



e)



f)

Figure 19. Photos of a) grass, b) dirt, and c) a combination of both. The thresholded images d), e), and f) of a), b), and c) respectively with only the ‘grass’ pixels shown. PCA with a Euclidean rectangle was used.

Appendix C

**List of peer reviewed papers, book chapters,
and conference presentations with copyright
permissions**

C. 1 Peer reviewed publications

H. Jull, R. Künnemeyer, and P. Schaare, "Considerations needed for sensing mineral nutrient levels in pasture using a benchtop laser-induced breakdown spectroscopy system," Unpublished.

H. Jull, J. Bier, R. Künnemeyer, and P. Schaare, "Classification of recyclables using laser-induced breakdown spectroscopy for waste management," submitted for publication.

H. Jull, R. Künnemeyer, and P. Schaare, "Nutrient detection in fresh and dried pasture using laser-induced breakdown spectroscopy," *Precision Agriculture*, accepted January 25 2018. Reproduced by permission of Springer at https://link.springer.com/article/10.1007/s11119-018-9559-4?wt_mc=Internal.Event.1.SEM.ArticleAuthorOnlineFirst

H. Jull, P. Ewart, R. Künnemeyer, and P. Schaare, "Selective Surface Sintering Using a Laser-Induced Breakdown Spectroscopy System," *Journal of Spectroscopy*, vol. 2017, p. 11, 2017. Reproduced by permission of H. Jull and available at: <https://www.hindawi.com/journals/jspec/2017/1478541/>

P. Ewart, H. Jull, R. Künnemeyer, and P. N. Schaare, "Identification of contamination levels and the microstructure of metal injection moulded titanium," in *Key Engineering Materials* vol. 704, T. Ebel and F. Pyczak, Eds., ed: Trans Tech Publications Ltd, 2016, pp. 161-169. Reproduced by permission of Key Engineering Materials and available at: <https://www.scientific.net/KEM.704.161>

C. 2 Presentations

H. Jull, R. Künnemeyer, and P. Schaare. "Considerations needed for sensing mineral nutrient levels in fresh pasture using LIBS," in *2017 Eleventh International Conference on Sensing Technology (ICST)*, Sydney, Australia, 2017.

H. Jull, R. Künnemeyer, and P. Schaare. "Chemometric analyses of agricultural spectra generated by laser-induced breakdown spectroscopy," in *Waikato Young Research Engineers Symposium*, Hamilton, New Zealand, 2017.

H. Jull, R. Künnemeyer, and P. Schaare. "Macro and micro-nutrient detection in pasture using laser-induced breakdown spectroscopy," in *IEEE Instrument & Measurement Workshop 2016*, Lincoln, New Zealand, 2016. Reproduced by permission of IEEE and available at: <http://ieeexplore.ieee.org/document/7081157/>

H. Jull, R. Künnemeyer, S. Talele, P. Schaare, "Internal Standard Considerations for Laser-induced Breakdown Spectroscopy Measurements on Pelletized Grass Samples," in *New Zealand Institute of Physics Conference 2015*, Hamilton New Zealand.

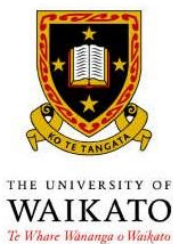
H. Jull, R. Künnemeyer, S. Talele, P. Schaare, and M. Seelye, "Laser-induced breakdown spectroscopy analysis of sodium in pelletised pasture samples," in *Automation, Robotics and Applications (ICARA), 2015 6th International Conference on*, Queenstown, New Zealand, 2015.

H. Jull, R. Künnemeyer, S. Talele, P. Schaare, and M. Seelye, "Sodium Determination in Pasture by Laser-Induced Breakdown Spectroscopy," in *2014 IEEE I&M Society Workshop*, Auckland, New Zealand, 2014.

H. Jull, R. Künnemeyer, S. Talele, P. Schaare, and M. Seelye, "Laser-induced breakdown spectroscopy analysis of sodium in pasture," in *ENZCon'14 21st Electronics New Zealand Conference*, Hamilton, New Zealand, 2014.

Appendix D

Co-authorship forms



Co-Authorship Form

Postgraduate Studies Office
 Student and Academic Services Division
 Wahanga Ratonga Matauranga Akonga
 The University of Waikato
 Private Bag 3105
 Hamilton 3240, New Zealand

This form is to accompany the submission of any PhD that contains research reported in published or unpublished co-authored work. **Please include one copy of this form for each co-authored work.** Completed forms should be included in your appendices for all the copies of your thesis submitted for examination and library deposit (including digital deposit).

Please indicate the chapter/section/pages of this thesis that are extracted from a co-authored work and give the title and publication details or details of submission of the co-authored work.

Chapter 3: N Nutrient quantification in fresh and dried mixtures of ryegrass and clover leaves using laserinduced breakdown spectroscopy
 Accepted in Precision Agriculture.

Nature of contribution by PhD candidate

Processed spectra, performed chemometric analysis, interpreted results, wrote the paper

Extent of contribution by PhD candidate (%)

60%



CO-AUTHORS

Name	Nature of Contribution
Rainer Künemeyer	Supervision, consultation, paper corrections
Peter Schaare	Supervision, consultation, paper corrections

Certification by Co-Authors

The undersigned hereby certify that:

- ❖ the above statement correctly reflects the nature and extent of the PhD candidate's contribution to this work, and the nature of the contribution of each of the co-authors; and

Name	Signature	❖ Date
Rainer Künemeyer		17 January 2018
Peter Schaare		17 January 2018



Co-Authorship Form

Postgraduate Studies Office
Student and Academic Services Division
Wahanga Ratonga Matauranga Akonga
The University of Waikato
Private Bag 3105
Hamilton 3240, New Zealand

This form is to accompany the submission of any PhD that contains research reported in published or unpublished co-authored work. **Please include one copy of this form for each co-authored work.** Completed forms should be included in your appendices for all the copies of your thesis submitted for examination and library deposit (including digital deposit).

Please indicate the chapter/section/pages of this thesis that are extracted from a co-authored work and give the title and publication details or details of submission of the co-authored work.

Chapter 4: Laser-Induced Breakdown Spectroscopy Analysis of Sodium in Pelletised Pasture Samples.
Published in 2015 6th International Conference on Automation, Robotics and Applications (ICARA).

Nature of contribution by PhD candidate	Processed spectra, performed chemometric analysis, interpreted results, wrote the paper
Extent of contribution by PhD candidate (%)	60%

CO-AUTHORS

Name	Nature of Contribution
Rainer Künnemeyer	Supervision, consultation, paper corrections
Sadhana Talele	Supervision, consultation, paper corrections
Peter Schaare	Supervision, consultation, paper corrections
Mark Seelye	Collected experimental data

Certification by Co-Authors

The undersigned hereby certify that:

- ❖ the above statement correctly reflects the nature and extent of the PhD candidate's contribution to this work, and the nature of the contribution of each of the co-authors; and

Name	Signature	❖ Date
Rainer Künnemeyer		31/01/2018
Peter Schaare		29/01/18
Mark Seelye		29/01/18
Sadhana Talele (Deceased)		



Co-Authorship Form

Postgraduate Studies Office
Student and Academic Services Division
Wahanga Ratonga Matauranga Akonga
The University of Waikato
Private Bag 3105
Hamilton 3240, New Zealand

This form is to accompany the submission of any PhD that contains research reported in published or unpublished co-authored work. **Please include one copy of this form for each co-authored work.** Completed forms should be included in your appendices for all the copies of your thesis submitted for examination and library deposit (including digital deposit).

Please indicate the chapter/section/pages of this thesis that are extracted from a co-authored work and give the title and publication details or details of submission of the co-authored work.

Chapter 5: Considerations needed for sensing mineral nutrient levels in pasture using a benchtop laser-induced breakdown spectroscopy system
To be submitted as a book chapter in Smart Sensors for Precision Agriculture

Nature of contribution
by PhD candidate

Processed spectra, performed chemometric analysis, interpreted results, wrote the chapter

Extent of contribution
by PhD candidate (%)

70%



CO-AUTHORS

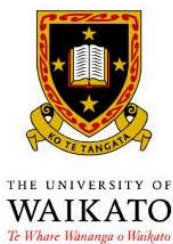
Name	Nature of Contribution
Rainer Künemeyer	Supervision, consultation, paper corrections
Peter Schaare	Supervision, consultation, paper corrections

Certification by Co-Authors

The undersigned hereby certify that:

- ❖ the above statement correctly reflects the nature and extent of the PhD candidate's contribution to this work, and the nature of the contribution of each of the co-authors; and

Name	Signature	❖ Date
Rainer Künemeyer		17 January 2018
Peter Schaare		17 January 2018



Co-Authorship Form

Postgraduate Studies Office
 Student and Academic Services Division
 Wahanga Ratonga Matauranga Akonga
 The University of Waikato
 Private Bag 3105
 Hamilton 3240, New Zealand

This form is to accompany the submission of any PhD that contains research reported in published or unpublished co-authored work. **Please include one copy of this form for each co-authored work.** Completed forms should be included in your appendices for all the copies of your thesis submitted for examination and library deposit (including digital deposit).

Please indicate the chapter/section/pages of this thesis that are extracted from a co-authored work and give the title and publication details or details of submission of the co-authored work.

Chapter 6 Identification of Contamination Levels and the Microstructure of Metal Injection Moulded Titanium.
 Published in Key Engineering Materials.

Nature of contribution
 by PhD candidate

Planned and performed LIBS experiments, collected EDS and SEM data, collected and processed LIBS spectra, interpreted LIBS results, developed autofocus mechanism, wrote LIBS and autofocus sections

Extent of contribution
 by PhD candidate (%)

15%


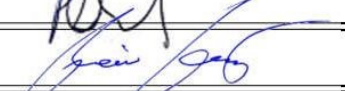

CO-AUTHORS

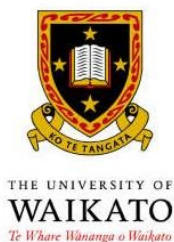
Name	Nature of Contribution
Paul Ewart	Wrote paper, created samples, performed titanium experiments, interpreted titanium results
Rainer Künne Meyer	Supervision, consultation, paper corrections
Peter Schaare	Supervision, consultation, paper corrections

Certification by Co-Authors

The undersigned hereby certify that:

- ❖ the above statement correctly reflects the nature and extent of the PhD candidate's contribution to this work, and the nature of the contribution of each of the co-authors; and

Name	Signature	❖ Date
Paul Ewart		15 Jan 2018
Rainer Künne Meyer		17 Jan 2018
Peter Schaare		17 Jan 2018



Co-Authorship Form

Postgraduate Studies Office
 Student and Academic Services Division
 Wahanga Ratonga Matauranga Akonga
 The University of Waikato
 Private Bag 3105
 Hamilton 3240, New Zealand

This form is to accompany the submission of any PhD that contains research reported in published or unpublished co-authored work. **Please include one copy of this form for each co-authored work.** Completed forms should be included in your appendices for all the copies of your thesis submitted for examination and library deposit (including digital deposit).

Please indicate the chapter/section/pages of this thesis that are extracted from a co-authored work and give the title and publication details or details of submission of the co-authored work.

Chapter 7: Selective Surface Sintering Using a Laser-Induced Breakdown Spectroscopy System.
 Published in Journal of Spectroscopy.

Nature of contribution
 by PhD candidate

Planned experimental design, collected and processed spectra, performed experiments,
 interpreted LIBS results, created autofocus mechanism, wrote the paper

Extent of contribution
 by PhD candidate (%)

50%


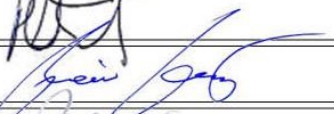

CO-AUTHORS

Name	Nature of Contribution
Paul Ewart	Created samples, performed titanium experiments, interpreted titanium results
Rainer Künнемeyer	Supervision, consultation, paper corrections
Peter Schaare	Supervision, consultation, paper corrections

Certification by Co-Authors

The undersigned hereby certify that:

- ❖ the above statement correctly reflects the nature and extent of the PhD candidate's contribution to this work, and the nature of the contribution of each of the co-authors; and

Name	Signature	❖ Date
Paul Ewart		15 January 2018
Rainer Künнемeyer		17 January 2018
Peter Schaare		17 January 2018



Co-Authorship Form

Postgraduate Studies Office
Student and Academic Services Division
Wahanga Ratonga Maturanga Akonga
The University of Waikato
Private Bag 3105
Hamilton 3240, New Zealand

This form is to accompany the submission of any PhD that contains research reported in published or unpublished co-authored work. **Please include one copy of this form for each co-authored work.** Completed forms should be included in your appendices for all the copies of your thesis submitted for examination and library deposit (including digital deposit).

Please indicate the chapter/section/pages of this thesis that are extracted from a co-authored work and give the title and publication details or details of submission of the co-authored work.

Chapter 8: Classification of recyclables using laser-induced breakdown spectroscopy for waste management.
In review by Spectroscopy Letters.

Nature of contribution
by PhD candidate

Planned experimental design, collected and processed spectra, interpreted results, wrote the paper, created autofocus mechanism

Extent of contribution
by PhD candidate (%)

70%

CO-AUTHORS

Name	Nature of Contribution
James Bier	Bioplastic sample preparation, contributed to experimental section, paper corrections
Rainer Künnemeyer	Supervision, consultation, paper corrections
Peter Schaare	Supervision, consultation, paper corrections

Certification by Co-Authors

The undersigned hereby certify that:

- ❖ the above statement correctly reflects the nature and extent of the PhD candidate's contribution to this work, and the nature of the contribution of each of the co-authors; and

Name	Signature	❖ Date
James Bier		17/1/2018
Rainer Künnemeyer		17/1/2018
Peter Schaare		29/01/18